Computation Of Information Theoretic Quantities Using Gauge/Gravity Correspondence

Thesis submitted for the degree of

Doctor of Philosophy **(Science)**

in

Physics (Theoretical)

by

Anirban Roy Chowdhury

Department of Physics,

University of Calcutta,

2025

to my parents

Acknowledgements

It's honestly difficult to put into words just how grateful I am to everyone who's backed me up throughout my doctoral journey. There are so many people-mentors, colleagues, friends, family-who have offered support, encouragement, and the occasional reality check when I needed it most. While it's impossible to list everyone or fully express my appreciation, I want to sincerely thank all those who contributed, in big ways and small, to this achievement. From the initial stages of my academic journey to the completion of this thesis, I have benefited greatly from the guidance, assistance, and motivation provided by colleagues, mentors, friends, and family. Their unwavering support has been essential in making this accomplishment possible.

Firstly, I would acknowledge S.N Bose National Centre for Basic Sciences (SNBNCBS) for the opportunity and financial support during the my PhD. I would like to express my gratitude to my supervisor Prof. Sunandan Gangopadhyay for the continuos support and encouragement during my Ph.D. journey. I would also like to thank my senior Dr. Ashis Sahafor his unwavering support and guidance from the very beginning of this journey. His insightful advice, encouragement, and willingness to help at every stage have been invaluable to me. Then I would like to thank my seniors Dr. Debabrata Ghorai, Dr. Rituparna Mandal, Dr. Ankur Shrivastav, Dr.Niraj Kumar, Dr.Anish Das, Ms. Manjari Dutta, Mr. Arnab Mukherjee for their support. I would also like to thank my juniors Soham, Souvik, Gopinath, Arpita for their invaluable assistance in helping me complete my research. Their enthusiasm, support, and constructive discussions have made this journey more enriching and enjoyable. I would also like to extend my sincere gratitude to the rest of my thesis committee, especially Prof. Archan S Majumdar and Prof. Amitabha Lahiri, for their encouragement, thought-provoking questions, and insightful comments. Their valuable feedback and critical perspectives have significantly contributed to the depth and clarity of this work.

Apart from my research group, I feel fortunate to have had the support of my friends and seniors at SNBNCBS, with whom I have shared both cherished moments and challenges throughout my PhD journey. I owe a sincere debt of gratitude to my batchmates- Animesh, Ankita, Avik, Arnab, Gaurav, Shubham, Soumen, Soham, Shinjini, Ishita, Rajdeep, Sudipta, and Koushik-for their steadfast support and camaraderie throughout this journey. Their encouragement, thoughtful conversations, and presence have played a crucial role in shaping both my academic pursuits and personal development Their constant encouragement, insightful discussions, and shared expe-

riences have made this academic pursuit not only smoother but also immensely enjoyable. I would also like to express my heartfelt gratitude to my seniors for their guidence.

Apart from my friends at SNB, I would also like to extend my gratitude to my friends from Gyandeep Vidyapith, especially Anuvab, Arindam, Dipanjan, Swadesh, Pradip, Singha, Arup, Ranit and others. Their unwavering support, cherished friendships, and the countless memories we have shared over the years have been a source of strength and motivation throughout this journey.

I would also like to express my heartfelt gratitude to my undergraduate college (Ramakrishna Mission Vivekananda Centenary College) teachers Dr. Ashok Kr. Paul, Dr. Atisdipankar Chakrabarty, Dr. Kalyan Chatterjee, Dr. Rajen Kundu, Dr. Chandan Kr. Das and Dr. Bhaskar Halder for their invaluable guidance and encouragement during my formative years. Their dedication to teaching and mentorship played a crucial role in shaping my academic foundation and inspiring me to pursue research.

Last but not least, I would like to express my deepest respect and heartfelt gratitude to all my family members. Their unwavering support, patience, and encouragement have been the foundation of my academic journey, and this achievement would not have been possible without them. My parents has always inspired me to follow my passion without any fear. They let me exercise my freedom regarding my academic matters and individual choices.

Certificate from the Supervisor

This is to certify that the thesis entitled " **Computation of Information Theoretic Quantities Using Gauge/Gravity Correspondence** " submitted by **Anirban Roy Chowdhury**, a Senior Research Fellow at S.N. Bose National Centre for Basic Sciences, Kolkata, to the University of Calcutta (C.U.), as a part of **5000 word thesis synopsis** for Ph.D. Programme in Physics, is absolutely based upon his own work under the supervision of **Prof. Sunandan Gangopadhyay**. Neither this thesis synopsis nor any part of it has been submitted for any degree/diploma or any other academic award anywhere before.

Anirban Roy Chowdhury
Senior Research Fellow
(Self-Declaration)

.....

Prof. Sunandan Gangopadhyay
(Professor)

List of publications on which the thesis is based

1. **Anirban Roy Chowdhury**, Ashis Saha and Sunandan Gangopadhyay "Entanglement wedge cross-section for noncommutative Yang-Mills theory ", JHEP02(2022)192.

2. **Anirban Roy Chowdhury**, Ashis Saha and Sunandan Gangopadhyay,"Mixed state information theoretic measures in boosted black brane", Annals Phys. 452 (2023) 169270.

3. **Anirban Roy Chowdhury**, Ashis Saha and Sunandan Gangopadhyay ,"Mixed state entanglement measures for the dipole deformed supersymmetric Yang-Mills theory", Annals Phys. 460 (2024) 169565

4. **Anirban Roy Chowdhury**, Ashis Saha and Sunandan Gangopadhyay *"Role of mutual information in the Page curve "*, Phys.Rev.D 106 (2022) 8, 086019

5. **Anirban Roy Chowdhury**, Ashis Saha and Sunandan Gangopadhyay *" Mutual information of subsystems and the Page curve for the Schwarzschild-de Sitter black hole"*,Phys.Rev.D 108 (2023) 2, 026003

NOT included in the thesis

6. **Anirban Roy Chowdhury**, Ashis Saha and Sunandan Gangopadhyay "Entropy function from the Einstein boundary term ", EPL 134 (2021) 60003.

7. Anish Das, **Anirban Roy Chowdhury** and Sunandan Gangopadhyay "Stability, quasinormal modes in a charged black hole in perfect fluid dark matter ", Class.Quant.Grav. 41 (2024) 1, 015018.

8. Ashis Saha,**Anirban Roy Chowdhury** and Sunandan Gangopadhyay, "Investigating the role of mutual information in the Page curve for a functional renormalization group improved Schwarzschild black hole",Eur. Phys. J. C (2025) 85:837.

9. Souvik Paul, **Anirban Roy Chowdhury**, Ashis Saha and Sunandan Gangopadhyay "Information theoretic measures for Lifshitz system",JHEP 10 (2024) 033.

List of conferences participated during Ph.D.

1. Participated in the in the "Future Trends in Gravitational Physics 2022", S. N. Bose National Centre for Basic Sciences.

2. Presented poster in the "Workshop on Gravity, Cosmology and Raychaudhuri's Equation", RCRC, Jadavpur University.

3. Presented poster in the "Field Theoretic Aspect in Gravity", BITs, Mesra.

4. Presented poster in the "Advances in Astroparticle Physics and Cosmology (AAPCOS-2023)", Saha Institute of Nuclear Physics.

5. Presented poster in "International Conference on Photonics, Quantum Information, and Quantum Communication (ICPQIQC) 2024", S. N. Bose National Centre for Basic Sciences.

6. Presented poster in "XXVI DAE-BRNS High Energy Physics Symposium-2024", Institute of Science, Banaras Hindu University,Varanasi. (Best poster award)

7. Presented poster in "STRINGS-25", NewYork University, Abu Dhabi (NYUAD).

Abstract

In this work, I have systematically examined key aspects of the Anti-de Sitter/Conformal Field Theory (AdS/CFT) correspondence, focusing on its foundational principles, mathematical structure, and physical consequences. Central to my investigation are information-theoretic quantities in strongly coupled field theories, approached through the powerful AdS/CFT duality. Specifically, I have calculated the entanglement entropy for a strip-like region in the conformal field theory, employing the Ryu-Takayanagi prescription. Rather than deriving entanglement entropy directly from the field theory, I utilized its gravitational dual in a higher-dimensional spacetime, which naturally leads to the notion of holographic entanglement entropy. Building on these results, I also computed the mutual information between two strip-like subsystems, again leveraging the holographic framework.

Beyond these measures, I explored various quantum correlation quantities relevant for mixed states. In particular, I calculated the entanglement wedge cross-section (the gravitational dual to entanglement of purification) and entanglement negativity. Additionally, holographic complexity and purification complexity were studied to further elucidate quantum information measures within the AdS/CFT context. All such computations were carried out for $\mathcal{N} = 4$ noncommutative super Yang-Mills theory, $\mathcal{N} = 4$ dipole-deformed super Yang-Mills theory, and a uniformly boosted $\mathcal{N} = 4$ strongly coupled thermal plasma, always by analyzing their respective gravitational duals. Furthermore, I addressed the longstanding black hole information loss paradox through the recently developed island formalism, which offers a new perspective on the black hole information problem. Within this framework, I demonstrated the essential role of mutual information between relevant subsystems in reconstructing the Page curve. I also proposed two conjectures regarding the connectivity of the entanglement wedge at different temporal regimes. The analysis shows that these methods successfully reproduce the expected Page curve for eternal black holes, thereby providing new insights into black hole information dynamics. Importantly, the proposals remain valid for eternal black holes in both asymptotically AdS and asymptotically de Sitter spacetimes. To give concrete evidence, I explicitly considered two black hole solutions: the eternal black hole in JT gravity and the Schwarzschild de Sitter black hole.

Contents

List of Figures

Chapter 1

Introduction and Motivation

In this chapter we have discussed various quatities which are useful to measure quantum correlation present in a system. These quantities are very useful in the context of quantum information theory. In this thesis I have computed some of these quantities in the context of the conformal field theory. In the subsequent sections we have discussed these information theoretic measures in details. We have started with the definition of pure and mixed states. Then I have moved on to discuss von-Neumann entropy, mutual information, entanglement negativity, entanglement of purification, complexity and complexicity of purification. After that we have discussed conformal field theory and a bit of Einstein gravity in the prsence of the negative cosmological constant briefly. Then we have proceed to describe the gauge/gravity duality and the holographic description of different information theoretic quantities in details.

1.1 Some Basics of Quantum Mechanics

Quantum mechanics is one of the most fasinating subject of modern physics. It describes physcics at very small length (Compton length) scale where classical theory does not work. In Quantum mechanics a system is described by a complex function dependens of the position on time, called wave function, $\psi(\vec{x},t)$. Time evolution of a quantum state is described by Schrödinger equation given as following [1]

$$i\hbar\frac{\partial\psi(\vec{x},t)}{\partial t} = H\psi(\vec{x},t)\ . \tag{1.1}$$

H is the Hamiltonian of the system. Any dynamical observable in this theory is described by Hermitiam operator. The expectation value of an dynamical observable is given by

$$\langle A \rangle_\psi = \frac{\int_{-\infty}^{\infty} \psi(\vec{x},t)^* A \psi(\vec{x},t)}{\int_{-\infty}^{\infty} \psi(\vec{x},t)\psi(\vec{x},t)^*} \ . \tag{1.2}$$

There are different pictures of quantum theory, depending on which kind of problem we are dealing with. The above picture is named as the Schrödinger picture. There are other two pictures Hisenberg picture and interaction picture. I will not discuss them here.

Alternatively there is another way to describe quantum mechanics which is independent of choice of basis. It is more abstract way to describe quantum mechanics. In this formalism the state of a system in described by $|\psi(t)\rangle$. The wave function is the position basis can be obtained by following

$$\psi(\vec{x},t) = \langle \vec{x}|\psi(t)\rangle \ . \tag{1.3}$$

We define an operator, known as density matrix with $|\psi(t)\rangle$, as following

$$\rho = |\psi\rangle \langle\psi| \ . \tag{1.4}$$

Alternatively instead of wavefunction, a system can also described by density matrix. In this formalism the expectation value of a dynamical observable is given by

$$\langle A \rangle = \mathrm{Tr}[\rho A] \ . \tag{1.5}$$

The density matrix have the follwing properties

1. It is a hermitian operator, this implies $\rho^\dagger = \rho$.
2. $\mathrm{Tr}[\rho] = 1$.
3. $\mathrm{Tr}[\rho^2] \leq 1$.
4. All the eigenvalues of the density matix is real and positive.

Depending on the third property a state is said to be either pure or mixed. A system is said to be in pure state if

$$\mathrm{Tr}[\rho^2] = 1 \ . \tag{1.6}$$

On the other hand, a system is said to be in mixed state if

$$\mathrm{Tr}[\rho^2] < 1 \ . \tag{1.7}$$

In the subsequent sections I have discussed different measures of qunatum correlation for both the pure and mixed state. For pure state, the quantum correlation is measured by von-Neuman entropy. On the other hand for mixed state there are several quantities like entanglement of purification, entnaglement negativity etc.

1.1.1 von-Neumann entropy and quantum entanglement

von-Neumann entropy is a reliable measure of quantum correlation when the system under consideration is in a pure state. One can define von-Neumann entropy for pure state in the following manner. Let us consider a bipartite system $A \cup B$, which is in a pure state. The Hilbert space associated with the full system can be expressed as $\mathcal{H}_{AB} = \mathcal{H}_A \otimes \mathcal{H}_B$, where $\mathcal{H}_A$ and $\mathcal{H}_B$ represents the Hilbert space associated with the subsystem A and B respectively. Now the state of the compositie system can be wriiten as $|\psi\rangle_{AB}$. The two subsystems are said to be entangled if the state of the composite system cannot be written as tensor product of two individual states. This means two subsystems are said to entangled if $|\psi\rangle_{AB} \neq |\psi\rangle_A \otimes |\psi\rangle_B$. On the other hand if, $|\psi\rangle_{AB} = |\psi\rangle_A \otimes |\psi\rangle_B$, then subsystems are said to be not entangled. Quantum entanglement between two subsystems is quantified in interms of the von-Neumann entropy. The desnity matrix associated with the composite system canbe written as $\rho_{AB} = |\psi_{AB}\rangle \otimes \langle\psi_{AB}|$. The reduced density matrix can be defined as $\rho_{A/B} = Tr_{B/A}[\rho_{AB}]$. The von-Neumann entropy between two subsystems can be defined as [2]

$$S_{vN}(\rho_A) = -Tr[\rho_A \log(\rho_A)] = -\sum_i \lambda_i \ln(\lambda_i) \tag{1.8}$$

where λ_i is the ith eigenvalue of the density matrix. It can be easily shown that $S_{vN}(\rho_A) = S_{vN}(\rho_B)$. The von-Neumann entropy is always a positive quantity, this implies $S_{vN}(\rho_{A(B)}) \geq 0$. If the von-Neumann entropy between two subsystems vanishes, then the two subsystems are not entangled. This in turns means that, there is quantum correlation between two subsystems if $S_{vN}(\rho_{A(B)}) = 0$. It is to be noted that, as the von-Neumann entropy measures the quantum entanglement between two subsystems, in literature it is also termed as entanglement entropy. In the subsequent chapters

we mostly use this term. Now I have discussed some intersting properties of von-Neumann entropy. The von-Neumann entropy has the following properties.

1. von-Neumann entropy is a positive definite quantity, that is, $S_{vN}(\rho_{A(B)}) \geq 0$.

2. von-Neumann entropy is invariant under suitable class of unitary transformation. This implies following, if the reduced density matrix is transformed in the following way

$$\rho_A \longrightarrow \rho'_A = U\rho U^\dagger \tag{1.9}$$

   where U is an unitary operator, then the von-Neumann entropy obtained from the new reduced density matrix is same as that of computed from the old one. This implies $S_{vN}(\rho_A) = S_{vN}(\rho'_A)$. This reflects the fact that, if a state is initially pure then it will remain pure in the future and similarly a mixed state will remain mixed. This is a very important property which just reflects the unitarity of time evolution of a quantum system. It means we are able to know about the past of the system by just going backwards in time under the action of a unitary operator.

3. For a pure state with density matrix ρ at zero temperature the von Neumann entropy of a subsystem A is equal to the entropy of its complemment. This manifestly shows that the entanglement entropy is not an extensive quantity. This equality is violated at finite temperature.

4. For a bipartite system ρ_{AB}

$$|S_{vN}(\rho_A) - S_{vN}(\rho_B)| \leq S_{vN}(\rho_{AB}) \tag{1.10}$$

   This is known as the Araki-Lieb bound.

5. von-Neumann entropy obey the subadditivity. For a bipartitie state ρ_{AB}

$$S_{vN}(\rho_A) + S_{vN}(\rho_B) \leq S_{vN}(\rho_{AB}) \ . \tag{1.11}$$

6. For a tripartite state ρ_{ABC}, von-Neumann entropy obey strong subadditivity. That is

$$S_{vN}(\rho_{ABC}) + S_{vN}(\rho_B) \leq S_{vN}(\rho_{AB}) + S_{vN}(\rho_{BC}) \ . \tag{1.12}$$

1.1.2 Quantum mutual information

Keeping the above concept of von-Neumann entropy I now discuss another measure of correlation in the context of information theory, mutual information ($I(A:B)$). Let us consider a bipartite quantum systems AB, described by a density matrix ρ_{AB}. The quatum mutual information between two subsystem A and B is defined by following [2]

$$I(A:B) = S_{vN}(\rho_A) + S_{vN}(\rho_B) - S_{vN}(\rho_{AB}) \tag{1.13}$$

where $S_{vN}(\rho_i)$ represents the von-Neumann entropy computed from the density matrix ρ_i. The mutual information has some interesting properties which are listed below

1. The mutual information measures total correlation present in the system. It includes both the classical and quantum correlation.

2. It a positive definite quantity, $I(A:B) \geq 0$, due to the subadditivity property of von-Neumann entropy.

3. The mutual information between two subsystems vanishes when the density matrix of the composite system can be written as direct product of density matrices of indivisual subsystems. This implies if $\rho_{AB} = \rho_A \otimes \rho_B$, $I(A:B) = 0$.

4. Mutual information is bounded by the smaller entropy of the two subsystems, this implies

$$I(A:B) \leq \min(S_{vN}(\rho_A), S_{vN}(\rho_B)) \ . \tag{1.14}$$

5. For a pure bipartite state $|\psi_{AB}\rangle$, the mutual information is maximal, reflecting the perfect correlations due to entanglement.

6. For a tripartite system A,B, C, one can show that the mutual information obey

$$I(A:B\cup C) \geq I(A:B) \ . \tag{1.15}$$

   The above property is named as the subadditivity.

7. Mutual information satisfies a monogamy-like relation in multipartite systems. For a tripartite system A,B, C the following inequality holds

$$I(A:B\cup C) \geq I(A:B) + I(B:C) \ . \tag{1.16}$$

These are some very interesting properties of mutual information. This concept of mutual information plays a very important role in subsequesnt chapters in his thesis.

1.1.3 Entanglement of purification

As we have already mention that, the von-Neumann entropy is a suitable measure of quantum correlation when the system under consideration is in the pure state. However, if the system is in a mixed state then, the von-Neumann entropy is not a suitable candidate which can measure the qunatum correlation present in the system. On the other hand the mutual information measures the total correlation present in the system. It includes both the classical and quantum correlation. Furthermore it is also to be noted that, mutual information is nothing but a particular algebric combination of von-Neumann entropy. This suggests the need for a distinct measure that can effectively quantify quantum correlation in a system, particularly when the system is in the mixed state.

Various studies in this direction have proposed several distinct measures to quantify quantum correlations in mixed states. Among these the entanglement of purification (EoP) [3] is one of the most promising candidate. The process of purification suggests that one has to construct a pure state $|\psi\rangle$ from the mixed density matrix ρ_{AB} by adding auxiliary degrees of freedom to the original Hilbert space $\mathcal{H}$

$$\rho_{AB} = tr_{A'B'} |\psi\rangle \langle\psi| \,;\ \psi \in \mathcal{H}_{AA'BB'} = \mathcal{H}_{AA'} \otimes \mathcal{H}_{BB'} \tag{1.17}$$

The states $|\psi\rangle$ are denoted as the purifications of ρ_{AB}. In this set up, the EoP can be computed as [3]

$$E_P(\rho_{AB}) \equiv E_P(A,B) = \min_{|\psi\rangle} S(\rho_{AA'});\ \rho_{AA'} = tr_{BB'} |\psi\rangle \langle\psi| \tag{1.18}$$

where the minimization is taken over any state $|\psi\rangle$ with the property $\rho_{AB} = tr_{A'B'} |\psi\rangle \langle\psi|$ being held constant. However, in the context of the QFT, it is a tricky task to compute the EoP. It has been observed that both $E_P(A,B)$ satisfies the following properties [4]

1. For pure state the entanglement of purification obey

$$E_P(A,B) = S_{EE}(A) = S_{EE}(B);\ \rho_{AB}^2 == \rho_{AB}\ . \tag{1.19}$$

2. For bipartite system $E_P(A,B)$ and the mutual information ($I(A:B)$) obey the following inequality

$$\frac{1}{2}I(A:B) \leq E_P(A,B) \leq min\left[S_{EE}(A), S_{EE}(B)\right] \tag{1.20}$$

3. The entanglement of purification decreases upon discarding of quantum system, this implies

$$E_P(A:BC) \geq E_P(A:B)\ . \tag{1.21}$$

4. For a tripartite system we have

$$\frac{I(A:B)+I(A:C)}{2} \leq E_P(A,BC)\ \ . \tag{1.22}$$

5. The entanglement of purification is polygamous for a tripartite pure state ρ_{ABC},

$$E_P(A:B)+E_P(A:C) \geq E_P(A:BC)\ . \tag{1.23}$$

1.1.4 Entanglement negativity

In this section we wolud like to discuss another measure of mixed state quantum correlation which is known as entanglement negativity. In order to define the entanglement negativity (EN), let us consider a tripartite quantum mechanical system with the subsystems denoted as A_1, A_2 and B. These subsystems are such that, they also obey the following condition, $A = A_1 \cup A_2$ and $B = A^c$ [5]. Now the Hilbert space associated with the subsystem A can be written as $\mathcal{H} = \mathcal{H}_1 \otimes \mathcal{H}_2$, where $\mathcal{H}_1$ represents the Hilbert space of the subsystem A_1 and $\mathcal{H}_2$ denotes the Hilbert space associated with the subsystem A_2. One can obtain the reduced density matrix of the subsystem A by computing the trace of full density matrix of the system with respect to its complement, that is, $A^c = B$. This results

$$\rho_A = \mathrm{tr}_{A^c}(\rho_{AB}) \tag{1.24}$$

where ρ_{AB} denotes the total (mixed) density matrix of the system. Now, according to the definition of EN, we have to take the partial transpose of the above computed reduced density matrix over one of the subsystems in the given bipartite system. One can do this by the following procedure. Let us assume that, $|e_i^{(1)}\rangle$ and $|e_i^{(2)}\rangle$ represent the basis of the Hilbert space associated with the

subsystems A_1 and A_2 respectively. The partial transpose of the reduced density matrix with respect to A_2 can be written as

$$\left\langle e_i^{(1)} e_j^{(2)} \right| \rho_A^{T_2} \left| e_k^{(1)} e_l^{(2)} \right\rangle = \left\langle e_i^{(1)} e_l^{(2)} \right| \rho_A \left| e_k^{(1)} e_j^{(2)} \right\rangle \tag{1.25}$$

where $\rho_A^{T_2}$ denotes the partial transpose of the total density matrix ρ with respect to A^c. EN measures the degree to which $\rho_A^{T_2}$ is negative, which signifies the term 'negativity'. The trace norm of the partial transposed reduced density matrix is represented by $\| \rho_A^{T_2} \|_1$. In this set up, it has been shown that one can actually define two quantities, one is negativity and another one is the entanglement negativity or logarithmic negativity. The negativity between two subsystems A_1 and A_2 is defined as [6]

$$\mathcal{N}(\rho) = \frac{\| \rho_A^{T_2} \|_1 - 1}{2} \ . \tag{1.26}$$

The above corresponds to the absolute value of the sum of negative eigenvalues of $\rho_A^{T_2}$. One can show that for a unentangled product state, $\mathcal{N}(\rho)$ vanishes. On the other hand, entanglement negativity or logarithmic negativity between two subsystems A_1 and A_2 is defined as [6]

$$E_N(\rho) = \ln\left(\| \rho_A^{T_2} \|_1 \right) \ . \tag{1.27}$$

Apart from EoP and entanglement negativity, there are other quantities such as odd entropy [7, 8], reflected entropy [9, 10, 11, 12] which are also proposed measures of quantum correlation for a system in mixed state.

Some important properties of entanglement negativity are listed below

1. Both the negativity and logarithmic negativity are positive definite. This implies

$$\mathcal{N}(\rho) \geq 0 \ \ ; \ \ E_N(\rho) \geq 0 \tag{1.28}$$

   the equality holds for separable states, meaning there is no quantum entanglement.

2. Both the $\mathcal{N}(\rho), E_N(\rho)$ are non-increasing under local operations and classical communication.

3. $E_N(\rho)$ is additive, meaning that for a tensor product state $\rho_{AB} \otimes \sigma_{CD}$

$$E_N(\rho_{AB} \otimes \sigma_{CD}) = E_N(\rho_{AB}) + E_N(\sigma_{CD}) \ . \tag{1.29}$$

   On the other hand, negativity ($\mathcal{N}(\rho)$) is not additive

1.1.5 Complexity

Along with the above measures of quantum correlation, quantum complexity is one of the most fundamental quantity in context of quantum information theory. The computational complexity has its roots in the subject of computer science [13, 14]. In classical computation, an algorithm simply means a function which maps set of input bits to specific set of output bits. However, we are interested in quantum complexity. Here the function transform to the unitary operator $\hat{U}$ which acts on some input state for some number of qubits and gives an output quantum state on equal number of qubits. The unitary operation is constructed by set of elementary gates. If our reference state is $|\psi_R\rangle$ and the target state is $|\psi_T\rangle$, then one has to implement the following operation

$$|\psi_T\rangle = \hat{U}\,|\psi_R\rangle \tag{1.30}$$

where $\hat{U}$ is an unitary operator which has been constructed with help of a set of elementary gates. Thus one can write the unitary operation as

$$\hat{U} = g_1 g_2 ... g_n \tag{1.31}$$

g_i denotes the elementary quantum gates. This in turn means that in order to reach the target state from the reference state one needs to implement the following operation in terms of the elementary gates

$$|\psi_T\rangle = \hat{U}\,|\psi_R\rangle = g_n g_{n-1} ... g_1\,|\psi_R\rangle \ . \tag{1.32}$$

Now the circuit complexity of the target state, $\mathcal{C}(|\psi_T\rangle)$ is defined as the minimum number of the gates which are needed to construct the unitary operation. This is the way by following which one can define the complexity in the state space. There are various different ways to compute the quantum complexity [15, 16, 17, 18]. Now the complexity of the target state $|\psi_T\rangle$, that is $\mathcal{C}(|\psi_T\rangle)$ is defined [19] as the minimum numbers of quantum elementary gates required to implement the quantum circuit. Now one can construct infinitely many possible circuits to get the correct target state. But we have chosen that one circuit which contains a minimum number of quantum gates, that is the optimal circuit. But it is very much difficult to find that one optimal circuit. This definition of complexity holds if we are in the wave function space.

We define complexity in the space of the unitary operators also. Suppose we start from a reference

operator U and we have to reach the target operator V then the relative complexity $\mathcal{C}_R(U,V)$ is defined as the minimum number of elementary gates required to reach the target unitary operator V. The relative complexity of a unitary operator with respect to the identity operator is known as the complexity of that operator. So the complexity of a unitary operator U can be written as [17, 20, 21]

$$\mathcal{C}(U) = \mathcal{C}_R(I,U) \ . \tag{1.33}$$

So we can see that in both cases it is very much difficult to identify that optimal circuit. This problem was first solved by Neilson. He came up with a very interesting solution to this problem. According to this approach, the problem of finding the optimal circuit is mapped to the problem of finding the minimal geodesic between the two states, and circuit complexity is given by the length of that minimal path. Here instead of considering the discrete elementary gates which form the unitary operator U, we will introduce a continuous representation of the unitary operator U in the following way [19, 22, 23]

$$U(\tau) = \overleftarrow{\mathcal{P}} exp\left(-i\int_0^\tau d\tilde{\tau} H(\tilde{\tau})\right) \tag{1.34}$$

where τ parametrizes a path in the Hilbert space. We usually choose τ to be in the range, $0 \leq \tau \leq 1$, $\tau = 0$ represents the reference state, and $\tau = 1$ represents the target state. $\overleftarrow{\mathcal{P}}$ represents the time ordering such that the circuit is built from right to left as τ increases. The operator $H(\tilde{\tau})$ can be expanded in terms of a basis of Hermitian operators (M_I) in the following way

$$H(\tilde{\tau}) = \sum_I Y^I(\tilde{\tau}) M_I \ \ . \tag{1.35}$$

Y_I in the above equation is known as the control functions indicating which gates are being applied at a particular value of the parameter τ. Thus we can think the elementary gates g_I can be constructed in the following way

$$g_I = exp(\epsilon M_I) \tag{1.36}$$

thus M_I can be thought of as the generator of the elementary gate g_I and ϵ is very small number. The control function can be obtained in the following way

$$Y_I = Tr(U\partial_\tau U(M^I)^T) \tag{1.37}$$

where $tr(M^I(M^J)^T) = \delta^{IJ}$. Then we can define the metric in the following way

$$ds^2 = G_{IJ}dY^I dY^{*J} \tag{1.38}$$

from the above metric, one can calculate geodesic with proper boundary conditions. After obtaining the geodesic we can compute its length which gives the complexity of a target state,

$$\mathcal{C}(|\psi_T\rangle) = \int_0^1 ds \quad . \tag{1.39}$$

On the other hand, we can also use the covariance matrix approach to compute the complexity of a target state. In this approach, we have to first compute the covariance matrices associated with both the reference state and the target state in the following way [24, 25, 26, 27, 28, 29, 30]

$$G^{ab}_{T/R} = \left\langle \psi_{T/R}(x,t) \right| \left(\xi^a \xi^b + \xi^b \xi^a\right) \left| \psi_{T/R}(x,t) \right\rangle \tag{1.40}$$

where T and R represent the target and the reference state and $\xi = \{x, p\}$. The covariance matrix is a real symmetric matrix with a unit determinant. Now we can always transform the reference covariance matrix in the following way

$$\tilde{G}^{\tau=0} = SG^{\tau=0}S^T \tag{1.41}$$

such that $\tilde{G}^{\tau=0}$ is identity matrix and S is a real symmetric matrix. We can also transform the target covariance matrix in a similar way

$$\tilde{G}^{\tau=1} = SG^{\tau=1}S^T \ . \tag{1.42}$$

The unitary operator U acts on the transformed covariance matrices in the following way

$$G^{\tilde{\tau}=1} = U(\tau)G^{\tilde{\tau}=0}U^T(\tau) \tag{1.43}$$

Then we can define a function $\mathcal{F}(U, \dot{U})$, which is known as the cost function. Then the complexity of the unitary operator U is defined as

$$\mathcal{C}(U) = \int_0^1 \mathcal{F}(U, \dot{U}) d\tau \quad . \tag{1.44}$$

Minimizing this cost function gives us the optimal set of Y^I, which in turn gives us the most efficient circuit by minimizing the circuit depth. There are various choices for the cost function.

Some choices of cost functions read [26, 31]

$$\begin{aligned}\mathcal{F}_1(U,Y) &= \sum_I \left|Y^I\right| \; ; \; \mathcal{F}_2(U,Y) = \sqrt{\sum_I (Y^I)^2} \\ \mathcal{F}_k(U,Y) &= \sum_I \left|Y^I\right|^k \; . \end{aligned} \tag{1.45}$$

The $\mathcal{F}_1$ measure can be recognized as the original concept of counting the number of gates. The $\mathcal{F}_2$ measure can be recognized as the proper distance in geometry and this choice reduces the problem of identifying the optimal circuit to finding the shortest geodesic connecting the reference and target states in this geometry. The third one, that is $\mathcal{F}_k(U,Y)$ can be thought of as a generalization of the $\mathcal{F}_1$ cost function.

Quantum complexity is not only important in the context of quantum computation or in quantum information. But for a mixed state, the computation of the complexity is a bit tricky. Various research in this direction shows that purification complexity is a quantity that can be used to compute the complexity of the mixed state. The purification complexity is defined as the minimal pure state complexity among all possible purifications available for a mixed state, subject to the constraint that every additional qubit of the purifying system ends up entangled with the original "physical" qubits,

$$C^P(\rho) = \min_{\psi \in \mathcal{P}} \mathcal{C}(\psi) \tag{1.46}$$

where $\mathcal{P}$ is the set of all purifications ψ of the mixed state density matrix ρ. In this context, mutual complexity plays an important role. If we have two subsystems A and B, then mutual complexity between two systems is defined as [32, 33, 34, 35, 36, 37, 38]

$$\Delta\mathcal{C} = \mathcal{C}(\rho_A) + \mathcal{C}(\rho_B) - \mathcal{C}(\rho_{AB}) \tag{1.47}$$

where ρ_i represents the density matrix corresponding to the i-th system. Mutual complexity is said to be subadditive if $\Delta\mathcal{C} > 0$ and superadditive if $\Delta\mathcal{C} < 0$. Apart from the quantum information theory complexity plays an important role in the theory of quantum chaos. In a quantum system, one can quantized chaos in terms of the complexity [25, 39, 40, 41, 42, 43, 44]. Quantum complexity is also a probe of quantum quench [45].

1.2 Entanglement entropy in the context of quantum field theory

In this section I would like to provide a brief review on the computation of entanglement entropy in the context of quantum field theory. To proceed we will first consider discrete lattice model with lattice spacing ϵ. We will assume that each lattice site has a finite dimensional Hilbert space, $\mathcal{H}_i$, i indicates the lattice site. Then, a pure quantum state of the system $|\psi\rangle \in \otimes_i \mathcal{H}_i$. Now I will briefly discuss how a subset of lattice degrees of freedom is entangled with the rest of the lattice for a given pure state of the total system. To do so we will devide the lattice sites into two regions by fiducial boundary across the lattice. Now we can label the region inside the boundary as $\mathcal{A}$ and the rest of the lattice is denoted as $\mathcal{A}^c$ and the artificial boundary separating these two regions, $\partial\mathcal{A}$ is the entangling surface. Therefore the Hilbet space of the toatl system can be as the following tensor product

$$\otimes_i \mathcal{H}_i \equiv \mathcal{H}_{\mathcal{A}} \otimes \mathcal{H}_{\mathcal{A}^c} \ . \tag{1.48}$$

Keeping this bipartition of the Hilbert space in mind we can define the density matrix of the full system as

$$\rho_{total} = |\psi\rangle \langle\psi| \ . \tag{1.49}$$

Now the reduced density matrix of the region $\mathcal{A}$ is formalised as

$$\rho_A = \mathrm{Tr}_{\mathcal{A}^c}(\rho_{total}) = \mathrm{Tr}_{\mathcal{A}^c}\Big(|\psi\rangle \langle\psi| \Big) \ . \tag{1.50}$$

Therefore the von-Neumann entropy of the reduced density matrix can be defined as

$$S_{\mathcal{A}} = -\mathrm{Tr}(\rho_{\mathcal{A}} \log \rho_{\mathcal{A}}) = -\sum_i \lambda_i \log \lambda_i \ . \tag{1.51}$$

We would like to mention that the above defination of the von-Neumann entropy in the discrete quantum field theory is very formal. Before proceeding to the continumm QFT I will discuss some other kinds of entropy which is useful to compute the von-Neumann entropy in the context of QFT. I will start with Renyi entropy. The Renyi entropy of order q, (where $q \in \mathbb{Z}_+$) is defined as

$$S^{(q)}_{\mathcal{A}} = \frac{1}{1-q} \log \mathrm{Tr}_{\mathcal{A}}\big(\rho^q_{\mathcal{A}}\big) = \frac{1}{1-q} \log\left(\sum_i \lambda_i^q \right) \ . \tag{1.52}$$

The above definition of Renyi entropy suggests that it captures the moments of the reduced density matrix. It is very useful to probe the purity of the system. Now in the limit $q \to 1$ one can obtained the von-Neumann entropy form the Renyi entropy. Therefore,

$$S_{\mathcal{A}} = \lim_{q \to 1} S_{\mathcal{A}}^{(q)} \ . \tag{1.53}$$

Now we will proceed to the continuum scenario, that is, we will consider the lattice spacing to be zero ($\epsilon \to 0$). In the continuum case, the concept of the bipartition can be generalised geometrically. to define the bipartition in the continuum case, we have to consider a Cauchy slice (Σ). On this Cauchy slice we would consider a codimension-1 region A and it's complement region $A^c = B$, such that, $A \cup A^c(B) = \Sigma$. Therefore the total Hilbert space to full system can be represented as $\mathcal{H}_\Sigma = \mathcal{H}_A \otimes \mathcal{H}_{A^c}$. We can define the entangling surface as the boundary of the region A, that is ∂A. Now the entanglement entropy for this bipartition can be computed by following the usual way to compute the von-Neumann entropy. This entropy depends of the geometry of the entangling surface, therefore it is also known as the geometric entanglement entropy. Now we would like to make some comments.To compute the von-Neumann entropy of the region A, first we have to obtain the reduced density matrix associated with the region A. This can be obtained by tracing out the full density matrix with respect to the degrees of freedom associated to the region A^c. However, this bipartition of Hilbert space is not well known. One can avoid this issue by using the replica trick. In this technique, instead of computing the von-Neumann entropy of subsystem directly one can compute the Renyi entropy, then taking the approriate limit one can obtain the von-Neumann of concerened subsystem.

The replica technique suggests one should compute $\mathrm{Tr}(\rho_A^n)$, instead of computing $\mathrm{Tr}(\rho_A \log \rho_A)$ directly. Thus the EE of a subsystem is given by

$$S_{EE}(A) = -\lim_{n \to 1} \frac{\partial}{\partial n} (\mathrm{Tr}(\rho_A^n)) \ . \tag{1.54}$$

Furthermore computing $\mathrm{Tr}(\rho_A^n)$ for generic real value of n is extremely difficult job. Therefore in this replica trick we compute $\mathrm{Tr}(\rho_A^n)$ for positive integer n, then we analytically continued it for generic value of n. Computation of $\mathrm{Tr}(\rho_A^n)$ reduces to calculating partition function on some complicated Riemann surface, which can be achived analytically for generic quantum field theory. The quantity $\mathrm{Tr}(\rho_A^n)$ can be computed by considering $n(n > 0, n \in \mathbb{Z}_+)$copies of theory and glue

them by imposing appropreiate boundary condition along the cuts. Thus computation of $\mathrm{Tr}(\rho_A^n)$ reduces to the following

$$\mathrm{Tr}(\rho_A^n) = \frac{Z_n(A)}{Z^n} \tag{1.55}$$

where $Z_n(A)$ indicates the partition function on the complicated n sheeted Riemann surface and Z represents the usual partition function. Keeping the result given in eq.(1.55), one can compute the Reyni entropy of order n by following

$$S_A^{(n)} = \frac{1}{1-n} \log\left(\frac{Z_n(A)}{Z^n(A)}\right) . \tag{1.56}$$

Now one can get the EE by taking the limit $n \to 1$, that is

$$S_{EE}(A) = \lim_{n\to 1} S_A^{(n)} . \tag{1.57}$$

It can be shown that both the formulas given in eq.(1.54) and eq.(1.57) are equivalent. Readers are reffered to [46, 47, 48, 49, 50] for further detials.

It was shown earlier that, the EE of a subsystem in this context is UV divergent. It is quite obvious because we do not introduce any cutoff to prevent the short distance correlation. One can regularised this EE by incorporating a UV cutoff in the theory. To avoid this divergence one can introduce a UV cutoff ϵ. Therefore after incorporating this one would have the following resuslt of EE (in d-dimensional QFT)

$$S_{EE}(A) = \alpha \frac{\mathrm{Area}(\partial A)}{\epsilon^{d-2}} + \text{subleading terms...} . \tag{1.58}$$

In the above result α is a constant represents the effective degrees of freedom of the geometric region A. The above result is very general and it is reffered to as the "*area law*" of entanglement [51, 48, 52, 53, 54]. One can show that the subleading terms in the above result of EE depends on the extrinsic and intrinsic geometry of the entangling surface. The above result shows that, it EE of in a generic QFT has a similarity with the Bekenstein-Hawking formula for black hole entropy. The Bekenstein-Hawking formula for black hole entrop is given by

$$S_{BH} = \frac{\mathrm{A_H}}{4G} \tag{1.59}$$

where A_H is the area of the event horizon, and G is the Newton's gravitational constant. Both of these entropies are extensive. Both the formulas suggest that, the information inside a volume V

is encoded on its boundary. The UV structure of the EE in relativistic QFT reads [55]

$$S_{EE}(A) = \begin{cases} a_{d-2}\left(\frac{L}{\epsilon}\right)^{d-2} + a_{d-4}\left(\frac{L}{\epsilon}\right)^{d-4} + ... + a_1\left(\frac{L}{\epsilon}\right) + (-1)^{\frac{d-1}{2}}\mathcal{S}_A + \mathcal{O}(\epsilon) & \text{for} d \text{ odd} \\ a_{d-2}\left(\frac{L}{\epsilon}\right)^{d-2} + a_{d-4}\left(\frac{L}{\epsilon}\right)^{d-4} + ... + (-1)^{\frac{d-1}{2}}\mathcal{S}_A \log\left(\frac{L}{\epsilon}\right) + \mathcal{O}(\epsilon^0) & \text{for} d \text{ even} \end{cases} \tag{1.60}$$

where L represents the size of the subsystem A. We would like to mention that the coefficients a_i's in the above equation does not have any physcial importance because they depends on the which scheme we follow to derive the entanglement entropy. On the other hand, one should emphasise on $\mathcal{S}_A$ contains non-trivial physical information.

1.3 Introduction to Gauge/Gravity duality

In this section we will discuss the gauge/gravity duality in detials. This duality relates two completely different theories. On one side of the duality, we have a quantum field theory, while on the other side, we have a classical theory of gravity. This duality emerges from the string theory. In the subsequent section we have briefly discuss conformal field theory, Anti de-Sitter spacetime, string theory, theory of D-branes and gauge theory. Finally, we end our discussion by reviewing the central idea of gauge/gravity duality (or AdS/CFT correspondence).

1.3.1 Brief introduction to conformal field theory (CFT)

Quantum field theory is one of the most fundamental theory of modern theoretical ohysics. It describes three fundamental interactions of nature namely, weak, strong and electromagnetic interaction successfully. QFT is also relevant in the context of condensed matter systems, where we deal with many body system and the quantized excitations are not necessarily elementary particles but so called quasiparticles. Quantum field theory works very well when the it is weakly coupled. However, when a set of weakly coupled degrees of freedom cannot be identified, the theory loses most of its predictivity. A relativistic QFT in d spacetime dimensions is invariant under the Poincaré transformation. The isometry group of QFT in d spacetime dimensions is ISO$(d-1,1)$. Conformal field theory is a very special class of quantum field theory, which is invariant under conformal transformation. Conformal transformations are very special class of coordinate transformation, under which the angle between two lines remain same. Conformal transformations

include Poincaré transformation along with the scale tranformation and special conformal transformation.

In d spacetime dimensions a conformal tranformation is defined as the set of coordinate tranformation under which the spacetime metric remains same upto a scale factor. That means if $x \to x'$, the spacetime metric $g_{\alpha\beta}(x)$ is transformed as

$$x \to x' \quad : \quad g_{\alpha\beta}(x) \to g_{\alpha\beta}(x')' = \Omega^2(x) g_{\alpha\beta}(x) \ . \tag{1.61}$$

The above equation suggests that, if $\Omega^2(x) = 1$ we can recover the Poincare transformation which leavs the Minkowski spacetime invariant. Now we would explore which kind of coordinate tranformations leave the spacetime metric invariant upto a conformal factor. To investigate that let us a general infinitisimal coordinate transformation of the following form

$$x^\mu \to x'^\mu = x^\mu + \epsilon(x^\mu) \ . \tag{1.62}$$

Due to this coordinate tranformation the change in the spacetime metric is given by

$$\delta g_{\mu\nu} = \partial_\mu \epsilon_\nu + \partial_\nu \epsilon_\mu \ . \tag{1.63}$$

Now we demand that, the change in the spacetime metric is proportional to the original metric, this results the following differential equation for ϵ

$$\begin{aligned} \partial_\mu \epsilon_\nu + \partial_\nu \epsilon_\mu &= \frac{2}{d} g_{\mu\nu}(x) \partial^\rho \epsilon_\rho \\ \Rightarrow (g_{\mu\nu}\partial_\rho \partial^\rho + (d-2)\partial_\mu \partial_\nu)\partial^\sigma \epsilon_\sigma &= 0 \ . \end{aligned} \tag{1.64}$$

The above equation suggests that, there is something very interesting when we consider $d = 2$. In this case the above equation boils down to the Cauchy-Riemann equations. We will discuss the $2d$-CFT later in this thesis. Now we will consider $d > 2$. The most general form of the infinitisimal transformation can be written as

$$\epsilon_\mu = a_\mu + \omega_{\mu\nu} x^\nu + \lambda x_\mu + b_\mu x^2 - 2(b.x) x_\mu \ . \tag{1.65}$$

The first two terms in the expression corresponds to translations and Lorentz transformations. This corresponds to the Poincare transformation. Now let us look at the following coordinate transformation

$$x^\mu \to x'^\mu = \alpha x^\mu \ . \tag{1.66}$$

The above transformation is known as the scale transformation. Under this scale transformation a scalar is transformed as

$$\phi(x) \to \phi'(x) = \phi(x - \lambda x) = \phi(x) - \lambda x^\mu \partial_\mu \phi(x) \tag{1.67}$$

Now let us consider the following infinitisimal coordinate transformation

$$x^\mu \to x^\mu + b^\mu x^2 - 2(b.x)x^\mu \ . \tag{1.68}$$

The above coordinate transformation is known as the special coordinate transformation (SCT). Under SCT a scalar is transformed as follows

$$\phi(x) \to \phi'(x) = \phi(x + bx^2 - 2(b.x)x) = \phi(x) - b^\mu(x^2\partial_\mu - x_\mu x^\nu \partial_\nu)\phi(x) \ . \tag{1.69}$$

Therefore conformal transformation includes the scale tranformation and special conformal tranformation along with the Poincare tranformation. For the completeness I have listed all the conformal transformation. To do so let us consider a CFT in $\mathbb{R}^d$ $(d > 2)$, with the flat spacetime metric $\eta_{\alpha\beta}$ with signature (p, q). The infinitisimal conformal transformations can be defined as

$$\begin{aligned}
\text{Translations} &: x'^\mu \to x^\mu + a^\mu \\
\text{Rotations} &: x'^\mu \to (\delta^\mu_\nu + m^\mu_\nu)\, x^\nu \\
\text{Scale transformations} &: x'^\mu \to \lambda x^\mu \\
\text{Special conformal transformations} &: x'^\mu \to x^\mu + 2\,(k.x)\, x^\mu + \left(x^2\right) k^\mu \ .
\end{aligned}$$

The generators of the above infinitisimal conformal transformation are given by

$$\begin{aligned}
\text{Generators of translations} &: \mathcal{P}_\mu = -i\partial_\mu \\
\text{Generators of rotations} &: \mathcal{L}_{\mu\nu} = i(x_\mu\partial_\nu - x_\nu\partial_\mu) \\
\text{Generators of scale transformations} &: \mathcal{D} = -ix^\mu\partial_\mu \\
\text{Generators of SCT} &: \mathcal{K}_\mu = -i(2x_\mu x^\nu\partial_\nu - x^2\partial_\mu) \ .
\end{aligned}$$

The algebra of the conformal generators are given as

$$\begin{aligned}
&[\mathcal{D}, \mathcal{P}_\mu] = i\mathcal{P}_\mu,\ [\mathcal{D}, \mathcal{K}_\mu] = -i\mathcal{K}_\mu,\ [\mathcal{K}_\mu, \mathcal{P}_\nu] = 2i\,(\eta_{\mu\nu}\mathcal{D} - \mathcal{L}_{\mu\nu}) \\
&[\mathcal{K}_\rho, \mathcal{L}_{\mu\nu}] = i\,(\eta_{\rho\mu}\mathcal{K}_\nu - \eta_{\rho\nu}\mathcal{K}_\mu)\,,\ [\mathcal{P}_\rho, \mathcal{L}_{\mu\nu}] = i\,(\eta_{\rho\mu}\mathcal{P}_\nu - \eta_{\rho\nu}\mathcal{P}_\mu) \\
&[\mathcal{L}_{\mu\nu}, \mathcal{L}_{\rho\sigma}] = i\,(\eta_{\nu\rho}\mathcal{L}_{\mu\sigma} + \eta_{\mu\sigma}\mathcal{L}_{\nu\rho} - \eta_{\mu\rho}\mathcal{L}_{\nu\sigma} - \eta_{\nu\sigma}\mathcal{L}_{\mu\rho}) \ .
\end{aligned} \tag{1.70}$$

The rest of the commutator between the generators vanishes. This generators form a group, known as the conformal group. The above algebra suggests that Poincare group is subgroup of conformal group. Now let us count the number of generators in d dimension. In d spacetime dimensions there are d number of translations, $\frac{d(d-1)}{2}$ number of rotations, 1 scale transformation and d SCTs. This implies in d spacetime dimension there are total $\frac{(d+2)(d+1)}{2}$ number of generators, which is the same number of generators of $SO(2,d)$ group. However, one can combine these generators in the following way

$$\begin{aligned}
\bar{\mathcal{L}}_{\mu\nu} &= \mathcal{L}_{\mu\nu} \\
\bar{\mathcal{L}}_{\mu d} &= \frac{1}{2}(\mathcal{K}_\mu - \mathcal{P}_\mu) \\
\bar{\mathcal{L}}_{\mu d+1} &= \frac{1}{2}(\mathcal{K}_\mu + \mathcal{P}_\mu) \\
\bar{\mathcal{L}}_{(d+1)d} &= \mathcal{D}
\end{aligned} \tag{1.71}$$

from this above representations of the conformal generators, it can be observed that, these are nothing but the generators of Lie grouo $SO(d,2)$, obeying the following algebra

$$[\bar{\mathcal{L}}_{AB}, \bar{\mathcal{L}}_{CD}] = i(\eta_{BC}\bar{\mathcal{L}}_{AD} - \eta_{AC}\bar{\mathcal{L}}_{BD} - \eta_{BD}\bar{\mathcal{L}}_{AC} + \eta_{AD}\bar{\mathcal{L}}_{BC}) \ . \tag{1.72}$$

This group leaves the metric $\eta_{AB} = diag(- + ... + -)$ invariant, where $\mu.\nu = 0, 1, ...(d-1)$ and $A, B = 0, 1..., (d+1)$.

Now we will briefly discuss about the representation of the conformal group $SO(d,2)$ in $\mathbb{R}^{1,d-1}$. To construct the representation of $SO(d,2)$ we decompose it as $SO(d-1,1) \times SO(1,1)$. The first factor represents the Lorentz group and the second one represents dilation ($\mathcal{D}$). $\mathcal{D}$ has eigenvalues $-i\Delta$, the fields or operators are transformed as

$$\phi(x) \to \lambda^{\Delta}\phi(\lambda x) \ . \tag{1.73}$$

The operator $\mathcal{P}_\mu$, raises the eigen value of $\mathcal{D}$. On the other hand $\mathcal{K}_\mu$ lower it. It is known that for an unitary field theory, there is a lower bound on the fields, which is known as the unitary bound. Therefore the unitary representation is "lowest weight representation".

In $d = 2$ spacetime dimensions one can observe that there are infinite number of conformal generators. This can be shown by using eq.(1.64). In two dimension the generators of conformal group

obey the Witt algebra, given as follows

$$\begin{aligned}
[l_m, l_n] &= (m-n)l_{m+n} \\
[\bar{l}_m, \bar{l}_n] &= (m-n)\bar{l}_{m+n} \\
[l_m, \bar{l}_n] &= 0 \ .
\end{aligned} \tag{1.74}$$

The generators of the 2-dimensional confromal transformation is given by

$$l_n = -z^{n+1}\partial_z \ \ ; \ \ \bar{l}_n = -\bar{z}^{n+1}\partial_{\bar{z}} \tag{1.75}$$

where z and $\bar{z}$ are considered as independent variables. One can construct any kind of conformal transfomations with these generatores. For example, l_{-1} generates translation, $(l_0 + \bar{l}_0)$ generates 2 dimensional scale transformation, the operator $i(l_0 - \bar{l}_0)$ gives rise to the rotation and finaly l_{-1} generates special conformal transformations. This above discussion implies that, the operators $\{l_{-1}, l_0, l_{+1}\}$ are the global conformal generator in two dimensions. They form a group structure given by $SL(2,\mathbb{C})/\mathbb{Z}_2$ group. Therefore $\{l_{-1}, l_0, l_{+1}\}$ generates the following coordinate transformation

$$z \to \frac{az+b}{cz+d} \ \ ; \ \ \text{with} \ \ a, b, c, d \in \mathbb{C} \ . \tag{1.76}$$

For the transformatoins to be invertible we would have the condition $ad - bc \neq 0$. Furthermore, the Witt algebra admits a central extension. The central extension of an algebra $\tilde{g} = g \oplus \mathbb{C}$ of a algebra g by $\mathbb{C}$ is

$$\begin{aligned}
[\tilde{x}, \tilde{y}]_{\tilde{g}} &= [x, y]_g + c\ p(x, y), \\
[\tilde{x}, c]_{\tilde{g}} &= 0 \ \ ; \ \ [\tilde{y}, c]_{\tilde{g}} = 0
\end{aligned} \tag{1.77}$$

where, $\tilde{x}, \tilde{y} \in \tilde{g}$, $x, y \in g$ and $c \in \mathbb{C}$. The central extension of algebra is related to the projective rpresentation. Let us label the central extension of Witt algebra by L_n, $n \in \mathbb{Z}$ and the commutation relation is give by

$$[L_n, L_m] = (m-n)L_{m+n} + cp(m, n) \ . \tag{1.78}$$

One can also do the similar analysis with the generators $\bar{l}_n \leftrightarrow \bar{L}_n$. One can obtain $p(m, n)$ by following [56]. Incase of the two dimensional CFT the central extension of Witt algebra is given

by

$$
\begin{aligned}
[L_m, L_n] &= (m-n)L_{m+n} + \frac{c}{12}(m^3 - m)\delta_{m+n,0} \\
[\bar{L}_m, \bar{L}_n] &= (m-n)\bar{L}_{m+n} + \frac{c}{12}(m^3 - m)\delta_{m+n,0} \\
[L_m, \bar{L}_n] &= 0
\end{aligned} \tag{1.79}
$$

where c represents the central charge of the two dimensional CFT.

Now we will discuss the energy momentum tensor of CFTs [56]. To do so let us recall the Neother's theorem. It states that for every continuous symmetry in field theory there is a conserved current, that is, $\partial_\mu j^\mu = 0$. In the present scenario we are interested in the theories with conformal symmetry, that is $x^\mu \to x^\mu + \epsilon^\mu$. Therefore in this case the conserve current can be written as

$$
j_\mu = T_{\mu\nu}\epsilon^\mu \tag{1.80}
$$

where $T_{\mu\nu}$ is the energy-momentum tensor, it is symmetric. Since the current is conserved, for a special case of $\epsilon^\mu = const$ we have

$$
\partial_\mu T^{\mu\nu} = 0 \ . \tag{1.81}
$$

On the other hand for general infinitisimal ϵ^μ we have [56]

$$
T^\mu_{\ \mu} = 0 \tag{1.82}
$$

Thus we can conclude the fact that the energy momentum tensor of CFTs are traceless.

Now we will discuss how one can obtain the correlation funtions in the context fof CFT from the symmetry arguments. The conformal symmetry plays a vital role to obtain the form of the correlators. For that let us consider two operators $\phi_1(x)$ and $\phi_1(x)$ with definite scaling dimension Δ_1 and Δ_2 respectively. We are now interested in computing the two point correlator of the form $\langle 0|\, \phi_1(x)\phi_1(x)\, |0\rangle$. Under the dilation the correlator transform as

$$
\langle 0|\, \phi_1(x)\phi_2(y)\, |0\rangle \to \lambda^{\Delta_1}\lambda^{\Delta_1} \langle 0|\, \phi_1(\lambda x)\phi_2(\lambda y)\, |0\rangle \ . \tag{1.83}
$$

Now using the fact that the correlator should have translational invariance, we can argue that, the correlation function depends only on the difference of two points. In other word the correlation function must be the function of the distance between two points. Another imporatnt fact is

that the correleator should be Lorentz invarinat. This implies, the correlation function must be a function of $(x-y)^2$. This implies

$$\langle 0|\, \phi_1(x)\phi_2(y)\, |0\rangle = f\Big((x-y)^2\Big)\ . \tag{1.84}$$

Now making a translation to the origin we have

$$\langle 0|\, \phi_1(x)\phi_2(0)\, |0\rangle = f(x^2)\ . \tag{1.85}$$

Now we will use the fact that, the vaccum stateare conformally invariant. This implies that the generators of the conformal algebra annahilates the vaccum state. Therefore we can use the algebra of the conformal generators to observer the restriction on the two point function

$$\begin{aligned} \langle 0|\, \phi_1(x)\phi_2(0)\mathcal{D}\, |0\rangle &= 0 \\ \Rightarrow \langle 0|\, \phi_1(x)[\phi_1(0), D]\, |0\rangle + \langle 0|\, \phi_1(x) D\phi_2(0)\, |0\rangle &= 0 \\ \Rightarrow i(\Delta_1 + \Delta_2 + x^\mu\partial_\mu) f(x^2) &= 0\ . \end{aligned} \tag{1.86}$$

The above differential equation has solutions of the following form

$$f(x^2) = \frac{C}{x^{\Delta_1+\Delta_2}} \tag{1.87}$$

where C is the integtarion constant. Therefor in a most general way the two point function can be written as

$$\langle 0|\, \phi_1(x)\phi_2(y)\, |0\rangle = \frac{C_{12}}{(x-y)^{\Delta_1+\Delta_2}}\ . \tag{1.88}$$

Similarly the three point function can be obtained as

$$\langle 0|\, \phi_1(x)\phi_2(y)\phi_3(z)\, |0\rangle = \frac{C_{123}}{(x-y)^{\Delta_1+\Delta_2-\Delta_3}(y-z)^{\Delta_2+\Delta_3-\Delta_1}(x-z)^{\Delta_1+\Delta_3-\Delta_2}}\ . \tag{1.89}$$

We would like to mention that upto a constant factor two point and three point functions can be obatine by using the conformal symmetry and conformal algebra. But the higher point functions cannot be obtained by this method.

1.3.2 Brief discussion on Anti-de-Sitter spacetime

Anti-de-Sitter spacetime is solution of Einstein filed equation in the presence of negative cosmological constant. It is a maximally symmetric spacetime. It can be defined in different ways. Before going into the details of the AdS spacetime let us understand what is meant by maximally symmetric spacetime. A spacetime of D dimensions is said to be maximally symmmetric if the spacetime has $\frac{D(D+1)}{2}$ number of Killing vector. That means, the spacetime has $\frac{D(D+1)}{2}$ number of symmetries. For example let us consider the flat Euclidean spacetime in D dimensions, $\mathbb{R}^D$. This spacetime has D number of translational symmetry in D possible directions, and $\frac{D(D-1)}{2}$ rotational symmetries. Thus, the D-dimensional flat Euclidean spacetime has total $\frac{D(D+1)}{2}$ symmetries. Therefore spacetimes this same number of symmetries are said to be maximally symmetric. Now if we want to find a maximally syemmetric curved spacetimes, the symmetry tells us that the curvature (R) of the spacetime should be constant. Therefore there are two possible choice one can make. Either the curvature is positive, $R > 0$, or negative, $R < 0$. The spacetime with positive curvature is known as the de-Sitter spacetime. On the other hand the spacetime with constant negative curvature is known as the Anti-de-Sitter spacetime. In this section I am interested to discuss the spacetime with negative curvature.

One can define Anti-de-Sitter spacetime in $d+1$ dimensions by embedding in $(d+2)$ dimensional Euclidean spacetime. To understand this let us consider a flat $d+2$ dimensional spacetime with the following line element

$$ds^2 = -dX_0^2 + \sum_{i=1}^{d} dX_i^2 - dX_{d+1}^2. \tag{1.90}$$

Anti-de-Sitter In this above spacetime we can embed a hypersurface of the following form

$$-X_0^2 + \sum_{i=1}^{d} X_i^2 - X_{d+1}^2 = -R^2 \tag{1.91}$$

where R is the radius of the hyperboloid and it is related to the cosmological constant Λ. I would like to mention that AdS_{d+1} is a maximally symmetric spacetime with $\frac{(d+1)(d+2)}{2}$ independent killing vectors.These linearly independent Killing vectors generate the isometry group $SO(2, d-1)$ which is the conformal group of Minkowski spacetime in $(d-1)$ dimensions. Let us recast this $(d+1)$-dimensional AdS spacetime in different forms by choosing different kind of parametrisation. First

we will look into the form of AdS_{d+1} spacetime in Global coordinates. For this let us consider the following coordinate transformations

$$\begin{aligned} X_0 &= R\cosh(\rho)\cos(\tau) \\ X_i &= R\ \Omega_i \sinh(\rho) \\ X_{d+1} &= R\cosh(\rho)\sin(\tau) \quad ; \quad i \in [1,..,d] \quad ; \quad \rho \in \mathbb{R}_+ \quad ; \quad \tau \in [0, 2\pi] \end{aligned} \tag{1.92}$$

where Ω_i is the usual parametrisation of $(d-1)$ dimensional sphere. In this new coordinate system the AdS_{d+1} spacetime looks like

$$ds^2 = R^2\left(-\cosh^2(\rho)d\tau^2 + d\rho^2 + \sinh^2(\rho)d\Omega^2_{d-1}\right) \tag{1.93}$$

where $d\Omega^2_{d-1}$ is metric on a unit sphere S^{d-1}. The above line element suggests that the all the metric coefficients asre independent of τ, this implies ∂_τ is Killing vector. However, this τ coordinate is periodic with 2π periodicity. This implies the fact that, the spacetime has closed timelike curve. To deal with this we unwrap the τ direction, by $\tau \in \mathbb{R}$. The boundary of this AdS spacetime plays a very important role. The boundary structure of AdS spacetime is very relevant in our analysis. To study the boundary structure of the the above spacetime let introduce a new parameter by $\tan(\theta) = \sinh(\rho)$, with $\theta \in \left[0, \frac{\pi}{2}\right)$. Using this parametrisation the elementary line element given in eq.(1.93) can be written as

$$ds^2 = \frac{R^2}{\cos^2\theta}\left(-d\tau^2 + d\theta^2 + \sin^2(\theta)d\Omega^2_{d-1}\right) \ . \tag{1.94}$$

It is aperant from the above line element is that, the metric diverges at $\theta = \frac{\pi}{2}$. Another important obeservation is that, the line element in the above equation is conformally flat. It is flat upto a conformal factor $\frac{R^2}{\cos^2\theta}$. Now we can perform the metric compatification by rescaling with the conformal factor. After the conformal compatification the line element reads

$$ds'^{\,2} = -d\tau^2 + d\theta^2 + \sin^2(\theta)d\Omega^2_{d-1} \ . \tag{1.95}$$

Now one can include the point $\theta = \frac{\pi}{2}$ as the boundary of AdS_{d+1} spacetime. The metric has topology of $\mathbb{R} \times \mathbb{S}^{d-1}$, which represents half of the Einstein static universe. On the other hand the conformal boundary $\theta = \frac{\pi}{2}$ has the topology of $\mathbb{R} \times \mathbb{S}^{d-2}$. Another point is that using global coordinates we do not have the full $SO(2,d)$ symmetry group of AdS_{d+1}.

Now concider the following coordinate transformations $(X_0, X_{d+1}, X_i) \to (t, z, x_i)$, with $i \in (1, .., d-1)$

$$\begin{aligned} X_0 &= \frac{1}{2z}\left(L^2 + z^2 + \vec{x}^2 - t^2\right), \\ X_{d+1} &= \frac{1}{2z}\left(L^2 - z^2 - \vec{x}^2 + t^2\right), \\ X_i &= \frac{x^i}{z}, \quad i = 1, 2, \ldots, d-1, \\ X_d &= \frac{t}{z}. \end{aligned} \tag{1.96}$$

The set of those coordinates cover only the half of the hyperboloid as $z > 0$. In terms of the these new coordinates the elementary line element given in eq.(1.90) can be recast as

$$ds^2 = \frac{L^2}{z^2}\left(-dt^2 + \sum_{i=1}^{d-1} d\vec{x}_i^2 + dz^2\right) . \tag{1.97}$$

The resulting spacetime is known as the Poincaré patch. The above metric suggests that there is a coordinate singularity at $z = 0$. Similar to the previous case of global coordinate after making conformal compatification one can include the point $z = 0$ in the patch. Thus the new metric becomes

$$ds^2 = -dt^2 + \sum_{i=1}^{d-1} d\vec{x}_i^2 . \tag{1.98}$$

The boundary is at $z = 0$.The boundary is conformally equivalent to the Minkowski space, $\mathbb{R}^{1,d-1}$.

1.3.3 Brief review on string theory

String theory is one of the most suitable candidate for a consistent theory of quantum gravity. In contrast to conventional quantum field theory, which governs the behavior of point-like particles, string theory is built upon the premise that the basic building blocks of the universe are one-dimensional entities known as strings. Strings are characterized by a specific length, referred to as the Planck length, denoted as $l_P = 1.6 \times 10^{-33}$cm. It is to be noted that, this length scale is much smaller than the shortest length scale which can be probed experimentally. One can charecterised strings by two parameters, namely the string tension (T_s) and dimensionless string coupling (g_s). One can express the string tension in terms of the string length (l_s) in the following way

$$T_s = \frac{1}{2\pi l_s^2} . \tag{1.99}$$

Now we would like to describe the dynamics of string qualitatively. Much like a point particle traces a one dimensional world line through spacetime, a string moves through spacetime by sweeping out a twodimensional surface known as a world sheet. Drawing inspiration from the action of a point particle, which is simply the length of its world line, we propose that the action for a string corresponds to the area of its world sheet. We can parametrised the string world sheet by $\xi^\alpha = \{\tau.\sigma\}$. We further assume that, the string is moving in a D dimensional spacetime which is described by the coordinates $X^a, \{a = 0, 1, 2..., D\}$. We can describe the trajectory of the string by specifying the functions $X^a = X^a(\xi)$. Now one can write down the induced metric on the two dimensional string world sheet as

$$g_{\alpha\beta} = G_{ab}\frac{\partial X^a}{\partial \xi^\alpha}\frac{\partial X^b}{\partial \xi^\beta} \tag{1.100}$$

where G_{ab} is the spacetime metric of D dimensional spacetime. Now we can write down the Numbo-Gotto action describing the strig dynamics as

$$S_{NG} = \frac{1}{2\pi\alpha'}\int d\tau d\sigma \sqrt{-\text{det} g_{\alpha\beta}}\ . \tag{1.101}$$

Quantisation of the above theory gives rise to the quantum mechanical description of strings. Quantisation of the string theory put restriction on the dimension of the spacetime in which the string propagates. For example, if we consider D dimensional Minkowski spacetime, then the dimension of the spacetime should be $D = 26$. Further, different states of the string spectrum represents different vibrational modes of the string. Each of these modes represents particles with specific mass (m) and spin (s). The spectrum of open string consists of finite number of mass less modes and infinite number of massive modes. On the contrary, the spectrum of closed string consists of spin-2 massless particles, which are interpreted as the gravitons. This explains why string theory is considered as a quantum theory of gravity. The graviton represents small perturbations in the spacetime metric, indicating that the spacetime we initially assumed is, in fact, dynamical.

It is also possible to construct other string theory by considering more degrees of freedom along with the string world sheet action. For example, in superstring theories, ensuring the absence of negative norm states imposes a strict condition on the spacetime dimension. This requirement uniquely determines the spacetime dimension to be $D = 10$. One of the most interesting example

of superstring theory is type-II B superstring theory which is obtained by adding two-dimensional world-sheet fermions to the above action. In addition to the graviton, the spectrum of type IIB superstring theory includes two scalar fields, multiple antisymmetric tensor fields, and various fermionic partners as dictated by supersymmetry. It is to be noted that, at low energy, one can integrate the massive modes, this leads us to write down an effective action for the massless modes. As the spectrum of the massless strings always contains the graviton, the effective action at the low energy limit is nothing but the Einstein gravity coupled to other massless modes

$$S_{low} = \frac{1}{16\pi G_D} \int d^D x \sqrt{-G}\mathcal{R} + ... \tag{1.102}$$

where $\mathcal{R}$ represents the Ricci scalar of the D-dimensional spacetime and "..." stands for additional terms containing other massless modes. This type-II B superstring theory contains a dilatonic scalar field ϕ which is related to the string coupling as $g_s = e^{\phi}$. The string coupling can vary over spacetime. In such case, we can still think of a coupling constant which is given by the asymptotic value of the dilaton at infinity, that is, $g_s = e^{\phi_\infty}$.

However, the fermions in the spectrum of closed string can have two kinds of chirality, namely, the left handed chirality and the right handed chirality. One can impose either the periodic boundary condition (Ramond sector) or the antiperiodic (Neveu-Schwarz sector) boundary condition on these fermions. Depending upon the chirality and the boundary conditions we can identify 24 different sectors: R-R, NS-NS, R-NS and NS-R. It is to be noted that, the R-R and the NS-NS sectors give spacetime bosons. On the other hand the R-NS and NS-R sectors give spacetime fermions. Interestingly, the NS-NS sector contains the graviton, the two-form field and the dilaton. While the the R-R sector contains the $(p+1)$ form field in the massless sector.

1.3.4 D-brane and gauge theory

A Dp-brane can be defined as a $(p+1)$-dimensional object moving in $(9+1)$ spacetime dimension with which string can interact. It is to be observed that, a closed string can break on a Dp brane and while an open string can end on a Dp brane. The endpoints of an open string are free to move along the $(p+1)$ directions of the Dp-brane, but they are confined to it and can move along the transverse directions. This implies the open strings obey Neumann boundary condition along the $(p+1)$-directions of the D brane. On the other hand, the open strings satisfies Drichlet

boundary condition along the $(9-p)$ directions transverse to the Dp brane. A Dp brane swipes out a $(p+1)$-dimensional world volume in the spacetime. It is to be mentioned that, the $D0$ brane acts as a point particle, $D1$ brane behaves as string and $D2$ branes are like membrane.

The concept of Dp-brane enhances the structural framework of string theory, providing deeper insights into its dynamics and interactions. As mentioned earlier, when a closed string interacts with a Dp-brane, it can break and transform into an open string with endpoints constrained to the brane. Just as the quantization of a closed string gives rise to dynamical fluctuations of space-time, the quantization of an open string leads to a spectrum that includes fluctuations of the Dp-brane. The open string spectrum consists of a finite set of massless modes along with an infinite tower of massive modes. For example, incase of a single Dp brane, the spectrum of massless modes consists of an abeliean gauge field A_μ $(\mu = 0, 1..., p)$, $(9-p)$ scalar fields $(\phi^i, i = 1, 2..., (9-p))$ and their superpartners. The $(9-p)$ scalar fields represent the fluctuations of the Dp-brane in the transverse directions, encompassing both possible deformations and linear motion of the brane. Dp-branes carry charge under the $(p+1)$-form field A_{p+1} originating from the R-R sector of Type II string theory. A remarkable feature of D-branes is the emergence of a non-Abelian gauge field when multiple D-branes are brought into proximity. It is also to be noted that, in case of the multiple D branes, new degrees of freedom arises from the strings that, stretch from one brane to another. To understand this let us consider a example of two Dp-branes which are separated by a distance d.In this setup, four types of strings can arise, classified by the brane on which their endpoints are located. In this scenario, strings with both endpoints attached to the same brane give rise to massless gauge fields, as mentioned earlier. We can denote these gauge fields as $(A_\mu)^1_1$ and $(A_\mu)^2_2$, where the upper (lower) index indicates the brane where the string originates (terminates). Additionally, there exists the possibility of strings stretching between the two branes, with one endpoint on brane 1 and the other on brane 2, or vice versa. These gives us to more massive vector fields $(A_\mu)^1_2$ and $(A_\mu)^2_1$. Now one can make the separation between these two branes to be zero, that is, two branes are now on top of each other. These results the spectrum of four massless vector fileds, denoted as $(A_\mu)^a_b$, where $a, b = 1, 2$. This is nothing but the gauge field of non-Abelian gauge group $U(2)$. On the other hand, the $(9-p)$ massless scalar fields become 2×2 matrix, $(\phi^i)^a_b$. These fields transform according to the adjoint representation of the $U(2)$ gauge group. With the fundamental intuition in mind, it's possible to generalised the analysis when N_c branes are

stacked together. We obtain a $U(N_c)$ multiplet of non-Abelian gauge fields, accompanied by (9 ? p) scalars that transform in the adjoint representation of $U(N_c)$. The low-energy dynamics emerge after integrating out the massive modes, revealing that they are described by a non-Abelian gauge theory. Now we consider a very well known examples of N_c numbers of $D3$ brane in type-IIB string theory. The massless spectrum of the theory is now consists of a gauge field A_μ, six scalar field ϕ_i and four Weyl fermions. Now if we restrict ourselves to theories with derivatives not higher than the second order, the low-energy effective action for these massless modes precisely corresponds to $\mathcal{N} = 4$ supersymmetric Yang-Mills (SYM) theory in $(3 + 1)$ dimensions, with the gauge group $U(N_c)$ [57, 58, 59]. One can write down the bosonic part of the action in the following way

$$\mathcal{L} = -\frac{1}{g_{\rm YM}}\mathrm{Tr}\left(\frac{1}{4}F^{\mu\nu}F_{\mu\nu} + \frac{1}{2}D_\mu\phi^i D^\mu\phi^i + \left[\phi^i, \phi^j\right]^2\right) . \tag{1.103}$$

The Yang-Mills coupling is connected to the string coupling through the relation

$$g^2_{YM} = 4\pi g_s \ . \tag{1.104}$$

It is to be noted that, the bosonic part of the Lagrangian is the most general renormalizable Lagrangian which is consistent with $\mathcal{N} = 4$ global supersymmetry. Because of its substantial supersymmetry, the theory possesses numerous fascinating characteristics. For instance, the β-function is zero, meaning the coupling constant remains constant across all scales, and the theory maintains conformal invariance. Another important feature of the Lagrangian is that the $U(1)$ component is free and can be decoupled.

1.3.5 D-brane and spacetime geometry

As the D-branes are massive objects they can defrom the neighbouring spacetime of it. The spacetime metric produced by N_c Dp-branes is determined by solving the supergravity equations of motion. The low-energy effective action of Type II supergravity, expressed in the Einstein frame, is given by

$$S = \frac{1}{16\pi G_{10}}\int d^{10}x\sqrt{-\mathrm{det}G}\left(\mathcal{R} - \frac{1}{2}g_{MN}\partial^M\phi\partial^N\phi - \frac{1}{2}\sum_n \frac{1}{n!}e^{a_n\phi}F_n^2 + ...\right) \tag{1.105}$$

where $a_n = -\frac{1}{2}(n-5)$, and G_{MN} represents the 10-dimensional spacetime metric.The dotted terms correspond to the fermionic terms and the NS-NS three-form field strength term. On the other

hand the n form field strength belongs to the R-R sector. It is to be noted that, in case of type IIA (IIB) theory, n is even (odd). The equations of motion derived from the above action are

$$R_{MN} = \frac{1}{2}\partial_M\phi\partial_N\phi + \frac{1}{2n!}e^{a\phi}\left(nF_{MK_2\ldots K_n}F_N^{\ K_2\ldots K_n} - \frac{n-1}{8}g_{MN}F_n^2\right) \tag{1.106}$$

$$\nabla^2\phi = \frac{1}{\sqrt{G}}\partial_M\left(\sqrt{G}G^{MN}\partial_N\phi\right) = \frac{a}{2n!}F_n^2 \tag{1.107}$$

$$\partial_M\left(\sqrt{G}e^{a\phi}F^{MK_2\ldots K_n}\right) = 0 \tag{1.108}$$

This is accompanied by the Bianchi identity given as

$$\partial_{[K_1}F_{K_2\ldots K_n]} = 0 \tag{1.109}$$

In obtaining the above equantion of motions we keep in mind that, F_n exits only for one value of n. So we can write $a_n \equiv a$. By solving the equations of motion, one can determine the spacetime metric generated by Dp-branes. Specifically, if the coupling with the dilaton vanishes, it can be shown that the spacetime metric reduces to the familiar form $\mathrm{AdS}_q \times S^{10-q}$. This takes place when the dilaton remains constant, specifically zero, with $n = 5$. In this scenario we can obtain the following metric sourced by stack of D-branes

$$ds^2 = H^{-1/2}\left(-dt^2 + dx_1^2 + dx_2^2 + dx_3^2\right) + H^{1/2}\left(dr^2 + r^2d\Omega_5^2\right) \tag{1.110}$$

where H is given by

$$H = 1 + \frac{R^4}{r^4} \quad ; \quad R^4 = 4\pi g_s N_c l_s^4 \ . \tag{1.111}$$

In the above spacetime metric, $\{t, x_1, x_2, x_3, x_3\}$ represents the world-volume coordinates on the $D3$ brane and y_i, with $i = \{1, 2, ..6\}$ denotes the transverse coordinates on the $D3$-brane with the condition

$$r^2 = \sum_{i=1}^{6} y_i^2 \ . \tag{1.112}$$

To gain insight into the geometry generated by the D3-brane, we analyze its behavior in two distinct limiting regimes. First, we consider the limit, $r >> R$. In this regime, $H \to 1$ which

implies, the metric simplifies, and the spacetime asymptotically approaches flat Minkowski space, that is, $\mathbb{R}^{1,9}$. On the other hand, in the limit $r \ll R$, the metric might initially appear singular. This geometry is known as the throat geometry. However, a suitable redefinition of the coordinates resolves this apparent singularity. To proceed further let us define a new coordinate

$$U = \frac{r}{l_s^2} \ . \tag{1.113}$$

In this new coordinate the spacetime metric given in eq.(1.110) can be written as

$$\begin{aligned} ds^2 &= l_s^2 \left(\frac{U^2}{\sqrt{4\pi g_s N_c}} dx_{(4)}^2 + \sqrt{4\pi g_s N_c} \left(\frac{dU^2}{U^2} + d\Omega_5^2 \right) \right) \\ &= \frac{U^2}{R^2} d\tilde{x}_{(4)}^2 + \frac{R^2}{U^2} dU^2 + R^2 d\Omega_5^2 \end{aligned} \tag{1.114}$$

where $\tilde{x} \equiv l_s^2\{t, x_1, x_2, x_3\}$ and we denote $dx_{(4)}$ as

$$dx_{(4)}^2 = -dt^2 + \sum_{i=1}^{3} dx_i^2 \ . \tag{1.115}$$

The metric, expressed in this form, explicitly takes the structure of a product geometry. One of the metric component is S^5 with the metric coefficient $R^2 d\Omega_5^2$, while the other component corresponds to AdS_5. As we will see later, the Maldacena conjecture requires us to take the "near-horizon limit", which corresponds to setting the string length to be zero, that is, $l_s \to 0$. Thus, we focus on a region very close to the surface of the $D3$-brane. In this region, only the $\mathrm{AdS}_5 \times S^5$ structure remains relevant, while the dynamics in the asymptotically flat spacetime decouple from the theory. This is why it is also referred to as the decoupling limit.

1.3.6 AdS/CFT correspondence

In the preceding subsection, we laid the foundation for discussing the AdS/CFT correspondence. In this section, we aim to motivate the AdS/CFT correspondence [60, 61, 62] by considering string theory in the presence of D-branes from two distinct perspectives. We start our analysis by considering type-IIB string theory in $(9+1)$-dimensional Minkowski spacetime and N_c number of parallel $D3$ brane. String theory in this background consists of two types of excitations: closed strings and open strings. Closed strings correspond to excitations of the vacuum, while open strings describe excitations of D-branes. Now if we restrict ourselves in the low energy regim of the theory, then only the massless strind states will persist. This considaration allows us to write down the effective action which describes the string interaction. It can be shown that, in ten dimensions, closed string spectrum contains gravity supermultiplet, and their low-energy dynamics are described by type-IIB supergravity. Conversely, the massless states of open strings constitute an $\mathcal{N}=4$ supermultiplet, with their low-energy dynamics governed by the Lagrangian of $\mathcal{N}=4$ super Yang-Mills (SYM) theory.

One can write down the effective action for the mass less modes as follows

$$S_{eff} = S_{\text{bulk}} + S_{\text{brane}} + S_{\text{int}} \ . \tag{1.116}$$

In the above action the first term S_{bulk} represents the action of ten-dimensional gravity along with the higher derivative correction terms. While the second term describes the action for $\mathcal{N}=4$ SYM theory. This term also include some correction terms. Finally, the last term, that is , S_{int} represents the interaction between the brane modes and the bulk modes. It is to be mentioned that, the bulk action can be expanded as free quadratic part which describes propagation of free massless modes including the gravitons along with some interaction with the bulk. In the low-energy limit, all interaction terms and higher derivative terms become negligible and do not contribute. As a result, we are left with pure $\mathcal{N}=4$ SYM theory in $(3+1)$ dimensions and a free gravity theory in the bulk.

Now we look into the same problem from a subtly different angle. In the previous section, we discussed how D-branes emerge as solutions of type II supergravity. Now we restrict ourselves only to the low energy regime. This involves considering excitations that possess infinitesimally small energy as observed by an observer in asymptotically Minkowski spacetime. We can identify

two distinct sets of excitations. One set consists of massless excitations propagating in the bulk, while the other includes excitations localized in the throat region. For such excitations, we can allow for any value of proper energy. This is because, for an observer in asymptotically Minkowski spacetime, the energy E_∞ is measured as

$$E_\infty = H^{-\frac{1}{4}} E \tag{1.117}$$

where E represents the energy as measured by an observer positioned at a radial coordinate r. As we approach the throat ($r \to 0$), for a fixed E, the energy measured by the observer at infinity, E_∞, approaches zero. Consequently, even the massive modes residing in the throat region will seem massless to the observer. In the low energy limit, these modes are pushed deeper into the throat and eventually decouple from the massless modes in the bulk. Thus, in the low-energy regime, we are left with two decoupled components: a free gravity theory in the bulk and the near-horizon geometry, which corresponds to $AdS_5 \times S^5$. From both perspectives, we observe that the low-energy limit consists of two decoupled theories. The gravity sector is common to both descriptions, making it natural to identify the remaining sectors. This leads to the equivalence of the following two theories:

- Type IIB string theory on $AdS_5 \times S^5$, where both subspaces share a common radius R, and the string coupling is g_s.
- $\mathcal{N} = 4$ SYM theory in (3+1) dimensions with gauge group $SU(N_c)$ and Yang-Mills coupling constant $g_{\rm YM}$, which is known to be a conformally invariant theory.

This forms the foundation of the AdS/CFT correspondence.

For two theories to be equivalent, a natural requirement is that they share the same symmetries. Let us now analyze the symmetries of these two theories. We start with the symmetry of $AdS_5 \times S_5$. The isometry group of AdS_5 is $SO(4,2)$, which becomes evident when we represent AdS_5 as a hyperboloid embedded in a higher-dimensional space (in $\mathbb{R}^{2,4}$). On the other hand the isometry group of S_5 is $SO(6)$. Therefore the full symmetry group of $AdS_5 \times S_5$. Further, in the CFT side, the symmetry group of $\mathcal{N} = 4$ SYM theory in $(3+1)$-spacetime dimension is described by $SO(4,2)$, including Poincaré transformations as well as scale transformations and special conformal transfomations. The six scalar fields ϕ^i and the four fermions in $\mathcal{N} = 4$ Super Yang-Mills (SYM)

theory are related through a global $SU(4) \sim SO(6)$ symmetry, which acts as the R-symmetry of the theory. This symmetry rotates the scalars and fermions among themselves and is a key feature of the superconformal algebra $SU(2,2|4)$. Both sides of the AdS/CFT correspondence share 32 supersymmetries

- Gravity Side ($\mathrm{AdS}_5 \times S^5$): supersymmetry appears as Killing spinors, which are solutions to the Killing spinor equation in the $\mathrm{AdS}_5 \times S^5$ background of type IIB supergravity, reflecting the maximal supersymmetry of the space.

- Gauge Theory Side ($\mathcal{N} = 4$ SYM): supersymmetry manifests through the superconformal algebra $SU(2,2|4)$, which includes both Poincaré and conformal supersymmetries, making it the most symmetric 4D supersymmetric field theory.

This symmetry matching strongly supports the duality between type IIB string theory on $AdS_5 \times S^5$ and $\mathcal{N} = 4$ SYM in four dimensions.

The most remarkable aspect of the AdS/CFT conjecture is that it establishes a dynamical equivalence between two fundamentally different theories in physics.This means that the conjecture allows us to study a strongly coupled gauge theory through its dual description in terms of the corresponding gravity theory in an asymptotically AdS spacetime. It is to be noted that, the gravitational theory exists in one higher dimension than the strongly coupled gauge theory. For this reason, the conjecture is often referred to as the *holographic duality*. This profound correspondence was first demonstrated by Juan M. Maldacena, who identified a duality between the large-N limit[1] of $3+1$-dimensional $SU(N)$ supersymmetric Yang-Mills (SYM) theory with four supercharges ($N = 4$) and the low-energy limit of Type IIB string theory in $AdS_5 \times S^5$ [60]. By a more rigorous argument, it can be observed that the parameters of the two theories are related as follows

$$4\pi g_s = g_{YM}^2;\ g_{YM}^2\ N = \lambda = \frac{L_{AdS}^4}{4\pi l_s^4}\ . \tag{1.118}$$

Here, g_s and g_{YM} represent the string coupling constant and the SYM coupling constant respectively.N denotes the number of $D3$-branes under consideration. Additionally, L_{AdS} denotes the AdS radius, λ is the t' Hooft coupling, and l_s is the string length. Based on these parameter relations, we now

[1]Here, N represents the rank of the gauge group.

discuss the several interesting physical limits.

In the large-N limit ($N \to \infty$, with the t' Hooft coupling $\lambda = g_{YM}^2 N$ kept constant and finite), one obtains the so-called planar sector of SYM theory [63]. In this regime, the corresponding string theory is effectively classical, as it only contains tree-level diagrams, with the string coupling scaling as $g_s \sim \frac{1}{N} \to 0$. This implies that all higher order loop corrections are suppressed in the large-N limit. On the other hand, in the limit $\lambda \gg 1$, the $\mathcal{N} = 4$ SYM gauge theory exhibits strong coupling behavior and becomes non-perturbative. In terms of string theory, it is evident (from the relations given (1.118)) that the strong coupling limit ($\lambda \gg 1$) corresponds to $L_{\text{AdS}} \gg l_s$. This means that the curvature of the $\text{AdS}_5 \times S^5$ background is much smaller than the string scale, ensuring the validity of the supergravity approximation. This limiting condition can also be expressed as $m_s^2 \gg \mathcal{R}$, where m_s is the string mass and $\mathcal{R}$ is the Ricci scalar. This ensures that stringy corrections remain suppressed, validating the supergravity approximation in the $\text{AdS}_5 \times S^5$ background. This in turn means that the limit $\lambda \gg 1$ suppresses all the stringy effects as the string theory lives on a weakly curved background, whereas $\lambda \ll 1$ means that the string theory lives on a curved spacetime background. Some further development in this direction can be found in [64, 65, 61, 66, 67, 62, 68].

Now we discuss another interesting features of AdS/CFT correspondence. This is known as the Gubser-Klebanov-Polchinski-Witten (GKP-W) relation[61, 62], which states that, the partition functions oftwo seemingly different theories are equivalent. This implies [61, 62]

$$Z_{QFT}|_{\mathsf{N}\to\infty} = Z_{AdS_5} \approx e^{-iS_{cl}[g_{\mu\nu}]}|_{\text{on-shell}}. \tag{1.119}$$

The above relation implies that the generating functional of correlators for a CFT in 3+1 spacetime dimensions can be obtained from the partition function of the dual gravity theory in AdS_5. This forms the foundation of the AdS/CFT correspondence, where boundary operators in the gauge theory correspond to bulk fields in AdS, establishing a holographic dictionary between the two theories.

1.3.7 Holographic dictionary

Based on numerous studies in this direction [69, 70, 71, 72, 73], one can establish a holographic dictionary, which provides a framework for understanding the equivalence between two fundamentally different theories. This correspondence can be summarized as follows

Gauge theory	**Gravitational theory**
CFT_d at the boundary ($z = 0$)	AdS_{d+1} in the bulk ($z > 0$)
CFT at temperature T	Black hole with Hawking temperature T
Scalar operator $\hat{\mathcal{O}}_s$/ Fermionic operator $\hat{\mathcal{O}}_f$	Scalar field ϕ/ Dirac field ψ
Stress tensor $T^{\mu\nu}$	Metric tensor $g^{\mu\nu}$
Global current J^{μ}	1-form A_{μ}
Chemical potential/charge density	Boundary value of the gauge potential
Spin/charge of the operator	spin/charge of the field
External source of the operator	Boundary value of the bulk field
Dimension (conformal) of the operator	Mass of the field
Phase transition	Instability of black hole
Global symmetry	local isometry

1.4 Holographic description of different information theoretic measures

In this section we would discuss how one can compute different information theoretic measures using the AdS/CFT correpondence. It is shown that every information theoretic measures of the boundary CFT can be mapped to a geometric quantity in the bulk. Here we will discuss how to compute those information theoretic measure holographically.

1.4.1 Holographic entanglement entropy

We would start with the holographic computation of entanglement entropy. This discussion is based on the Ryu-Takyanagi prescription [74, 75, 76] of computing entnaglement entropy of a subsystem

on the CFT side by using the gravity dual in the bulk. The RT presecription of computing the holographic entanglement entropy can be stated as following.

Let us consider a d-dimensional CFT which lives on the boundary of a $(d+1)$-dimensional Anti-de-Sitter spacetime. The bulk $(d+1)$-dimensional Anti-de-Sitter spacetime is denoted by $\mathcal{M}_{d+1}$, therefore the boundary of the AdS_{d+1} is labeled by $\partial\mathcal{M}_d$. One can compute EE of a subsystem A in CFT_d by calculating the area of a codiemnsion-2 static minimal surface γ_A^{min}. This static codimension-2 minimal surface is known as the Ryu-Takyanagi surface. Therefore, the holographic entanglement entropy of spatial region in CFT side is given by

$$S_{HEE}(A) = \frac{\text{Area}(\gamma_A^{min})}{4G_N} \ . \tag{1.120}$$

In [77], it was shown that one proof the above formula by using the GKP-W relation and the replica tricks. We wolud also provide a heuristic proof of the above formula in the following. The proof of the RT formula is based upon the basic principle of AdS/CFT correpondence, which is given as

$$Z_{\text{CFT}} = Z_{\text{AdS gravity}} \ . \tag{1.121}$$

The above equation relates the partition function of the CFT to that of the AdS gravity theory. Now to obatin the EE in the CFT side one need to compute the patition function on the d-dimensional n-sheeted geometry. Let us denote this n sheeted complicated geometry as $\mathcal{B}_n$. One can characterise this geometry by the deficit angle $\delta = 2\pi(1-n)$ on the entangling surface ∂A. Next to proceed further one need to a $(d+1)$ dimensional backreacted geometry $\mathcal{S}_n$ in the dual AdS space by solving the Einstein equation in the presence of the negative cosmological constant, such that the metric goes to the $\mathcal{B}_n$ in the boundary limit. This seems to be very difficult mathematically. To avoid this issue we will make a simple assumption given in [**?**]. In this work it was suggested that, the backreacted geometry $\mathcal{S}_n$ is given by n sheeted AdS_{d+1} which can be defined by putting the deficit angle δ localised on codimension two surface γ_A. Keeping this assumption in mind, one can obatain Ricci scalar for $\mathcal{S}_n$ as

$$R = 4\pi(1-n)\delta(\gamma_A) + R^{(0)} \tag{1.122}$$

where $\delta(\gamma_A)$ is delta function localised on the codimension-2 surface γ_A and $R^{(0)}$ is the Ricci scalar associated to the pure AdS background. Our next task is to compute the logarithm of the partition

function on the gravity side by keeping all this in mind. Therefore, we have

$$\begin{aligned}\log(Z_n) &= -\frac{1}{16\pi G_N^{(d+1)}}\int d^{d+1}x\sqrt{-g}(R+\Lambda)+... \\ &= -4\pi\frac{(1-n)\text{Area}(\gamma_A)}{16\pi G_N^{(d+1)}}-\frac{1}{16\pi G_N^{(d+1)}}\int d^{d+1}x\sqrt{g}(R^{(0)}+\Lambda)+... \ . \end{aligned} \tag{1.123}$$

Now using the bulk boundary condition given in eq.(1.121) one can obtain

$$\log(Z_{CFT})=\log(Z_{AdS})=\frac{(1-n)\text{Area}(\gamma_A)}{4\pi G_N^{(d+1)}}+\ \text{(q independent terms)} \tag{1.124}$$

Next we need to compute the Reiny entropy by using the formula given in eq.(1.56). Then taking the $n\to 1$ limit we have the following result of HEE

$$S_{HEE}(A)=\frac{\text{Area}(\gamma_A^{min})}{4G_N}\ . \tag{1.125}$$

This completes the heuristic proof of the RT- formula of computing the EE of a region in CFT side by using the gauge/gravity duality. For further details one can go through [77].

However, in case of two dimensional CFT, the EE of a subsystem obatined by replica trick matches exactly with that of obtained by the above mentioned RT prescription. Therefore it is belived that this prescription of computing EE works for any dimensions. We would like to mention that the HEE obtained by this way obey all the properties of EE listed in section(1.1.1). It is much more eaiser to proof those properties geometrically.

1.4.2 Holographic mutual information

Mutual information is another important quantity in the context of quantum information. In this section we will discuss how one can compute this quantity holographically. Let us consider two sub systems A and B in the CFT side, therefore the holographic mutual information (HMI) between these two sub systems are given by

$$I(A:B)=S_{HEE}(A)+S_{HEE}(B)-S_{HEE}(A\cup B)\ . \tag{1.126}$$

In the above expression $S_{HEE}(A)$, $S_{HEE}(B)$ and $S_{HEE}(A\cup B)$ represent the holographic entanglement entropy of the A, B and $A\cup B$ repecetively. It can be shown that, HMI ($I(A:B)$) is positive definite quantity, that is $I(A:B)\geq 0$. It measures total correlation in the system, both the classical and quantum correlation. Furthermore it is also easy to show that holographic mutual information obey all the properties of mutual information which we have discussed in section(1.1.2).

1.4.3 Holographic description of EoP: Entanglement wedge cross-section

As we have discussed earlier, the EE captures the quantum correlation present in a system as long as the system under consideration is in a pure state. If state of system under consideration is in a mixed state, then EE is not good candidate to capture the quantum correlation. Therefore, various research in this direction shows that, entanglement of purification is one potential candidtae, which can measure quantum correlation in system, when it is in the mixed state. It is to be mentioned that, the computation of EoP is extremely difficult in the context of field theory. Thus gauge/gravity duality plays an important role to provide a nice prescription to compute EoP holographically. The holographic analogue of EoP is termed as the entanglement wedege cross section (EWCS). We now holographically compute EoP, which is one of the potential candidates to quantify entanglement for mixed states. This computation holographically probes EoP on the basis of $E_P = E_W$ duality [4, 78, 79, 80].

To proceed further we consider two strip like subsystems on the boundary $\partial\mathcal{M}$ ($\partial\mathcal{M}$ is the boundary of the canonical time-slice $\mathcal{M}$ that has been considered in the gravity dual). Let us denote these subsystems as A and B with both of them having the same length l. Further we assume that the subsystems, A and B are separated by a distance x with the condition $A \cap B = 0$. The Ryu-Takayanagi surfaces associated to A, B and AB can be denoted as Γ_A^{min}, Γ_B^{min} and Γ_{AB}^{min} respectively. Therefore, the co-dimension-0 domain of entanglement wedge M_{AB} can be characterized by the following boundary

$$\partial\mathcal{M}_{AB} = A \cup B \cup \Gamma_{AB}^{min} = \bar{\Gamma}_A \cup \bar{\Gamma}_B \tag{1.127}$$

where $\bar{\Gamma}_A = A \cup \Gamma_{AB}^A$, $\bar{\Gamma}_B = B \cup \Gamma_{AB}^B$. In the above expression we have used the condition $\Gamma_{AB}^{min} = \Gamma_{AB}^A \cup \Gamma_{AB}^B$. In this secnario, one can define the holographic entanglement entropies $S(\rho_{A\cup\Gamma_{AB}^A})$ and $S(\rho_{B\cup\Gamma_{AB}^B})$. This can be computed by identifying a static RT surface Σ_{AB}^{min} with the following condition

$$\partial\Sigma_{AB}^{min} = \partial\bar{\Gamma}_A = \partial\bar{\Gamma}_B \ . \tag{1.128}$$

We would like to mention that, the splitting condition $\Gamma_{AB}^{min} = \Gamma_{AB}^A \cup \Gamma_{AB}^B$ is not unique and there can be infinite number of possible choices. Further, this means that there can be infinite number of choices for the surface Σ_{AB}^{min}. The EWCS is computed by minimizing the area of Σ_{AB}^{min} over all

possible choices for Σ_{AB}^{min}. This reads

$$E_W(\rho_{AB}) = \min_{\bar{\Gamma}_A \subset \partial M_{AB}} \left[\frac{A\left(\Sigma_{AB}^{min}\right)}{4G_{d+1}} \right] . \tag{1.129}$$

EWCS is bounded by HMI, given by following

$$E_W \geq \frac{I(A:B)}{2} . \tag{1.130}$$

1.4.4 Holographic computation of Entanglement negativity

We now consider another important measure of quantum correlation for mixed states, the entanglement negativity (also known as the logarithmic negativity) (E_N) . In section (1.1.4), we have discussed the concept of entanglement negativity and its importance in context of quantum information theory. Noe we will proceed to discuss how one can compute entanglement negativity holographically. Two different proposals have been suggested by various literatures in this direction.

In one of proposal, it was stated that, E_N can be computed by calculating the area of an extremal cosmic brane that terminates at the boundary of the entanglement wedge [81, 82]. This proposal is motivated by the quantum error correcting codes and states that the logarithmic negativity is equivalent to the cross-sectional area of the entanglement wedge with a bulk correction term. However, for a general entangling surface this is difficult to compute due to the backreaction of the cosmic brane. This calculation simplifies a lot for a ball shaped subregion. In this set up, the backreaction is accounted for by an overall constant to the area of the entanglement wedge cross-section. Then it is conjectured that [81, 82, 83]

$$E_N = \chi_d \frac{E_W}{4G_N} + E_{bulk} \tag{1.131}$$

where E_W is the minimal cross-sectional area of the entanglement wedge associated with the concerned boundary region and χ_d is a constant which depends on the dimension of the spacetime. E_{bulk} is the quantum correction term corresponding to the logarithmic negativity between the bulk fields on either sides of the entanglement wedge cross-section.

Another proposal suggests that the entanglement negativity is given by certain combinations of co-dimension-two static minimal bulk surfaces [84, 85, 86, 87, 88, 89]. Both of these proposals

reproduce the exact known result of entanglement negativity in CFT. In this paper, we follow the second proposal where entanglement negativity is given by the a certain combination of the area of co-dimension-two static minimal surfaces in the bulk. These combinations can be obtained from the dual CFT correlators. Some recent works in this directions can be found in [90, 91, 92, 93, 94, 95, 96, 97, 98].

We now compute E_N by considering two different set ups, namely, for two adjacent strip like subsystems and for two disjoint strip like subsystems. At first we consider adjacent scenario. Let us consider two strip like subsystems A and B with lengths l_1 and l_2 with zero-overlapping. In the case of such adjacent subsystems the entanglement negativity (E_N) is defined as [84, 85, 86, 87, 88, 89]

$$E_{N_{adj}} = \frac{3}{4}\left[S_{EE}(l_1) + S_{EE}(l_2) - S_{EE}(l_1 + l_2)\right] \ . \tag{1.132}$$

As we have mentioned earlier, we now consider two disjoint strip like subsystems A and B with length l_1 and l_2. The subsystems under consideration are separated by a length x. In this case the entanglement negativity reads [99, 100]

$$E_{N_{dis}} = \frac{3}{4}\left[S_{EE}(l_1 + x) + S_{EE}(l_2 + x) - S_{EE}(l_1 + l_2 + x) - S_{EE}(x)\right] \ . \tag{1.133}$$

1.4.5 Holographic computation of complexity

The holographic derivation of quantum complexity was first proposed by *L. Susskind* [21, 20]. In these works he proposed that the quantum computational complexity associated to a state of the CFT which lies at the boundary is equal to some extremal volume inside the bulk. To be precise, it has been noted that the *Einstein-Rosen (ER) bridge* (in simple language the wormhole) which connects the both of boundaries of a two-sided eternal black hole (which is nothing but the dual analogy of thermofield doublet or TFD state), has an ever-growing nature (which is expressed in terms of the thermalization time-scale of the black hole). This growth sustains much longer in comparison with the growth of EE between the mentioned two-boundaries of the eternal black hole. Susskind proposed that this growth of the ER bridge is a dual manifestation of the growth property of the complexity associated to the TFD state of the boundary CFT [20].

Complexity=Volume conjecture

This first proposal which was given regarding the holographic computation of complexity, is known as the *Complexity=Volume* (CV) conjecture. It is to be noted that this proposal was given regarding the whole state of the CFT living at the boundary as there was no notion of subregions in this conjecture.

According to this proposal, the quantum complexity can be holographically computed by evaluating the extremal volume associated to a codimension-1 surface inside the higher dimensional gravitational theory, defined on a Cauchy-slice σ which associated to the boundary state. This can expressed as

$$\mathcal{C}_{\text{volume}}(\sigma) = \max_{\sigma=\partial\gamma_A} \left(\frac{\text{Volume}(\gamma_A)}{G_N L_{AdS}} \right) \tag{1.134}$$

where the mentioned extremal surface is denoted by γ_A. Furthermore, this proposal also suggests that the state defined on σ is a pure state [101].

Complexity=Action conjecture

Another proposal regarding the holographic computation of complexity was later given in [102, 103]. In this conjecture, it was suggested that the complexity can be holographically computed by computing the classical gravitational action which resides inside a causal domain of dependence, denoted as the *Wheeler-DeWitt (WDW) patch*. It is to be mentioned that the mentioned patch is the domain of dependence of each and every space-like hypersurface which is anchored on boundary time-slice σ. Keeping in mind these properties, this conjecture has been dubbed as the *Complexity=Action* (CA) conjecture which can be mathematically represented in the following way

$$\mathcal{C}_{\text{action}}(\sigma) = \frac{I_{WDW}}{\pi\hbar} \tag{1.135}$$

where I_{WDW} denotes the gravitational action on the WDW patch. The factor $\frac{1}{\pi}$ was fixed in order to satisfy the *Lloyd's bound* [104]. The gravitational action on the WDW patch has the following generic form [105, 106]

$$I_{WDW} = I_{Einstein} + I_{GHY} + I_{null} + I_{ct} + I_{joint} \tag{1.136}$$

where

$$
\begin{aligned}
I_{Einstein} &= \frac{1}{16\pi G_N}\int d^{d+1}x\sqrt{-g}\,[R-2\Lambda]+I_{matter},\\
I_{GHY} &= \frac{1}{8\pi G_N}\int d^{d}x\sqrt{-h}K,\\
I_{null} &= \frac{1}{8\pi G_N}\int d\lambda d\Omega_{d-1}\sqrt{-\gamma}\mathcal{K},\\
I_{ct} &= \frac{1}{8\pi G_N}\int d\lambda d\Omega_{d-1}\sqrt{-\gamma}\log(l_{ct}\Theta),\\
I_{joint} &= \frac{1}{8\pi G_N}\int d\Omega_{d-1}\sqrt{-\sigma}a_{joint}\ .
\end{aligned}
\tag{1.137}
$$

In the above expressions, $I_{Einstein}$ represents the classical Einstein-Hilbert action. In WDW patch, one needs to introduce boundary terms corresponding to timelike/ spacelike/ null-like boundaries, in order to yield a well-defined boundary value problem. The Gibbons-Hawking-York term I_{GHY} [107, 108] has been used to take care of the spacelike/ timelike boundaries in WDW patch. On the other hand, the null-like boundaries is taken care by the boundary term I_{null} [105, 109]. Further, in WDW patch, the spacelike/ timelike boundaries sometimes intersect with each other. These kind of contributions have been taken care of by the terms I_{joint} [110, 111]. If one of these boundaries is a null-like boundary then the associated contribution is represented by I_{ct} [105].
However, similar to the CV conjecture, the CA conjecture does not have a notion of subregion at the boundary. This implies it probes the complexity associated to the whole state.

Holographic subregion complexity

As we have mentioned, both of the above mentioned holographic proposals of computing complexity corresponds to the whole state of the boundary theory. However, in [112] a proposal was given in order to compute the complexity associated to a subregion at the boundary theory (which generally gives us a mixed state). This proposal was inspired by the the previously mentioned CV conjecture, with some subtle differences. This we shall discuss now.
The RT prescription to holographically compute the EE suggests that one first needs to identify the codimension-2 static minimal surface. As we know, the area of this surface is proportional to the EE associated to the boundary subsystem namely A. On the other hand, Alishahiha proposed that the volume enclosed by this extremal surface (RT surface) shall lead us to the complexity

associated to the chosen geometric region A which we denote as the boundary subregion [112]. This has been denoted as the *holographic subregion complexity* (HSC) proposal which has the following mathematical form

$$\mathcal{C}(\mathsf{A}) = \frac{\text{Volume}(\gamma_{\mathsf{A}}^{min})}{8\pi L_{AdS} G_N} \ . \tag{1.138}$$

The above proposal has been argued to measure the complexity of preparing the reduced density matrix associated to the boundary state. In chapter (5), we have used this proposal to calculate HSC. We have also used this conjecture to calculate the mutual complexity which quantifies the mixed state complexity.

1.4.6 Holographic analogy of mixed state complexity

As we have discussed in section (1.1.5), the CoP has emerged as the measure of complexity associated to a mixed density matrix. In [32, 35, 113], it was suggested that *mutual complexity* is the holographic counter part of CoP. It has the following mathematical form

$$\Delta\mathcal{C} = \mathcal{C}(\rho_{\mathsf{A}}) + \mathcal{C}(\rho_{\mathsf{B}}) - \mathcal{C}(\rho_{\mathsf{AB}}) \tag{1.139}$$

where $\mathsf{A}^c = \mathsf{B}$. The mentioned quantity enables us to measure the rate complexification rate in any of the two subsystem and its effect on the rate of complexity growth in the other subsystem. Furthermore, the roleplay of non-vanishing correlations (between A and B) on the complexity growth can also be probed via $\Delta\mathcal{C}$. One can also verify whether the growth rate of complexity (of a subsystem) can be enhanced by introducing another subsystem or not. However, the concerned subsystems must be correlated to each other. It is easy to note that the definition of $\Delta\mathcal{C}$ can be thought as a combination of multiple complexities and one can apply any of the holographic proposals (CA proposal, CV proposal or the HSC proposal) to compute them. However, the resulting expressions for various holographic proposals are very unlikely to match and this could mean something very interesting is happening here. For example, if one of the holographic proposals leads to the result $\Delta\mathcal{C} > 0$, that is $\mathcal{C}(\rho_{\mathsf{A}}) + \mathcal{C}(\rho_{\mathsf{B}}) > \mathcal{C}(\rho_{\mathsf{AB}})$, then based upon the properties of CoP, one can conclude that they are having the separable result (provided in eq.(**??**)). As opposed to that, if the resulting form reads $\Delta\mathcal{C} < 0$, that is $\mathcal{C}(\rho_{\mathsf{A}}) + \mathcal{C}(\rho_{\mathsf{B}}) < \mathcal{C}(\rho_{\mathsf{AB}})$, then eq.(**??**) suggests that the computed result corresponds to a entangled state.

Chapter 2

Computation of information theoretic measures for deformed $\mathcal{N} = 4$ supersymmetric Yang-Mills theory

In this chapter [1] we would like to discuss different information theoretic measures for deformed super symmetric Yang-Mills theory (SYM). Here we will consider two different kind of diformation of SYM theory, namely, the noncommutative super Yang Mills theory (NCSYM) and dipole deformed super Yang-Mills theory(DSYM). We will use the technique described in section(1.4) to compute different information theoretic measures holographically. These diferomation makes the theory non-local. This motivates us to look into the effct of non locality on different information theoretic measures. We have also found the effect of both noncommutativity and dipole deformation on the different measures of quantum correlation separately. In both the theories, we have found that, there exists a critical length scale above which the HEE obey the area law, and below that length scale HEE obey a volume like law. This is one of most interesting features arises due to the non locality. We have computed different measures of quantum correlations in both the domains of the theory. In the subsequent section we have described those in details. First we have considered the NCSYM theory and it gravity dual to compute those measures. We have also carried out our computation for fininite temperature NCSYM theory by considering black hole in

[1] this chapter is based on [114, 115].

the bulk spacetime. Then we have proceed to the DSYM theory and consider its gravity dual to compute all the mentioned information theoretic measures. In ace of DSYM we have only consider the zero temperature scenario. Another interesting features of NCSYM theory is that, it has the UV-IR mixing properties. On the other hand, in case of DSYM theory we donot have the UV-IR miixing. We will put stress on it in the subsequent discussion.

2.1 Information theoretic measures for NCSYM theory

Noncommutative geometry is one of the very facinating topic of research in recent days for both the physicists and mathematicians. In terms of mathematics, noncommutative geometry is equivalent to a program of unification under the umbrella of the quantum apparatus, which includes the theory of operators and C^*-algebras. Here we will not discuss the mathematical presprective in details, for further details one can go through. Noncommutativity also has wide range of application in different area of physics the reinterpretation of the phenomenological Standard Model of particle physics as a new spacetime geometry, to the quantum Hall effect, strings, renormalization and more in quantum field theory.

One can find the more concrete proof of spacetime noncommutativity from the string theory. In string theory we have an intrinsic length scale l_s, to probe physics at smaller length scale. Therefore we cannot probe the physics at length scale smaller than this characteristics length. Furthermore, very high energy string scattering amplitude suggests the following form of the string modified Heisenberg uncertainty principle

$$\Delta x = \frac{\hbar}{2}\left(\frac{1}{\Delta p} + l_s^2 \Delta p\right) . \tag{2.1}$$

We can recover the ususal quantum mechanical result in the limit $l_s \to 0$.

One can define a noncommutative space, we need to replace the local corrdinates x^i of $\mathbb{R}^d$ by Hermitian operator $\hat{x}^i$, with the following commutation relation

$$[\hat{x}_i, \hat{x}_j] = i\theta_{ij} \tag{2.2}$$

where θ^{ij} is an antisymmetric tensor in i,j, where i,j can take all possible values. In our work we will assume noncommutativity only in a plane, therefore only one coordinate pair of θ_{ij} will be

non-zero. Now we would briefly discuss about the Moyal star product. To motivate this Moyal star product let us consider two dimensional noncommutative plane such that,

$$[\hat{x}_1, \hat{x}_2] = i\theta \;\; ; \;\; [t, \hat{x}_i] = 0 \;\; ; \;\; i = 1, 2 \tag{2.3}$$

where time t is the commutating parameter. At this point, one can either proceed with the quantisation program using operator-valued coordinates or degrade the operators $\hat{x}_1$ and $\hat{x}_2$ to regular c-numbered valued coordinates, where the Moyal star product [116] must perform the compositions of any pair of functions thereof. We would now describe this heuristically, by considering Wely's prescription of constructing Weyl ordered operator $\mathcal{W}[f(\vec{x})]$, from the $c$numbered valued function $g(\vec{x})$ of two commutating variable x_1, x_2. This prescription tells us that, we need to replace $\vec{x}$ occuring in the exponent of the following identity

$$f(\vec{x}) = \frac{1}{(2\pi)^2} \int d^2k \; d^2y e^{\vec{k}.(\vec{x}-\vec{y})} \; f(\vec{y}) \; . \tag{2.4}$$

Now for the operator $\hat{\vec{x}}$, the Weyl order operator is given by

$$\mathcal{W}[f(\vec{x})] = \frac{1}{(2\pi)^2} \int d^2k \; d^2y e^{\vec{k}.(\hat{\vec{x}}-\vec{y})} \; f(\vec{y}) \; . \tag{2.5}$$

Keeping this above definition one can show that, for any pair of functions $f(x_i)$ and $g(x_i)$ the composition should be modified as following

$$\mathcal{W}[f(x_i)]\mathcal{W}[g(x_i)] = \mathcal{W}[(f \star g)(x_i)] \tag{2.6}$$

where

$$(f \star g)(x_i) = e^{(i/2)\theta\epsilon_{ij}\partial_i^x \partial_j^y} f(x_i) g(y_i)|_{y=x} \tag{2.7}$$

In this section we have considered noncommutative super Yang-Mills theory. To make the gauge theory noncommutative we need to define the product of two ordinary function as follows

$$(f \star g)(x) = e^{(i/2)\vartheta^{ij} \frac{\partial}{\partial x^i} \frac{\partial}{\partial x^j}} f(x) g(y)|_{y=x} \; ; \; i, j = 2, 3 \; ; \; x_2 = x, \; x_3 = y \tag{2.8}$$

where $f(x)$ and $g(x)$ are two ordinary functions. The above product is known as the star product [117, 118, 119]. The main motivation to study this kind of deformed star product gauge theory are that, it is non-local in nature and it exhibits the UV-IR mixing properties.

In this chapter we would discuss the effect of noncommutativity on different information theoretic

measures. We have considered a strip like subsystem to compute different information theoretic measures holographically. We have found that, there is critical length scale $\left(\frac{l_c}{a}\right)$, which depends on the UV cut-off. Above this critical length scale HEE follows area like law, and below that length scale HEE obey volume like law. We have obtained the result of HEE both analytically and numerically in different domains of the theory. We have also obtained the relation between the subsystem length $\left(\frac{l}{a}\right)$ and the turning point (au_t) both numerically and analytically. The relationship between the subsystem size (in dimensionless form) $\frac{l}{a}$ and the turning point (in dimensionless form) introduces three domains in the theory. These regions are named as, the deep UV domain ($l < l_c$; $au_t \gg 1$, $au_t \sim au_b$), deep noncommutative domain ($l > l_c,\ au_b > au_t \gg 1$) and deep IR domain ($l > l_c,\ au_t \ll 1$). This in turn means that the length scale l_c distinctly points out the UV/IR mixing property of the non-local theory under consideration. Then we have moved on to the holographic study of entanglement entropy for each of these domains by both analytical and numerical techniques. The broken Lorentz symmetry induced by noncommutativity has motivated us to redefine the entropic c-function. We have obtained the noncommutative correction to the c-function upto leading order in the noncommutative parameter. We have also looked at the behaviour of this quantity over all the domains of the theory. We then move on to compute the minimal cross-section area of the entanglement wedge by considering two disjoint subsystems A and B. Then we proceed to compute entanglement of purification holographically by following the $E_P = E_W$ dualitye. The correlation between two subsystems, namely, the holographic mutual information $I(A : B)$ has also been computed. Moreover, the computations of E_W and $I(A : B)$ has been done for each of the domains in the theory. We have then briefly discussed the effect of the UV cut-off on the IR behaviours of these quantities. Finally, we consider finite temperature NCSYM by considering a black hole geometry with a noncommutative parameter and study the influence of both noncommutativity and finite temperature on the various measures of quantum entanglement.

2.1.1 Dual description of noncommutative super Yang-Mills theory at zero temperature

In [120], it was shown that the non-zero NS-NS B-field leads to noncommutative space on the D-brane which decouples from the closed string excitations. The B-field is introduced by performing a T-duality in a particular direction while the other directions are compactified on a torus. In [121, 122], a stack of $D3$-branes with non-zero B-field (in a certain plane) was considered and it was shown that at a particular decoupling limit, a holographic dual of $SU(N)$ noncommutative super Yang-Mills theory exists. This type IIB gravity dual is described by the following metric in the string frame [121, 122]

$$ds^2 = R^2\left[-u^2dt^2+u^2dy_1^2+u^2h(u)(dy_2^2+dy_3^2)+\frac{du^2}{u^2}\right]+R^2d\Omega_5^2 \tag{2.9}$$

where $h(u)=\frac{1}{1+a^4u^4}$ and $a=\lambda^{1/4}\sqrt{\vartheta}$ is the renormalized noncommutative scale or the NC parameter. The NC parameter is non-zero only in the y_2-y_3 plane with the commutator $[y_2,y_3]=i\vartheta$. The non-vanishing dilaton profile is specified as $e^{2\Phi}=g_s^2h(u)$ where g_s is the string coupling. The t'Hooft coupling constant is related with the AdS radius as $\sqrt{\lambda}=\frac{R^2}{\alpha'}$ where α' is the string tension. Further the only non-vanishing component of the NS-NS B-field reads $B_{23}=R^2a^2u^4h(u)$.
We would like to make a comment now. The (y_2,y_3)-plane collapses in the UV limit, that is, as $u\to\infty$. Hence it is necessary to introduce a UV cutoff. We shall see subsequently that the introduction of this cutoff leads to the presence of a critical length, and the study of entanglement of regions smaller than this critical length needs to be done carefully. For cylindrical entangling regions, the necessity of the cutoff is the following. Without the cutoff, all bulk surfaces would correspond to the same boundary region in the collapsing (x_2,x_3)-plane [123].

2.1.2 Holographic computation of entanglement entropy and UV/IR mixing

To start our computation of information theoretic measures holographically, let us consider a strip like subsystem, A. We can specify the subsystem by the volume $V_{sub}=L^2l$, where $-\frac{l}{2}\leq y_2\leq\frac{l}{2}$ and $y_1,y_3\in[-L,L]$ with $L\to\infty$. We have also assumed that the widths along y_1 and y_3 are fixed and only the width along y_2 can vary. We have made this choice of the subsystem such that,

the effect of nonncommutativity can be captured. Now we would proceed to compute the HEE by following the RT prescription. We would construct the codimension-2 RT surface by considering the parametrization $u = u(y_2)$. Furthermore, the metric given in eq.(2.9) is written in the 10-dimensional string frame with a non-vanishing dilaton, but the calculation should be done in the Einstein frame. Therefore one can rewrite the metric in the Einstein frame by using the following transformation

$$g^E_{\mu\nu} \to e^{-\frac{\phi}{2}} g^S_{\mu\nu} \ . \tag{2.10}$$

Now using the above transformation, we have $\sqrt{g^E_8} = e^{-2\phi}\sqrt{g^S_8}$. Therefore the generalised RT formula for 10-dimensional string frame is given by

$$\begin{aligned} S_{HEE} &= \frac{Area(\Gamma^{min}_A)}{4G^{(10)}} \\ &= \frac{1}{4G^{(10)}_N}\int d^8\xi\ e^{-2\phi}\sqrt{g^S_8} \\ &= \frac{2R^8L^2\mathrm{Vol}(\Omega_5)}{4g_s^2G^{(10)}_N}\int_{-l/2}^{0} u^3\sqrt{1+\frac{u'^2}{u^4h(u)}}dy_2 \quad ; \ u' \equiv \frac{du}{dy_2} \end{aligned} \tag{2.11}$$

where $G^{(10)}_N$ is the $10d$ Newton's constant. It is related with the $5d$ Newton's constant as $G^{(10)}_N = \pi^3R^5G^{(5)}_N$. The integrand in the above equation can be thought as the Lagrangian, then it is easy to see that y_2 is a cyclic coordinate. This means there is a conserved Hamiltonian of the following form

$$\mathcal{H} = -\frac{u^3}{\sqrt{1+\frac{u'^2}{u^4h(u)}}} = constant(c) \ . \tag{2.12}$$

Now we will use the fact that, at the turning point $u = u_t$, $\frac{du}{dx_2} = 0$. Thus one can fix the value of the constant $c = -u_t^3$, which gives us the following differential equation

$$\frac{du}{dx_2} = \sqrt{u^4h(u)\left(\left(\frac{u}{u_t}\right)^6 - 1\right)} \ . \tag{2.13}$$

Now we substitute eq.(2.13) in eq.(2.11) and use the following boundary conditions (this implements the UV cutoff)

$$u(x_2 = \pm\frac{l}{2}) = u_b = \frac{1}{\epsilon} \tag{2.14}$$

this results the following dimensionless form of HEE

$$a^2S_{HEE} = \frac{2R^8L^2\mathrm{Vol}(\Omega_5)}{4g_s^2G^{(10)}_N}(au_t)^2\int_{\frac{au_t}{au_b}}^{1}\frac{\sqrt{p^4+(au_t)^4}}{p^5\sqrt{1-p^6}}dp \tag{2.15}$$

where $p = \frac{au_t}{au}$. On the other hand the subsyemtem length (in dimensionless form) in terms of the bulk coordinate is given by

$$\frac{l}{a} = \frac{2}{au_t}\int_{\frac{au_t}{au_b}}^{1} dp \frac{p\sqrt{p^4+(au_t)^4}}{\sqrt{1-p^6}} \ . \tag{2.16}$$

We can find a explicit relation between the subsystem length and the turning point by performing the above integral by both the numerical and analytical way. Before doing this we would found this relation between turning point and susbsystem length in two different domains of the theory. First we consider the deep IR limit by considering the fact that $au_t << 1$. In deep IR limit one can obtain the following relation

$$\begin{aligned}\left(\frac{l}{a}\right)_{deep\ IR} &\approx \frac{2}{au_t}\int_0^1 dp \frac{p^3}{\sqrt{1-p^6}} \\ &= \frac{2}{(au_t)}\sqrt{\pi}\frac{\Gamma(2/3)}{\Gamma(1/6)} \ .\end{aligned} \tag{2.17}$$

The above result suggests that the deep IR limit leads to the result of ordinary commutative $\mathcal{N}=4$ super Yang-Mills gauge theory ($AdS_5 \times S^5$) in $3+1$-dimensions. This in turn means that one can denote the deep IR limit as the commutative limit of this theory. On the other hand, the deep noncommutative (NC) limit can be incorporated by the fact that, $au_t \gg 1$, and $au_t \ll au_b$ [124], this leads to

$$\begin{aligned}\left(\frac{l}{a}\right)_{deep\ NC} &\approx 2(au_t)\int_0^1 dp \frac{p}{\sqrt{1-p^6}} \\ &= \frac{\sqrt{\pi}}{3}\frac{\Gamma(1/3)}{\Gamma(5/6)}(au_t) \ .\end{aligned} \tag{2.18}$$

The deep UV limit, on the other hand, needs to be analysed very carefully as we shall see later. Our goal is to find an analytical solution by which we can probe the UV-IR mixing property. To proceed further we wolud find the relation between the subsystem length and turning point in two different domains, namely in the domain $au_t \leq 1$ and $au_t \geq 1$. First we will consider the domain where $au_t \leq 1$. In this doamin eq.(2.16) can be written as

$$\frac{l}{a} = \frac{2}{(au_t)}\left[\int_{\frac{au_t}{au_b}}^{au_t} dp \frac{p\sqrt{p^4+(au_t)^4}}{\sqrt{1-p^6}} + \int_{au_t}^{1} dp \frac{p\sqrt{p^4+(au_t)^4}}{\sqrt{1-p^6}}\right] \ . \tag{2.19}$$

In the above eq.(2.19), we have divided the whole integral in two parts. The first integral suggests that, $0 \leq p \leq (au_t)$ and hence $\frac{p}{(au_t)} < 1$. Similarly for the second integral $(au_t) \leq p \leq 1$ and hence

$\frac{(au_t)}{p} < 1$. Now we can make a binomial expansion by keepinng terms upto $\mathcal{O}\left(\frac{p}{au_t}\right)^4$ in the first integral and terms upto $\mathcal{O}\left(\frac{au_t}{p}\right)^4$ in the second integral. This results the following expression for the subsystem size (for $au_t \leq 1$)

$$\begin{aligned}\frac{l}{a} &\approx \frac{\sqrt{\pi}}{2(au_t)}\frac{\Gamma(\frac{5}{3})}{\Gamma(\frac{7}{6})} - (au_t)^3\ln(au_t) + (au_t)^3\sum_{n=1}^{\infty}\frac{1}{\sqrt{\pi}}\frac{\Gamma(n+\frac{1}{2})}{\Gamma(n+1)}\frac{1}{(6n)} - \sum_{n=1}^{\infty}\frac{1}{\sqrt{\pi}}\frac{\Gamma(n+\frac{1}{2})}{\Gamma(n+1)}\frac{(au_t)^{(6n+3)}}{(6n)} \\ &+ \left(\sum_{n=0}^{\infty}\frac{2}{\sqrt{\pi}}\frac{\Gamma(n+\frac{1}{2})}{\Gamma(n+1)}\left[\frac{1-(1/au_b)^{6n+2}}{(6n+2)} - \frac{1}{(6n+4)} + \frac{1-(1/au_b)^{6n+6}}{2(6n+6)}\right]\right)(au_t)^{(6n+3)} \ . \quad (2.20)\end{aligned}$$

On the other hand, in the domain $au_t \geq 1$, the expression for $\left(\frac{l}{a}\right)$ (in eq.(2.16)) reads

$$\begin{aligned}\left(\frac{l}{a}\right) &= 2(au_t)\int_{\frac{au_t}{au_b}}^{1} dp \sum_{n=0}^{\infty}\sum_{m=0}^{\infty}\frac{p}{\sqrt{\pi}}\frac{\Gamma(n+\frac{1}{2})}{\Gamma(n+1)}\frac{\Gamma(\frac{3}{2})}{\Gamma(m+1)\Gamma(\frac{3}{2}-m)}p^{6n}\left(\frac{p}{au_t}\right)^{4m} \\ &= \sum_{n,m=0}^{\infty}\frac{\Gamma(n+\frac{1}{2})}{\Gamma(n+1)\Gamma(m+1)\Gamma(\frac{3}{2}-m)}\frac{1}{(au_t)^{4m-1}}\frac{1}{(6n+4m+2)}\left[1-\left(\frac{au_t}{au_b}\right)^{6n+4m+2}\right] \\ &\approx \sum_{n=0}^{\infty}\frac{\Gamma(n+\frac{1}{2})}{\Gamma(n+1)\Gamma(\frac{3}{2})}(au_t)\frac{1}{(6n+2)}\left[1-\left(\frac{au_t}{au_b}\right)^{6n+2}\right] \\ &\quad + \sum_{n=0}^{\infty}\frac{\Gamma(n+\frac{1}{2})}{\Gamma(n+1)\Gamma(2)\Gamma(\frac{1}{2})}\frac{1}{(au_t)^3}\frac{1}{(6n+6)}\left[1-\left(\frac{au_t}{au_b}\right)^{6n+6}\right] \quad (2.21)\end{aligned}$$

to get the above result we have used the following identities

$$\begin{aligned}\sqrt{1+\left(\frac{p}{au_t}\right)^4} &= \sum_{m=0}^{\infty}\frac{\Gamma(\frac{3}{2})}{\Gamma(m+1)\Gamma(\frac{3}{2}-m)}\left(\frac{p}{au_t}\right)^{4m} \ ; \ \left(\frac{p}{au_t}<1\right) \\ \frac{1}{\sqrt{1-p^6}} &= \sum_{n=0}^{\infty}\frac{1}{\sqrt{\pi}}\frac{\Gamma(n+\frac{1}{2})}{\Gamma(n+1)}(p)^{6n} \ ; \ (p<1) \ . \quad (2.22)\end{aligned}$$

One can observe that, in the limit $a \to 0$, eq.(2.20) one can reproduce the result of commutative SYM theory.

$$\left(\frac{l}{a}\right)_{\text{SYM}} = \frac{2}{\sqrt{\pi}(au_t)}\sum_{n=0}^{\infty}\frac{\Gamma(n+\frac{1}{2})}{\Gamma(n+1)}\frac{1}{(6n+4)}\left[1-\left(\frac{au_t}{au_b}\right)^{6n+4}\right] \ . \quad (2.23)$$

Now we will perform numerically the perform the integral given in eq.(2.16) and compare it with our analytically obtained result given in eq.(2.20) and eq.(2.21).

We would observe that, our analytically computed result matches perfectly with the numerically computed result from Fig.(2.1). The plots have been made for two different values of cutoff

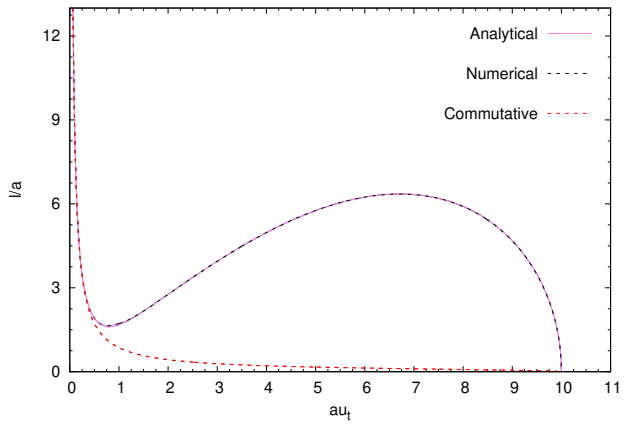

$au_b = 10$

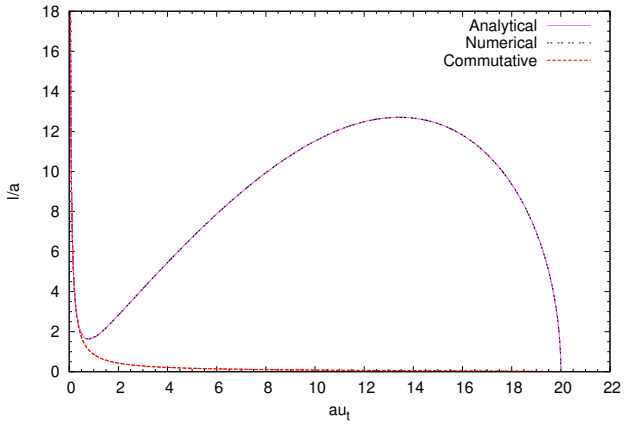

$au_b = 20$

Figure 2.1: In the above figure we have shown the variation of subsystem length (in dimensionless form$\frac{l}{a}$) with respect to turning point (in dimensionless form au_t) for two different values of the cutoff ($au_b = 10, 20$). The dotted curve represents the numerical result and the solid curve dontes the analytical results given in eqs.(2.20,2.21) . The red dotted curve shows the commutative result. To get the analytical plots corresponds to noncommutative case we have used eq.(s)((2.20),(2.21)). It is to be noted that, the value of both the functions matches at $au_t = 1$ and is equal to 1.7255 (for $au_b = 10$) and 1.733 (for $au_b = 20$).

$au_b = 10, 20$. It is to be noted that, for $au_b = 10$, $\frac{l}{a}$ has the first local minimum $\left(\frac{l}{a}\right)_{min} \approx 1.61$ which occurs at $(au_t)_c^{num} \approx 0.78$ (obtained numerically), and for $au_b = 20$, $\left(\frac{l}{a}\right)_{min} \approx 1.64$ at $(au_t)_c^{appr} \approx 0.77$ (obtained using eq.(2.20))[2]. This implies that the domain upto $(au_t)_c$ can be treated as the IR domain, and beyond $(au_t)_c$ it probes the deep noncommutative domain (where $\frac{l}{a}$ is proportional to au_t), and then the deep UV domain. We now try to estimate the value of $(au_t)_c$ analytically by using the results given in eq.(s)(2.17),(2.18). By equating these results of $\frac{l}{a}$ corresponding to deep NC and deep IR limits at $au_t = (au_t)_c$, leads to the following

$$\begin{aligned} \frac{2}{(au_t)_c^{ana}}\sqrt{\pi}\frac{\Gamma(2/3)}{\Gamma(1/6)} &= \frac{\sqrt{\pi}}{3}\frac{\Gamma(1/3)}{\Gamma(5/6)}(au_t)_c^{ana} \\ \Rightarrow (au_t)_c^{ana} &= 0.784\ . \end{aligned} \tag{2.24}$$

We can observe that the analytically estimated value of $(au_t)_c^{ana}$ matches well with that obtained graphically (using the approximate expression for $\frac{l}{a}$ given in eq.(2.20)) and numerically. We can

[2] $(au_t)_c$ is the value of au_t where $\frac{l}{a}$ has the first local minimum.

also observe from Fig.(2.1) the fact that, l goes to zero for large au_t (that is, $au_t \to au_b$) reflecting the fact that extremal surfaces exist for any l. Another important fact is that, there exists some lengths l for which there are more then one turning points. This is one of the signature of UV-IR mixing property. This completes our analysis about the relation of subsystem length and turning point.

Now we shall proceed to compute the expression of $a^2 S_{HEE}$ (given in eq.(2.15)). Similar to the previous analysis, we first compute the expressions of HEE corresponding to the deep IR and deep NC limits. As we have observed earlier, in the deep IR limit, we can get the commutative results. By using this fact and eq.(2.17), we obtain the finite piece of HEE in the deep IR (commutative limit). This reads

$$\left(a^2 \bar{S}_{HEE}|^{finite}\right)_{deep\ IR} = -\frac{\sqrt{\pi}}{4}\frac{\Gamma(2/3)}{\Gamma(1/6)}(au_t)^2 = -(\pi)^{3/2}\left(\frac{\Gamma(2/3)}{\Gamma(1/6)}\right)^3\left(\frac{a}{l}\right)^2 \tag{2.25}$$

where we have used the scaling $\bar{S}_{HEE} = \left(\frac{g_s^2 G_N^{(10)}}{R^8 L^2 \text{Vol}(\Omega_5)}\right) S_{HEE}$. Similarly in the deep NC limit ($\frac{1}{au_t} \approx 0$), the finite piece of HEE reads

$$\left(a^2 \bar{S}_{HEE}|^{finite}\right)_{deep\ NC} = \frac{1}{16\pi^{3/2}}\left(\frac{3\Gamma(5/6)}{\Gamma(1/3)}\right)^3\left(\frac{l}{a}\right)^4 . \tag{2.26}$$

Our next goal is to obtain a general expression of HEE in terms of the turning point. To do this we have followed the similar prescription that we have used to find the relation between subsystem length and the turning point. Therefore, first we will obtain the HEE in the doamin $au_t \leq 1$ by using the result given in eq.(2.15). Keeping this approximation ($au_t \leq 1$) in mind the result of HEE (in the domain $au_t \leq 1$) is given by

$$\begin{aligned}
a^2 \bar{S}_{HEE} &= \frac{(au_t)^2}{2}\left[(au_t)^2 \int_{\frac{au_t}{au_b}}^{au_t} dp \frac{\sqrt{1+(\frac{p}{au_t})^4}}{p^5\sqrt{1-p^6}} + \int_{au_t}^{1} dp \frac{\sqrt{1+(\frac{au_t}{p})^4}}{p^3\sqrt{1-p^6}}\right] \\
&\approx a^2 \bar{S}_{div} + \left(\sum_{n=1}^{\infty}\frac{1}{2\sqrt{\pi}}\frac{\Gamma(n+\frac{1}{2})}{\Gamma(n+1)}\left[\frac{1}{(6n-4)}+\frac{1}{(12n)}-\frac{1}{(6n-2)}\right]\right)(au_t)^{(6n)} \\
&- \sum_{n=2}^{\infty}\frac{1}{4\sqrt{\pi}}\frac{\Gamma(n+\frac{1}{2})}{\Gamma(n+1)}\frac{(au_t)^{(6n)}}{(6n-6)} + \sum_{n=2}^{\infty}\frac{1}{4\sqrt{\pi}}\frac{\Gamma(n+\frac{1}{2})}{\Gamma(n+1)}\frac{(au_t)^6}{(6n-6)} + \sum_{n=0}^{\infty}\frac{1}{2\sqrt{\pi}}\frac{\Gamma(n+\frac{1}{2})}{\Gamma(n+1)}\frac{(au_t)^2}{(6n-2)} \\
&+ \left[\frac{1}{6}-\frac{(au_t)^6}{24}-(au_t)^6\frac{\Gamma(\frac{3}{2})\log(au_t)}{4\sqrt{\pi}}\right] .
\end{aligned} \tag{2.27}$$

In the above result of HEE there is a divergent term which is independent of the turning point, hence it is independent of susbsystem length. The divesrgent piece [51] reads

$$a^2\bar{S}_{div} = \frac{1}{8}(au_b)^4 + \frac{\log(au_b)}{4} \ . \tag{2.28}$$

However, to obtain the correct result correponding to commutative SYM theory we need to take the limit $a \to \frac{1}{u_b}$. Therefore in this limit the finite piece of eq.(2.27) gives the HEE corresponding to the commutative SYM (given in eq.(2.25))

$$a^2\bar{S}_{HEE}|_{deep\ IR} = \sum_{n=0}^{\infty} \frac{1}{2\sqrt{\pi}} \frac{\Gamma(n+\frac{1}{2})}{\Gamma(n+1)} \frac{1}{(6n-2)} (au_t)^2 = -\frac{\sqrt{\pi}}{4} \frac{\Gamma(2/3)}{\Gamma(1/6)} (au_t)^2 \ . \tag{2.29}$$

On the other hand, the expression of HEE in the domain $au_t \geq 1$ reads

$$\begin{aligned} a^2\bar{S}_{HEE} \ \approx \ & \frac{1}{8}\left((au_b)^4 - (au_t)^4\right) - \frac{1}{4}\ln\left(\frac{au_t}{au_b}\right) + \frac{(au_t)^4}{2} \sum_{n=1}^{\infty} \frac{1}{\sqrt{\pi}} \frac{\Gamma(n+\frac{1}{2})}{\Gamma(n+1)} \frac{1}{(6n-4)} \left(1 - \left(\frac{au_t}{au_b}\right)^{6n-4}\right) \\ & + \frac{1}{4}\sum_{n=1}^{\infty} \frac{1}{\sqrt{\pi}} \frac{\Gamma(n+\frac{1}{2})}{\Gamma(n+1)} \frac{1}{6n} \left(1 - \left(\frac{au_t}{au_b}\right)^{6n}\right) \\ & + \frac{1}{4}\sum_{m=2}^{\infty} \frac{\sqrt{\pi}}{\Gamma(m+1)\Gamma(\frac{3}{2}-m)} \frac{1}{(au_t)^{4(m-1)}} \frac{\left(1 - \left(\frac{au_t}{au_b}\right)^{4(m-1)}\right)}{4(m-1)} \\ & + \frac{1}{4}\sum_{n=1}^{\infty}\sum_{m=2}^{\infty} \frac{\Gamma(n+\frac{1}{2})}{\Gamma(n+1)\Gamma(m+1)\Gamma(\frac{3}{2}-m)} \frac{1}{(au_t)^{4(m-1)}} \frac{1}{(6n+4(m-1))} \left(1 - \left(\frac{au_t}{au_b}\right)^{6n+4(m-1)}\right) \ . \end{aligned} \tag{2.30}$$

Note that if we naively pick the limit $a \to 0$, the calculated result of HEE does not yield the commutative result, in contrast to the computed result of $\frac{l}{a}$. The reason for this is that we introduced a dimensionless cut-off au_b to alter the divergence structure. This change links the NC parameter to the cut-off, which is similar to the UV/IR mixing property. The reason for this is as follows. The dual field theory's momentum cut-off, which is inversely proportional to the lattice spacing, is represented by the radial cut-off u_b. Furthermore, the NC parameter ϑ is connected to the momentum cut-off u_b of the lattice field theory for a noncommutative field theory (with noncommutative parameter ϑ). Consequently, it is impossible to use a limiting value of $a = \lambda^{1/4}\sqrt{\vartheta}$ without affecting the momentum.

Now we will reprent our numerical and analytical results graphically. In fig.(2.2), we have compared

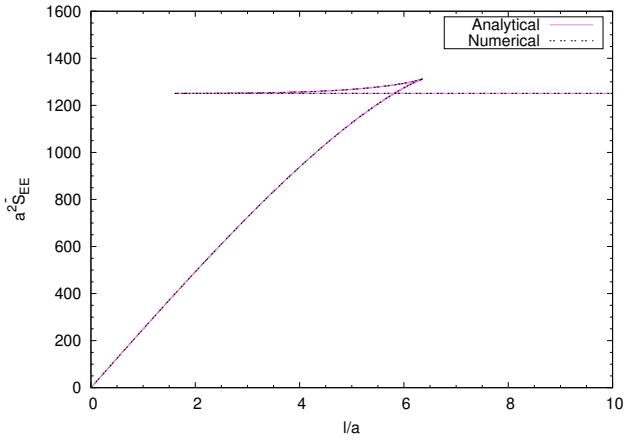

$au_b = 10$

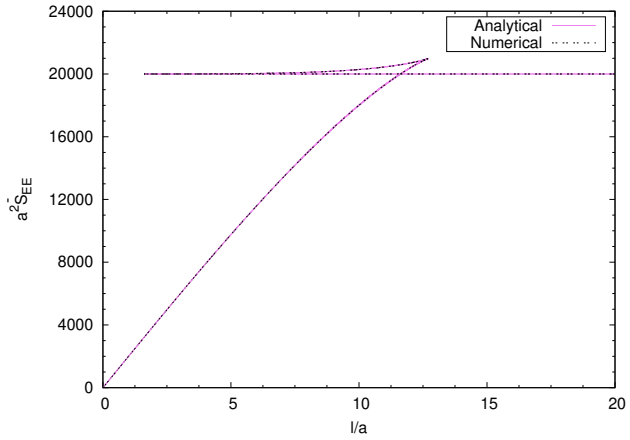

$au_b = 20$

Figure 2.2: The above figure represents the variation of HEE ($a^2\bar{S}_{EE}$) with respect to the subsystem length (in dimensionless form $\frac{l}{a}$) for two different values of cutoff ($au_b = 10, 20$). The solid curve denotes the analytical results which can be obtained by using the results given in eq.(s)((2.20),(2.21),(2.27),(2.30)). On the other hand, the dotted curve represents the numerical result. It is to be observed that, for the noncommutative case, the value of both the functions matches at $au_t = 1$ and is equal to 1250 (for $au_b = 10$) and 2×10^4 (for $au_b = 20$).

our analytically computed result $a^2\bar{S}_{EE}$ (given in eqs.(2.27 , 2.30)) with that obtained numerically from eq.(2.15). We have used only the finite pieces of EE. It is to be noted that, our analytical result is in very good agreement with that obtained numerically. The plots have been made both numerically and analytically for $au_b = 10, 20$.

Now we will proceed to make our analysis in the deep UV domain. To proceed further we would follow [125]. In [125], it was argued that for studying surfaces anchored on small strips, $u(y_2)$ can be expanded in a power series of y_2 (for small y_2)

$$u(y_2) = u_0 + u_1 y_2 + u_2 y_2^2 + \dots . \tag{2.31}$$

Using the fact $u(y_2 = 0) = u_t$ and the boundary condition in eq.(2.14) and substituting this in eq.(2.13), we obtain

$$u(y_2) = u_t + \frac{3}{2}\frac{u_t^3}{[1 + a^4 u_t^4]} y_2^2 + \dots . \tag{2.32}$$

Now substituting $y_2 = \frac{l}{2}$ in the above equation we get [125]

$$u_b = u_t + \frac{3}{8}\frac{u_t^3}{[1 + (au_t)^4]} l^2 + \mathcal{O}\left((l/a)^4\right) . \tag{2.33}$$

This result can be substituted in eq.(2.11) to get

$$\begin{aligned} a^2\bar{S}_{HEE} &= \frac{a^2}{2}\left(\frac{l}{\epsilon^3}-\frac{3}{8}\frac{l^3}{\epsilon a^4}\frac{1}{[1+(\epsilon/a)^4]}-\frac{9}{8}\frac{l^5}{a^8}\frac{\epsilon}{[1+(\epsilon/a)^4]^2}+\mathcal{O}\left((l/a)^7\right)\right) \\ &= \frac{1}{2}\left((au_b)^3\frac{l}{a}-\frac{3}{8}\left(\frac{l}{a}\right)^3\frac{(au_b)}{(1+(1/au_b)^4)}-\frac{9}{8}\left(\frac{l}{a}\right)^5\frac{1}{au_b}\frac{1}{(1+(1/au_b)^4)^2}\right) \\ &+ \mathcal{O}\left((l/a)^7\right) \ . \end{aligned} \tag{2.34}$$

It is to be noted that, we have also provided the finite terms apart from the leading oreder term given in [125]. These finite terms vanishes in the limit $\epsilon \to 0$ in the above equation. To obtain the critical length scale l_c below which we have the deep UV region, we need to equate the leading order leading order divergence term of the above result with that obtained in eq.(2.28). This yields the critical length l_c to be [3]

$$l_c \approx \frac{a^2 u_b}{2} \ . \tag{2.35}$$

One can recast the above result in the dimensionless form as follows

$$\frac{l_c}{a} \approx \frac{a u_b}{2} \ . \tag{2.36}$$

These two results suggest that the critical length scale depends on the UV cutoff of the theory. This is a clear signature of the UV-IR mixing property.

Therefore, the result of HEE given in eq.(2.34) holds for $l < l_c$ and eqs.(2.27 , 2.30) holds for $l > l_c$. Using the relation given in eq.(2.35), one can recast the expression of S_{EE} (given in eq.(2.34)) in the following form

$$\begin{aligned} a^2\bar{S}_{HEE} &= \frac{a^2}{2}\left(\frac{l_c l}{a}\right)\left[\frac{8l_c^2}{a^5}-\frac{3}{4}\left(\frac{1}{1+(\frac{a}{2l_c})^4}\right)\left(\frac{l^2}{a^5}\right)-\frac{9}{16}\left(\frac{1}{1+(\frac{a}{2l_c})^4}\right)^2\left(\frac{l^4}{l_c^2 a^5}\right)+....\right] \\ &= \frac{l_c l}{2}\left[\frac{8l_c}{a^3}-\frac{3}{4}\left(\frac{1}{1+(a/2l_c)^4}\right)\left(\frac{l^2}{a^3}\right)-\frac{9}{16}\left(\frac{1}{1+(a/2l_c)^4}\right)^2\left(\frac{l^4}{a^3 l_c^2}\right)+...\right] \ . \end{aligned} \tag{2.37}$$

We shall now investigate the c-function of the dual field theory holographically. We shall carry out our investigation for $l > l_c$. As we shall see in the subsequent discussion that the deep UV solution (for $l < l_c$) poses problems in the determination of the c-function. For this we now

[3] The left panel of Fig.(2.1) has been plotted for $au_b = 10$. This gives $\frac{l_c}{a} = 5$. Hence, we can see that the critical length $\frac{l_c}{a}$ below which we have the deep UV limit is larger than $\left(\frac{l}{a}\right)_{min}$ which means that an observer in the field theory will not realise that there is a minimum length $\left(\frac{l}{a}\right)_{min}$.

proceed to write down the expression of $a^2\bar{S}_{EE}|^{finite}$ (given in eq.(2.27) for $au_t \leq 1$) in terms of the dimensionless form of the subsystem size $\frac{l}{a}$ (given in eq.(2.20) for $au_t \leq 1$). Keeping the leading order noncommutative correction, eq.(2.20) can be recast as

$$\frac{l}{a} \simeq \frac{\sqrt{\pi}}{2(au_t)}\frac{\Gamma(\frac{5}{3})}{\Gamma(\frac{7}{6})}\left[1+\frac{1}{3\sqrt{\pi}}\frac{\Gamma(7/6)}{\Gamma(5/3)}\left(4+\log 4-6\log(au_t)-6\left(\frac{1}{au_b}\right)^2-\left(\frac{1}{au_b}\right)^6\right)(au_t)^4\right] . \tag{2.38}$$

Now with the above expression in hand and assuming au_t to be very small ($au_t << 1$), we can solve it perturbatively and write down au_t in terms of $\frac{l}{a}$. This reads (for $au_t << 1$)

$$au_t\left(\frac{l}{a}\right) = \frac{\alpha_0}{(\frac{l}{a})}+\frac{\alpha_1}{(\frac{l}{a})^5}+\frac{\alpha_0^4\log(\frac{l}{a})}{(\frac{l}{a})^5} \tag{2.39}$$

where $\frac{au_t}{au_b}$ has been neglected since it is very small. Similarly, we now approximate the expression for $a^2\bar{S}_{EE}|^{finite}$ (given in eq.(2.27)) by keeping the leading order NC correction terms only. This leads to the following expression (for $au_t << 1$)

$$a^2\bar{S}_{HEE}|^{finite} \simeq \frac{1}{6}-\frac{\sqrt{\pi}}{4}\frac{\Gamma(2/3)}{\Gamma(1/6)}(au_t)^2+\frac{1}{48}\left(3+\log 4-6\log(au_t)\right)(au_t)^6 . \tag{2.40}$$

By substituting the expression of turning point au_t (given in eq.(2.39)) in eq.(2.40), we obtain

$$\begin{aligned} a^2\bar{S}_{HEE}\left(\frac{l}{a}\right)|^{finite} &= \frac{1}{6}-\left[\frac{\sqrt{\pi}}{4}\frac{\Gamma(2/3)}{\Gamma(1/6)}-\frac{(3+\log 4)}{48}\left[\frac{\alpha_0}{(\frac{l}{a})}+\frac{\alpha_1}{(\frac{l}{a})^5}+\frac{\alpha_0^4\log(\frac{l}{a})}{(\frac{l}{a})^5}\right]^4\right] \\ &\times \left[\frac{\alpha_0}{(\frac{l}{a})}+\frac{\alpha_1}{(\frac{l}{a})^5}+\frac{\alpha_0^4\log(\frac{l}{a})}{(\frac{l}{a})^5}\right]^2-\left(\frac{1}{8}\right)\left[\frac{\alpha_0}{(\frac{l}{a})}+\frac{\alpha_1}{(\frac{l}{a})^5}+\frac{\alpha_0^4\log(\frac{l}{a})}{(\frac{l}{a})^5}\right]^6 \\ &\times \log\left[\frac{\alpha_0}{(\frac{l}{a})}+\frac{\alpha_1}{(\frac{l}{a})^5}+\frac{\alpha_0^4\log(\frac{l}{a})}{(\frac{l}{a})^5}\right] \end{aligned} \tag{2.41}$$

where

$$\alpha_0 = \frac{\sqrt{\pi}}{2}\frac{\Gamma(\frac{5}{3})}{\Gamma(\frac{7}{6})}; \quad \alpha_1 = \frac{2}{3}\alpha_0^4+\frac{\alpha_0^4}{6}\log 4-\alpha_0^4\log\alpha_0 .$$

The expression given in eq.(2.41) represents HEE for a strip-like subsystem at the boundary. Using the above expression we can holographically compute the c-function of the dual field theory which we shall carry out in the next section.

2.1.3 Holographic computation of the c-function

The c-function is a monotonically decreasing function (under renormalization group flow) measuring the degrees of freedom of the theory and is stationary at the fixed points of the renormalization group flow. Further, the value of the c-function at the fixed points are related to the central charge of the two-dimensional conformal field theory (CFT). In [126, 127], a c-function in terms of the entanglement entropy was computed for two-dimensional CFT. This was a entropic reformulation of the Zamolodchikov theorem [128].

For the EE corresponding to a single interval of length l, the c-function for 2D CFT reads [126, 127, 129]

$$c = 3l\frac{dS_{HEE}}{dl} . \tag{2.42}$$

Following this direction, in [130] a c-function in terms of the EE, for a $d+1$-dimensional CFT has been proposed. It is known that the HEE corresponding to a 'slab' like subsystem is given by [75]

$$S_{HEE} = \alpha\frac{L^{d-1}}{\epsilon^{d-1}} - \frac{1}{(d-1)}\frac{C_d}{\beta}\left(\frac{L}{l}\right)^{d-1} \tag{2.43}$$

where α and β are dimensionless constants, ϵ is the UV regulator and C_d is the central charge. Following the idea of 2D CFT, the following c-function along the RG flow for a $d+1$-dimensional CFT was proposed [130]

$$c = \left(\frac{\beta}{L^{d-1}}\right) l^d \frac{dS_{HEE}}{dl} . \tag{2.44}$$

Without loss of generality, we use the above c-function to characterize the degrees of freedom of NC SYM. It is to be noted that the above mentioned c-function has been proposed for Lorentz invariant theories. On the other hand the full Lorentz symmetry for NC SYM is broken as $SO(3,1) \to SO(1,1) \times SO(2)$. It remains an open problem to construct a c-function for systems with broken Lorentz symmetry. However, we shall use the above definition of the c-function since it can still probe the degrees of freedom of the system and observe the effect of noncommutativity on it. Firstly, we look at the deep IR limit of the NC SYM. In this limit, we have the commutative SYM and the EE reads (given in (2.25))

$$S_{HEE} = \left(\frac{R^8 L^2 \text{Vol}(\Omega_5)}{g_s^2 G_N^{(10)}}\right)\left[S_{div}^{SYM} - \pi^{3/2}\left(\frac{\Gamma(2/3)}{\Gamma(1/6)}\right)^3\left(\frac{1}{l}\right)^2\right] \tag{2.45}$$

where S_{div}^{SYM} represents the universal divergent term of SYM. Now by correctly identifying β and by using the definition (given in (2.44)) for $d = 3$, the c-function for the commutative SYM is obtained to be

$$c = \frac{2R^8 \mathrm{Vol}(\Omega_5)}{g_s^2 G_N^{(10)}} = C^{sym} \ . \tag{2.46}$$

This is also the central charge of the $\mathcal{N} = 4$ SYM theory in $3+1$-dimensions. It is to be noted that this identification of dimensionless quantity β is difficult to carry out for the expression of S_{EE} corresponding to NC SYM (given in (2.27)). Hence, we proceed with the expression given in eq.(2.41). We can recast the expression in the following form

$$\begin{aligned} S_{HEE} &= -\frac{C^{sym}L^2}{2}\frac{1}{\beta_0}\left(\frac{1}{l}\right)^2 + C^{sym}L^2\left[\frac{1}{12a^2} - \frac{a^4\alpha_0^6}{16l^6}\log\Big(\frac{\alpha_0 a}{l}\Big)\right] \\ &+ C^{sym}L^2\frac{a^4\alpha_0}{l^6}\left[\frac{\alpha_0^5(3+\log 4)}{96} - \frac{\sqrt{\pi}}{4}\frac{\Gamma(2/3)}{\Gamma(1/6)}\alpha_1 - \frac{\sqrt{\pi}}{4}\frac{\Gamma(2/3)}{\Gamma(1/6)}\alpha_0^4\log\left(\frac{l}{a}\right)\right] \end{aligned} \tag{2.47}$$

where we have identified $C^{sym} = \frac{R^8 Vol(\Omega_5)}{g_s^2 G_N^{10}}$ and $\beta_0 = \frac{4\Gamma(1/6)}{\sqrt{\pi}\Gamma(2/3)\alpha_0^2}$. It is to be noted that the first term is the usual one which we get from the commutative SYM in $3+1$-spacetime dimensions. We now introduce a l-dependent β, namely, $\beta(l)$ and recast the above expression in the form

$$S_{HEE} = \frac{C^{sym}L^2}{12a^2} - \frac{C^{sym}L^2}{2\beta(l)l^2} \tag{2.48}$$

where

$$\begin{aligned} \frac{1}{\beta(l)} &= \frac{1}{\beta_0} - \alpha_0\left(\frac{a}{l}\right)^4\left\{\frac{\alpha_0^5(3+\log 4)}{48} - \frac{\sqrt{\pi}}{2}\frac{\Gamma(2/3)}{\Gamma(1/6)}\alpha_1 - \frac{\sqrt{\pi}}{2}\frac{\Gamma(2/3)}{\Gamma(1/6)}\alpha_0^4\log\left(\frac{l}{a}\right)\right. \\ &- \left.\frac{\alpha_0^5}{8}\log\Big(\frac{\alpha_0 a}{l}\Big)\right\} \end{aligned} \tag{2.49}$$

We now define the entropic c-function in the following way

$$c = \frac{\beta(l)}{L^2}l^3\frac{dS_{HEE}}{dl} \ . \tag{2.50}$$

Computation of the above expression leads to the following

$$\begin{aligned} \frac{c}{C^{sym}} &= 1 - \beta_0\left(\frac{a}{l}\right)^4\alpha_0\left[\frac{(3+\log 4)}{24}\alpha_0^5 - \sqrt{\pi}\frac{\Gamma(2/3)}{\Gamma(1/6)}\alpha_1 - \sqrt{\pi}\frac{\Gamma(2/3)}{\Gamma(1/6)}\alpha_0^4\log\left(\frac{l}{a}\right) - \frac{\alpha_0^5}{4}\log\Big(\frac{\alpha_0 a}{l}\Big)\right. \\ &+ \left.\frac{\sqrt{\pi}}{4}\alpha_0^4\frac{\Gamma(2/3)}{\Gamma(1/6)} + \frac{\alpha_0^5}{16}\right] \ . \end{aligned} \tag{2.51}$$

It can be observed that the first term in the above equation is the central charge of the commutative theory whereas the rest probes the signature of a Lorentz violating theory induced by noncommutativity. It can be noted that in the deep IR limit the c-function of the NCYM approaches the constant value C^{sym} corresponding to the commutative Yang-Mills theory. For large $\frac{l}{a}$, (for $au_b = 10$), eq.(2.51) yields $\frac{c}{C^{sym}} = 1$ which agrees very well with the numerical result. There is a small difference between the two results only at the third decimal place.

Before ending this discussion we would like to point out that in the deep UV limit ($l < l_c$), the definition of c-function (given in eq.(2.44)) runs into a problem because of the non-locality of the theory which leads to the violation of area law for S_{EE}. To see this we compute and graphically represent the c-function for all possible values of $\frac{l}{a}$.

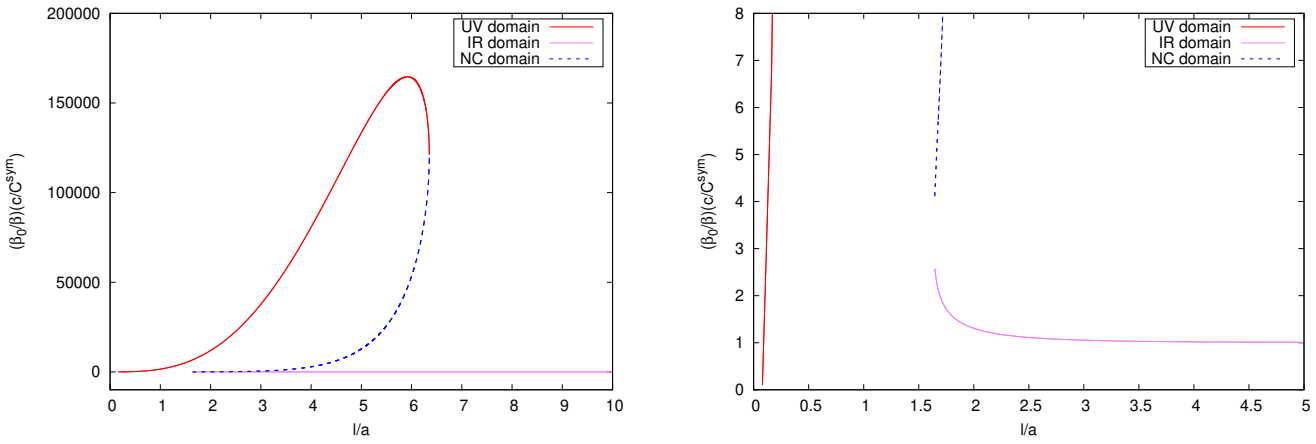

Behaviour of the c-function in each domain

Discontinous nature of the c-function

Figure 2.3: The above figure represents the varition of the c-function for all possible values of subsystem length $\frac{l}{a}$. To get this plot we set au_b=10.

In Fig.(2.3), we have plotted $\left(\frac{\beta_0}{\beta}\right)\left(\frac{c}{C^{sym}}\right)$ in the vertical axis and in the horizontal axis we have plotted $\frac{l}{a}$. In the left panel of Fig.(2.3), we observe that in the IR domain the ratio $\left(\frac{\beta_0}{\beta}\right)\left(\frac{c}{C^{sym}}\right)$ apporaches unity, that is, the c-function of NC SYM matches with that of SYM. Interestingly, we observe that there are discontinuous jumps in the quantity (see right panel of Fig.(2.3)) which is due to the swallowtail behaviour of the HEE. These jumps appear at the junction between the IR and NC domains of the theory, and the junction between the NC and UV domains (see Fig.(2.4)) of the theory. The discontinuities in the c-function therefore correspond to the transitions from one domain to the other, in particular the discontinuity between the IR and the NC domains

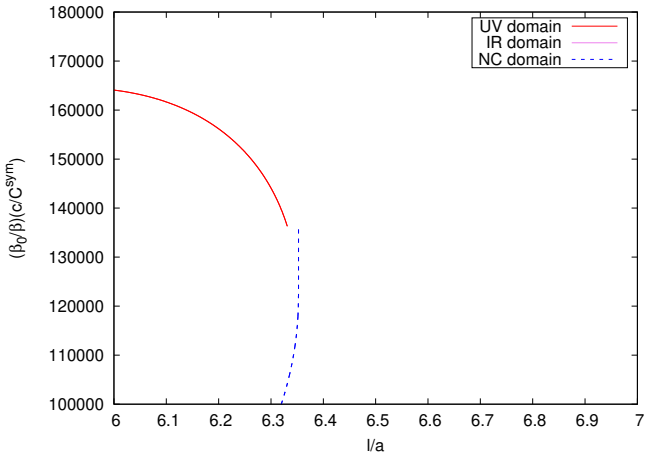

Figure 2.4: This figure reprensents the discontinuty in the c-function at the UV and the NC junction.

correspond to a transition from the area to the volume law for the HEE.

2.1.4 Entanglement wedge cross section

Now we will proceed to compute the entanglement of purification holographically. The holographic counterpart of EoP is knowns as the entanglement wedge cross section. The computation is based on the $E_P = E_W$ duality [4]. We have discussed this duality in details in section(1.4.3). To proceed further we would consider following setup. We would consider two strip like subsystems on the boundary theory ∂M (∂M is the boundary of a time-slice M we have considered in the gravity dual). We denote these subsystems as A and B with both of them having the same length l. Further we consider that A and B are separated by a distance d with the condition $A \cap B = 0$. This in turn means that EWCS is the vertical constant y_2 hypersurface with minimal area which splits the entanglement wedge of AB (that is,M_{AB}) into two domains corresponding to A and B. The time induced metric on this constant y_2 hypersurface reads

$$ds^2_{ind} = R^2\left[u^2 dy_1^2 + u^2 h(u) dy_3^2 + \frac{du^2}{u^2}\right] + R^2 d\Omega_5^2 \ . \tag{2.52}$$

Now using this above induced metric and the formula given in eq.(1.129). This results the following expression of EWCS

$$\begin{aligned} a^2 E_W &= a^2 \frac{R^8 L^2 \text{Vol}(\Omega_5)}{4 g_s^2 G_N^{(10)}} \int_{u_t(2l+d)}^{u_t(d)} u\sqrt{1+a^4u^4}\, du \\ &= \frac{R^8 L^2 \text{Vol}(\Omega_5)}{4 g_s^2 G_N^{(10)}} \left[\frac{1}{4}\left((au_t(d))^2\sqrt{1+(au_t(d))^4} - (au_t(2l+d))^2\sqrt{1+(au_t(2l+d))^4}\right)\right. \\ &+ \left.\frac{1}{4}\left(\sinh^{-1}\left((au_t(d))^2\right) - \sinh^{-1}\left((au_t(2l+d))^2\right)\right)\right] \quad . \end{aligned} \tag{2.53}$$

Keeping this result in mind we will explicitly check the following inequality

$$E_W \geq \frac{1}{2} I(A:B) \ . \tag{2.54}$$

where $I(A:B)$ is the holographic mutual information (HMI) defined as

$$I(A:B) = 2S_{HEE}(l) - S_{HEE}(d) - S_{HEE}(2l+d) \ . \tag{2.55}$$

In the above expression we have used the fact $S_{HEE}(A\cup B) = S_{HEE}(2l+d) + S_{HEE}(d)$, for "small" d/l.

In [4] it is shown that, for a given subsystem length (l), there exists a critical separation distance ($d_c < l$) between the two subsystems A and B above which there is no connected phase. We shall also see this feature in our study. This means that the codimension-0 bulk region M_{AB} (entanglement wedge) will be disconnected and therefore results in vanishing $E_W(\rho_{AB})$. Up to this critical separation length d_c, the mutual information $I(A:B)$ is non-zero and the RT surface Γ_{AB}^{min} is in connected phase which leads to a non-vanishing E_W. However beyond this critical separation length d_c, the mutual information $I(A:B) = 0$ and Γ_{AB}^{min} is in disconnected phase which results in a vanishing E_W. The value of this critical separation length d_c can be computed from the vanishing condition of the mutual information at $d = d_c$. This can be formally written as [123, 131]

$$I(A:B) = 2S_{HEE}(l) - S_{HEE}(d_c) - S_{HEE}(2l+d_c) = 0 \ . \tag{2.56}$$

In the domain $au_t \leq 1$, the result of EWCS in eq.(2.53) can be simplified as

$$a^2 \bar{E}_W = \frac{1}{8}\left[\left(au_t\left(d\right)\right)^2 - \left(au_t\left(2l+d\right)\right)^2\right] + \frac{1}{32}\left[\left(au_t\left(d\right)\right)^6 - \left(au_t\left(2l+d\right)\right)^6\right] \tag{2.57}$$

where $\bar{E}_W = \left(\frac{g_s^2 G_N^{(10)}}{R^8 L^2 \text{Vol}(\Omega_5)}\right) E_W$. In the above expression, $au_t\left(d\right)$ and $au_t\left(2l+d\right)$ represents the turning points associated with the RT surfaces Γ_d^{min} and Γ_{2l+d}^{min}.

To investigate the bound mentioned in eq.(2.54), we must calculate the expression of $I(A:B)$. In order to accomplish this, we use the expressions for $a^2\bar{S}_{HEE}\left(\frac{l}{a}\right)$ for $au_t \leq 1$ provided in eq.((2.27)) and $\frac{l}{a}$ for $au_t \leq 1$ given in eq.(2.20). Only finite piece of HEE will contribute to the HMI. Similarly expressions of HEE for subsystems of length $(2l+d)$ and d can be obtained from eq.(2.27). [4] For our further analysis we will consider the following dimensionless form of holographic mutual information

$$a^2\bar{I}(A:B) = 2a^2\bar{S}_{HEE}\left(\frac{l}{a}\right) - a^2\bar{S}_{HEE}\left(\frac{d}{a}\right) - a^2\bar{S}_{HEE}\left(\frac{2l+d}{a}\right) \tag{2.58}$$

where $a^2\bar{S}_{EE}$ is given in eq.(2.27), and we have used the scaling $\bar{I} = \left(\frac{g_s^2 G_N^{(10)}}{R^8 L^2 \text{Vol}(\Omega_5)}\right) I$. We would compute the result of EWCS and HMI in different doamins of the theory. We will start with deep-IR domain. In the deep IR (commutative, $au_t << 1$) limit, the expressions for E_W and $I(A:B)$ (in dimensionless form) reads

$$a^2\bar{E}_W|_{deep\ IR} = \frac{1}{8}\left(2\sqrt{\pi}\frac{\Gamma(2/3)}{\Gamma(1/6)}\right)^2\left[\frac{1}{\left(\frac{d}{a}\right)^2} - \frac{1}{\left(\frac{2l+d}{a}\right)^2}\right] \tag{2.59}$$

$$a^2\bar{I}(A:B)|_{deep\ IR} = -\pi^{3/2}\left(\frac{\Gamma(2/3)}{\Gamma(1/6)}\right)^3\left[\frac{2}{\left(\frac{l}{a}\right)^2} - \frac{1}{\left(\frac{d}{a}\right)^2} - \frac{1}{\left(\frac{2l+d}{a}\right)^2}\right]. \tag{2.60}$$

Siliarly, in the deep noncommutative limit ($1 << au_t << au_b$), the expressions for E_W and $I(A:B)$ (in dimensionless form) reads

$$a^2\bar{E}_W|_{deep\ NC} = \frac{1}{16}\left(\frac{3}{\sqrt{\pi}}\frac{\Gamma(5/6)}{\Gamma(1/3)}\right)^4\left[\left(\frac{d}{a}\right)^4 - \left(\frac{2l+d}{a}\right)^4\right] \tag{2.61}$$

$$a^2\bar{I}(A:B)|_{deep\ NC} = \frac{1}{16\pi^{3/2}}\left(\frac{3\Gamma(5/6)}{\Gamma(1/3)}\right)^3\left[2\left(\frac{l}{a}\right)^4 - \left(\frac{d}{a}\right)^4 - \left(\frac{2l+d}{a}\right)^4\right]. \tag{2.62}$$

Now in the deep UV limit to get the result of EWCS we substitute eq.(2.33) in eq.(2.53). This

[4] The divergent pieces of the HEEs are independent of subsystem size information so they cancel out and do not contribute.

results

$$
\begin{aligned}
16a^2\bar{E}_W &= \left(au_b - \frac{3}{8}\frac{(au_b)^3}{1+(au_b)^4}\left(\frac{d}{a}\right)^2\right)^2\sqrt{1+\left(au_b - \frac{3}{8}\frac{(au_b)^3}{1+(au_b)^4}\left(\frac{d}{a}\right)^2\right)^4} \\
&- \left(au_b - \frac{3}{8}\frac{(au_b)^3}{1+(au_b)^4}\left(\frac{2l+d}{a}\right)^2\right)^2\sqrt{1+\left(au_b - \frac{3}{8}\frac{(au_b)^3}{1+(au_b)^4}\left(\frac{2l+d}{a}\right)^2\right)^4} \\
&+ \sinh^{-1}\left(\left(au_b - \frac{3}{8}\frac{(au_b)^3}{1+(au_b)^4}\left(\frac{d}{a}\right)^2\right)^2\right) - \sinh^{-1}\left(\left(au_b - \frac{3}{8}\frac{(au_b)^3}{1+(au_b)^4}\left(\frac{2l+d}{a}\right)^2\right)^2\right).
\end{aligned}
\tag{2.63}
$$

Similarly in this doamin the expression of HMI can be obtained by substituting eq.(2.34) in the expression for mutual information eq.(2.58) [5]. This yields

$$
\begin{aligned}
a^2\bar{I}(A:B) &= \left(-\left(\frac{d}{a}\right)(au_b)^3 + \left(\frac{3}{16}\right)(au_b)\frac{6\left(\frac{l}{a}\right)^3 + 2\left(\frac{d}{a}\right)^3 + 12\left(\frac{l}{a}\right)^2\left(\frac{d}{a}\right) + 6\left(\frac{l}{a}\right)\left(\frac{d}{a}\right)^2}{1+(\frac{1}{au_b})^4}\right. \\
&+ \left.\left(\frac{9}{16au_b}\right)\frac{30\left(\frac{l}{a}\right)^5 + 2\left(\frac{d}{a}\right)^5 + 80\left(\frac{l}{a}\right)^4\left(\frac{d}{a}\right) + 40\left(\frac{l}{a}\right)^2\left(\frac{d}{a}\right)^3 + 10\left(\frac{l}{a}\right)\left(\frac{d}{a}\right)^4}{(1+(\frac{1}{au_b})^4)^2}\right).
\end{aligned}
\tag{2.64}
$$

The above result suggests that, the holographic mutual information is a divergent quantity in the deep UV regime. However, we know that the mutual information is in general UV finite quantity. As the divergent part of HEE in this doamin depends on the subsystem size, therefore the diverget pieces are not cancelled. That is why the HMI is a divergent quantity in the dee-UV domain. This observation was made earlier in [125]. On the other hand, EWCS is also a divergebt quantity in this deep UV domain. Further, we note that, in the deep UV limit, the evaluation of $a^2\bar{I}(A:B)$ (given in eq.(2.64)) produces negative values for all possible $\frac{d}{a}$. The result therefore indicates that this phase is not physical.

We now represent our results graphically and find out how the noncommutativity effects the EWCS and holographic mutual information.

The plots given in Fig.(2.5) shows the variation of $a^2\bar{E}_W$ and $\frac{a^2}{2}\bar{I}(A:B)$ with respect to the separation distance $\frac{d}{a}$ for both noncommutative (given in eq.(s)(2.57),(2.58)) and commutative

[5] Once again we consider two subsystems of equal length $l < l_c$ kept at a distance $d < l$, and also consider $2l + d < l_c$.

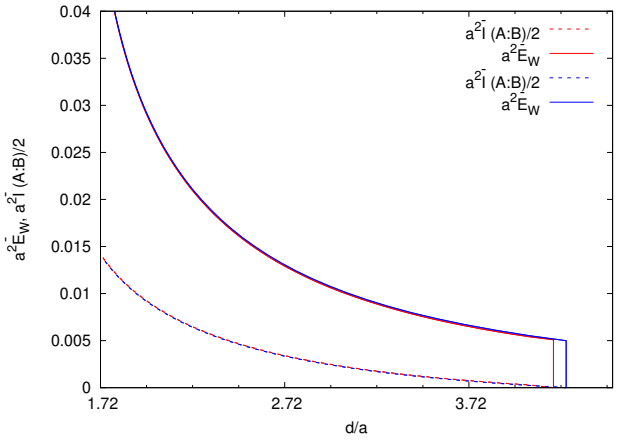

Noncommutative Yang-Mills theory

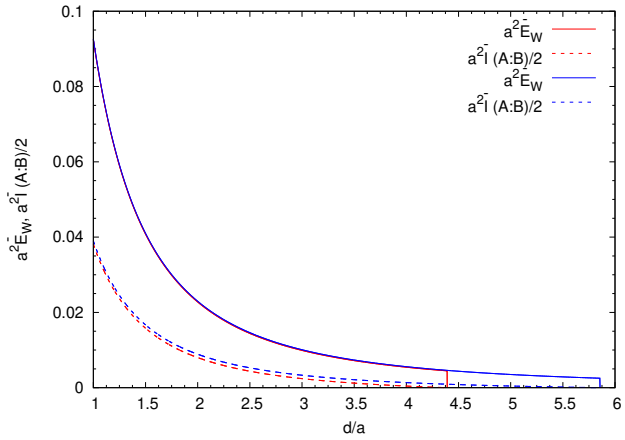

Commutative (deep IR) Yang-Mills theory

Figure 2.5: In this figure we have represented the effect of noncommutativity on EWCS and HMI (we have chosen two values for $\frac{l}{a}$, $\frac{l}{a} = 6$ (red) and $\frac{l}{a} = 8$ (blue)). In the left panel of figure we have plotted the analytical results of EWCS and HMI with repect to the separation distance, which are given by eqs.(2.57,2.58) (for $au_t \leq 1$) with $au_b = 10$. The curve in the right panel depicts the analytical results of EWCS and HMI given in eqs.(2.139,2.132) (deep IR/ commutative limit) .

Yang-Mills theory. To get these plots for $a^2\bar{E}_W$ and $\frac{a^2}{2}\bar{I}(A:B)$ in the noncommuative domain, we need the help of rsults given in eq.(s)(2.20, 2.27) which are valid for $au_t \leq 1$. Onecan obtain the results of the commuatative theory (given in eq.(s)(2.59),(2.60)) by taking the deep IR limit. The polts suggests that, the bound $a^2E_W \geq \frac{1}{2}a^2I(A:B)$ holds for both the commoutative and nocommutative domain. One can also observe that, the value of critical separation point or the point of phase transition (from connected to disconnected phase of M_{AB}) increases for increase in the value of $\frac{l}{a}$. We would also like to mention that, to get the polts for noncommuataive case we have chosen the lower limit of the $\frac{d}{a}$ axis in such a way so that $au_t(d) \leq 1$. Furthermore, the values of $\frac{l}{a}$ are also chosen in order to make $au_t(2l+d),\ au_t(l) \leq 1$. The domain for which $\frac{d}{a} < 1.61$ is not allowed as it corresponds to $au_t >> 1$ for which the above analysis breaks down.
Furthermore, its is to be noted that, the expressions $a^2\bar{E}_W$ and $a^2\bar{I}(A:B)$ (given in eq(s).(2.61),(2.62)) produces negative values for all possible values of $\frac{d}{a}$ in the deep NC limit. Therefore this result indicates that it cannot be a physical phase, which signals that the disconnected phase is the physical phase and therefore both E_W and $I(A:B)$ are zero.
We now study the effect of UV/IR mixing on the EWCS and HMI. By UV/IR mixing we intend

to investigate the effect of the UV cut-off on the IR result [125]. We compute the above quantities for two different values of the UV cut-off, namely, $au_b = 10, 20$.

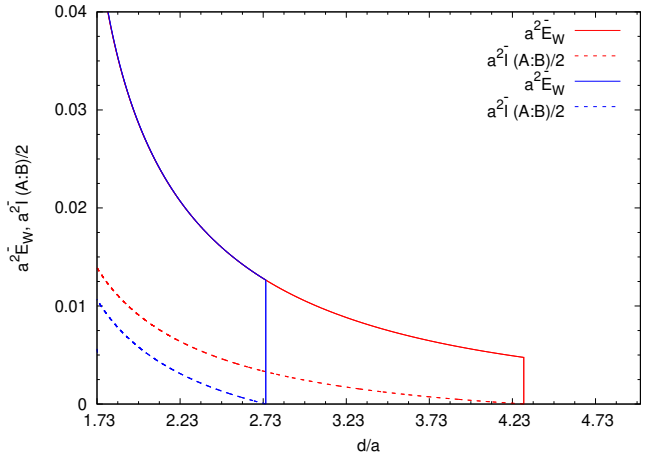

Figure 2.6: In the above figure we have depicted the effect of UV/IR mixing on EWCS and HMI . In the above plot the blue curves (both solid and dotted) correspond to $au_b = 20$ and the red curves (both solid and dotted) correspond to $au_b = 10$. We have set $\frac{l}{a} = 6$.

From Fig.(2.6), we can see clearly the prominent effect of the UV cut-off on the EWCS and HMI. The effect of the UV cut-off on these quantities is a signature of the UV/IR mixing [125]. In particular, we observe that for a fixed subsystem length $\frac{l}{a}$, the HMI and EWCS vanishes at a smaller value of separation $\frac{d}{a}$ for a larger cut-off value. This shows the sensitivity of the IR results on the UV cut-off. We make one more comment. In the IR domain, the HEE obeys an area law (eq.(2.28)) in contrast to the UV domain (eq.(2.34)) where it obeys a volume law. This is consistent with the fact that in the deep IR limit, the HEE reduces to the Bekenstein-Hawking entropy of the black hole. The fact that in the UV limit, the HEE obeys a volume law implies that it has an extensive behaviour unlike the IR behaviour.

2.1.5 Holographic entanglement entropy at finite temperature

So far we have discussed different measures of quantum correlation for zero temperature scenario. Now we would proceed to the information theoretic aspects of NC Yang-Mills theory at a finite temperature. To make further progress we have considered a black hole geometry in the bulk

to include the effect of temperature. The dual gravitational theory is described by the following metric

$$ds^2 = R^2\Big[-u^2 f(u)dt^2 + u^2 dy_1^2 + u^2 h(u)(dy_2^2+dy_3^2) + \frac{du^2}{u^2 f(u)}\Big] + R^2 d\Omega_5^2 \tag{2.65}$$

where $f(u) = 1-\left(\frac{u_H}{u}\right)^4$ and u_H is black hole horizon. Further it is related with the Hawking temperature T_H of the black hole as $T_H = \frac{u_H}{\pi}$.

Now we will proceed to compute the HEE of a strip like subsystem A at the boundary by following the same set up we have used previously given in section.(2.1.2). This leads to the following integral for HEE(S_{HEE})

$$S_{HEE} = \frac{2R^8 L^2 Vol(\Omega_5)}{4g_s^2 G_N^{10}} \int_{-l/2}^{0} \frac{u^2}{\sqrt{h(u)}} \left(u^2 h(u) + \frac{u'^2}{u^2 f(u)}\right)^{\frac{1}{2}} dy_2 \ . \tag{2.66}$$

Again considering the integrant of the above equation as Lagrangian one can argue that, y_2 is a cyclic coordinate. This gives rise to the following conserved Hamiltonian

$$\mathcal{H} = -\frac{u^4}{\left(u^2 + \frac{u'^2}{u^2 f(u)h(u)}\right)^{\frac{1}{2}}} = constant(c') = -u_t^3 \ . \tag{2.67}$$

We can find the constant using the fact that at the turning point (u_t), $\frac{du}{dy_2}$ vanishes. This now results in the following differential equation

$$\frac{du}{dy_2} = \sqrt{u^4 h(u) f(u)\left(\left(\frac{u}{u_t}\right)^6 - 1\right)} \ . \tag{2.68}$$

Now substituting the result in eq.(2.66) and using the boundary condition 2.14 yields

$$a^2 \bar{S}_{HEE} = \frac{1}{2}(au_t)^2 \int_{\frac{au_t}{au_b}}^{1} \frac{\sqrt{p^4+(au_t)^4}}{p^5\sqrt{1-p^6}\sqrt{1-\eta^4 p^4}} dp \ ; \quad \eta = \frac{au_H}{au_t} \quad ; \quad p = \frac{au_t}{au} \ . \tag{2.69}$$

We have performed the above integral analytically by incorporating the low temperature approximation. This can be done by assuming the fact that, the dimensionless parameter $\eta \ll 1$ is small.

Thus in the domain $au_t \leq 1$, we have the following expression for HEE

$$
\begin{aligned}
a^2\bar{S}_{HEE} &\simeq \frac{1}{2}(au_t)^2\left[\int_{\frac{au_t}{au_b}}^{1}\frac{\sqrt{p^4+(au_t)^4}}{p^5\sqrt{1-p^6}}dp+\frac{\eta^4}{2}\int_{\frac{au_t}{au_b}}^{1}\frac{\sqrt{p^4+(au_t)^4}}{p\sqrt{1-p^6}}dp\right] \\
&\approx a^2\bar{S}_{div}+\left(\sum_{n=1}^{\infty}\frac{1}{2\sqrt{\pi}}\frac{\Gamma(n+\frac{1}{2})}{\Gamma(n+1)}\left[\frac{1}{(6n-4)}+\frac{1}{(12n)}-\frac{1}{(6n-2)}\right]-\sum_{n=2}^{\infty}\frac{1}{4\sqrt{\pi}}\frac{\Gamma(n+\frac{1}{2})}{\Gamma(n+1)}\frac{1}{(6n-6)}\right) \\
&\times (au_t)^{(6n)}+\sum_{n=2}^{\infty}\frac{1}{4\sqrt{\pi}}\frac{\Gamma(n+\frac{1}{2})}{\Gamma(n+1)}\frac{(au_t)^6}{(6n-6)}+\sum_{n=0}^{\infty}\frac{1}{2\sqrt{\pi}}\frac{\Gamma(n+\frac{1}{2})}{\Gamma(n+1)}\frac{(au_t)^2}{(6n-2)} \\
&+ \left[\frac{1}{6}-\frac{(au_t)^6}{24}-(au_t)^6\frac{\Gamma(\frac{3}{2})\log(au_t)}{4\sqrt{\pi}}\right]+\frac{\eta^4}{4}\left[(au_t)^2\sum_{n=0}^{\infty}\frac{1}{\sqrt{\pi}}\frac{\Gamma(n+(1/2))}{\Gamma(n+1)}\frac{1}{6n+2}\right. \\
&+ \frac{(au_t)^4}{2}\sum_{n=0}^{\infty}\frac{1}{\sqrt{\pi}}\frac{\Gamma(n+(1/2))}{\Gamma(n+1)}\frac{1}{6n-2}+\left(\sum_{n=0}^{\infty}\frac{1}{\sqrt{\pi}}\frac{\Gamma(n+(1/2))}{\Gamma(n+1)}\left[\frac{1}{2(6n+4)}-\frac{1}{6n+2}-\frac{1}{6n-2}\right]\right. \\
&\left.\left.+\sum_{n=1}^{\infty}\frac{1}{\sqrt{\pi}}\frac{\Gamma(n+(1/2))}{\Gamma(n+1)}\frac{1}{6n}\right)(au_t)^{6n+4}\right]. \qquad (2.70)
\end{aligned}
$$

The above expression suggests that, similar to the zero temperature secnario in this case case also the HEE contains a universal divergent piece, which is independent of subsystem length. The divergent piece in the above expression reads

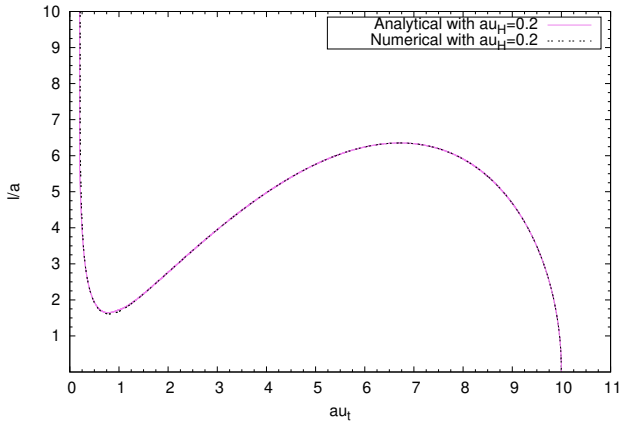

Variation of $\frac{l}{a}$ with respect to au_t with $au_H = 0.2$.

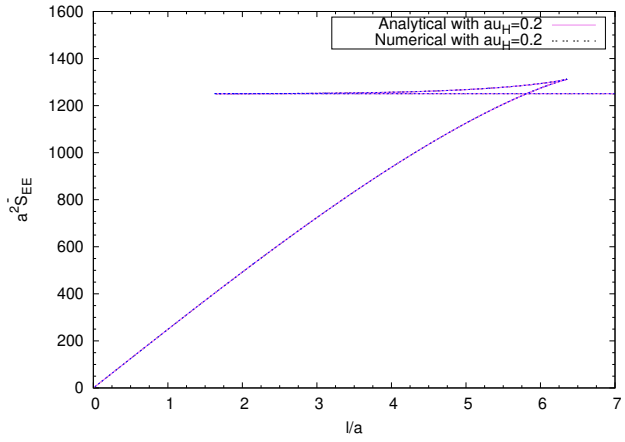

Variation of the $a^2\bar{S}_{EE}$ with respect to $\frac{l}{a}$ at $au_H = 0.2$.

Figure 2.7: In the left panel of the above figure we have represented the variation of subsystem length ($\frac{l}{a}$) with respect to turning point (au_t), and in the right panel we have shown the variation of HEE ($a^2\bar{S}_{EE}$) with respect to subssytem length ($\frac{l}{a}$). In both the plots we have set $au_b = 10$.

$$a^2\bar{S}_{div} = \frac{1}{8}(au_b)^4 + \frac{\log(au_b)}{4} + \frac{(a\pi T)^4}{4}\log(au_b)\ . \tag{2.71}$$

The above expression of the divergent term suggests that, it contains a temperature dependent term. In the limit $T \to 0$ we can recover the divergent term corresponding to the zero temperature scenario. We can interpert this as one of the unique feature of NCSYM theory as in general the divergent piece does not depend on the temperature.

Now we will proceed to find a expression of the finite part of HEE at the low temperature limit. In this limit $au_H \ll au_t \leq 1$ the finite part of HEE reads

$$\begin{aligned} a^2\bar{S}_{HEE}|^{finite} &\simeq \left[\frac{1}{6} - \frac{\sqrt{\pi}}{4}\frac{\Gamma(2/3)}{\Gamma(1/6)}(au_t)^2 + \frac{1}{48}\left(3 + \log 4 - 6\log(au_t)\right)(au_t)^6\right] \\ &- \eta^4\left[\frac{(au_t)^4}{32} + \frac{\sqrt{\pi}(au_t)^6}{16}\frac{\Gamma(2/3)}{\Gamma(1/6)} - \frac{\sqrt{\pi}(au_t)^2}{8}\frac{\Gamma(4/3)}{\Gamma(5/6)} + \frac{(au_t)^{10}}{240}\right]\ . \end{aligned} \tag{2.72}$$

Now we would proceed to compute the result of HEE for $au_t \geq 1$. The result of HEE in this doamin reads

$$\begin{aligned} a^2\bar{S}_{HEE} &= \frac{1}{8}\left((au_b)^4 - (au_t)^4\right) - \frac{1}{4}\ln\left(\frac{au_t}{au_b}\right) + \frac{1}{4}\sum_{m=2}^{\infty}\frac{\sqrt{\pi}}{\Gamma(m+1)\Gamma(\frac{3}{2}-m)}\frac{1}{(au_t)^{4(m-1)}}\frac{\left(1-\left(\frac{au_t}{au_b}\right)^{4(m-1)}\right)}{4(m-1)} \\ &+ \frac{1}{4}\sum_{n=1}^{\infty}\sum_{m=0}^{\infty}\frac{\Gamma(n+\frac{1}{2})}{\Gamma(m+1)\Gamma(\frac{3}{2}-m)\Gamma(n+1)}\frac{1}{\sqrt{\pi}}\frac{1}{(au_t)^{4(m-1)}}\frac{\left(1-\left(\frac{au_t}{au_b}\right)^{6n+4(m-1)}\right)}{6n+4(m-1)} \\ &+ \frac{(au_H)^4}{4}\Bigg[\ln(au_b) + \sum_{m=1}^{\infty}\frac{\Gamma(3/2)}{\Gamma(m+1)\Gamma(\frac{3}{2}-m)}\frac{1}{(au_t)^{4m}}\frac{\left(1-\left(\frac{au_t}{au_b}\right)^{4m}\right)}{4m} \\ &+ \sum_{n=1}^{\infty}\sum_{m=0}^{\infty}\frac{\Gamma(\frac{3}{2})}{\Gamma(m+1)\Gamma(\frac{3}{2}-m)}\frac{\Gamma(n+1)}{\Gamma(n+\frac{1}{2})\sqrt{\pi}}\frac{1}{(au_t)^{4m}}\frac{\left(1-\left(\frac{au_t}{au_b}\right)^{6n+4m}\right)}{6n+4m}\Bigg]\ . \end{aligned} \tag{2.73}$$

We can recover the result of HEE for $au_t \geq 1$ at $T = 0$ given in eq.(2.30) by setting $u_H = 0$ in the above expression.

To obtain the expression of HEE in terms of the subsystem length $\frac{l}{a}$, we need to find the relation between the subsystem length and turning point. To do this we note that the subsystem size in terms of the bulk coordinate can be written as

$$\frac{l}{a} = \frac{2}{au_t}\int_{\frac{au_t}{au_b}}^{1}\frac{p\sqrt{p^4+(au_t)^4}}{\sqrt{1-p^6}\sqrt{1-\eta^4p^4}}\,dp\ . \tag{2.74}$$

We would evaluate the above integral in the low temperature approximation. Under this approximation the subsystem size $\frac{l}{a}$ in the domain $au_t \leq 1$ reads

$$\begin{aligned}
\frac{l}{a} &\simeq \frac{2}{(au_t)}\left[\int_{\frac{au_t}{au_b}}^{1} dp\frac{p\sqrt{p^4+(au_t)^4}}{\sqrt{1-p^6}} + \frac{\eta^4}{2}\int_{\frac{au_t}{au_b}}^{1} dp\frac{p^5\sqrt{p^4+(au_t)^4}}{\sqrt{1-p^6}}\right] \\
&\approx \frac{\sqrt{\pi}}{2(au_t)}\frac{\Gamma(\frac{5}{3})}{\Gamma(\frac{7}{6})} - (au_t)^3\ln(au_t) + (au_t)^3\sum_{n=1}^{\infty}\frac{1}{\sqrt{\pi}}\frac{\Gamma(n+\frac{1}{2})}{\Gamma(n+1)}\frac{1}{(6n)} - \sum_{n=1}^{\infty}\frac{1}{\sqrt{\pi}}\frac{\Gamma(n+\frac{1}{2})}{\Gamma(n+1)}\frac{(au_t)^{(6n+3)}}{(6n)} \\
&+ \left(\sum_{n=0}^{\infty}\frac{2}{\sqrt{\pi}}\frac{\Gamma(n+\frac{1}{2})}{\Gamma(n+1)}\left[\frac{1-(1/au_b)^{6n+2}}{(6n+2)} - \frac{1}{(6n+4)} + \frac{1-(1/au_b)^{6n+6}}{2(6n+6)}\right]\right)(au_t)^{(6n+3)} \\
&+ \eta^4\Bigg[\frac{\sqrt{\pi}}{8}\frac{\Gamma(7/3)}{\Gamma(11/6)}\frac{1}{au_t} + \frac{\sqrt{\pi}}{8}\frac{\Gamma(5/3)}{\Gamma(7/6)}(au_t)^3 + \sum_{n=0}^{\infty}\frac{1}{\sqrt{\pi}}\frac{\Gamma(n+(1/2))}{\Gamma(n+1)}\Bigg(\frac{1-(1/au_b)^{6n+6}}{6n+6} \\
&- \frac{1}{6n+8} - \frac{1}{2(6n+4)} + \frac{1}{2}\frac{1-(1/au_b)^{6n+10}}{6n+10}\Bigg)(au_t)^{6n+7}\Bigg] . \qquad (2.75)
\end{aligned}$$

The above result suggests that, it contains a temperature dependent term. Furthermore, we can recover the relation between the subsystem length and turning point at zero temperature in the limit $T \to 0$. Following the similar procedure we now find the relation between the subsystem length and turning point in the deep IR and deep NC limit. Once gain the deep IR domain is indentified by $au_t << 1$. In the domain the expression given in the above equation reduces to

$$\left(\frac{l}{a}\right)_{deep\ IR} \approx \frac{2\sqrt{\pi}}{(au_t)}\frac{\Gamma(2/3)}{\Gamma(1/6)} + \frac{(au_H)^4}{(au_t)^5}\frac{\sqrt{\pi}}{8}\frac{\Gamma(7/3)}{\Gamma(11/6)} . \qquad (2.76)$$

On the other hand in the deep noncommuatitive limit ($(au_t) \gg 1$, and $au_t \ll au_b$ [124]) the relation between the subsystem length and turning point reduces to

$$\left(\frac{l}{a}\right)_{deep\ NC} \approx \frac{\sqrt{\pi}}{3}\frac{\Gamma(1/3)}{\Gamma(5/6)}(au_t) + \frac{1}{3}\frac{(au_H)^4}{(au_t)^3} . \qquad (2.77)$$

It is to be mentioned that all the above results are obtained by considered terms upto $\mathcal{O}((au_H)^4)$. Now we would perform our analysis in the domain $au_t \geq 1$. In this domain the subsystem length in terms of the turning point is given by

$$\begin{aligned}
\frac{l}{a} &= \sum_{m=0}^{\infty}\sum_{n=0}^{\infty}\frac{\Gamma(n+\frac{1}{2})}{\Gamma(m+1)\Gamma(\frac{3}{2}-m)\Gamma(n+1)}\frac{1}{(au_t)^{4m-1}}\frac{\left(1-\left(\frac{au_t}{au_b}\right)^{6n+4m+2}\right)}{6n+4m+2} \\
&+ \eta^4\sum_{m=0}^{\infty}\sum_{n=0}^{\infty}\frac{\Gamma(n+\frac{1}{2})}{\Gamma(n+1)\Gamma(m+1)\Gamma(\frac{3}{2}-m)}\frac{1}{(au_t)^{4m-1}}\frac{\left(1-\left(\frac{au_t}{au_b}\right)^{6n+4m+6}\right)}{6n+4m+6} . \qquad (2.78)
\end{aligned}$$

Now we compare our analytical result with that of the numerical one. In the left panel of fig.(2.7), we have graphically represented this comparison for $au_H = 0.2$. The analytical expression of $\left(\frac{l}{a}\right)$ has been obtained from eqs.(2.75,2.78) by following the technique introduced for the zero temperature case. From this figure, it can be seen that the numerical and analytical results are in good agreement with each other. We now proceed to compute the value of $(au_t)_c$ at which the length scale $\left(\frac{l}{a}\right)_{min}$ appears. This can be done by equating the results given in eq.(2.76)and eq.(2.77) at $au_t = (au_t)_c$, thus we obtain an equation of the form

$$2\sqrt{\pi}\frac{\Gamma(2/3)}{\Gamma(1/6)}(au_t)_c^4 - \frac{\sqrt{\pi}}{3}\frac{\Gamma(1/3)}{\Gamma(5/6)}(au_t)_c^6 - (au_H)^4\left(\frac{(au_t)_c^2}{3} - \frac{\sqrt{\pi}}{8}\frac{\Gamma(7/3)}{\Gamma(11/6)}\right) = 0\ . \tag{2.79}$$

The above equation suggests that, it very much difficult to provide an exact analytical solution for $(au_t)_c$.

To make further progress we choose $au_H = 0.2$, the yields the value of $(au_t)_c$ to be $(au_t)_c \approx 0.784$. This matches perfectly with the numerical findings also. Furthermore, the value of $\left(\frac{l}{a}\right)_{min}$ is found to be $\left(\frac{l}{a}\right)_{min} \approx 1.649$. We conclude that in the finite temperature scenario, the values of $(au_t)_c$ and $\left(\frac{l}{a}\right)_{min}$ depend on the choice of (au_H). In the limit $au_H \ll au_t \ll 1$, the expression given in eq.(2.75) reduces to

$$\begin{aligned}\frac{l}{a} &\simeq \frac{\sqrt{\pi}}{2(au_t)}\frac{\Gamma(5/3)}{\Gamma(7/6)}\left[1 + \frac{1}{3\sqrt{\pi}}\frac{\Gamma(7/6)}{\Gamma(5/3)}\left(4 + \log 4 - 6\log(au_t)\right)(au_t)^4\right] \\ &+ \left(\frac{au_H}{au_t}\right)^4\left[\frac{\sqrt{\pi}(au_t)^3}{8}\frac{\Gamma(5/3)}{\Gamma(7/6)} + \frac{\sqrt{\pi}}{8(au_t)}\frac{\Gamma(7/3)}{\Gamma(11/6)} - \frac{(au_t)^7}{30}\right]\ .\end{aligned} \tag{2.80}$$

Following the perturbative approach, we can express the turning point au_t in terms of the subsystem length $\frac{l}{a}$, for large $\frac{l}{a}$. This reads

$$\begin{aligned}au_t &= \left[\frac{\alpha_0}{\left(\frac{l}{a}\right)} + \frac{\alpha_1}{\left(\frac{l}{a}\right)^5} + \frac{\alpha_0^4\log\left(\frac{l}{a}\right)}{\left(\frac{l}{a}\right)^5}\right] + \frac{(a\pi T)^4}{4}\left[\frac{\alpha_0}{\left(\frac{l}{a}\right)} + \frac{1}{\alpha_0^4}\frac{\Gamma(7/3)}{\Gamma(11/6)}\left(\frac{l}{a}\right)^3 - \frac{4}{30}\frac{\alpha_0^4}{\left(\frac{l}{a}\right)^5}\right] \\ &\equiv l_1 + \frac{(a\pi T)^4}{4}l_2\end{aligned} \tag{2.81}$$

where l_1 and l_2 are given by

$$l_1 = \frac{\alpha_0}{\left(\frac{l}{a}\right)} + \frac{\alpha_1}{\left(\frac{l}{a}\right)^5} + \frac{\alpha_0^4\log\left(\frac{l}{a}\right)}{\left(\frac{l}{a}\right)^5};\quad l_2 = \frac{\alpha_0}{\left(\frac{l}{a}\right)} + \frac{1}{\alpha_0^4}\frac{\Gamma(7/3)}{\Gamma(11/6)}\left(\frac{l}{a}\right)^3 - \frac{4}{30}\frac{\alpha_0^5}{\left(\frac{l}{a}\right)^5}\ .$$

In the above result given in eq.(2.81) a temperature dependent term has appeared due to the thermal excitation. It is to be noted that in the above computation we have kept terms upto

$\mathcal{O}(T^4)$. We now substitute the above expression for the turning point au_t (eq.(2.81)) in eq.(2.72) and obtain the following expression for the finite part of HEE (for $au_t << 1$, large $\frac{l}{a}$)

$$a^2\bar{S}_{HEE}|^{finite}\left(\frac{l}{a}\right) = a^2\bar{S}_{HEE}\left(\frac{l}{a}\right)|^{finite} + \frac{(a\pi T)^4}{4}\Delta\left(a^2\bar{S}_{HEE}\right) \ . \tag{2.82}$$

The first term in the above expression, $a^2\bar{S}_{HEE}\left(\frac{l}{a}\right)|^{finite}$ represents the finite piece of HEE corresponding to $T = 0$ case and the expression is given in eq.(2.41). Further, thes expression of $\Delta\left(a^2\bar{S}_{HEE}\right)$ which represents the change in HEE due to the thermal excitation, is given by following expression

$$\begin{aligned}\Delta\left(a^2\bar{S}_{HEE}\right) &= \frac{\sqrt{\pi}}{2l_1^2}\frac{\Gamma(4/3)}{\Gamma(5/6)} - \frac{\sqrt{\pi}}{2}\frac{\Gamma(2/3)}{\Gamma(1/6)}l_1l_2 + \frac{(3+\log 4)}{8}l_1^5l_2 - \frac{\sqrt{\pi}}{4}\frac{\Gamma(2/3)}{\Gamma(1/6)}l_1^2 - \frac{l_1^6}{60} \\ &- \frac{1}{8}l_1^5l_2\log(l_1) - \frac{l_1^5l_2}{8} - \frac{1}{8} \ .\end{aligned} \tag{2.83}$$

The change in the HEE due to thermal excitation plays a crucial role in context of entanglement thermodynamics[132, 133, 134, 135, 136]. In the right panel of fig.(2.7), we have graphically represented $a^2\bar{S}_{HEE}|^{finite}\left(\frac{l}{a}\right)$ as a function of (l/a) (given in eq.(2.82)). The presence of the length scale $(\frac{l}{a})_{min}$ can be noticed from the plot in the left panel. One can also observe the effect of temperature from the plot in the right panel.

We would like to end this discussion by providing the result of HEE at the deep IR limit, which corresponds to the commutative Yang-Mills theory. This reads

$$\left(a^2\bar{S}_{HEE}|^{finite}\left(\frac{l}{a}\right)\right)_{deep\ IR} = \left(a^2\bar{S}_{HEE}|^{finite}\left(\frac{l}{a}\right)\right)^{T=0}_{deep\ IR} + \frac{(a\pi T)^4}{4}\Delta\left(a^2\bar{S}_{HEE}\right)_{deep\ IR} \tag{2.84}$$

where $\left(a^2\bar{S}_{HEE}|^{finite}\left(\frac{l}{a}\right)\right)^{T=0}_{deep\ IR}$ represents the temperature independent piece (given in eq.(2.25)) and $\Delta\left(a^2\bar{S}_{HEE}\right)_{deep\ IR}$ probes the change in HEE (due to thermal excitation) with the following expression

$$\Delta\left(a^2\bar{S}_{HEE}\right)_{deep\ IR} = \frac{1}{\sqrt{\pi}}\left(\frac{\Gamma(7/6)}{\Gamma(5/3)}\right)^2\left(\frac{\Gamma(1/3)}{\Gamma(5/6)}\right)\left(\frac{l}{a}\right)^2\left[\frac{4}{3} - \frac{432}{5^5}\left(\frac{\Gamma(7/6)}{\Gamma(5/3)}\right)\right] \ . \tag{2.85}$$

However, it is to be noted that, all the above analysis is valid for a strip length l larger than some critical length l_c which we shall see now. It has been observed in [125] that to study the surfaces anchored on small strips, $u(y_2)$ has to be expanded in a power series of y_2 (see eq.(2.31)).

Substituting this power series in eq.(2.68) and using $u(y_2 = 0) = u_t$ and the boundary condition given in eq.(2.14), we get the profile of the RT surface to be

$$u(y_2) = u_t + \frac{3}{2}\frac{u_t^3}{1+(au_t)^4}\left(1 - \left(\frac{u_H}{u_t}\right)^4\right) y_2^2 + \dots \ . \tag{2.86}$$

Now substituting $y_2 = \frac{l}{2}$, we get

$$u_b = u_t + \frac{3}{8}\frac{u_t^3}{[1+(au_t)^4]}\left(1 - \left(\frac{u_H}{u_t}\right)^4\right) l^2 + \mathcal{O}\left((l/a)^4\right) \ . \tag{2.87}$$

Now using the above result in eq.(2.66), we get the HEE as

$$\begin{aligned} a^2\bar{S}_{HEE} &= \frac{a^2}{2}\left(\frac{l}{\epsilon^3} - \frac{3}{8}\frac{l^3}{\epsilon a^4}\frac{(1-(\epsilon u_H)^4)}{[1+(\epsilon/a)^4]} - \frac{9}{8}\frac{l^5\epsilon}{a^8}\frac{[1+3(\epsilon u_H)^4/10]}{[1+(\epsilon/a)^4]^2} + \mathcal{O}\left((l/a)^7, \epsilon^6\right)\right) \\ &= \frac{1}{2}\left((au_b)^3\frac{l}{a} - \frac{3}{8}\left(\frac{l}{a}\right)^3\frac{(au_b)(1-(au_H/au_b)^4)}{(1+(1/au_b)^4)} - \frac{9}{8}\left(\frac{l}{a}\right)^5\frac{(1+\frac{3}{10}(au_H/au_b)^4)}{au_b\,(1+(1/au_b)^4)^2}\right) \\ &+ \mathcal{O}\left((l/a)^7, \epsilon^6\right) \ . \end{aligned} \tag{2.88}$$

The above result matches with the zero temperature result eq.2.34 if we set $u_H = 0$. We observe that temperature arises only in the finite terms of the above expression. Now to obtain the critical length l_c, we equate the leading order divergent terms appearing in eq.(2.88) and eq.(2.71). This results in [123]

$$l_c = \frac{a^2 u_b}{2} + \left(\frac{1+(a\pi T)^4}{a^2 u_b^3}\right)\ln(au_b) \ . \tag{2.89}$$

Again the above expression suggests that, the critical length scale depends on the Uv cut off. This clearly indicates the effect of UV-IR mixing property of NCSYM theory.

2.1.6 EWCS and HMI at finite temperature

In this section we proceed to compute the EWCS which is the holographic dual of EoP, in the finite temperature scenario. Similar to the zero temperature case, we again consider two disjoint subsystems, namely, A and B (along the direction y_2) with length l and separated by a distance d. The induced metric on constant y_2 hypersurface at finite temperature reads

$$ds^2_{ind} = R^2\left[u^2 dy_1^2 + u^2 h(u) dy_3^2 + \frac{du^2}{u^2 f(u)}\right] + R^2 d\Omega_5^2 \ . \tag{2.90}$$

The above induced metric leads to the following result for EWCS

$$
\begin{aligned}
a^2\bar{E}_W &= \frac{a^2}{4}\int_{u_t(2l+d)}^{u_t(d)} \frac{u\sqrt{1+a^4u^4}}{\sqrt{f(u)}}\,du \\
&= \frac{a^2}{16}\Bigg[(au_t(d))^2\sqrt{1+(au_t(d))^4}\sqrt{1-\left(\frac{au_H}{au_t(d)}\right)^4}+(1+(au_H)^4)\sinh^{-1}\left(\frac{(au_t(d))^2\sqrt{1-\left(\frac{au_H}{au_t(d)}\right)^4}}{\sqrt{1+(au_H)^4}}\right) \\
&- (au_t(2l+d))^2\sqrt{1+(au_t(2l+d))^4}\sqrt{1-\left(\frac{au_H}{au_t(2l+d)}\right)^4} \\
&- (1+(au_H)^4)\sinh^{-1}\left(\frac{(au_t(2l+d))^2\sqrt{1-\left(\frac{au_H}{au_t(2l+d)}\right)^4}}{\sqrt{1+(au_H)^4}}\right)\Bigg] \ . \qquad (2.91)
\end{aligned}
$$

The above result of EWCS simplifies to the following result in the domain $au_t \leq 1$

$$
\begin{aligned}
a^2\bar{E}_W &= \frac{1}{8}\left[(au_t(d))^2-(au_t(2l+d))^2\right]+\frac{1}{32}\left[(au_t(d))^6-(au_t(2l+d)^6)\right] \\
&+ \frac{(au_H)^4}{16}\left[\frac{1}{(au_t(2l+d))^2}-\frac{1}{(au_t(d))^2}\right]+\frac{3}{64}(au_H)^4\left[(au_t(2l+d))^2-(au_t(d))^2\right] \qquad (2.92)
\end{aligned}
$$

We can express the result of EWCS in the deep IR (commutative) limit in terms of the subsystem size as follows

$$
\begin{aligned}
a^2\bar{E}_W|_{deep\ IR} &= \frac{1}{8}\left[\left(\frac{\alpha_0}{\left(\frac{d}{a}\right)}+\left(\frac{d}{a}\right)^2 A\ (a\pi T)^4\right)^2-\left(\frac{\alpha_0}{\left(\frac{2l+d}{a}\right)}+\left(\frac{2l+d}{a}\right)^2 A\ (a\pi T)^4\right)^2\right] \\
&+ \frac{(a\pi T)^4}{16}\left[\frac{1}{\left(\frac{\alpha_0}{\left(\frac{2l+d}{a}\right)}+\left(\frac{2l+d}{a}\right)A\ (a\pi T)^4\right)^2}-\frac{1}{\left(\frac{\alpha_0}{\left(\frac{d}{a}\right)}+\left(\frac{d}{a}\right)A\ (a\pi T)^4\right)^2}\right] \qquad (2.93)
\end{aligned}
$$

where A is given by

$$
A=\frac{\Gamma(\frac{7}{3})}{12\sqrt{\pi}\Gamma(\frac{11}{6})}\left(\frac{\Gamma(\frac{1}{6})}{\Gamma(\frac{2}{3})}\right)^2 \ .
$$

Now we would proceed to compute HMI in the finite termperature scenario in similar set up , we have just described. The holographic mutual information at finite temperature reads (for $au_t \leq 1$)

$$
a^2\bar{I}(A:B) = 2a^2\bar{S}_{HEE}\left(\frac{l}{a}\right)-a^2\bar{S}_{HEE}\left(\frac{d}{a}\right)-a^2\bar{S}_{HEE}\left(\frac{2l+d}{a}\right) \qquad (2.94)
$$

where $a^2\bar{S}_{HEE}(l/a)$ is given by eq.(2.70). Once again to compute $a^2\bar{I}(A:B)$, we need to use the analytical expressions in eq.(s)(2.70,2.75). In order to find the effect of temperature of HMI we

can recast the above expression of HMI in the following way

$$a^2\bar{I}(A:B) \;=\; a^2\bar{I}(A:B)|_{T=0} + \frac{(a\pi T)^4}{4}\Delta\left(a^2\bar{I}(A:B)\right) \tag{2.95}$$

where, $a^2\bar{I}(A:B)|_{T=0}$ represents the temperature independent piece (given in eq.(2.58)) and $\Delta\left(a^2\bar{I}(A:B)\right)$ gives us the change in HMI due to thermal excitation. This temperature dependent piece has the following expression

$$\Delta\left(a^2\bar{I}(A:B)\right) = \left[2\Delta\left(a^2\bar{S}_{EE}\left(\frac{l}{a}\right)\right) - \Delta\left(a^2\bar{S}_{EE}\left(\frac{d}{a}\right)\right) - \Delta\left(a^2\bar{S}_{EE}\left(\frac{2l+d}{a}\right)\right)\right] \;. \tag{2.96}$$

On the other hand, in the deep IR limit (commutative limit), the EWCS is obtained to be

$$a^2\bar{E}_W|_{deep\ IR} = a^2\bar{E}_W|^{T=0}_{deep\ IR} + \frac{(a\pi T)^4}{4}\Delta\left(a^2\bar{E}_W\right)_{deep\ IR} \tag{2.97}$$

where the temperature independent piece $a^2\bar{E}_W|^{T=0}_{deepIR}$ is given in eq.(2.59) and $\Delta\left(a^2\bar{E}_W\right)_{deep\ IR}$ represents the change in EWCS due to thermal excitation in the deep IR limit. Using eq.(2.93), $\Delta\left(a^2\bar{E}_W\right)_{deep\ IR}$ is given by

$$\Delta\left(a^2\bar{E}_W\right)_{deep\ IR} \;=\; A\ \alpha_0\left(\left(\frac{d}{a}\right) - \left(\frac{2l+d}{a}\right)\right) + \frac{1}{4}\left(\frac{1}{\left(\frac{\alpha_0}{\left(\frac{2l+d}{a}\right)}\right)^2} - \frac{1}{\left(\frac{\alpha_0}{\left(\frac{d}{a}\right)}\right)^2}\right) \;. \tag{2.98}$$

We now graphically represent our computed results in order to have a better understanding of the above discussion.

In the right panel of Fig.(2.8), we have shown the effect of noncommutativity on EWCS and HMI at finite temperature graphicaly. To do this plot we have taken two different values of temperature, namely, $aT = \frac{0.1}{\pi}$ (red) and $aT = \frac{0.2}{\pi}$ (blue). We have observed that, the value of the critical separation length $\left(\frac{d}{a}\right)_c$ decreases with the increase in the temperature. The above plots also suggest that $a^2E_W \geq \frac{1}{2}a^2I(A:B)$ for all valid temperatures. Once again we choose the lower limit of the d/a axis (for the noncommutative case in the left panel of Fig.(5.5)) to be $d/a = 1.649$ (for $T = \frac{0.2}{\pi}$) so that $au_t(d/a) \leq 1$.

In Fig.(2.9), we once again probe the effect of UV/IR mixing on the EWCS and HMI, at a finite temperature. Similar to the zero temperature scenario, we observe that for a fixed subsystem length $\frac{l}{a}$, the HMI and EWCS vanishes at a smaller value of separation $\frac{d}{a}$ for a larger cut-off value.

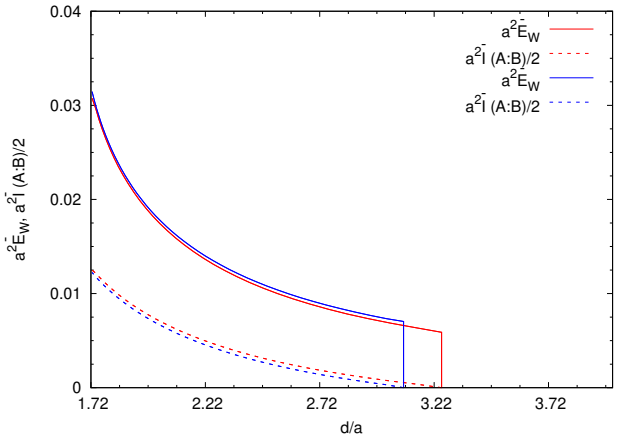

Noncommutative Yang-Mills theory

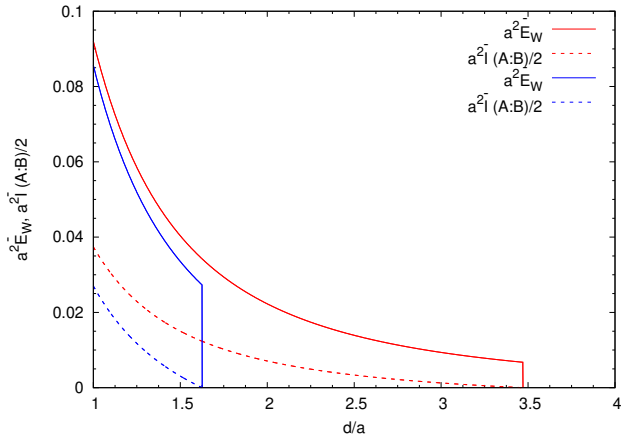

Commutative (deep IR) Yang-Mills theory

Figure 2.8: The effect of noncommutativity on EWCS and HMI at finite temperature with $aT = \frac{0.1}{\pi}$ (red curve) and $aT = \frac{0.2}{\pi}$ (blue curve) (we have set $\frac{l}{a} = 6$) is shown in the left panel of the figure. The curve depict the analytical results. The value of $au_b = 10$ for which eq.(2.89) gives $\frac{l_c}{a} = 5.0023$ for $aT = \frac{0.1}{\pi}$, and $\frac{l_c}{a} = 5.00232$ for $aT = \frac{0.2}{\pi}$. The right panel depicts the corresponding results in the commutative domain.

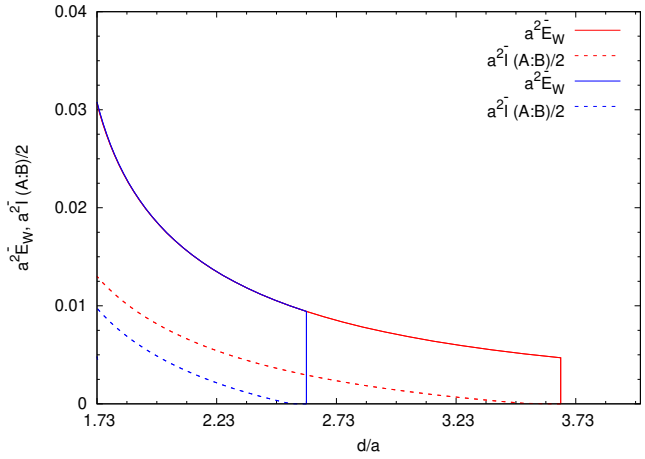

Figure 2.9: The above figure describes the effect of UV/IR mixing on EWCS and HMI at finite temperature $aT = \frac{0.1}{\pi}$. In the above plot, the red curves (both solid and dotted) correspond to $au_b = 10$ while, the blue curves (both solid and dotted) correspond to $au_b = 20$. The subsystem size has been fixed at, $\frac{l}{a} = 6$.

This again shows the sensitivity of the IR results on the UV cut-off.

Now we will consider again the behaviour of the holographic mutual information (HMI) below

the critical length l_c given in eq.(2.89). Following the same procedure to obtain the holographic mutual information below the critical length for zero temperature, we obtain the holographic mutual information at finite temperature using eq.(2.88). In this case it reads

$$\begin{aligned} a^2\bar{I}(A:B) &= \frac{1}{2}\Bigg[-2\left(\frac{d}{a}\right)(au_b)^3+\frac{3}{8}(au_b)\frac{\left(1-\left(\frac{au_H}{au_b}\right)^4\right)}{\left(1+(\frac{1}{au_b})^4\right)}\Bigg\{6\left(\frac{l}{a}\right)^3+2\left(\frac{d}{a}\right)^3 \\ &+ 12\left(\frac{l}{a}\right)^2\left(\frac{d}{a}\right)+6\left(\frac{l}{a}\right)\left(\frac{d}{a}\right)^2\Bigg\}+\frac{9}{8}\frac{1}{au_b}\frac{\left(1+(\frac{3}{10})\left(\frac{au_H}{au_b}\right)^4\right)}{(1+(\frac{1}{au_b})^4)^2}\Bigg\{30\left(\frac{l}{a}\right)^5 \\ &+ 2\left(\frac{d}{a}\right)^5+80\left(\frac{l}{a}\right)^4\left(\frac{d}{a}\right)+40\left(\frac{l}{a}\right)^2\left(\frac{d}{a}\right)^3+10\left(\frac{l}{a}\right)\left(\frac{d}{a}\right)^4\Bigg\}\Bigg]\,. \end{aligned} \tag{2.99}$$

Once can see that the mutual information at zero temperature given in eq.(2.64) is recovered by setting $u_H = 0$ in the above result. In this case also, the HMI is a divergent quantity. All the discussions made earlier in the zero temperature case also hold in this case.

2.2 Mixed state entanglement measures for the dipole deformed supersymmetric Yang-Mills theory

Now we would discuss similar information theoretic measures for dipole deformed super Yang-Mills (DSYM) theory. It is to be noted that, dipole deformation induces non-locality which is characterized by a length-scale $a = \lambda^{\frac{1}{2}}\tilde{L}$. We would compute different measures of quantum correlation for DSYM theory holographically. we have first conisered a strip like subsystem of length $\frac{l}{a}$ and compute the holographic entanglement entropy both analytically and numerically. We have carried out our computation different domains of the theory, namely, $au_t \leq 1$, $1 \leq au_t < au_b$ and $au_t \sim au_b$, where au_b is the UV cut-off. The choice of these domains helps us to identify the expansion parameter for carrying out the binomial expansion. The entanglement measures expectedly displays a smooth behaviour with respect to the subsystem size as the geometry has a smooth transition between the mentioned regions. Now using these results of HEE we then proceed to compute the holographic mutual information for two disjoint subsystems A and B. Based upon the $E_P = E_W$ duality, the entanglement of purification (E_P) is then computed and the effects of dipole deformation in this context have been studied. Finally, we proceed to compute

entanglement negativity for this theory and compare the obtained result with that of the standard SYM theory in order to get a better understanding about the effects of the non-locality.

2.2.1 Dipole deformed supersymmetric Yang-Mills theory and its gravity dual

In this section we would discuss the dipole deformed $\mathcal{N} = 4$ super Yang-Mills theory and its gravity dual of it in the strong coupling limit. One can introduce the dipole deformation by introducing an external dipole deformation which breaks the Lorentz symmetry. Deu to the dipole deformation one need to modify the action of $\mathcal{N} = 4$ SYM theory by incorporating a new term which is proportional to product of the dipole moment and gauge field. It is to be noted that, the new theory is still a supersymmetric theory, which in turn emans that it has symmetry that relates bosonic and fermionic degrees of freedom. Due to the defromation there is new length scales appears in the theroy which depends on the size of the dipole [137, 138].

Emergence of this length scale affects the behaviour of the theory at both low and high energies. For instance, at low energies, the dipole deformation leads to the appearance of a non-trivial ground state, which breaks the supersymmetry of the theory [139, 140, 141, 142]. This ground state is characterized by a set of vortices that are responsible for the formation of a condensate of the gauge field. At high energies, the dipole deformation affects the scattering amplitudes of the gauge bosons [140, 143], leading to the emergence of new kinematical regions that are not present in the original theory. For instance, in the behaviour of the scattering amplitudes in the presence of a background magnetic field, where the dipole deformation leads to a modification of the Landau levels of the charged particles. Some related work in the context of dipole deformed field theory can be found [144, 145, 146].

In the dipole deformed SYM theory the ordinary algebric product of two fields is deformed in the following way [147, 141, 148]

$$(f\tilde{\star}g)(\vec{x}) = f\left(\vec{x} - \frac{\vec{L_f}}{2}\right) g\left(\vec{x} + \frac{\vec{L_g}}{2}\right) \tag{2.100}$$

where $\vec{L_f}$ and $\vec{L_g}$ are dipole vectors associated to the fields f and g respectively. In order to make this new product associative, one needs to assign dipole vector $\vec{L_f} + \vec{L_g}$ to $(f\tilde{\star}g)(\vec{x})$. Here, we

will consider $\vec{L} = L\hat{x}$ corresponding to some fixed length scale L, this implies that our theory is non-local only in the x-direction. There is also another kind of deformation possible for the SYM theory which is known as the noncommutatitve deformation [120, 119, 149]. Unlike the noncommutative SYM theory, the dipole deformed SYM theory does not exhibit any UV/IR mixing property [125, 114].

In the gauge/gravity duality set up, the gravitational dual of dipole-deformed SYM theory is a type IIB string theory in AdS_5 which contains a non-trivial dilaton and axion fields [140, 150, 151]. As mentioned earlier, the dipole deformation deals with the fact that one has to introduce an external dipole moment which in turn breaks the Lorentz symmetry of the theory. In the gravity dual, this deformation is realized with the presence of a non-trivial dilaton field along with a non-trivial axion field. The dilaton field is related to the coupling constant of the SYM theory, while the axion field is related to the dipole moment [152]. The gravity dual of dipole-deformed SYM theory has been extensively studied in the literature, and several important results have been obtained. For example, it has been shown that the dual theory exhibits a nontrivial scaling behavior, which is related to the presence of the dipole moment. The holographic dual also predicts the existence of a new phase in the SYM theory, which is characterized by the breaking of the conformal symmetry and the presence of a dipole moment. This phase is known as the dipole phase. One of the important applications of the gravity dual of dipole-deformed SYM theory is the study of quark-antiquark potential. The holographic calculation of the potential shows that it has a Coulomb-like behavior at short distances, while at large distances it exhibits a linear confinement [153, 154]. The metric associated to the gravity dual of dipole deformed SYM theory (in string frame) reads [125, 155]

$$\begin{aligned} ds^2 &= R^2\left[u^2\left(-dt^2+f(u)dx^2+dy^2+dz^2\right)+\frac{du^2}{u^2}\right]+\text{metric on the deformed } S^5 \\ e^{2\phi} &= g_s^2 f(u)\ ;\ f(u)=\frac{1}{1+a^2u^2}\ ;\ B_{x\psi}=-\frac{1-f(u)}{\tilde{L}}=-\frac{R^2}{\alpha'}au^2f(u) \end{aligned} \tag{2.101}$$

where $a=\lambda^{\frac{1}{2}}\tilde{L}$ with $\tilde{L}=\frac{L}{2\pi}$ is the scale of non locality in the strong coupling limit and ϕ is the non-zero dilaton profile. The S_5 part of the metric in the gravity dual is deformed by expressing S_5 as S_1 fibration over $\mathbb{CP}^2$ [155]. ψ is the global angular 1-form of the Hopf fibration.

2.2.2 Computation of holographic entanglement entropy

We would start our analyasis by computing the HEE of a strip like subsystem A by using the RT prescription [74, 75]. We can specify the subsystem by its volume $V_{sub} = L^2 l$, with $-\frac{l}{2} \leq x \leq \frac{l}{2}$, and $y, z \in [0, L]$ with $L \to \infty$. We further assume that, the width of the subsystem along y and z direction is fixed and we can vary the length only in the x direction. Now we would consider the parametrisation $u = u(x)$ to compute the surface area of the co-dimension two RT surface Γ_A^{min}. However, we would like to mention that the gravity dual of this theory given in eq(2.101) is in the string frame. But all the computations shold be done in the Einstein frame. To transform the metric from string frame to the Einstein frame one can use the following transform

$$g^E_{\mu\nu} \to e^{-\frac{\phi}{2}} g^S_{\mu\nu} \tag{2.102}$$

Using the above transformation we can obtain

$$\sqrt{g^E_8} = e^{-2\phi} \sqrt{g^S_8} \ . \tag{2.103}$$

Taking into account the results discussed above, we now move forward to calculate the HEE. This is expressed as follows [125]

$$\begin{aligned} S_{\rm HEE} &= \frac{\text{Area}(\Gamma^A_{\rm min})}{4G_N} \\ &= \frac{2L^2\pi^3 R^8}{4G_N^{(10)} g_s^2} \int_{-\frac{l}{2}}^{0} dx \ u^2 \left(1 + \frac{u'^2}{f(u)u^4}\right)^{\frac{1}{2}} \ ; \ u' = \frac{du}{dx} \ . \end{aligned} \tag{2.104}$$

It is evident that the integrand in the above expression does not depend on the x coordinate. As a result, x acts as a cyclic coordinate in this setup. This leads to the emergence of the following conserved quantity

$$\mathcal{H} = -\frac{u^3}{\left(1 + \frac{u'^2}{f(u)u^4}\right)^{\frac{1}{2}}} = \text{constant} \equiv c \ . \tag{2.105}$$

We can determine the constant c, by using the fact, $u' = \frac{du}{dx}$ vanishes at the turning point $u = u_t$. This results the following

$$\frac{du}{dx} = \sqrt{u^4 f(u) \left[\left(\frac{u}{u_t}\right)^6 - 1\right]} \ . \tag{2.106}$$

Substituting the above expression into equation (2.104), we derive the result for the HEE in dimensionless form. Thus HEE can be expressed in terms of the bulk coordinate as follows

$$a^2 S_{\rm HEE} = \frac{2L^2\pi^3 R^8}{4G_N^{(10)} g_s^2}(au_t)^2 \int_{\frac{au_t}{au_b}}^1 \frac{dp}{p^4}\frac{(p^2+(au_t^2))^{\frac{1}{2}}}{\sqrt{1-p^6}} \;;\; p=\frac{au_t}{au} \; . \tag{2.107}$$

To regularise the area functional we have used the following boundary condition

$$u\left(x=\pm\frac{l}{2}\right)=u_b=\frac{1}{\epsilon} \; . \tag{2.108}$$

Combining the above boundary condition with the expression provided in equation (2.106), we obtain the subsystem length (in dimensionless form) expressed in terms of the bulk coordinate as follows

$$\frac{l}{a}=\frac{2}{au_t}\int_{\frac{au_t}{au_b}}^1 dp\;\frac{p^2\sqrt{p^2+(au_t)^2}}{\sqrt{1-p^6}} \; . \tag{2.109}$$

We now move forward to calculate the subsystem size in terms of the turning point. To do this analytically we would consider three different domains of the theory, which are characterised by $au_t \leq 1$, $1 \leq au_t < au_b$ and $au_t \sim au_b$. These choices enable us to determine the appropriate expansion parameter needed to carry out the relevant binomial expansions. We have also verified that the result obtained for $au_t \leq 1$ matches smoothly with that obtained for $1 \leq au_t < au_b$ at $au_t = 1$.

Similar to the NCSYM case we first compute the subsystem length in terms of the turing point in the doamin $au_t \leq 1$. In this doamin eq.(2.109) can be recast to the following form

$$\frac{l}{a}=\frac{2}{au_t}\left[\int_{\frac{au_t}{au_b}}^{au_t} dp\frac{p^2\sqrt{p^2+(au_t)^2}}{\sqrt{1-p^6}}+\int_{au_t}^1 dp\frac{p^2\sqrt{p^2+(au_t)^2}}{\sqrt{1-p^6}}\right] \; . \tag{2.110}$$

The above expression suggests that, in the first integral $0 \leq p \leq au_t$, which implies that one can assume $\frac{p}{au_t} < 1$ and perform an expansion to keep terms upto $\mathcal{O}\left(\frac{p}{au_t}\right)^2$. On the other hand in the second integral we have $(au_t) \leq p \leq 1$ and once again we can do an expansion by assuming $\frac{au_t}{p} < 1$ and keep terms upto $\mathcal{O}\left(\frac{au_t}{p}\right)^2$. Keeping this approximation in mind we can rewrite the subsystem length in terms of the turning point as

$$\begin{aligned}\frac{l}{a} \;\approx\; & \frac{\sqrt{\pi}}{2(au_t)}\frac{\Gamma\left(\frac{5}{3}\right)}{\Gamma\left(\frac{7}{6}\right)}+\frac{\sqrt{\pi}}{2}\frac{\Gamma\left(\frac{4}{3}\right)}{\Gamma\left(\frac{5}{6}\right)}(au_t)-\sum_{n=0}^{\infty}\frac{1}{\sqrt{\pi}}\frac{\Gamma\left(n+\frac{1}{2}\right)}{\Gamma\left(n+1\right)}\left[\frac{2}{(6n+4)}+\frac{1}{(6n+2)}\right](au_t)^{6n+3} \\ & + \sum_{n=0}^{\infty}\frac{1}{\sqrt{\pi}}\frac{\Gamma\left(n+\frac{1}{2}\right)}{\Gamma\left(n+1\right)}\left[\frac{2\left(1-(1/au_b)^{6n+3}\right)}{(6n+3)}+\frac{\left(1-(1/au_b)^{6n+5}\right)}{(6n+5)}\right](au_t)^{6n+3} \; .\end{aligned} \tag{2.111}$$

The turning point can also be expressed in terms of the subsystem length by inverting the above expression. This yields ($au_t \leq 1$)

$$\begin{aligned} au_t &\approx \frac{\sqrt{\pi}}{2}\frac{\Gamma\left(5/3\right)}{\Gamma\left(7/6\right)}\frac{1}{\left(\frac{l}{a}\right)}\Bigg[1+\frac{\Gamma\left(4/3\right)\Gamma\left(7/6\right)}{\Gamma\left(5/6\right)\Gamma\left(5/3\right)}\left(\frac{\frac{\sqrt{\pi}}{2}\frac{\Gamma(5/3)}{\Gamma(7/6)}}{\left(\frac{l}{a}\right)}\right)^2 \\ &\quad -\frac{2\Gamma\left(7/6\right)}{\sqrt{\pi}\Gamma\left(5/3\right)}\left(\frac{\frac{\sqrt{\pi}}{2}\frac{\Gamma(5/3)}{\Gamma(7/6)}}{\left(\frac{l}{a}\right)}\right)^3\left(\frac{2}{15}+\frac{2}{3}\frac{1}{(au_b)^3}+\frac{1}{5(au_b)^5}\right)\Bigg] \\ &\equiv \frac{\lambda_1}{\left(\frac{l}{a}\right)}+\frac{\lambda_2}{\left(\frac{l}{a}\right)^3}+\frac{\lambda_3}{\left(\frac{l}{a}\right)^4}\ . \end{aligned} \tag{2.112}$$

where in the above result λ_1, λ_2 and λ_3 are given as

$$\begin{aligned} \lambda_1 &= \frac{\sqrt{\pi}}{2}\frac{\Gamma\left(5/3\right)}{\Gamma\left(7/6\right)} \\ \lambda_2 &= \frac{\sqrt{\pi}}{2}\frac{\Gamma\left(4/3\right)}{\Gamma\left(5/6\right)}\left(\frac{\sqrt{\pi}}{2}\frac{\Gamma\left(5/3\right)}{\Gamma\left(7/6\right)}\right)^2 \\ \lambda_3 &= -\left(\frac{\sqrt{\pi}}{2}\frac{\Gamma\left(5/3\right)}{\Gamma\left(7/6\right)}\right)^3\left(\frac{2}{15}+\frac{2}{3}\frac{1}{(au_b)^3}+\frac{1}{5(au_b)^5}\right)\ . \end{aligned} \tag{2.113}$$

In the domain $1 \leq au_t < au_b$, the subsystem length in terms of the turning point can be written down as

$$\begin{aligned} \frac{l}{a} &= 2\int_{\frac{au_t}{au_b}}^{1} dp \sum_{n=0}^{\infty}\sum_{m=0}^{\infty}\frac{\Gamma\left(n+\frac{1}{2}\right)}{\Gamma\left(n+1\right)\Gamma\left(m+1\right)\Gamma\left(\frac{3}{2}-m\right)}\frac{p^{6n+2m+2}}{(au_t)^{2m}} \\ &= \sum_{n=0}^{\infty}\sum_{m=0}^{\infty}\frac{\Gamma\left(n+\frac{1}{2}\right)}{\Gamma\left(n+1\right)\Gamma\left(m+1\right)\Gamma\left(\frac{3}{2}-m\right)}\frac{1}{(au_t)^{2m}}\frac{1}{(6n+2m+3)}\left[1-\left(\frac{au_t}{au_b}\right)^{6n+2m+3}\right] \end{aligned} \tag{2.114}$$

To obtain the above result, we have used the following identities

$$\begin{aligned} \sqrt{1+\left(\frac{p}{au_t}\right)^2} &= \sum_{m=0}^{\infty}\frac{\Gamma\left(\frac{3}{2}\right)}{\Gamma\left(m+1\right)\Gamma\left(\frac{3}{2}-m\right)}\left(\frac{p}{au_t}\right)^{2m}\ ;\ \left(\frac{p}{au_t}\right)<1 \\ \frac{1}{\sqrt{1-p^6}} &= \sum_{n=0}^{\infty}\frac{1}{\sqrt{\pi}}\frac{\Gamma\left(n+\frac{1}{2}\right)}{\Gamma\left(n+1\right)}p^{6n}\ . \end{aligned}$$

We have found that the results given in eq.(2.111) and eq.(2.114) smoothly matches at $au_t = 1$. Similar kind of approach for the analytical computations can also be found in [156, 157, 158, 159, 114]. Before proceeding further, it is to be mentioned that we can obtain the relation between the

subsystem size in terms of the turning point for the standard $\mathcal{N}=4$ supersymmetric Yang-Mills (SYM) theory by setting $a=0$ in the eq.(2.111). This reads [74, 75, 76]

$$\left(\frac{l}{a}\right)_{\rm SYM}=\frac{2}{\sqrt{\pi}(au_t)}\sum_{n=0}^{\infty}\frac{\Gamma\left(n+\frac{1}{2}\right)}{\Gamma\left(n+1\right)}\frac{1}{(6n+4)}\left[1-\left(\frac{au_t}{au_b}\right)^{6n+4}\right]\ . \tag{2.115}$$

For the completeness of the analysis we have aslo find the expression of the subsystem size in terms of the turning point for the domain $au_t\sim au_b$. In this domain, we can approximate $f(u)$ as, $f(u)\sim(au)^{-2}$ and by using this approximation we recast the differential equation given in eq.(2.106) as

$$dx=\frac{a}{u_t}\frac{\left(\frac{u_t}{u}\right)^4du}{\sqrt{1-\left(\frac{u_t}{u}\right)^6}}\ . \tag{2.116}$$

Upon solving the above differential equation, one can obtain the following result [125]

$$u=\frac{u_t}{\left[\cos\left(\frac{3x}{a}\right)\right]^{\frac{1}{3}}}\ . \tag{2.117}$$

By using the fact $x=\frac{l}{2}$ along with the boundary condition given in eq.(2.108), the above expression leads us to the following relation [125]

$$u_t=u_b\left(\cos\left(\frac{3l}{2a}\right)\right)^{\frac{1}{3}}\ . \tag{2.118}$$

In Fig.(2.10), we have depicted the variation of the subsystem size with respect to the turning point. We have plotted both the numerical and analytically obtained results. We have chosen two different values of for the cut-off. Fig.(3.134) shows that for each subsystem size there exits an unique value of the turning point and the extremal surface exists for any subsystem length.

Our next task is to compute the HEE of a strip like subsystem. For this computation we again consider three different domains of the theoey as we have discueed above. Therefore, first we consider the doamin $au_t\leq 1$. In this doamin the expression given in eq.(2.107) can be reformulated in the following way (here $\bar{S}_{\rm HEE}=\frac{g_s^2G_N^{(10)}}{R^8L^2\pi^3}S_{\rm HEE}$)

$$a^2\bar{S}_{\rm HEE}\ =\ \frac{(au_t)^2}{2}\left[(au_t)\int_{\frac{au_t}{au_b}}^{au_t}dp\frac{\left(1+\left(\frac{p}{au_t}\right)^2\right)^{\frac{1}{2}}}{p^4\sqrt{1-p^6}}+\int_{au_t}^{1}dp\frac{\left(1+\left(\frac{au_t}{p}\right)^2\right)^{\frac{1}{2}}}{p^3\sqrt{1-p^6}}\right]\ . \tag{2.119}$$

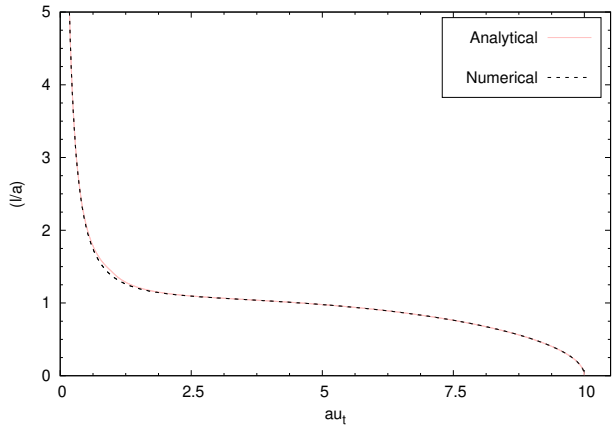

$au_b = 10$

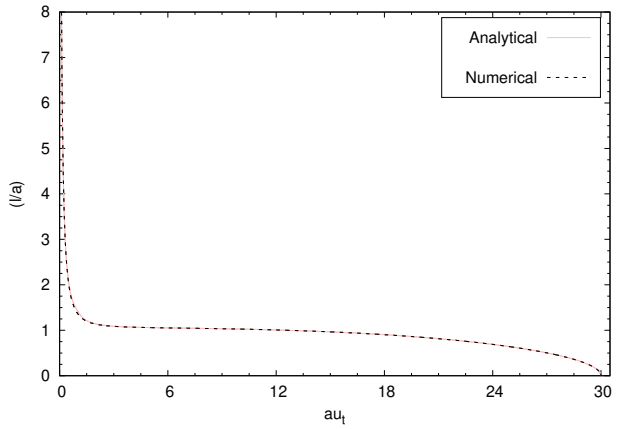

$au_b = 30$

Figure 2.10: The figures above depict how the subsystem size changes as a function of the turning point. Analytical results, derived from Eqs. (2.111) and (2.114), are shown as solid curves, whereas the dotted curves illustrate the outcomes of numerical computations.

Now we would follow the approximation that we have already used to obtain eq.(2.111). Following these approximations lead us to the following result of HEE (for $au_t \leq 1$)

$$\begin{aligned} a^2\bar{S}_{\rm HEE} \approx\ & a^2\bar{S}_{\rm div} - \frac{5}{48} + \frac{(au_t)^2}{2}\sum_{n=0}^{\infty}\frac{1}{\sqrt{\pi}}\frac{\Gamma\left(n+\frac{1}{2}\right)}{\Gamma\left(n+1\right)}\frac{1}{(6n-2)} + \frac{(au_t)^4}{4}\sum_{n=0}^{\infty}\frac{1}{\sqrt{\pi}}\frac{\Gamma\left(n+\frac{1}{2}\right)}{\Gamma\left(n+1\right)}\frac{1}{(6n-4)} \\ &+ \frac{1}{2}\sum_{n=1}^{\infty}\frac{1}{\sqrt{\pi}}\frac{\Gamma\left(n+\frac{1}{2}\right)}{\Gamma\left(n+1\right)}\left[\frac{(1-(1/au_b)^{6n})}{(6n-3)} + \frac{(1-(1/au_b)^{6n})}{2(6n-1)} - \frac{1}{2(6n-4)} - \frac{1}{(6n-2)}\right](au_t)^{6n} \ . \end{aligned} \tag{2.120}$$

From the above equation it can be observed that, the HEE contains a divergent term which is independent of turning point and hence the subsystem length. Therefore the divergent piece of HEE reads

$$a^2\bar{S}_{\rm div} = \frac{1}{6}(au_b)^3 + \frac{1}{4}(au_b) \ . \tag{2.121}$$

It is to be noted that, we can recover the result of HEE corresponding to SYM theory can be obtained by taking the limit $a \to \frac{1}{u_b}$. This reads [74, 75, 76]

$$a^2\bar{S}_{\rm HEE}|^{\rm finite}_{\rm SYM} = \frac{(au_t)^2}{2}\sum_{n=0}^{\infty}\frac{1}{\sqrt{\pi}}\frac{\Gamma\left(n+\frac{1}{2}\right)}{\Gamma\left(n+1\right)}\frac{1}{(6n-2)} = -\frac{\sqrt{\pi}}{4}\frac{\Gamma(2/3)}{\Gamma(1/6)}(au_t)^2 \ . \tag{2.122}$$

For future purposes, we will use the following simplified expression for the HEE, under the condition $au_t \leq 1$

$$a^2\bar{S}_{HEE} \approx a^2\bar{S}_{div} - \frac{5}{48} + \frac{14}{1000}(au_t)^6 - \frac{\sqrt{\pi}}{16}\frac{\Gamma(1/3)}{\Gamma(-1/6)}(au_t)^4 - \frac{\sqrt{\pi}}{4}\frac{\Gamma(2/3)}{\Gamma(1/6)}(au_t)^2 \ . \quad (2.123)$$

To obtain the above result, we have performed follwing sums appearing in eq.(2.120) exactly

$$\begin{aligned}\sum_{n=0}^{\infty}\frac{1}{\sqrt{\pi}}\frac{\Gamma\left(n+\frac{1}{2}\right)}{\Gamma\left(n+1\right)}\frac{1}{(6n-2)} &= -\frac{\sqrt{\pi}}{2}\frac{\Gamma(2/3)}{\Gamma(1/6)}\\ \sum_{n=0}^{\infty}\frac{1}{\sqrt{\pi}}\frac{\Gamma\left(n+\frac{1}{2}\right)}{\Gamma\left(n+1\right)}\frac{1}{(6n-4)} &= -\frac{\sqrt{\pi}}{4}\frac{\Gamma(1/3)}{\Gamma(-1/6)}\end{aligned}$$

and approximated the last sum in eq.(2.120) as follows (by neglecting the terms $\mathcal{O}\left(\frac{1}{au_b}\right)^6$)

$$\frac{1}{2}\sum_{n=0}^{\infty}\frac{1}{\sqrt{\pi}}\frac{\Gamma\left(n+\frac{1}{2}\right)}{\Gamma\left(n+1\right)}\left[\frac{(1-(1/au_b)^{6n})}{(6n-3)}+\frac{(1-(1/au_b)^{6n})}{2(6n-1)}-\frac{1}{2(6n-4)}-\frac{1}{(6n-2)}\right](au_t)^{6n} \approx \frac{14}{1000}(au_t)^6 \ .$$

We can now express this result in terms of the subsystem size $(\frac{l}{a})$ by using eq.(2.112). This yields

$$\begin{aligned}a^2\bar{S}_{HEE} &\approx a^2\bar{S}_{div} - \frac{5}{48} + \frac{14}{1000}\left(\frac{\lambda_1}{\left(\frac{l}{a}\right)}+\frac{\lambda_2}{\left(\frac{l}{a}\right)^3}+\frac{\lambda_3}{\left(\frac{l}{a}\right)^4}\right)^6 - \frac{\sqrt{\pi}}{16}\frac{\Gamma(1/3)}{\Gamma(-1/6)}\left(\frac{\lambda_1}{\left(\frac{l}{a}\right)}+\frac{\lambda_2}{\left(\frac{l}{a}\right)^3}+\frac{\lambda_3}{\left(\frac{l}{a}\right)^4}\right)^4\\ &- \frac{\sqrt{\pi}}{4}\frac{\Gamma(2/3)}{\Gamma(1/6)}\left(\frac{\lambda_1}{\left(\frac{l}{a}\right)}+\frac{\lambda_2}{\left(\frac{l}{a}\right)^3}+\frac{\lambda_3}{\left(\frac{l}{a}\right)^4}\right)^2\\ &= \frac{1}{6}(au_b)^3+\frac{1}{4}(au_b) - \frac{5}{48} + \frac{14}{1000}\left(\frac{\lambda_1}{\left(\frac{l}{a}\right)}+\frac{\lambda_2}{\left(\frac{l}{a}\right)^3}+\frac{\lambda_3}{\left(\frac{l}{a}\right)^4}\right)^6\\ &- \frac{\sqrt{\pi}}{16}\frac{\Gamma(1/3)}{\Gamma(-1/6)}\left(\frac{\lambda_1}{\left(\frac{l}{a}\right)}+\frac{\lambda_2}{\left(\frac{l}{a}\right)^3}+\frac{\lambda_3}{\left(\frac{l}{a}\right)^4}\right)^4 - \frac{\sqrt{\pi}}{4}\frac{\Gamma(2/3)}{\Gamma(1/6)}\left(\frac{\lambda_1}{\left(\frac{l}{a}\right)}+\frac{\lambda_2}{\left(\frac{l}{a}\right)^3}+\frac{\lambda_3}{\left(\frac{l}{a}\right)^4}\right)^2 \quad .(2.124)\end{aligned}$$

Now we would look into the result of HEE in the domain $1 \leq au_t < au_b$. In this doamin the expression of HEE is given by

$$\begin{aligned}a^2\bar{S}_{\text{HEE}} &\approx \frac{1}{6}\left(au_b^3-au_t^3\right)+\frac{1}{4}(au_b-au_t)+\frac{(au_t)^3}{2}\sum_{n=1}^{\infty}\sqrt{\pi}\frac{\Gamma\left(n+\frac{1}{2}\right)}{\Gamma\left(n+1\right)}\frac{1-\left(\frac{au_t}{au_b}\right)^{6n-3}}{(6n-3)}\\ &+ \frac{(au_t)}{4}\sum_{n=1}^{\infty}\frac{1}{\sqrt{\pi}}\frac{\Gamma\left(n+\frac{1}{2}\right)}{\Gamma\left(n+1\right)}\frac{1-\left(\frac{au_t}{au_b}\right)^{6n-1}}{(6n-1)}+\frac{1}{2}\sum_{m=2}^{\infty}\frac{\Gamma(3/2)}{\Gamma\left(m+1\right)\Gamma\left(\frac{3}{2}-m\right)(au_t)^{2m-3}}\frac{1-(au_t/au_b)^{2m-3}}{(2m-3)}\\ &+ \frac{1}{2}\sum_{n=1}^{\infty}\sum_{m=2}^{\infty}\frac{1}{\sqrt{\pi}}\frac{\Gamma(3/2)}{\Gamma\left(m+1\right)\Gamma\left(\frac{3}{2}-m\right)}\frac{\Gamma\left(n+\frac{1}{2}\right)}{\Gamma\left(n+1\right)(au_t)^{2m-3}}\frac{1}{(6n+2m-3)}\left[1-\left(\frac{au_t}{au_b}\right)^{6n+2m-3}\right]\end{aligned}$$

. (2.125)

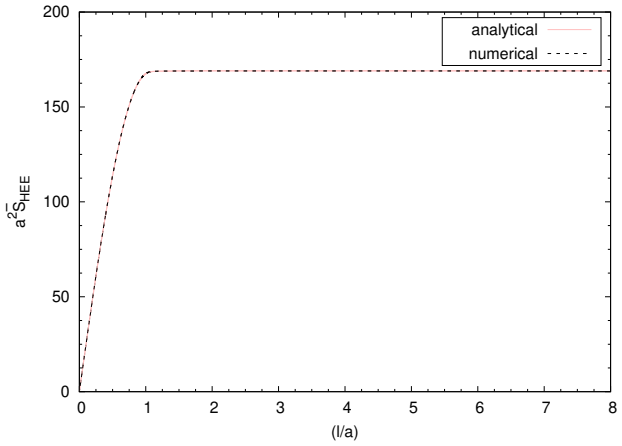

$au_b = 10$

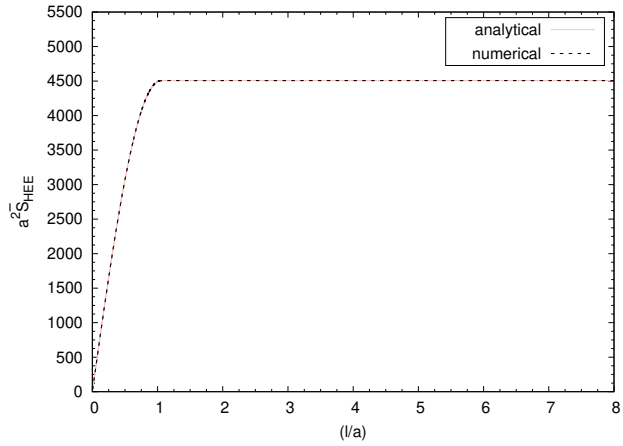

$au_b = 30$

Figure 2.11: The above figures show the variation of holographic entanglement entropy with respect to the sub system size if the dimensionless form. The dotted curves represent the analytical result which is obtained by using eq(s).(2.120, 2.125, 2.111, 2.114). On the other hand the solid curve represents the numerical results. We have plotted for different values of the UV cut-off.

Finally, we compute the HEE for the domain $au_t \sim au_b$. As it is already mentioned that in this domain we can approximate $f(u)$ as $f(u) \sim (au)^{-2}$ and then by using this approximation along with eq.(s)(2.117),(2.104), the HEE is found to be [125]

$$\begin{aligned} S_{\text{HEE}} &= \frac{2R^8\pi^3L^2}{4G_N^{(10)}g_s^2}u_b^3\left[\frac{a}{3}\sin\left(\frac{3l}{2a}\right)\right] \\ &= \frac{2R^8\pi^3L^2}{4G_N^{(10)}g_s^2}u_b^3\left[\frac{a}{3}\left(\frac{3l}{2a}-\frac{1}{3!}\left(\frac{3l}{2a}\right)^3+...\right)\right] \\ &\approx \frac{R^8\pi^3L^2}{4G_N^{(10)}g_s^2}\frac{l}{\epsilon^3} \end{aligned} \tag{2.126}$$

in the second line we have expanded $\sin\left(\frac{3l}{2a}\right)$ in power series since in the domain $au_t \sim au_b$, $\frac{l}{a}$ is very small. In Fig.(2.11), we have represent our results graphically. In this figure we have plotted both the analytical and numerical results. It is to be mentioned that the analytically computed result is well agreed with that of obtained numerically.

We would end this discussion by some useful comments. As we have already discussed earlier that, due to the presence of non-locality in a particular direction (in our case it is the x-direction) in the bulk metric, there are two different length scales involved in the theory. Due to this non locality, there exists a minimum length scale $\frac{l_c}{a}$ below which HEE is proportional to the subsystem

size (l) and above this minimum length scale, the HEE is given by eq.(2.120) (for $au_t \leq 1$), and eq.(2.125) (for $1 \leq au_t < au_b$) obeying the usual area like law. One can find this critical length scale by equating the leading order term of eq.(2.126) to the divergent piece of the HEE (given in eq.(2.121)). This in turn leads us to the following

$$\frac{l_c}{a} = \frac{2}{3} \ . \tag{2.127}$$

The above result suggests that the critical length scale (in the dimensionless form) above which HEE follows the area law is independent of the UV cut-off. Furthermore, this result also indicates the fact that the dipole deformed SYM theory does not exhibit the UV/IR mixing property. In our earlier work [114] we have shown that for the noncommutative deformation of the SYM theory, this minimum length scale (in the dimension less form) depends on the UV cut-off and NCYM theory shows the UV/IR mixing phenomena.

2.2.3 Holographic mutual information and minimal cross section of the entanglement wedge

Now we have studied the holographic mutual information (HMI) and entanglement wedge cross section (EWCS) for two disjoint strip-like subsystems A and B of equal length l. we have furthermore assumed that, they are separated by a length scale d. So we can define the HMI in this set up as folllows

$$I(A:B) = S_{\rm HEE}(A) + S_{\rm HEE}(B) - S_{\rm HEE}(A \cup B) \ . \tag{2.128}$$

Futhermore, we have assumed that, the distance of separation between the subsystems is smaller than the length of the subsystems (that is, $\frac{d}{l} < 1$). Under this assumption eq.(2.128) reduces to

$$I(A:B) = 2S_{\rm HEE}(l) - S_{\rm HEE}(d) - S_{\rm HEE}(2l+d) \tag{2.129}$$

where in the above expression we have used the fact that $S_{\rm HEE}(A \cup B) = S_{\rm HEE}(2l+d) + S_{\rm HEE}(d)$ for $\frac{d}{l} < 1$. Another important point to note is that since all the results have been expressed in dimensionless form, the computation of the HMI requires considering the following form [114]

$$a^2 \bar{I}(A:B) = 2a^2 \bar{S}_{\rm HEE}\left(\frac{l}{a}\right) - a^2 \bar{S}_{\rm HEE}\left(\frac{d}{a}\right) - a^2 S_{\rm HEE}\left(\frac{2l+d}{a}\right) \tag{2.130}$$

where $\bar{I} = \frac{g_s^2 G_N^{(10)}}{R^8 L^2 \pi^3} I$. Now we would proceed to compute the HMI in different domains of the theory by considering $au_t \leq 1$, $1 \leq au_t < au_b$ and $au_t \sim au_b$.

We would first discuss about the computation of HMI in the domain $au_t \leq 1$. To compute the HMI in this domain we have used the result of HEE given in eq.(2.124)[6] in the expression of form of HMI given in eq.(2.130). We have also graphically represented our result in Fig.(2.13). Then we would proceed to the computation of HEE in the domain $1 \leq au_t < au_b$. Now to perform the computation of HMI in the mentioned range of the turning point we have to use the expression of HEE (given in eq.(2.125)) along with the relation between the subsystem length and the turning oint (given by eq(2.114)) in the expression of HMI given in eq.(2.130). We have also graphically represented our result of HMI in this domain in Fig(2.12).

Now we would like to mention few important comments regarding the computation of HMI in the domain $1 \leq au_t < au_b$. Firstly, it is to be noted that, in the expression of HMI in eq.(2.130), there are three three RT surfaces corresponding to the length $\frac{l}{a}$, $\frac{d}{a}$ and $\frac{2l+d}{a}$. This implies there are three turning points all of which lies $au_b > au_t \geq 1$. With all these facts in mimd, we have choosen the subsystem length $\frac{l}{a}$ to be 0.5 which corresponds to the turning point $au_t\left(\frac{l}{a}\right) = 9.02$. This value of turning point can be obtained from the relation between the subsystem length and turning point given in eq.(2.114). Further, this relation also depicts the fact that the maximum value of $\frac{2l+d}{a}$ can be 1.41 which is associated to the turning point $au_t\left(\frac{2l+d}{a}\right) = 1$. This implies that the allowed range for the separation length $\frac{d}{a}$ is $[0, 0.42]$, which corresponds to the turning point range $[9.32, 10]$, where $au_t = 9.32$ corresponds to $\frac{d}{a} = 0.42$, and $au_t = 10$ corresponds to $\frac{d}{a} = 10$. The plot shows that the HMI in this domain decreases with the increase in the separation distance and it vanishes for a particular value of the separation distance, namely, $\frac{d}{a} = 0.24$.

Finally we compute HMI for the scenario $au_t \sim au_b$. The result of HMI in this doamin can be obtained by substituing the result of HEE (given in eq.(2.126)) in the expression of HMI (given by eq.(2.129)). Therefore the expression of HMI in the domain $au_t \sim au_b$ reads

$$I(A:B) = \frac{2R^8\pi^3 L^2}{4G_N^{(10)} g_s^2} u_b^3 \frac{a}{3}\left[2\sin\left(\frac{3l}{2a}\right) - \sin\left(\frac{3d}{2a}\right) - \sin\left(\frac{3(2l+d)}{2a}\right)\right] . \tag{2.131}$$

The HMI in this domain is a divergent quantity because in this case the divergent part of HEE

[6]The detailed expressions of the individual terms appearing in eq.(2.130) are given in Appendix A.

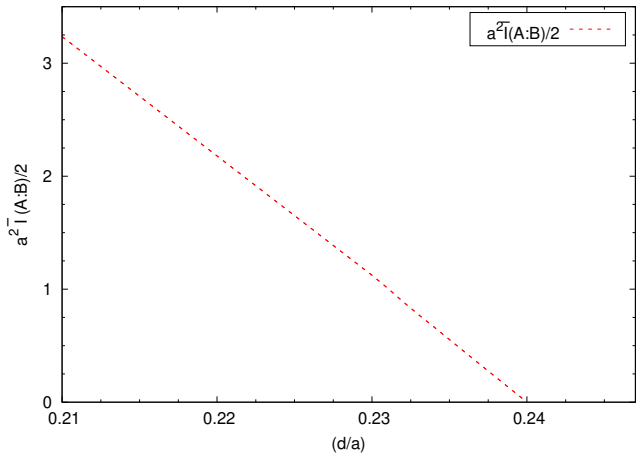

Figure 2.12: The above figure shows the variation of HMI with resepct to separation distance between the two subsystems in the doamin $1 \leq au_t < au_b$. We have set the subsystem size $\frac{l}{a} = 0.5$.

depends on the subsystem size explicitly.

One can obtain the result of HMI for the standard SYM theory by using eq(s).(2.115, 2.122) in eq.(2.130). This results in

$$a^2\bar{I}(A:B)|_{\text{SYM}} = -\pi^{3/2}\left(\frac{\Gamma(2/3)}{\Gamma(1/6)}\right)^3\left[\frac{2}{\left(\frac{l}{a}\right)^2} - \frac{1}{\left(\frac{d}{a}\right)^2} - \frac{1}{\left(\frac{2l+d}{a}\right)^2}\right] . \tag{2.132}$$

We now proceed to compute the holographic counterpart of entanglement of purification (EoP), known as the minimal cross section of the entanglement wedge (EWCS). This can be done by using the $E_P = E_W$ duality [4, 78, 79, 80] already discussed in section.(1.4.3) . Some recent works in this direction can be found in [160, 161, 162, 163, 164, 165, 113, 166, 167, 168, 169].

Similar to the setup used for the computation of the Holographic Mutual Information (HMI), here we also consider two strip-like subsystems on the boundary ∂M (where ∂M is the boundary of the canonical time-slice M considered in the gravity dual). We denote these subsystems as A and B, both of which have the same length l. Furthermore, we assume that A and B are separated by a distance d, with the condition $A \cap B = 0$. This means that to compute EWCS by following prespcription given in section.(1.4.3), we have to calculate the vertical constant x hypersurface with minimal area which splits M_{AB} into two domains corresponding to A and B. The time

induced metric on this constant x hypersurface reads

$$ds^2 = R^2\left[u^2\left(dy^2+dz^2\right)+\frac{du^2}{u^2}\right]+\text{metric on the deformed } S^{5'} \tag{2.133}$$

Now we can obtain the minimum cross sectional area of entanglement wedge by using the above induced metric along with the formula given in eq.(1.129). This results the following expression of EWCS

$$\begin{aligned} E_W &= \frac{L^2R^8\pi^3}{4G_N^{(10)}g_s^2}\int_{au_t\left(\frac{2l+d}{a}\right)}^{au_t\left(\frac{d}{a}\right)} u\sqrt{1+(au)^2}du \\ &= \frac{L^2R^8\pi^3}{4G_N^{(10)}g_s^2}\frac{1}{3a^2}\left[\left(1+\left(au_t\left(\frac{d}{a}\right)\right)^2\right)^{\frac{3}{2}}-\left(1+\left(au_t\left(\frac{2l+d}{a}\right)\right)^2\right)^{\frac{3}{2}}\right] \end{aligned} \tag{2.134}$$

where $au_t\left(\frac{d}{a}\right)$ and $au_t\left(\frac{2l+d}{a}\right)$ indicates the turning points corresponding to the RT surfaces $\Gamma^{\min}_{\left(\frac{d}{a}\right)}$ and $\Gamma^{\min}_{\left(\frac{2l+d}{a}\right)}$ respectively. Keeping this result of EWCS (given in eq.(2.134)) in mind, we now compute EWCS for different domains of the theory.

We first consider the domain $au_t \leq 1$. In this domain we can recast the eq.(2.134) as ($\bar{E}_W = \frac{g_s^2G_N^{(10)}}{R^8L^2\pi^3}E_W$)

$$a^2\bar{E}_W = \frac{1}{8}\left[\left(au_t\left(\frac{d}{a}\right)\right)^2-\left(au_t\left(\frac{2l+d}{a}\right)\right)^2\right]+\frac{1}{32}\left[\left(au_t\left(\frac{d}{a}\right)\right)^4-\left(au_t\left(\frac{2l+d}{a}\right)\right)^4\right] \tag{2.135}$$

We now express the above result in terms of the subsystem length. This can be done by using the relation between subsystem length and turning point in the domain $au_t \leq 1$ given in eq.(2.112). This yields

$$\begin{aligned} a^2\bar{E}_W &= \frac{1}{8}\left[\left(\frac{\lambda_1}{\left(\frac{d}{a}\right)}+\frac{\lambda_2}{\left(\frac{d}{a}\right)^3}+\frac{\lambda_3}{\left(\frac{d}{a}\right)^4}\right)^2-\left(\frac{\lambda_1}{\left(\frac{2l+d}{a}\right)}+\frac{\lambda_2}{\left(\frac{2l+d}{a}\right)^3}+\frac{\lambda_3}{\left(\frac{2l+d}{a}\right)^4}\right)^2\right] \\ &+ \frac{1}{32}\left[\left(\frac{\lambda_1}{\left(\frac{d}{a}\right)}+\frac{\lambda_2}{\left(\frac{d}{a}\right)^3}+\frac{\lambda_3}{\left(\frac{d}{a}\right)^4}\right)^4-\left(\frac{\lambda_1}{\left(\frac{2l+d}{a}\right)}+\frac{\lambda_2}{\left(\frac{2l+d}{a}\right)^3}+\frac{\lambda_3}{\left(\frac{2l+d}{a}\right)^4}\right)^4\right]. \end{aligned} \tag{2.136}$$

Now we would like to mention few comments. In [4], it was demonstrated that the HMI (given in eq.(2.130)) vanishes at a specific value of the separation length, known as the critical separation distance d_c, which depends on the fixed sizes of the subsystem length. At this critical separation

length, the EWCS exhibits a discontinuity, indicating a phase transition from the connected phase to the disconnected phase of the entanglement wedge. For separations $d \leq d_c$, the connected phase is physically relevant, while for $d > d_c$, the disconnected phase becomes the physically relevant configuration. Some recent works in this direction can be found in [38, 114, 160, 170, 171, 37, 172, 173, 136, 174, 175, 176, 177, 178]. We have depicted this fact in Fig.(2.13). We would also like to

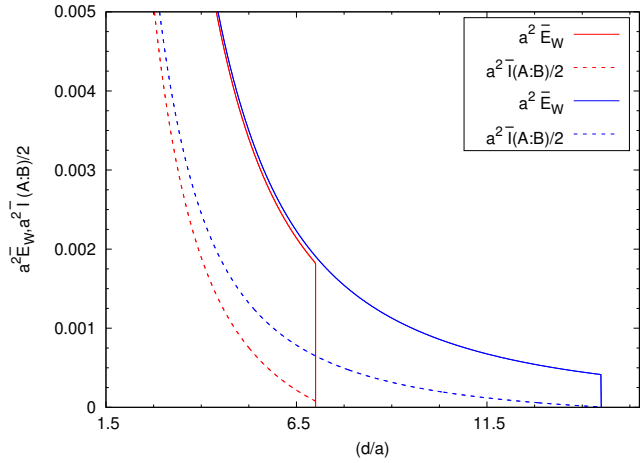

Figure 2.13: The above figure depicts the variation of EWCS and HMI with the separation between two subsystems in the doamin $au_t \leq 1$. To do these plots we have considered two different values of the subsystem size. The red curves are for the susbsystem length ,$\frac{l}{a} = 10$ and the blue curves denote the results for $\frac{l}{a} = 20$.

mention that EWCS and HMI both obey the following inequality

$$E_W \geq \frac{1}{2} I(A:B) \ . \tag{2.137}$$

We have also verified the above inequality in Fig.(2.13). We can recover the result of EWCS for supersymmetric Yang-Mills theory by setting $a = 0$ in the eq.(2.135). This yields

$$a^2 \bar{E}_W|_{\rm SYM} = \frac{1}{8}\left[\left(au_t\left(\frac{d}{a}\right)\right)^2 - \left(au_t\left(\frac{2l+d}{a}\right)\right)^2\right] \ . \tag{2.138}$$

To obtain the result of EWCS for SYM theory in terms of the subsystem size we have to use eq.(2.115) in eq.(2.138). This reads

$$a^2 \bar{E}_W|_{\rm SYM} \ = \ \frac{1}{8}\left(2\sqrt{\pi}\frac{\Gamma(2/3)}{\Gamma(1/6)}\right)^2\left[\frac{1}{\left(\frac{d}{a}\right)^2} - \frac{1}{\left(\frac{2l+d}{a}\right)^2}\right] \ . \tag{2.139}$$

Now we would move on to compute EWCS for $1 \leq au_t < au_b$. In this case, the EWCS has the following form

$$a^2\bar{E}_W \approx \frac{1}{12}\left[\left(au_t\left(\frac{d}{a}\right)\right)^3 - \left(au_t\left(\frac{2l+d}{a}\right)\right)^3\right] . \tag{2.140}$$

To obtain the above result we have used the fact that,$au_t\left(\frac{2l+d}{a}\right) > 1$ and $au_t\left(\frac{d}{a}\right) > 1$ in eq.(2.134). So we have obtained the desired result of EWCS for this domain by following the same approach as we have shown for the computation of HMI. We have graphically represented the result in Fig(2.14). We have chosen the subsystem size $\frac{l}{a} = 0.5$ and observe that the connected to disconnected phase

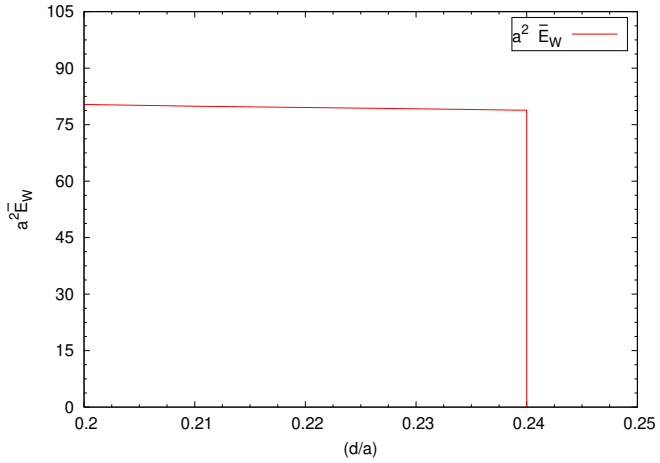

Figure 2.14: Variation of EWCS with the separation between two subsystems in the domain $1 \leq au_t < au_b$ is shown in the above figure. To make this plot we have fixed $\left(\frac{l}{a}\right) = 0.5$

transition for EWCS happens at $\frac{d}{a} = 0.24$. Furthermore, EWCS and HMI obey the universal bound given in eq.(2.137). This can be verified by comparing the plots given in Figures(2.12),(2.14). Finally, we compute EWCS for the case where $au_t \sim au_b$. In this scenario, the EWCS can be derived using the results provided in eq(s).(2.140, 2.118). This yields the following expression:

$$a^2\bar{E}_W = \frac{(au_b)^3}{12}\left[\cos\left(\frac{3d}{2a}\right) - \cos\left(\frac{3(2l+d)}{2a}\right)\right] . \tag{2.141}$$

The above result indicates that for $au_t \sim au_b$, EWCS is not a finite quantity, as it diverges (this divergence has been regularized using the UV cut-off). In eq.(2.131), we have already shown that the holographic mutual information is also a divergent quantity in this regime. Consequently, in this domain, both the HMI and EWCS are physically relevant.

Next, we will compare the results for the holographic mutual information and the entanglement wedge cross section in the context of dipole-deformed supersymmetric Yang-Mills theory with those of the standard supersymmetric Yang-Mills theory.

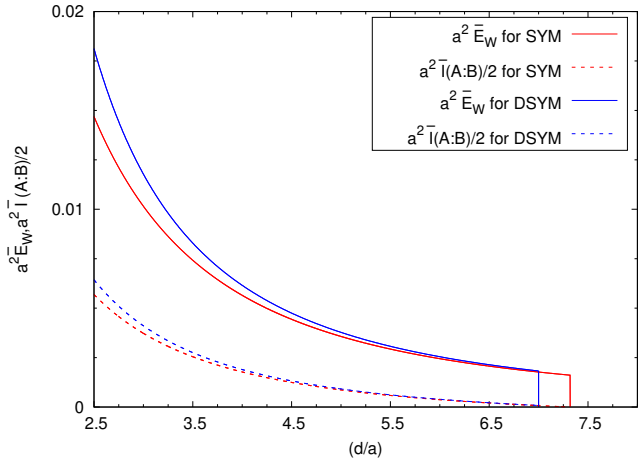

Figure 2.15: In this plot, we have compared the results of EWCS and HMI between dipole deformed supersymmetric Yang-Mills theory and standard supersymmetric Yang-Mills theory. We have done these plots by choosing the subsystem size, $\frac{l}{a} = 10$. The red curve denotes the results for the standard SYM theory. On the other hand , the blue curve represents the results for DSYM theory.

In Fig(2.15), we present a comparison of the results for the entanglement wedge cross section and holographic mutual information between the two theories mentioned above. The blue curves (where the dotted curve represents HMI and the solid curve represents EWCS) correspond to the results for dipole-deformed supersymmetric Yang-Mills theory in the regime $au_t \leq 1$, while the red curves represent the results for the standard supersymmetric Yang-Mills theory. The figure clearly demonstrates that for DSYM theory, both the EWCS and HMI vanish earlier compared to the SYM theory.

Finally, to complete the analysis, we compare the results of the entanglement wedge cross section and holographic mutual information for dipole-deformed supersymmetric Yang-Mills theory with those of noncommutative supersymmetric Yang-Mills theory, as obtained earlier in [114]. In [114], it was found that both the EWCS and HMI are physically meaningful only in the domain $\tau_t < 1$, while for other scenarios, they are not physically relevant. However, for dipole-deformed supersymmetric Yang-Mills theory, we observe that both the EWCS and HMI remain physically meaningful not

only for $au_t \leq 1$ but also for $1 \leq au_t < au_b$. Additionally, these quantities exhibit a smooth transition, as they match precisely at $au_t = 1$.

2.2.4 Holograhic computation of the entanglement negativity

We now move on to compute another measure of quantum correlation known as the entanglement negativity (or logarithmic negativity) (E_N), which quantifies entanglement for mixed states. Earlier, we briefly discussed the concept of entanglement negativity and its significance in the context of quantum information theory. The holographic description of computing the entanglement negativity is given in section(1.4.4). We have two different proposals to holographically compute entanglement negativity. One of the proposal states that, E_N is related to the area of an extremal cosmic brane that ends at the boundary of the entanglement wedge [81, 82]. Another proposal suggests that the entanglement negativity is given by an appropriate combinations holographic entanglement entropy [84, 85, 86, 87, 88, 89]. Both of these proposals reproduce the exact known result of entanglement negativity in CFT.

In this work, we follow the second proposal to compute E_N. Some recent works in this directions can be found in [90, 91, 92, 93, 94, 95, 96, 97, 98, 179, 180]. To compute the entanglement negativity holographically we have considered two different scetups. First we have considered two strip-like adjacent subsystems A and B of lengths l_1 and l_2. In the case of such adjacent subsystems the entanglement negativity (E_N) is defined as [84, 85, 86, 87, 88, 89]

$$a^2\bar{E}_{N_{adj}} = \frac{3}{4}\left[a^2\bar{S}_{EE}\left(\frac{l_1}{a}\right) + a^2\bar{S}_{EE}\left(\frac{l_1}{a}\right) - a^2\bar{S}_{EE}\left(\frac{l_1+l_2}{a}\right)\right] \tag{2.142}$$

where $\bar{E}_{N_{\rm adj}} = \frac{g_s^2 G_N^{(10)}}{R^8 L^2 \pi^3} E_{N_{adj}}$ and $\bar{S}(l_i)$ is the HEE of a subsystem of length l_i. To compute the entanglement negativity for adjacent subsystems for the doain $au_t \leq 1$, we have used eq.(2.124). On the other hand for $1 \leq au_t < au_b$, the entanglement negativity can be computed by using eq(s).(2.125, 2.114). It is to be noted that, the entanglement negativity for adjacent set up, is a divergent quantity for both the domain $au_t \leq 1$ and $1 \leq au_t < au_b$. On the other hand, entanglement negativity for two adjacent subsystems for $au_t \sim au_b$ reads

$$a^2\bar{E}_{N_{adj}} = \frac{3}{4}\frac{(au)^3}{3}\left[\sin\left(\frac{3l_1}{2a}\right) + \sin\left(\frac{3l_2}{2a}\right) - \sin\left(\frac{3(l_1+l_2)}{2a}\right)\right] . \tag{2.143}$$

The above expression suggests that entanglement negativity is divergent also for the consideration $au_t \sim au_b$.

Next we have considered two disjoint subsystems to compute E_N holographically. Now we would consider two disjoint subsystems A and B with length l_1 and l_2 respectively along with the fact that they are separated by a distance d. In this setup, entanglement negativity reads [99, 100]

$$a^2\bar{E}_{N_{\rm dis}} = \frac{3a^2}{4}\left[\bar{S}_{\rm HEE}(l_1+x)+\bar{S}_{\rm HEE}(l_2+x)-\bar{S}_{\rm HEE}(l_1+l_2+x)-\bar{S}_{\rm HEE}(x)\right] \quad . \tag{2.144}$$

Now we would consider a special case where we take two disjoint subsystems of equal length $l_1 = l_2 \equiv l$, we get the following result

$$a^2\bar{E}_{N_{dis}} = \frac{3}{4}\left[2a^2\bar{S}_{HEE}\left(\frac{l+d}{a}\right)-a^2\bar{S}_{HEE}\left(\frac{2l+d}{a}\right)-a^2\bar{S}_{HEE}\left(\frac{d}{a}\right)\right] \quad . \tag{2.145}$$

To compute the entanglement negativity for the domain $au_t \leq 1$, we could use of the eq(s).(2.124,2.145) [7] Similarly, for $1 \leq au_t < au_b$, one can obtain the result of entanglement negativity for two disjoint subsystems by using eq(s).(2.114, 2.125) along with the definition given in eq.(2.145). The definition of entanglement negativity (given in eq.(2.145)) suggests that for two disjoint subsystems, the entanglement negativity is a divergence free quantity.

The result of entanglement negativity of two disjoint subsystems of equal length for the standard supersymmetric Yang-Mills (SYM) theory can be obtained by using eq(s).(2.115, 2.122) along eq.(2.145). This results

$$a^2\bar{E}_{N_{dis}}|^{\rm SYM} = \frac{3\sqrt{\pi}}{8}\frac{\Gamma(2/3)}{\Gamma(1/6)}\left(\frac{\sqrt{\pi}\Gamma(5/3)}{2\Gamma(7/6)}\right)^2\left[\frac{1}{\left(\frac{d}{a}\right)^2}+\frac{1}{\left(\frac{2l+d}{a}\right)^2}-\frac{1}{\left(\frac{l+d}{a}\right)^2}\right] \quad . \tag{2.146}$$

We have graphically shown the variation of entanglement negativity with respect to the separation distance. In Fig.(2.16) where the plot is given for the domain $au_t \leq 1$. The red curve represents the entanglement negativity for the dipole deformed supersymmetric Yang-Mills (DSYM) theory for $au_t \leq 1$ and the blue curve depicts the entanglement negativity for the usual supersymmetric Yang-Mills theory.

To compute the entanglement negativity for the scenario $1 \leq au_t < au_b$, we have followed the same procedure as we have discussed earlier to plot HMI and EWCS in the domain $1 \leq au_t < au_b$. Furthermore, it can be observed that EN measures the quantum correlation between two disjoint

[7] The detailed expression of the individual terms are in given in Appendix B.

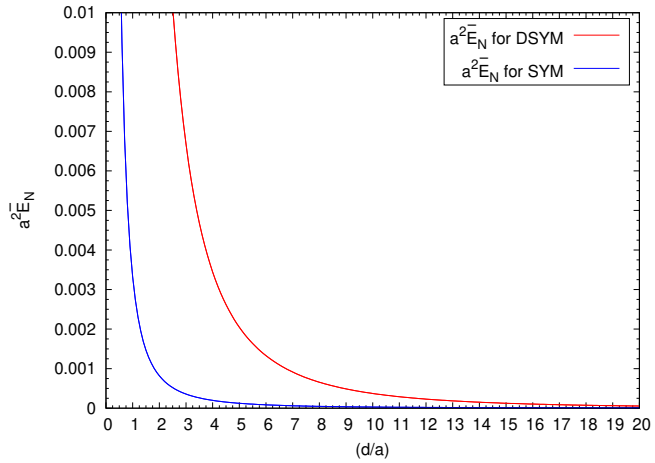

Figure 2.16: The figure shows the variation of E_N with respect to the separation distance. The blue curve represents the E_N for standard SYM theory and the red curve represents the result of DSYM theory. We have chosen the subsystem size $\frac{l}{a} = 20$ for both the plots.

subsystems even though they are not in the connected phase [8] . We have graphically represented the result of EN for two disjoint subsystem of equal length in the domain $1 \leq au_t < au_b$ in Fig.(2.17).

On the other hand, in this set up, the result of entanglement negativity for $au_t \sim au_b$ can be obtained by substituting eq.(2.126) in eq.(2.145). This reads

$$a^2 \bar{E}_{N_{\rm dis}}|_{l_1=l_2} = \frac{3}{4}\frac{(au)^3}{3}\left[2\sin\left(\frac{3(l+d)}{2a}\right) - \sin\left(\frac{3(2l+d)}{2a}\right) - \sin\left(\frac{3d}{2a}\right)\right] . \tag{2.147}$$

2.3 Conclusion

Now we summarize our findings to draw conckusion. In this chapter we have discussed different measures of quantum correlation for deformed $\mathcal{N} = 4$ super Yang-Mills theory. In particular we have considered noncommutative deformation and dipole deformation to the $\mathcal{N} = 4$ SYM theory. In section(2.1) we have computed different measures of quantum correlation for noncommutative super Yang-Mills theory. We have first briefly discuss about the NCSYM theory and its gravity dual at zero temperature. We have also seen from that the noncommutative plane get collapsed in

[8]This is because the HMI and EWCS at some value of the separation distance, but entanglement negativity never vanishes for any value of the separation distance.

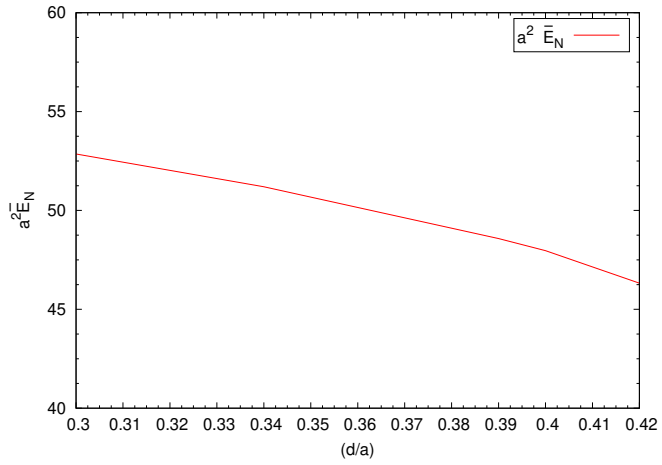

Figure 2.17: Variation of entanglement negativity of dipole deformed supersymmetric Yang-Mills theory for the consideration $1 \leq au_t < au_b$ is depicted in the above figure. To do this plot we have choosen the subsystem size to be $\frac{l}{a} = 0.5$.

the UV limit. So it is necessery to introduce a UV cut off to regulate the theory. This UV cutoff leads to a critical length scale. One should carried out the computation of informatrion theoretic measures very carefully. First we would compute the subsystem length $\frac{l}{a}$ (in dimensionless form) in terms of the turning point (au_t) in different domains of the theory analytically. Then we have compared our analytical and numerical results graphically. We have shown that the analytically obtained result matched prefectly with that of the numerically computed result. We have found there exists a critical length scale $\frac{l_c}{a}$. This points out the fact that, there are two distinct length scale involved in the theory, namely, one is for $l > l_c$ and other one is for $l < l_c$. The domain $l < l_c$ and $au_t \gg 1$, $au_t \sim au_b$ is identified as the deep UV domain of the theory. On the other hand the domain $l > l_c$ has two different solutions depending on the value of the turning point. For $l > l_c$ and $au_t \ll 1$ is identified as the deep IR domain and the domain with $l > l_c$ and $1 << au_t < au_b$ corresponds to the deep noncommutative doamin. Then we have moved on the computation of entanglement entropy of a strip like subsystem A holographically in different domains of the theory analytically. We then graphically compared these nuemrical and analytical results. We have also found that HEE obey an area like law for the domain $l > l_c$. In this domain the divergent part of the HEE is independent of the turning point and hence this divergent part is indpendent of the subsystem length. On the other hand in the domain $l < l_c$, HEE obey a volume

like law. In this domain we have observed that the divergent part of HEE explicitely depends on the subsystem length. Furthermore, we have also found the expression of the critical length scale $\frac{l_c}{a}$ (in dimension less form) by equating the leading order divergent piece of HEE in these two different length scale. We have seen that this critical length scale depends on the UV cutoff, au_b. this clearly indicates the UV-IR mixing property of NCSYM theory. Kepping this result of HEE in mind we have proceed to compute the holographic mutual information for two disjoint subsystems of equal length. Then we have computed EoP in this set up by following the $E_P = E_W$ duality in different domains of the theory. We would like to mention that, EWCS and HMI has physical relevance only in the doamin $au_t \leq 1$. In other doamins of theory these quantities are not physical. Then we have represented the result of EWCS and HMI graphically. We have made these plots for fixed subsystem size. We have found that, the HMI between two subsystems vanishes for a particular value of the separation distance $\left(\frac{d_c}{a}\right)$. This impiles there is phase transition from the connected phase to the disconnected phase. We have also made a graphical comparison of these result for NCSYM and SYM theory. With these results of HMI and EWCS we have also shown the effect of UV-IR mixing on these quantities graphically. Then we moved on to the computation of all these quantities in the finite temperature scenarion. One could incorporate the notion of temperature in the bulk metric by including a black hole geometry. To obtain the analytical results we have considered the low temperature approximation. This low temperature approximation can be realised by considering $au_H << au_t < 1$. In this case also we have found that there is critical length scale l_c which depends on both the UV cut off and the temeperature. We have also made a similar computation as we have done for zero temperature scenario. We have obtained the relation between the subsystem length and the turning point in different domain of the theory analytically. We have compared the analytical and numerical results graphically. Then we have calculated HEE in different domains and compared these analytical results with that of obtained numerically. We have found that our analytically obtained result matches perfectly with the numerical results. In case of HEE we would like to mention that, the divergent part in the in the finite temperature case contained a a term which depends on the temperature. This is one of the unique features of finite temperature NCSYM theory. Then we have computed HMI and EWCS for two disjoint subsystems and made similar kind of analysis that we have done for zero temperature scenario. In this case also we have observed that, both the EWCS and HMI is physically relevant in the

domain $au_t \leq 1$. We have aslo found the collective effect of temperature and noncommutativity on these quantities. We have also shown the effect of UV-IR mixing of these quantities.

Now I would like to make few comments to discuss the dipole deformed super Yang-Mills theory and different measures of quantum correlation that we have computed hologoprahically. For DSYM theroy we are only considering the the zero temperature scenario. Unlike to the noncommutative deformation which acts in a plane, the dipole deformation acts along a particular direction. This dipole deformation introduces non-locality in the usual SYM theory which is manifested by the appearance of a new length scale $a = \lambda^{\frac{1}{2}}\tilde{L}$. In this work we have also investigated the effect of nonlocality on different measures of quantum correlations. First we have considered a strip like subssytem and then expressed the subsystem length $\frac{l}{a}$ (in dimensionless form) in terms of the turning point, au_t. To do this we have consider three different domains of theory, given by,$au_t \leq 1$, $1 \leq au_t < au_b$ and $au_t \sim au_b$, where au_b is the UV regulator of the theory. We have also compared both the analytically and numerically obtained results. Then we have moved on to compute the HEE in the different domains of the theory analytically. In this case also there is critical length scale l_c below which the HEE obey the volume like law, this implies that the divergent piece of HEE depends on the subsystem length. On the other hand, for $l > l_c$, HEE obey area like law. This critical in this context is independent of the UV cut off. This implies DSYM does not exhibit UV-IR mixing property in contrast to the NCSYM theory. Keeping this result of HEE in mind we now proceed to compute HMI and EoP for two disjoint subsystems by following $E_P = E_W$ duality. We have computed these quantities in different mentioned domains of the theory. We have observed that for DSYM theory both the HMI and EWCS are physically relevant in both the domain $au_t \leq 1$ and $1 \leq au_t < au_b$. Whereas for NCSYM theory we have found that EWCS and HMI is physically relevant only in the doamin $au_t \leq 1$. Then we have graphically represented these results of HMI and EWCS. These plots suggest that there exist a critical separation distance between two subsystems for fixed subsystem length, for which there is phase trantition from connected phase to disconnected phase. We have also compared the result of EWCS and HMI of DSYM theory with that of the standard SYM theory. We have also verified that $a^2 E_W(A:B) \geq \frac{1}{2}a^2 I(A:B)$ holds for these two mentioned scenarios. Then we have computed entanglement negativity holographically. To compute this we have first considered two adjoint subsystems. It is to be mentioned that for adjoint subsystems entanglement negativity is a divergent quabtity for all the three domains of

the theory. On the other habd, in case of the disjoint subsystems we have find that it is physically relevant in the domain $au_t \leq 1$ and $1 \leq au_t < au_b$. However, in the domain $au_t \sim au_b$, EN is a divergent quantity. We have also graphically represented the results of entnaglement negativity for both the domain $au_t \leq 1$ and $1 \leq au_t < au_b$.

Before concluding our discussion, we would like to highlight that it would be intriguing to explore other entanglement measures for mixed states, such as odd entropy and reflected entropy, from a holographic perspective. Additionally, investigating holographic subregion complexity for pure states and the complexity of purification for mixed states using holographic methods presents a promising avenue for future research. We plan to pursue these investigations in our upcoming work.

2.4 Appendix A: Expressions required to compute HMI for the consideration $au_t \leq 1$

In this Appendix, we will provide the expressions of the individual terms appearing in the result of HMI associated to the consideration $au_t \leq 1$. The expression given in eq.(2.130) suggests that we need the following expressions of HEE

$$\begin{aligned} a^2\bar{S}_{HEE}\left(\frac{l}{a}\right) &= a^2\bar{S}_{div} - \frac{5}{48} + \frac{14}{1000}\left(\frac{\lambda_1}{\left(\frac{l}{a}\right)} + \frac{\lambda_2}{\left(\frac{l}{a}\right)^3} + \frac{\lambda_3}{\left(\frac{l}{a}\right)^4}\right)^6 - \frac{\sqrt{\pi}}{16}\frac{\Gamma(1/3)}{\Gamma(-1/6)}\left(\frac{\lambda_1}{\left(\frac{l}{a}\right)} + \frac{\lambda_2}{\left(\frac{l}{a}\right)^3} + \frac{\lambda_3}{\left(\frac{l}{a}\right)^4}\right)^4 \\ &- \frac{\sqrt{\pi}}{4}\frac{\Gamma(2/3)}{\Gamma(1/6)}\left(\frac{\lambda_1}{\left(\frac{l}{a}\right)} + \frac{\lambda_2}{\left(\frac{l}{a}\right)^3} + \frac{\lambda_3}{\left(\frac{l}{a}\right)^4}\right)^2 . \end{aligned} \tag{2.148}$$

$$\begin{aligned} a^2\bar{S}_{HEE}\left(\frac{d}{a}\right) &= a^2\bar{S}_{div} - \frac{5}{48} + \frac{14}{1000}\left(\frac{\lambda_1}{\left(\frac{d}{a}\right)} + \frac{\lambda_2}{\left(\frac{d}{a}\right)^3} + \frac{\lambda_3}{\left(\frac{d}{a}\right)^4}\right)^6 - \frac{\sqrt{\pi}}{16}\frac{\Gamma(1/3)}{\Gamma(-1/6)}\left(\frac{\lambda_1}{\left(\frac{d}{a}\right)} + \frac{\lambda_2}{\left(\frac{d}{a}\right)^3} + \frac{\lambda_3}{\left(\frac{d}{a}\right)^4}\right)^4 \\ &- \frac{\sqrt{\pi}}{4}\frac{\Gamma(2/3)}{\Gamma(1/6)}\left(\frac{\lambda_1}{\left(\frac{d}{a}\right)} + \frac{\lambda_2}{\left(\frac{d}{a}\right)^3} + \frac{\lambda_3}{\left(\frac{d}{a}\right)^4}\right)^2 \end{aligned} \tag{2.149}$$

$$\begin{aligned} a^2\bar{S}_{HEE}\left(\frac{2l+d}{a}\right) &= a^2\bar{S}_{div} - \frac{5}{48} + \frac{14}{1000}\left(\frac{\lambda_1}{\left(\frac{2l+d}{a}\right)} + \frac{\lambda_2}{\left(\frac{2l+d}{a}\right)^3} + \frac{\lambda_3}{\left(\frac{2l+d}{a}\right)^4}\right)^6 - \frac{\sqrt{\pi}}{16}\frac{\Gamma(1/3)}{\Gamma(-1/6)}\left(\frac{\lambda_1}{\left(\frac{2l+d}{a}\right)} + \frac{\lambda_2}{\left(\frac{2l+d}{a}\right)^3}\right. \\ &+ \left.\frac{\lambda_3}{\left(\frac{2l+d}{a}\right)^4}\right)^4 - \frac{\sqrt{\pi}}{4}\frac{\Gamma(2/3)}{\Gamma(1/6)}\left(\frac{\lambda_1}{\left(\frac{2l+d}{a}\right)} + \frac{\lambda_2}{\left(\frac{2l+d}{a}\right)^3} + \frac{\lambda_3}{\left(\frac{2l+d}{a}\right)^4}\right)^2 . \end{aligned} \tag{2.150}$$

Using the above results in eq.(2.130), we can obtaine the desired result of HMI for $au_t \leq 1$.

2.5 Appendix B: Expressions required to compute entanglement negativity for the consideration $au_t \leq 1$

In this Appendix, we will provide the expression of individual terms appearing in the expression of entanglement negativity. The expression of entanglement negativity for adjoint subsystems given in (2.142), suggestes that we need the following expression of HEE

$$\begin{aligned} a^2\bar{S}_{HEE}\left(\frac{l_1}{a}\right) &= a^2\bar{S}_{div} - \frac{5}{48} + \frac{14}{1000}\left(\frac{\lambda_1}{\left(\frac{l_1}{a}\right)} + \frac{\lambda_2}{\left(\frac{l_1}{a}\right)^3} + \frac{\lambda_3}{\left(\frac{l_1}{a}\right)^4}\right)^6 \\ &- \frac{\sqrt{\pi}}{16}\frac{\Gamma(1/3)}{\Gamma(-1/6)}\left(\frac{\lambda_1}{\left(\frac{l_1}{a}\right)} + \frac{\lambda_2}{\left(\frac{l_1}{a}\right)^3} + \frac{\lambda_3}{\left(\frac{l_1}{a}\right)^4}\right)^4 - \frac{\sqrt{\pi}}{4}\frac{\Gamma(2/3)}{\Gamma(1/6)}\left(\frac{\lambda_1}{\left(\frac{l_1}{a}\right)} + \frac{\lambda_2}{\left(\frac{l_1}{a}\right)^3} + \frac{\lambda_3}{\left(\frac{l_1}{a}\right)^4}\right)^2 \end{aligned} \tag{2.151}$$

$$\begin{aligned} a^2\bar{S}_{HEE}\left(\frac{l_2}{a}\right) &= a^2\bar{S}_{div} - \frac{5}{48} + \frac{14}{1000}\left(\frac{\lambda_1}{\left(\frac{l_2}{a}\right)} + \frac{\lambda_2}{\left(\frac{l_2}{a}\right)^3} + \frac{\lambda_3}{\left(\frac{l_2}{a}\right)^4}\right)^6 \\ &- \frac{\sqrt{\pi}}{16}\frac{\Gamma(1/3)}{\Gamma(-1/6)}\left(\frac{\lambda_1}{\left(\frac{l_2}{a}\right)} + \frac{\lambda_2}{\left(\frac{l_2}{a}\right)^3} + \frac{\lambda_3}{\left(\frac{l_2}{a}\right)^4}\right)^4 - \frac{\sqrt{\pi}}{4}\frac{\Gamma(2/3)}{\Gamma(1/6)}\left(\frac{\lambda_1}{\left(\frac{l_2}{a}\right)} + \frac{\lambda_2}{\left(\frac{l_2}{a}\right)^3} + \frac{\lambda_3}{\left(\frac{l_2}{a}\right)^4}\right)^2 \\ a^2\bar{S}_{HEE}\left(\frac{l_1+l_2}{a}\right) &= a^2\bar{S}_{div} - \frac{5}{48} + \frac{14}{1000}\left(\frac{\lambda_1}{\left(\frac{l_1+l_2}{a}\right)} + \frac{\lambda_2}{\left(\frac{l_1+l_2}{a}\right)^3} + \frac{\lambda_3}{\left(\frac{l_1+l_2}{a}\right)^4}\right)^6 \\ &- \frac{\sqrt{\pi}}{16}\frac{\Gamma(1/3)}{\Gamma(-1/6)}\left(\frac{\lambda_1}{\left(\frac{l_1+l_2}{a}\right)} + \frac{\lambda_2}{\left(\frac{l_1+l_2}{a}\right)^3} + \frac{\lambda_3}{\left(\frac{l_1+l_2}{a}\right)^4}\right)^4 \\ &- \frac{\sqrt{\pi}}{4}\frac{\Gamma(2/3)}{\Gamma(1/6)}\left(\frac{\lambda_1}{\left(\frac{l_1+l_2}{a}\right)} + \frac{\lambda_2}{\left(\frac{l_1+l_2}{a}\right)^3} + \frac{\lambda_3}{\left(\frac{l_1+l_2}{a}\right)^4}\right)^2 \end{aligned} \tag{2.152}$$

On the other hand, for two disjoint interval we can obtain entanglement negativity by using eqs.(2.145,2.124). The expression of entanglement negativity suggests that we need the following

results of HEE for $au_t \leq 1$

$$a^2\bar{S}_{HEE}\left(\frac{l+d}{a}\right) = a^2\bar{S}_{div} - \frac{5}{48} + \frac{14}{1000}\left(\frac{\lambda_1}{\left(\frac{l+d}{a}\right)} + \frac{\lambda_2}{\left(\frac{l+d}{a}\right)^3} + \frac{\lambda_3}{\left(\frac{l+d}{a}\right)^4}\right)^6 - \frac{\sqrt{\pi}}{16}\frac{\Gamma(1/3)}{\Gamma(-1/6)}\left(\frac{\lambda_1}{\left(\frac{l+d}{a}\right)} + \frac{\lambda_2}{\left(\frac{l+d}{a}\right)^3} + \frac{\lambda_3}{\left(\frac{l+d}{a}\right)^4}\right)^4 - \frac{\sqrt{\pi}}{4}\frac{\Gamma(2/3)}{\Gamma(1/6)}\left(\frac{\lambda_1}{\left(\frac{l}{a}\right)} + \frac{\lambda_2}{\left(\frac{l}{a}\right)^3} + \frac{\lambda_3}{\left(\frac{l}{a}\right)^4}\right)^2 \tag{2.153}$$

$$a^2\bar{S}_{HEE}\left(\frac{d}{a}\right) = a^2\bar{S}_{div} - \frac{5}{48} + \frac{14}{1000}\left(\frac{\lambda_1}{\left(\frac{d}{a}\right)} + \frac{\lambda_2}{\left(\frac{d}{a}\right)^3} + \frac{\lambda_3}{\left(\frac{d}{a}\right)^4}\right)^6 - \frac{\sqrt{\pi}}{16}\frac{\Gamma(1/3)}{\Gamma(-1/6)}\left(\frac{\lambda_1}{\left(\frac{d}{a}\right)} + \frac{\lambda_2}{\left(\frac{d}{a}\right)^3} + \frac{\lambda_3}{\left(\frac{d}{a}\right)^4}\right)^4 - \frac{\sqrt{\pi}}{4}\frac{\Gamma(2/3)}{\Gamma(1/6)}\left(\frac{\lambda_1}{\left(\frac{d}{a}\right)} + \frac{\lambda_2}{\left(\frac{d}{a}\right)^3} + \frac{\lambda_3}{\left(\frac{d}{a}\right)^4}\right)^2 \tag{2.154}$$

$$a^2\bar{S}_{HEE}\left(\frac{2l+d}{a}\right) = a^2\bar{S}_{div} - \frac{5}{48} + \frac{14}{1000}\left(\frac{\lambda_1}{\left(\frac{2l+d}{a}\right)} + \frac{\lambda_2}{\left(\frac{2l+d}{a}\right)^3} + \frac{\lambda_3}{\left(\frac{2l+d}{a}\right)^4}\right)^6 - \frac{\sqrt{\pi}}{16}\frac{\Gamma(1/3)}{\Gamma(-1/6)}\left(\frac{\lambda_1}{\left(\frac{2l+d}{a}\right)} + \frac{\lambda_2}{\left(\frac{2l+d}{a}\right)^3} + \frac{\lambda_3}{\left(\frac{2l+d}{a}\right)^4}\right)^4 - \frac{\sqrt{\pi}}{4}\frac{\Gamma(2/3)}{\Gamma(1/6)}\left(\frac{\lambda_1}{\left(\frac{2l+d}{a}\right)} + \frac{\lambda_2}{\left(\frac{2l+d}{a}\right)^3} + \frac{\lambda_3}{\left(\frac{2l+d}{a}\right)^4}\right)^2 . \tag{2.155}$$

Now using these above expressions of holographic entanglement entropy, we can compute the entanglement negativity by using eq.(2.145) in the domain $au_t \leq 1$.

Chapter 3

Mixed state information theoretic measures in boosted black brane

In this chapter [1] would discuss about our work on the computation of different measures of quantum correlation for boosted black brane geometry holographically. This boosted black brane geometry is holographic dual of strongly correlated plasma moving in a particular direction. We have made the computation of different measures of quantum correlation by considering string like subsystem. We have considered two different setups, namely striplike subsystem taken along the boost and perpendicular to the direction of boost. In our study we have mainly focused on the computation of those quantities which measure quantum correlation present in a system when the system under consideration is in a mixed state. We have calculated entanglement wedge cross section, entanglement negativity, and purification complexity. To perform the computation we have incorporated the thin strip approximation because we are interested only on the leading order change in these quantities due to the boost. Then we have related these quantities computed holographically to the energy and pressure of the boundary theory. Then we have found the assyemtry ratio associated with those quantities. This computation tells us that the asymmetry ration is independent of the subsystem length. Then we have proceed to compute these mentioned quantities for very special class of geometry arises in the special limit of boosted geometry.

[1] This chapter is based on [37].

3.1 Brief discussion on the boosted black brane geometry

In this section we would briefly discuss about the boosted black brane geometry and its dual field theory. As we have already mentioned that boosted black brane geometry is holographic dual of a strongly correlated plasma moving with a constant velocity in a particular direction. Before going to the discussion on this boosted black brane geometry we would like to provide some important motivation to study this kind of theory in the context of AdS/CFT duality.

The AdS/CFT duality originally emerged from string theory, where it was primarily discussed in the context of theoretical particle physics. AdS/CFT offers a promising alternative by enabling the study of strongly-coupled gauge theories through the lens of AdS spacetime. Consequently, there have been numerous efforts to leverage AdS/CFT to analyze and better understand the strong force, providing new insights into its behavior in regimes where traditional methods are inadequate. There are so many attempts to understand QCD via AdS/CFT. Quark gluon plasma (QGP) is one of such example. According to the QCD the fundamental constituent of matter is quarks and gluons, and they are confiend indise the protons and neutrons. However, at high temperature the quark and gluons are deconfined and formed the QGP plasma. Furthermore, in the result of relativistic heavy ion collider (RHIC) it was stated that the QGP behaves like a perfect fluid in contrast to ideal gas. It was also observed that the quark gluon plasma has a small viscocity which arises due the momentum transfer. This momentum transfer becomes less effective at strong coupling. It is to be noted that, according to RHIC, QGP has very small viscosity hence, QGP is strongly coupled. Here is an intuitive explanation of how black holes relate to viscosity. Imagine a system at rest, like a pond of water. If we drop a ball into this pond, waves form and spread out but eventually die down, returning the pond to stillness. This settling is due to viscosity, which causes the energy of the waves to dissipate. Similarly, when we throw an object into a black hole, the event horizon gets disturbed, becoming momentarily irregular. However, this disturbance quickly fades away, and the black hole reverts to its original, symmetrical shape. This process can be seen as a form of dissipation, akin to viscosity in fluids, where the perturbation gets absorbed by the black hole. Thus, we can conceptualize a kind of "viscosity" for black holes, which could theoretically be calculated based on how quickly these disturbances are absorbed back into the black hole. Therefore the motivation to study this system is that boosted AdS black brane background

corresponds to a strongly coupled anisotropic thermal plasma uniformly boosted (with respect to an obsever seating in a static reference frame attached to the flat boundary spacetime) in a certain direction in the boundary theory [181, 182]. Such studies are important due to the experimental investigations of strongly coupled QCD plasma at RHIC and LHC [183, 184, 185, 186, 187].

The study of this system is motivated by the observation that the boosted brane establishes a connection between boundary field theory and string theory. In terms of the AdS/CFT correspondence, when a pp wave travels along a specific direction on the world volume of a classical p-brane, two scenarios can emerge based on whether the Bogomo'lnyi-Prasad-Sommerfield (BPS) bound is saturated. If the BPS bound is not saturated, introducing a pp wave is akin to applying a local Lorentz boost in the wave's direction of travel, but this is true only if the wave's propagation direction is not compactified. However, if the propagation direction is compactified on a circle, this equivalence holds only locally.

Furthermore, the boosted black brane geometry is the sole regular solution to Einstein's field equations that corresponds to a dual field theory on flat spacetime, representing a uniform and constant stress tensor, as discussed in [188]. These solutions are found to give a generalised first law of entanglement thermodynamics which contain the effects of chemical potential and charge density. Further, the effect of IR deformation (excitations in the CFT side) can be captured by computing the HEE of the boosted black brane. The rotational symmetry in the boundary theory breaks down due to the boost along a specific direction, in other words boost introduces anisotropy in the boundary theory. Hence, boosted black brane geometries in the bulk are important in investigating anisotropies of boundary field theories. It is also to be noted that the boost direction is compactified on a circle which results in Kaluza-Klein gauge charges. Interestingly, boosted black brane compatified along one of its lightcone coordinates gives rise to Lifshitz theory [189]. Various physical quantities such as energy, momentum and pressure can be obtained by expanding the bulk AdS geometry eq.(3.1)) in suitable Feffermann-Graham asymptotic coordinates [190, 191].

3.2 Boosted black brane in AdS_{d+1}

The AdS_{d+1} boosted black brane can be represented by the following metric [192, 193]

$$ds^2 = \frac{1}{z^2}\left(-\frac{f(z)}{K(z)}dt^2 + K(dy-\omega)^2 + dx_1^2 + ... + dx_{d-2}^2 + \frac{dz^2}{f(z)}\right) \tag{3.1}$$

where

$$f(z) = 1 - \frac{z^d}{z_0^d} \quad , \quad K(z) = 1 + \beta^2\gamma^2\frac{z^d}{z_0^d} \ . \tag{3.2}$$

In the above, β is the boost parameter which is constrained as $0 \leq \beta \leq 1$ and it is related to the Lorentz factor as $\gamma = \frac{1}{\sqrt{1-\beta^2}}$. Further, z_0 is the position of the event horizon. From the metric above, it is clear that the boost is along the y direction which in turn introduces anisotropy in that particular direction. The Kaluza-Klein 1-form ω reads

$$\omega = \beta^{-1}\left(1 - \frac{1}{K(z)}\right)dt \ . \tag{3.3}$$

In the following sections we will holographically compute various information theoretic measures by considering a strip like subsystem in both along the boost and perpendicular to the boost direction. We shall also investigate the effect of the boost parameter on these quantities.

3.3 Computation of information theoretic measures for strip like subsystem along the boost

Now we would consider a strip like subsystem A at the boundary theory to compute different mesaures of quantum correlation holographically. We specify the subsystem by its volume $\mathcal{V} = L^{d-2}l$, with $-\frac{l}{2} \leq y \leq \frac{l}{2}$, and $x_1, ..., x_{d-2} \in [0, L]$ with $L \to \infty$. We consider that length can vary only in the direction of the boost, that is, along the y-direction because we are interested to capture the effect of boost on the different measures of quantum correlation for subystem along the boost and width along other directions are kept to be fixed.

3.3.1 Holographic entanglement entropy

Now we would proceed to compute the entanglement entropy of strip like subsystem as described above holographically. It is to be noted that the boosted black geometry given in eq.(3.1) is not a static spacetime because the metric is not diagonal. So we cannot follow the RT prescription to compute the HEE because this technique is valid only foe static and stationary spacetime. In this case we have to use the more general prescription to compute the HEE. Therefore we would apply the HRT formalism to compute the HEE [194]. We choose the parametrization $z = z(y)$ and $t = t(y)$ in order to compute the surface area of the co-dimension two HRT surface $\Gamma_A^{min}(t)$ which leads us to the following result of HEE

$$\begin{aligned} S_{HEE}^{\parallel} &= \frac{Area(\Gamma_A^{min}(t))_{\parallel}}{4G_{d+1}} \\ &= \frac{V_{d-2}}{2G_{d+1}}\int_{-\frac{l}{2}}^{0}\frac{dy}{z^{d-1}}\sqrt{K(z)+\frac{z'^2}{f(z)}-t'^2\left(\frac{f(z)}{K(z)}-\frac{K(z)}{\beta^2}\left[1-\frac{1}{K(z)}\right]^2\right)-\frac{2t'(K(z)-1)}{\beta}} \end{aligned} \quad . \tag{3.4}$$

Now identifying the integrant of the above equation as Lagrangian $\mathcal{L} = \mathcal{L}(z, z', t, t')$, we can observe that y is a cyclic coordinate. This cyclic coordinate leads to the following conserved quantity

$$\mathcal{H} = \frac{-K(z)\left(1-\frac{t'(1-\frac{1}{K(z)})}{\beta}\right)}{z^{d-1}\sqrt{K+\frac{z'^2}{f(z)}-t'^2\left(\frac{f(z)}{K(z)}-\frac{K(z)}{\beta^2}\left[1-\frac{1}{K(z)}\right]^2\right)-\frac{2t'(K(z)-1)}{\beta}}} = constant = c \quad . \tag{3.5}$$

We fix the above constant by introducing the turning point $(z_t^{\parallel}, t_t^{\parallel})$ inside the bulk at which z' and t' vanishes which fixes the above constant to be $c = -\frac{\sqrt{K(z_t^{\parallel})}}{z_t^{\parallel(d-1)}}$. This results in the following equation

$$\begin{aligned} \frac{K^2(z)}{K(z_t^{\parallel})}\left(\frac{z_t^{\parallel}}{z}\right)^{2(d-1)}\left[1-\frac{t'}{\beta}\left(1-\frac{1}{K(z)}\right)\right]^2 &= K(z)+\frac{z'^2}{f(z)}-t'^2\left(\frac{f(z)}{K(z)}-\frac{K(z)}{\beta^2}\left[1-\frac{1}{K(z)}\right]^2\right) \\ &- \frac{2t'(K(z)-1)}{\beta} \end{aligned} \tag{3.6}$$

Substituting the above expression in eq.(3.4), we obtain the HEE to be

$$S_{HEE}^{\parallel} = \frac{V_{d-2}}{2G_{d+1}}\int_{-\frac{l}{2}}^{0}\frac{dy}{z^{d-1}}\frac{K(z)}{\sqrt{K(z_t^{\parallel})}}\left(\frac{z_t^{\parallel}}{z}\right)^{d-1}\left(1-\frac{t'}{\beta}\left[1-\frac{1}{K(z)}\right]\right). \tag{3.7}$$

Now we want to make few comments about the above result. We have observed that the first term in the above expression represents HEE obtained by following the RT-prescription which can be obtained by setting $dt = 0$ in the metric and by choosing the parametrization $z = z(y)$. On the other hand the second term represents a correction term which arises due to the HRT formalism [194].

Now we can express dy in terms of dz by using eq.(3.6). This reads

$$\frac{dy}{dz} = \frac{\left(\frac{z}{z_t^{\parallel}}\right)^{d-1}\left[1-\frac{\left(\frac{z}{z_t^{\parallel}}\right)^{2d-2}\left[t'^2\left(\frac{f(z)}{K(z)}-\frac{K(z)}{\beta^2}(1-\frac{1}{K(z)})^2\right)+\frac{2t'(K(z)-1)}{\beta}\right]}{K(z)\left[\frac{K(z)}{K(z_t^{\parallel})}\left(1-\frac{t'}{\beta}\left[1-\frac{1}{K(z)}\right]\right)^2-\left(\frac{z}{z_t^{\parallel}}\right)^{2d-2}\right]}\right]^{\frac{1}{2}}}{\sqrt{K(z)f(z)}\left[\frac{K(z)}{K(z_t^{\parallel})}\left(1-\frac{t'}{\beta}\left[1-\frac{1}{K(z)}\right]\right)^2-\left(\frac{z}{z_t^{\parallel}}\right)^{2d-2}\right]^{\frac{1}{2}}}. \tag{3.8}$$

We can proceed further by incorporating the thin strip approximation, that is, $\left(\frac{z_t^{\parallel}}{z_0}\right)^d << 1$. This approximation can be incorporated by considering terms upto $\mathcal{O}\left(\left(\frac{z}{z_t^{\parallel}}\right)^d\right)$ and neglect the higher order terms in eq.(3.8). Thus the above expression simplifies to the following

$$dy = \frac{\left(\frac{z}{z_t^{\parallel}}\right)^{d-1} dz}{\sqrt{K(z)f(z)}\left[\frac{K(z)}{K(z_t^{\parallel})}\left(1-\frac{t'}{\beta}\left[1-\frac{1}{K(z)}\right]\right)^2-\left(\frac{z}{z_t^{\parallel}}\right)^{2d-2}\right]^{\frac{1}{2}}} \tag{3.9}$$

Now substituting eq.(3.9) in eq.(3.7) along with the boundary conditions $z(y=0) = z_t^{\parallel}, z(y = \pm\frac{l}{2}) = \epsilon$[2], we can write down HEE in the following form

$$\begin{aligned} S_{EE}^{\parallel} &= \frac{V_{d-2}}{2G_{d+1}}\int_{\epsilon}^{z_t^{\parallel}} dz \frac{\sqrt{K(z)/K(z_t^{\parallel})}}{z^{d-1}\sqrt{f(z)}} \frac{1}{\sqrt{\frac{K(z)}{K(z_t^{\parallel})}\left(1-\frac{t'}{\beta}\left[1-\frac{1}{K(z)}\right]\right)^2-\left(\frac{z}{z_t^{\parallel}}\right)^{2d-2}}} \\ &- \frac{V_{d-2}}{2G_{d+1}}\int_{\epsilon}^{z_t^{\parallel}} dz \frac{\sqrt{K(z)/K(z_t^{\parallel})}}{z^{d-1}\sqrt{f(z)}} \frac{\frac{t'}{\beta}\left(1-\frac{1}{K(z)}\right)}{\sqrt{\frac{K(z)}{K(z_t^{\parallel})}\left(1-\frac{t'}{\beta}\left[1-\frac{1}{K(z)}\right]\right)^2-\left(\frac{z}{z_t^{\parallel}}\right)^{2d-2}}}. \end{aligned} \tag{3.10}$$

Before proceeding further we would like to make few comments. In this work we are only interested in the leading order change in HEE ariese due to boost. It is also to be noted that, one can obtain the leading order correction in HEE due to the boost in the thin strip approximation by considering

[2] ϵ is the UV cut-off which has been introduced to regularize the area functional.

the constant time slice [192, 193, 195]. This implies that, when it comes to compute the leading order correction in the HEE (next to pure AdS), it is sufficient to work with the constant time slice co-dimension two RT-surface. The deviations in the geometry of the extremal surface away from the constant time slice contribute only to the second order terms in the perturbative expansion [192, 193, 195]. To proceed further we will assume that all the computations are done in constant time slice, that is, we will set $t' = 0$. Therefore, under this approximation one can write down the subsystem size in terms of the bulk coordinate (by using eq.(3.9)) as [192, 193]

$$\frac{l}{2} = \int_0^{z_t^{\parallel}} dz \frac{(z/z_t^{\parallel})^{d-1}}{\sqrt{f(z)K(z)}\left[\frac{K(z)}{K(z_t^{\parallel})} - (z/z_t^{\parallel})^{2d-2}\right]^{1/2}} \ . \tag{3.11}$$

The above discussion suggests that, we can write the expression of HEE (by setting $t' = 0$) in the following form [192, 193, 195]

$$S_{EE}^{\parallel} = \frac{V_{d-2}}{2G_{d+1}} \int_{\epsilon}^{z_t^{\parallel}} dz \frac{\sqrt{K(z)/K(z_t^{\parallel})}}{z^{d-1}\sqrt{f(z)}} \frac{1}{\sqrt{\frac{K(z)}{K(z_t^{\parallel})} - \left(\frac{z}{z_t^{\parallel}}\right)^{2d-2}}} \ . \tag{3.12}$$

As we have mentioned earlier, we will now use the thin strip approximation which implies

$$\left(\frac{z_t^{\parallel}}{z_0}\right)^d << 1 \quad , \quad \beta^2\gamma^2\left(\frac{z_t^{\parallel}}{z_0}\right)^d << 1 \tag{3.13}$$

and we will keep terms upto $\mathcal{O}(\beta^2\gamma^2)$. Keeping this approximation in mind we can obtain $\frac{K(z)}{K(z_t^{\parallel})}$ as [192, 193]

$$\frac{K(z)}{K(z_t^{\parallel})} \approx 1 + \beta^2\gamma^2\left(\frac{z_t^{\parallel}}{z_0}\right)^d \left[\left(\frac{z}{z_t^{\parallel}}\right)^d - 1\right] \ . \tag{3.14}$$

Keeping this thin strip approximation in mind and by using the result given in eq.(3.14), the subsystem size in terms of the turning point is obtained to be [192, 193]

$$l = 2z_t^{\parallel}\left[b_0 + \frac{1}{2}\left(\frac{z_t^{\parallel}}{z_0}\right)^d \left(b_1 + \beta^2\gamma^2 I_l\right)\right] \tag{3.15}$$

where the expressions corresponding to the constant terms b_0, b_1 and I_l are given in the appendix. One can recover the subsystem size - turning point relation corresponding to the pure AdS_{d+1} geometry by taking the limits $\beta \to 0$ and $z_0 \to \infty$. This reads [75]

$$l = 2b_0\bar{z}_t \tag{3.16}$$

where $\bar{z}_t$ represents the turning point for pure AdS_{d+1} geometry. We can relate the turning point of boosted geometry with that of pure AdS geomtry by using eq.(3.15) and eq.(3.16). This results in [192, 193]

$$z_t^{\parallel} = \frac{l/2}{\left[b_0 + \frac{1}{2}\left(\frac{z_t^{\parallel}}{z_0}\right)^d (b_1 + \beta^2\gamma^2 I_l)\right]} \approx \frac{\bar{z}_t}{1 + \frac{1}{2}\left(\frac{\bar{z}_t}{z_0}\right)^d \left(\frac{b_1}{b_0} + \frac{\beta^2\gamma^2}{b_0} I_l\right)} . \tag{3.17}$$

The explicit form of HEE can be obtained by using eq.(s)(3.10,3.14). Under the thin strip approximation, the expression of HEE reads [192, 193]

$$S_{EE}^{\parallel} = S_{div} + \frac{V_{d-2}}{2G_{d+1}} \frac{a_0}{(z_t^{\parallel})^{d-2}} \left[1 + \frac{p^d}{2}\frac{a_1}{a_0} + \frac{q^d}{2}\left(\frac{d+1}{d-1}\frac{b_1}{a_0} - \frac{1}{d-1}\frac{b_0}{a_0}\right)\right] \tag{3.18}$$

where S_{div} represents the subsystem independent divergent term $S_{div} = \frac{V_{d-2}}{2G_{d+1}(d-2)}\frac{1}{\epsilon^{d-2}}$ and a_0 is a constant term, given in the appendix. Furthermore, $p^d = \left(\frac{z_t^{\parallel}}{z_0}\right)^d$ and $q^d = \beta^2\gamma^2\left(\frac{z_t^{\parallel}}{z_0}\right)^d$. We can express the HEE in terms of the subsystem length by using eq.(3.16), eq.(3.17) and eq.(3.18). This reads [192, 193]

$$S_{EE}^{\parallel} = S_{div} + \frac{V_{d-2}a_0}{2G_{d+1}}\left[\left(\frac{2b_0}{l}\right)^{d-2} + \frac{1}{2z_0^d}\left(\frac{l}{2b_0}\right)^2 \frac{b_1}{a_0}\left(\frac{d-1}{2} + \beta^2\gamma^2\right)\right] . \tag{3.19}$$

The higher order terms in the above expresiion of entanglement entropy is obtained in [196]. For the pure AdS_{d+1} background, the HEE of a strinp like subsystem reads [3] [75]

$$S_{EE}^{pure} = S_{div} + \frac{V_{d-2}a_0}{2G_{d+1}}\left(\frac{2b_0}{l}\right)^{d-2} \tag{3.20}$$

We now define a quantity $\delta S_{EE}^{\parallel}$, in order to remove divergent piece and to represent the change in HEE due to the boost. This reads [192, 193]

$$\delta S_{EE}^{\parallel} \equiv S_{EE}^{\parallel} - S_{EE}^{pure} = \frac{V_{d-2}(d+1)b_1 l^2}{32G_{d+1}b_0^2 z_0^d}\left[\frac{d-1}{d+1} + \frac{2\beta^2\gamma^2}{d+1}\right] . \tag{3.21}$$

The expression of HEE in eq.(3.19) suggests that the entanglement entropy increases in the presence of the boost. A possible reason for this increase in the entanglement entropy is an increase in the area of the strip residing in the CFT side. Increase in the boost also leads to more excitations in the CFT side, and this may also be a reason for the increase in the entanglement entropy from the CFT point of view.

[3] This can also be obtained from eq.(3.19) by taking the limits $\beta \to 0$ and $z_0 \to \infty$.

3.3.2 EWCS and Holographic mutual information

As we have mentioned earlier, the EE is a good way to quantify quantum entanglement as long as the system under consideration is in a pure state. We now holographically compute EoP, which is one of the promising candidates to quantify entanglement for mixed states. This we do by computing the EWCS for the boosted black brane. This computation holographically probes EoP on the basis of $E_P = E_W$ duality [4, 78, 79, 80], already discussed in section.(1.4.3).

We consider two strip like subsystems on the boundary ∂M (∂M is the boundary of the canonical time-slice M that has been considered in the gravity dual). We denote these subsystems as A and B with both of them having the same length l. Further we consider that A and B are separated by a distance x with the condition $A \cap B = 0$. This means that to compute EWCS we have to calculate the vertical constant y hypersurface with minimal area which splits M_{AB} into two domains corresponding to A and B. The time induced metric on this constant y hypersurface reads

$$ds^2 \mid_{ind} = \frac{1}{z^2}\left(dx_1^2 + ... + dx_{d-2}^2 + \frac{dz^2}{f(z)}\right) \quad . \tag{3.22}$$

By using this above mentioned induced metric and the formula given in eq.(**??**), the minimal cross-section of the entanglement wedge (M_{AB}) is found to be

$$\begin{aligned} E_W^{\parallel} &= \frac{V_{d-2}}{4G_{d+1}} \int_{z_t^{\parallel}(x)}^{z_t^{\parallel}(2l+x)} \frac{dz}{z^{d-1}\sqrt{f(z)}} \\ &\approx \frac{V_{d-2}}{4G_{d+1}} \int_{z_t^{\parallel}(x)}^{z_t^{\parallel}(2l+x)} \frac{dz}{z^{d-1}} \left[1 + \frac{1}{2}\left(\frac{z_t^{\parallel}}{z_0}\right)^d \left(\frac{z}{z_t^{\parallel}}\right)^d\right] \\ &= \frac{V_{d-2}}{4G_{d+1}(d-2)} \left[\frac{1}{(z_t^{\parallel}(x))^{d-2}} - \frac{1}{(z_t^{\parallel}(2l+x))^{d-2}}\right] + \frac{V_{d-2}}{16G_{d+1}z_0^d}\left[(z_t^{\parallel}(2l+x))^2 - (z_t^{\parallel}(x))^2\right] \end{aligned} \tag{3.23}$$

where in the second line we have used the thin strip approximation. By using eq.(3.17), we can recast the above result of EWCS in terms of the subsystem size l and the separation distance x. This reads

$$\begin{aligned} E_W^{\parallel} &= \frac{V_{d-2}}{4(2b_0)^2 G_{d+1}} \left[\frac{(2b_0)^d}{d-2}\left(\frac{1}{x^{d-2}} - \frac{1}{(2l+x)^{d-2}}\right)\right. \\ &+ \left.\left(\frac{1}{2z_0^d}\left[\left(1 + \frac{2\beta^2\gamma^2}{d-1}\right)\frac{b_1}{b_0} - \frac{\beta^2\gamma^2}{d-1}\right] - \frac{1}{2}\right)\left(x^2 - (2l+x)^2\right)\right] . \end{aligned} \tag{3.24}$$

The EWCS for the pure AdS_{d+1} geometry (with similar setup) can be obtained by taking the limit $\beta \to 0$, $z_0 \to \infty$ of the above expression, which gives

$$E_W^{pure} = \frac{V_{d-2}(2b_0)^{d-2}}{4G_{d+1}(d-2)} \left[\frac{1}{x^{d-2}} - \frac{1}{(2l+x)^{d-2}} \right] . \tag{3.25}$$

We now introduce a scaling for the sake of simplification. This reads

$$\bar{E}_W^{para} = \frac{2G_{d+1}}{V_{d-2}} E_W^{\parallel} \quad \text{and} \quad \bar{E}_W^{pure} = \frac{2G_{d+1}}{V_{d-2}} E_W^{pure} . \tag{3.26}$$

It has been observed that both E_P and E_W satisfies the bound $E_W(A:B) \geq \frac{1}{2} I(A:B)$. To verify this inequalty for the case in hand, we need to compute the explicit expression of the mutual information.

The holographic mutual information (HMI) has the following form in this set up

$$I(A:B) = S_{EE}^{\parallel}(A) + S_{EE}^{\parallel}(B) - S_{EE}^{\parallel}(A \cup B) \equiv 2S_{EE}^{\parallel}(l) - S_{EE}^{\parallel}(x) - S_{EE}^{\parallel}(2l+x) . \tag{3.27}$$

In the above we have used $S_{EE}^{\parallel}(A \cup B) = S_{EE}^{\parallel}(2l+x) + S_{EE}^{\parallel}(x)$ (for x/l "small"). Keeping this definition in mind, we can compute HMI (for this setup described above) by using eq.(3.19) in the above expression of HMI. This turns out to be

$$\begin{aligned} I^{\parallel}(A:B) &= \frac{V_{d-2}}{2G_{d+1}} \left[\frac{2^{d-2} b_0^{d-1}}{d-2} \left(-\frac{2}{l^{d-2}} + \frac{1}{x^{d-2}} + \frac{1}{(2l+x)^{d-2}} \right) \right. \\ &+ \left. \frac{b_1}{(2b_0)^2 z_0^d} \left(\frac{d-1}{2} + \beta^2 \gamma^2 \right) \left(l^2 - \frac{x^2}{2} - \frac{(2l+x)^2}{2} \right) \right] . \end{aligned} \tag{3.28}$$

We can recover the result of HMI for pure AdS_{d+1} background by taking the limit $\beta \to 0$, $z_0 \to \infty$ of the above expression. Thus we get

$$I^{pure}(A:B) = \frac{V_{d-2} 2^{d-2} b_0^{d-1}}{2G_{d+1}(d-2)} \left(-\frac{2}{l^{d-2}} + \frac{1}{x^{d-2}} + \frac{1}{(2l+x)^{d-2}} \right) . \tag{3.29}$$

Similar to EWCS, we now introduce the scaling $\bar{I}(A:B) = \frac{2G_{d+1}}{V_{d-2}} I(A:B)$. By incorporating this, we define

$$\bar{I}^{para}(A:B) = \frac{2G_{d+1}}{V_{d-2}} I^{\parallel}(A:B) \quad \text{and} \quad \bar{I}^{pure}(A:B) = \frac{2G_{d+1}}{V_{d-2}} I^{pure}(A:B) . \tag{3.30}$$

We shall now find the critical separation distance x_c at which the HMI between two subsystems under consideration vanishes and EWCS shows a phase transition. We shall try to express this

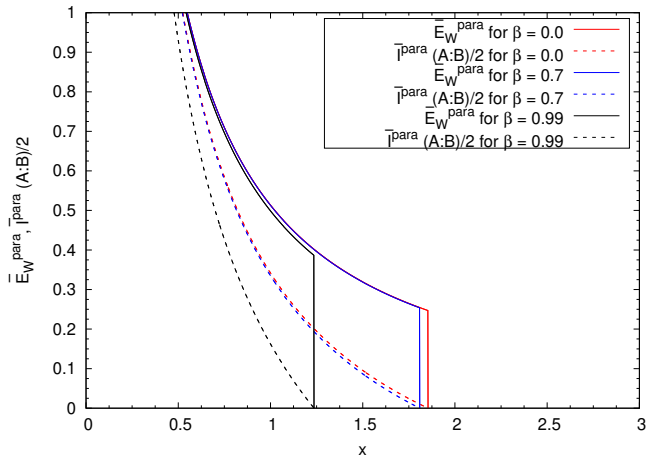

Figure 3.1: In the above figure, we show how the EWCS and HMI vary with respect to the separation distance for different values of the boost parameter. The solid curves represent the EWCS and the dotted curves represent the HMI. To make these polts we have considered $d = 3$, $l = 3$ and $z_0 = 10$.

critical separation in terms of the subsystem length and boost parameter. It is very much difficult to obtain an explicit analytical expression of x_c in terms of the subsystem length and boost parameter. Therefore we shall simplify our analysis by fixing the spacetime dimension, namely, we perform the computations for $d = 3$ and $d = 4$. In $d = 3$, the condition $I^{\parallel}(A : B) = 0$ at $x = x_c$ gives the following equation

$$2\left(\frac{\sqrt{\pi}\Gamma(3/4)}{\Gamma(1/5)}\right)^2\left[-\frac{2}{l}+\frac{1}{x_c}+\frac{1}{2l+x_c}\right]+\frac{\sqrt{\pi}\frac{\Gamma(3/4)}{4}(1+\beta^2\gamma^2)}{\left(\frac{2\sqrt{\pi}\Gamma(3/4)}{\Gamma(1/5)}\right)^2(10)^3}\left[l^2-\frac{x_c^2}{2}-\frac{(2l+x_c)^2}{2}\right] = 0 \quad . \tag{3.31}$$

On the other hand, for $d = 4$ we get

$$2\left(\sqrt{\pi}\frac{\Gamma(4/6)}{\Gamma(1/7))}\right)^3\left[-\frac{2}{l^2}+\frac{1}{x_c^2}+\frac{1}{(2l+x_c)^2}\right]+\frac{\frac{\sqrt{\pi}\Gamma(4/3)}{5\Gamma(5/6)}\left(\frac{3}{2}+\beta^2\gamma^2\right)}{\left(2\sqrt{\pi}\frac{\Gamma(4/6)}{\Gamma(1/7)}\right)^2(10)^4}\left[l^2-\frac{x_c^2}{2}-\frac{(2l+x_c)^2}{2}\right] = 0 \quad . \tag{3.32}$$

One needs to solve the above equations in order represent x_c in terms of the subsystem size l. We now graphically represent our observations in Fig.(3.1).

It has been pointed out in [4] that mutual information vanishes at a critical separation length,

namely, x_c for a fixed subsystem size. This in turn means that at $x = x_c$, EWCS shows a discontinuity which represent a phase transition between the connected phase and disconnected phase of the entanglement wedge. Upto $x = x_c$, connected phase is the physical whereas beyond $x > x_c$ disconnected phase is physical. Some recent works in this direction can be found in [38, 114, 160, 170, 171]. In order to compute the critical length x_c for the case in hand, we firstly fix the parameters $d = 3$, $l = 3$ and $z_0 = 10$. We then plot the expressions of EWCS and HMI, namely $\bar{E}_W^{para}$ and $\bar{I}^{para}(A : B)$, for various values of the boost parameter β. We observe that increasing the value of the boost parameter causes earlier saturation of the HMI and in turn means earlier phase transition for the corresponding entanglement wedge. This has been shown in Fig.(3.1).

Similar to the HEE, we now compute the change in HMI and EWCS due to inclusion of the anisotropy (boost) in the boundary field theory. This has been given below

$$\begin{aligned}\delta E_W^{\parallel} &\equiv E_W^{\parallel} - E_W^{pure} \\ &= \frac{V_{d-2}}{32 G_{d+1} z_0^d b_0^2}\left[\frac{1}{2} - \left(1 + \frac{2\beta^2\gamma^2}{d-1}\right)\frac{b_1}{b_0} + \frac{\beta^2\gamma^2}{d-1}\right]\left[(2l+x)^2 - x^2\right]\end{aligned} \tag{3.33}$$

and by using eq.(s)(3.28,3.29)

$$\begin{aligned}\delta I^{\parallel}(A:B) &\equiv I^{\parallel}(A:B) - I^{pure}(A:B) \\ &= \frac{V_{d-2} b_1 (d+1)}{32 G_{d+1} b_0^2 z_0^d}\left(\frac{d-1}{d+1} + \frac{2\beta^2\gamma^2}{d+1}\right)\left(2l^2 - x^2 - (2l+x)^2\right)\end{aligned} \tag{3.34}$$

.

Now we shall try to relate this change in EWCS due to the boost with the excitation energy and pressure of the boundary CFT. To do this we first take the adjacent subsystem limit, that is, $x \to 0$ in eq.(3.33) and then compare it with the change in HEE given by the expression in eq.(3.21). Thus we get

$$\delta E_W^{\parallel} = \lambda_1 \, \delta S_{EE}^{\parallel} \, . \tag{3.35}$$

This above result shows that the change in EWCS due to the presence of boost is proportional to the boost initiated change in HEE upto a constant factor λ_1[4]. We should keep in momd that, we have obtained the above result under the thin strip approximation. The above relation can be used

[4]The explicit expression of λ_1 has been given in Appendix B.

to relate the leading order change in EWCS to the excitation energy and pressure of the boundary CFT. This can be done by using the relation for the change in HEE ($\delta S^{\parallel}_{EE}$) with the boundary field theoretic quantities like excitation energy and pressure. This relation reads [192, 193]

$$\delta S^{\parallel}_{EE} = \frac{1}{T_E}\left(\Delta E_{\parallel} - \frac{d-1}{d+1}\mathcal{V}\Delta P_{\parallel}\right) \tag{3.36}$$

where $\Delta E_{\parallel}$, $\Delta P_{\parallel}$, T_E, $\mathcal{V} = V_{d-2}l$ are the excitation energy, pressure, entanglement temperature and volume of the subsystem respectively. The expressions for these quantities read [192, 193]

$$\begin{aligned}
\Delta E_{\parallel} &= \frac{V_{d-2}l}{16\pi G_{d+1}}\left(\frac{d-1}{d}+\beta^2\gamma^2\right)\frac{d}{z_0^d} \\
\Delta P_{\parallel} &= \frac{d}{16\pi G_{d+1}}\left(\frac{1}{d}+\beta^2\gamma^2\right)\frac{1}{z_0^d} \\
T_E &= \frac{b_0^2 d}{a_1\pi l}\,.
\end{aligned} \tag{3.37}$$

Now by substituting eq.(3.36) in eq.(3.35), we obtain

$$\delta E^{\parallel}_{W} = \frac{\lambda_1}{T_E}\left(\Delta E_{\parallel} - \frac{d-1}{d+1}\mathcal{V}\Delta P_{\parallel}\right)\,. \tag{3.38}$$

The above result shows that, the change in EWCS is related to the excitation energy and pressure of the boundary theory.

3.3.3 Entanglement negativity

We now turn our attention to another entanglement measure called the entanglement negativity, also referred to as the logarithmic negativity (E_N). This measure is considered a strong candidate for quantifying entanglement in mixed states. In section(1.1.4), we have briefly discussed the concept of entanglement negativity and its significance in context of quantum information theory. However, to proceed further we now qualitatively discuss how one can compute entanglement negativity holographically in section(1.4.4). Two different proposals have been suggested by various literatures in this direction. One of the proposal suggests that, E_N can be computed by calculating the area of an extremal cosmic brane that ends at the boundary of the entanglement wedge [81, 82]. Another proposal states that, the entanglement negativity is given by certain combinations holographic entanglement entropy [84, 85, 86, 87, 88, 89]. Both of these proposals reproduce the exact known result of entanglement negativity in CFT. In our work we have followed the second

proposal to compute the entanglement negativity holographically.

To compute E_N holographically we first consider two adjacent strip like subsystems. Let us conider two strip like adjacent subsystems A and B with length l_1 and l_2 respectively. In the case of such adjacent subsystems the entanglement negativity (E_N) is defined as [84, 85, 86, 87, 88, 89]

$$E^{\parallel}_{N_{adj}} = \frac{3}{4}\left[S^{\parallel}_{EE}(l_1) + S^{\parallel}_{EE}(l_2) - S^{\parallel}_{EE}(l_1+l_2)\right] \ . \tag{3.39}$$

Substitutig eq.(3.19) in the above expression, one can find the entanglement negativity for adjacent subsystems. This results

$$\begin{aligned} E^{\parallel}_{N_{adj}} &= \frac{3V_{d-2}a_0}{8G_{d+1}}\Bigg[(2b_0)^{d-2}\left[\frac{1}{l_1^{d-2}}+\frac{1}{l_2^{d-2}}-\frac{1}{(l_1+l_2)^{d-2}}\right] \\ &+ \frac{1}{2z_0^d(2b_0)^2}\frac{b_1}{a_0}\left(\frac{d-1}{2}+\beta^2\gamma^2\right)\left[l_1^2+l_2^2-(l_1+l_2)^2\right]\Bigg] + \frac{3}{4}S_{div} \ . \end{aligned} \tag{3.40}$$

Furthermore, one can get the entanglement negativity for two adjacent subsystem for pure AdS_{d+1} background by taking the limit $\beta \to 0$, $z_0 \to \infty$ of the above result. This reads

$$E^{pure}_{N_{adj}} = \frac{3V_{d-2}a_0(2b_0)^{d-2}}{8G_{d+1}}\left[\frac{1}{l_1^{d-2}}+\frac{1}{l_2^{d-2}}-\frac{1}{(l_1+l_2)^{d-2}}\right] + \frac{3}{4}S_{div} \ . \tag{3.41}$$

It is to be noted from eq.(s)(3.40,3.41) that, for adjacent subsystems E_N is a divergent quantity. We now compute the change in E_N due to the inclusion of boost, this we define as

$$\begin{aligned} \delta E^{\parallel}_{N_{adj}} &\equiv E^{\parallel}_{N_{adj}} - E^{pure}_{N_{adj}} \\ &= \frac{3V_{d-2}b_1}{16z_0^dG_{d+1}(2b_0)^2}\left[\frac{d-1}{2}+\beta^2\gamma^2\right]\left(l_1^2+l_2^2-(l_1+l_2)^2\right) \ . \end{aligned} \tag{3.42}$$

Furthermore, if we consider a special case where, the subsystems to be of equal length, that is, $l_1 = l_2 = l$, we then obtain the following expression of $\delta E^{\parallel}_{N_{adjacent}}$

$$\delta E^{\parallel}_{N_{adj}}|_{l_1=l_2} = -\frac{3V_{d-2}b_1l^2}{8z_0^dG_{d+1}(2b_0)^2}\left[\frac{d-1}{2}+\beta^2\gamma^2\right] \ . \tag{3.43}$$

This completes our analysis of computing E_N for two adjacent subsystems.

We now consider two disjoint strip like subsystems A and B with length l_1 and l_2. The subsystems under consideration are separated by a length x. In this case the entanglement negativity reads [99, 100]

$$E^{\parallel}_{N_{dis}} = \frac{3}{4}\left[S^{\parallel}_{EE}(l_1+x) + S^{\parallel}_{EE}(l_2+x) - S^{\parallel}_{EE}(l_1+l_2+x) - S^{\parallel}_{EE}(x)\right] \ . \tag{3.44}$$

Now to obtain the explict expression of E_N we have to use the expression of HEE given in eq.(3.19) in the above result. This results

$$E^{\parallel}_{N_{dis}} = \frac{3V_{d-2}a_0}{8G_{d+1}}\Bigg[(2b_0)^{d-2}\left(\frac{1}{(l_1+x)^{d-2}}+\frac{1}{(l_2+x)^{d-2}}-\frac{1}{(l_1+l_2+x)^{d-2}}-\frac{1}{x^{d-2}}\right) + \frac{b_1/a_0}{2z_0^d(2b_0)^2}\left(\frac{d-1}{2}+\beta^2\gamma^2\right)\left((l_1+x)^2+(l_2+x)^2-(l_1+l_2+x)^2-x^2\right)\Bigg] . \quad (3.45)$$

Similar to the adjacent case, in the limit $\beta \to 0$ and $z_0 \to \infty$ of the above expression, we get the the pure AdS_{d+1} result. This reads

$$E^{pure}_{N_{dis}} = \frac{3V_{d-2}a_0}{8G_{d+1}}(2b_0)^{d-2}\left(\frac{1}{(l_1+x)^{d-2}}+\frac{1}{(l_2+x)^{d-2}}-\frac{1}{(l_1+l_2+x)^{d-2}}-\frac{1}{x^{d-2}}\right) . \quad (3.46)$$

Furthermore, it is to be noted that in the disjoint set up, the entanglement negativity does not receive any contribution from the divergent piece. Therefore the entnaglement negtaivity for disjoint subsystems is a finite quantity. On the other hand, the change in entanglement negativity (disjoint case) due to the boost can be defined as

$$\begin{aligned}\delta E^{\parallel}_{N_{dis}} &\equiv E^{\parallel}_{N_{dis}} - E^{pure}_{N_{dis}} \\ &= \frac{3V_{d-2}b_1}{16z_0^d(2b_0)^2}\left(\frac{d-1}{2}+\beta^2\gamma^2\right)\left((l_1+x)^2+(l_2+x)^2-(l_1+l_2+x)^2-x^2\right) . \quad (3.47)\end{aligned}$$

So far we have considered the subsystems with different lengths l_1 and l_2. We now consider a special scenario where the lengths of the two strip like subsystems A and B are equal, that is, $l_1 = l_2 = l$. At this condition, the expressions given in eq.(s)(3.45,3.46) get simplified to the following forms

$$\begin{aligned}\bar{E}^{para}_{N_{dis}}|_{l_1=l_2} &= \frac{3}{4}\Bigg[a_0(2b_0)^{d-2}\left(\frac{2}{(l+x)^{d-2}}-\frac{1}{(2l+x)^{d-2}}-\frac{1}{x^{d-2}}\right) \\ &+ \frac{b_1/a_0}{2z_0^d(2b_0)^2}\left(\frac{d-1}{2}+\beta^2\gamma^2\right)\left(2(l+x)^2-(2l+x)^2-x^2\right)\Bigg] \quad (3.48) \\ \bar{E}^{pure}_{N_{dis}}|_{l_1=l_2} &= \frac{3a_0}{4}(2b_0)^{d-2}\left(\frac{2}{(l+x)^{d-2}}-\frac{1}{(2l+x)^{d-2}}-\frac{1}{x^{d-2}}\right) . \quad (3.49)\end{aligned}$$

where we have used the scaling $\bar{E}_N = \frac{2G_{d+1}}{V_{d-2}}E_N$. On the similar note, the change in entanglement negativity with the condition $l_1 = l_2 = l$ reads

$$\delta E^{\parallel}_{N_{dis}}|_{l_1=l_2} = \frac{3V_{d-2}b_1}{16z_0^d(2b_0)^2G_{d+1}}\left(\frac{d-1}{2}+\beta^2\gamma^2\right)\left(2(l+x)^2-(2l+x)^2-x^2\right) . \quad (3.50)$$

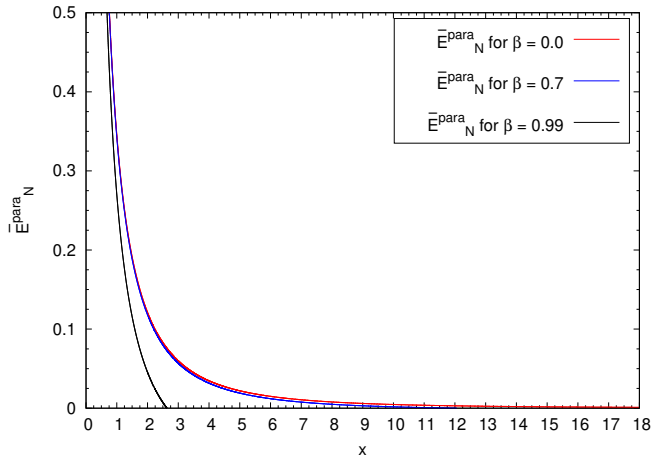

Figure 3.2: Variation of entanglement negativity for two disjoint subsystems (with equal length $l = 3$) with repect to the separation distance between the two subsystems is plotted in the above figure. To obtain these polts we have fixed $d = 3$ and $z_0 = 10$.

It is also reassuring to observe that if we consider the adjacent subsystem limit $x \to 0$ in eq.(3.50), we obtain eq.(3.43).

In order to understand the effect of the boost parameter on the entanglement negativity, we plot the result of E_N of two disjoint subsystems of equal length l (given in eq.(3.48)) with respect to the separation distance. We consider different values of the boost parameter β. We find that for $\beta \to 0$ and $z_0 \to \infty$, the entanglement negativity does not vanish at any value of the separation distance between two subsystems.This corresponds to the outcome for the entanglement negativity in the case of two disjoint subsystems of equal length within a pure AdS_{d+1} geometry. However, for a non-zero, finite value of the boost parameter β, we observe that entanglement negativity vanishes at a critical separation distance x'_c. Furthermore we have also observed that, the value of this critical separation length x'_c decreases with the increase in the value of the boost parameter β. Thus, one can say that entanglement negativity measures correlation between two disjoint subsystems even when they are not in the connected phase because entanglement negativity vanishes at a larger value of the separtion compared to mutual information and EWCS.

On the other hand, comparing the expression given in eq.(3.43) with eq.(3.21), we obtain the following relation

$$\delta E^{\parallel}_{N_{adj}}|_{l_1=l_2} = \lambda_2 \; \delta S^{\parallel}_{EE} \; . \tag{3.51}$$

The above relation suggests that the change in entanglement negativity due to the presence of boost is proportional to the change in HEE upto a constant factor λ_2[5]. This has also been observed in case of EWCS.

3.3.4 Holographic subregion complexity

Quantum complexity is another fundamental quantity in the context of quantum information theory. The basic concept of circuit complexity has already been discussed earlier in section(1.1.5). In this section we compute complexity holographically. There are different proposals to compute the complexity holographically. We have discueed these proposals in details in section (1.4.5). In our study we are particularly interested in the computation of holograhic subregion complexity. It relates co-dimension one volume ($V(\gamma)$) enclosed by the extremal RT surface to the complexity [112]

$$\mathcal{C}_V = \frac{V(\gamma)}{8\pi R G_{d+1}} \ . \tag{3.52}$$

Some interesting works related to the holographic computation of complexity can be found in [197, 198, 199, 200, 201, 202, 203, 204, 205, 206, 207, 208, 209, 210, 211].

Now in this set up (where the subsystem is taken to be along the direction of the boost), if $V(\gamma)^{\parallel}$ denotes the maximal co-dimension-one volume enclosed by the co-dimension-two static, minimal Ryu-Takayanagi (RT) surface in the bulk. Then the holographic subregion complexity (HSC) reads

$$\mathcal{C}_V^{\parallel} = \frac{V(\gamma)^{\parallel}}{8\pi R G_{d+1}} \ . \tag{3.53}$$

It is to be kept in mind that, in this case where the subsystem is placed parallel to the boost direction, the volume of the corresponding RT surface can be obtained by using eq.(3.1) and eq.(3.9). This in turn leads to the following [212]

$$\begin{aligned}\mathcal{C}_V^{\parallel} &= \frac{V_{d-2}}{8\pi G_{d+1}(d-1)}\left[\frac{l}{\epsilon^{d-1}} - \frac{2^{d-2}\pi^{\frac{d-1}{2}}}{(d-1)}\left(\frac{\Gamma(\frac{d}{2d-2})}{\Gamma(\frac{1}{(2d-2)})}\right)^{d-3}\frac{1}{l^{d-2}}\right. \\ &- \left.\frac{l^2}{4b_0^2 z_0^d}\left[\left(\frac{(d-2)\pi b_1}{2(d-1)b_0^2} + (2-d)c_0\right) + \beta^2\gamma^2\left(\frac{(d-2)\pi}{2(d-1)^2 b_0}\left(\frac{2b_1}{b_0} - 1\right) + c_2 - c_0 d\right)\right]\right] .\end{aligned} \tag{3.54}$$

[5]The explicit expression of λ_2 has been given in Appendix B.

where we have set AdS radius $R = 1$. Similarly the holographic subregion complexity for a subsystem of length l for pure AdS_{d+1} geometry reads

$$\mathcal{C}_V^{pure} = \frac{V^{pure}}{8\pi G_{d+1}} = \frac{1}{8\pi G_{d+1}}\left[\frac{V_{d-2}}{d-1}\frac{l}{\epsilon^{d-1}} - \frac{2^{d-2}\pi^{\frac{d-1}{2}}}{(d-1)^2}\left(\frac{\Gamma(\frac{d}{2d-2})}{\Gamma(\frac{1}{(2d-2)})}\right)^{d-3}\frac{V_{d-2}}{l^{d-2}}\right]. \tag{3.55}$$

The above result can also be obtained by taking the limits $\beta \to 0$ and $z_0 \to \infty$ of eq.(3.54). We compute the change in complexity due to the presence of the boost parameter. This we define as $\delta\mathcal{C}_V^{\parallel} \equiv \mathcal{C}_V^{\parallel} - \mathcal{C}_V^{pure}$. By substituting the corresponding expressions, we get

$$\delta C_V^{\parallel} = -\frac{1}{8\pi G_{d+1}}\frac{V_{d-2}l^2}{4b_0^2 z_0^d(d-1)}\left[\left(\frac{(d-2)\pi b_1}{2(d-1)b_0^2} + (2-d)c_0\right) + \beta^2\gamma^2\left(\frac{(d-2)\pi}{2(d-1)^2 b_0}\left(\frac{2b_1}{b_0} - 1\right) + c_2 - c_0 d\right)\right]. \tag{3.56}$$

3.3.5 Mutual complexity

In order to find the complexity for mixed states, we follow the purification complexity (CoP) protocol. It is defined as the minimal complexity among all possible purifications of the mixed state. This protocol suggests we need to compute the mutual complexity in order to compute the mixed state complexity [33, 32, 34, 113]. We have discussed the purification complexity in the context of quantum information in section(). We have also described the holographic computation of mutual complexity earlier.

To compute the mutual complexity holographically, we consider two disjoint subsystems A and B of equal length l on the boundary Cauchy slice, separated by a distance x. For $\frac{x}{l} < 1$, the mutual complexity is given by [32, 33, 34, 35, 36, 38]

$$\begin{aligned}\Delta\mathcal{C}^{\parallel} &= \mathcal{C}_V^{\parallel}(A) + \mathcal{C}_V^{\parallel}(B) - \mathcal{C}_V^{\parallel}(A\cup B)\\ &= 2\mathcal{C}_V^{\parallel}(l) - \mathcal{C}_V^{\parallel}(2l+x) + \mathcal{C}_V^{\parallel}(x)\end{aligned} \tag{3.57}$$

where in the last line we have used $C_V^{\parallel}(A\cup B) = C_V^{\parallel}(2l+x) - C_V^{\parallel}(x)$, for $\frac{x}{l} < 1$. This relation is valid in general for two subsystems of equal length and with separation x [113]. Now by using

eq.(3.54), we find the mutual complexity as

$$\begin{aligned}\Delta\mathcal{C}^{\parallel} &= \frac{V_{d-2}}{8\pi G_{d+1}(d-1)}\Bigg[\frac{2^{d-2}\pi^{\frac{d-1}{2}}}{(d-1)}\left(\frac{\Gamma(\frac{d}{2d-2})}{\Gamma(\frac{1}{(2d-2)})}\right)^{d-3}\left(\frac{1}{(2l+x)^{d-2}}-\frac{1}{x^{d-2}}-\frac{2}{l^{d-2}}\right)\\ &- \frac{1}{4b_0^2 z_0^d}\Bigg[\left(\frac{(d-2)\pi b_1}{2(d-1)b_0^2}+(2-d)c_0\right)\\ &+ \beta^2\gamma^2\left(\frac{(d-2)\pi}{2(d-1)^2 b_0}\left(\frac{2b_1}{b_0}-1\right)+c_2-c_0 d\right)\Bigg]\left(2l^2+x^2-(2l+x)^2\right)\Bigg]\end{aligned} \tag{3.58}$$

where the expressions corresponding to the constant terms c_0, c_1 and c_2 are given in the Appendix. On the other hand, the mutual complexity for pure AdS_{d+1} background is obtained to be

$$\Delta\mathcal{C}^{pure} = \frac{V_{d-2}}{8\pi G_{d+1}(d-1)}\frac{2^{d-2}\pi^{\frac{d-1}{2}}}{(d-1)}\left(\frac{\Gamma(\frac{d}{2d-2})}{\Gamma(\frac{1}{(2d-2)})}\right)^{d-3}\left(\frac{1}{(2l+x)^{d-2}}-\frac{1}{x^{d-2}}-\frac{2}{l^{d-2}}\right). \tag{3.59}$$

Keeping this result in hand, the change in mutual complexity can be computed by

$$\begin{aligned}\delta\mathcal{C}^{\parallel} &\equiv \Delta\mathcal{C}^{\parallel}-\Delta\mathcal{C}^{pure}\\ &= -\frac{V_{d-2}}{8\pi G_{d+1}(d-1)}\frac{1}{4b_0^2 z_0^d}\Bigg[\left(\frac{(d-2)\pi b_1}{2(d-1)b_0^2}+(2-d)c_0\right)\\ &+ \beta^2\gamma^2\left(\frac{(d-2)\pi}{2(d-1)^2 b_0}\left(\frac{2b_1}{b_0}-1\right)+c_2-c_0 d\right)\Bigg]\left(2l^2+x^2-(2l+x)^2\right) \quad .\end{aligned} \tag{3.60}$$

Similar to the previously computed quantities, we scale the mutual complexity in the following way

$$\bar{I}_C^{para}=\frac{2G_{d+1}}{V_{d-2}}\Delta\mathcal{C}^{\parallel} \text{ and } \bar{I}_C^{pure}=\frac{2G_{d+1}}{V_{d-2}}\Delta\mathcal{C}^{pure}\ . \tag{3.61}$$

We now proceed to represent our results graphically. It has been noted that the mutual complexity can either be subadditive if $\Delta\mathcal{C}>0$ or it can be superadditive if $\Delta\mathcal{C}<0$. In order to observe this for the case in hand, we take the help of fig.(3.3). We observe that the mutual complexity is super-additive for every possible value of the boost parameter β. Furthermore, the effect of the boost on the mutual complexity can be observed from the mentioned figure.

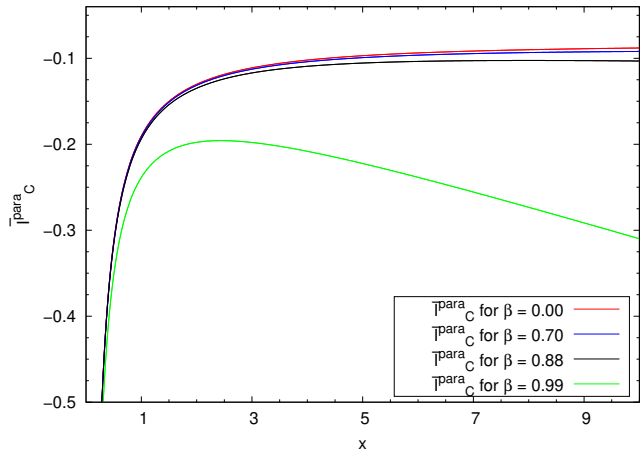

Figure 3.3: The figure reprents the change of the mutual complexity with respect to the separation distance (x) between the two subsystems for different values of boost parameter. In order to get these plots we have set $l = 3$, $d = 3$ and $z_0 = 10$.

3.4 Strip perpendicular to the boost

In this section we consider a strip like subsystem having orientation perpendicular to the boost direction and compute various information theoretic measures as we have done in the previous section for parall strips. Further, we assume that the subsystem is placed along the x_1 direction while boost is along the y direction. The subsystem is specified by the $-\frac{l}{2} \leq x_1 \leq \frac{l}{2}$, $0 \leq y \leq l_y$, and $0 \leq x_i \leq l_i$. l_y and l_i is taken to be very large, that is $l_y, l_i >> l$. Furthermore we assume that that the lengths along the directions other than x_1 are fixed.

3.4.1 Holographic entanglement entropy

We now again use the HRT prescription to obtain the HEE of a strip perpendicular to the boost. The co-dimension two static minimal surface Γ_A^{min} can be parametrised by $z = z(x_1)$ and $t = t(x_1)$. This leads to the following expression of HEE

$$S_{EE}^{\perp} = \frac{V_{d-2}}{2G_{d+1}} \int_{-\frac{l}{2}}^{0} \frac{dx_1}{z^{d-1}} \sqrt{K(z)} \left[1 + \frac{z'^2}{f(z)} - t'^2 \left(\frac{f(z)}{K(z)} - \frac{K(z)}{\beta^2} \left(1 - \frac{1}{K(z)} \right)^2 \right) \right]^{\frac{1}{2}} . \quad (3.62)$$

Identifying the integrant of the above expression as Lagrangian $\mathcal{L} = \mathcal{L}(z, z', t, t')$, we note that x_1 is a cyclic coordinate. This results in the following conserved quantity

$$\mathcal{H} = -\frac{\sqrt{K(z)}}{z^{d-1}\sqrt{1+\frac{z'^2}{f(z)} - t'^2\left(\frac{f(z)}{K(z)} - \frac{K(z)}{\beta^2}\left(1-\frac{1}{K(z)}\right)^2\right)}} = constant = c\ . \tag{3.63}$$

The constant c, can be fixed by introducing the turning point $(z_t^\perp, t_t^\perp)$ inside the bulk at which z' and t' vanishes. This fixes the above constant to be $c = -\frac{\sqrt{K(z_t^\perp)}}{z_t^{\perp(d-1)}}$. By using this value of the constant c in eq.(3.63), we obtain the following equation

$$1 + \frac{z'^2}{f(z)} - t'^2\left(\frac{f(z)}{K(z)} - \frac{K(z)}{\beta^2}\left(1-\frac{1}{K(z)}\right)^2\right) = \frac{K(z)}{K(z_t^\perp)}\left(\frac{z_t^\perp}{z}\right)^{2d-2}\ . \tag{3.64}$$

Substituting the above expression in eq.(3.62), the HEE of the strip is given by

$$S_{EE}^\perp = \frac{V_{d-2}}{2G_{d+1}}\int_{-\frac{l}{2}}^{0}\frac{dx_1}{z^{d-1}}\frac{K(z)}{\sqrt{K(z_t^\perp)}}\left(\frac{z_t^\perp}{z}\right)^{d-1}\ . \tag{3.65}$$

It is to be mentioned that, one can obtain the similar result by following the RT formalism. To proceed further, we now write the boundary coordinate in terms of the bulk coordinate. This can be done by simplifying eq.(3.64). Thus we can write dx_1 in terms of dz in the following way

$$dx_1 = \frac{dz\left(\frac{z}{z_t^\perp}\right)^{d-1}\left[1 - \frac{t'^2(z/z_t^\perp)^{2d-2}\left(\frac{f(z)}{K(z)} - \frac{K(z)}{\beta^2}\left(1-\frac{1}{K(z)}\right)^2\right)}{\left[\frac{K(z)}{K(z_t^\perp)} - \left(\frac{z}{z_t^\perp}\right)^{2d-2}\right]}\right]^{\frac{1}{2}}}{\sqrt{f(z)}\left[\frac{K(z)}{K(z_t^\perp)} - \left(\frac{z}{z_t^\perp}\right)^{2d-2}\right]^{\frac{1}{2}}}\ . \tag{3.66}$$

To proceed further, we have to consider the thin strip approximation. This can be incorporated by keeping terms upto $\mathcal{O}\left((z/z_t^\perp)^d\right)$ and neglect the higher order terms in the above expression. This results

$$dx_1 = \frac{dz\left(\frac{z}{z_t^\perp}\right)^{d-1}}{\sqrt{f(z)}\left[\frac{K(z)}{K(z_t^\perp)} - \left(\frac{z}{z_t^\perp}\right)^{2d-2}\right]^{\frac{1}{2}}}\ . \tag{3.67}$$

Substituting the above result in eq.(3.65) we can obtain the following form of HEE [192, 193]

$$S_{EE}^\perp = \frac{V_{d-2}}{2G_{d+1}}\int_\epsilon^{z_t^\perp}\frac{dz}{z^{d-1}\sqrt{f(z)}\left[1 - \left(\frac{z}{z_t^\perp}\right)^{2d-2}\frac{K(z)}{K(z_t^\perp)}\right]^{\frac{1}{2}}}\ . \tag{3.68}$$

It is to be mentioned that, in the thin strip approximation one can simplify $\frac{K(z)}{K(z_t^\perp)}$ as follows

$$\frac{K(z_t^\perp)}{K(z)} \approx 1+\beta^2\gamma^2\left[1-\left(\frac{z}{z_0}\right)^d\right]\left(\frac{z_t^\perp}{z_0}\right)^d \ . \tag{3.69}$$

In the above result we have kept terms upto $\mathcal{O}\left((z/z_t^\perp)^d\right)$. Using the above expression, the HEE of the strip is obtained to be [192, 193]

$$S_{EE}^\perp = S_{div}+\frac{V_{d-2}a_0}{z_t^{\perp(d-2)}}\left(1+\left(\frac{p'^d+q'^d}{2}\right)\frac{a_1}{a_0}+\frac{q'^d}{2}\left[\frac{d+1}{d-1}\frac{b_1}{a_0}-\frac{1}{d-1}\frac{b_0}{a_0}\right]\right) \tag{3.70}$$

where G_{d+1} is the $(d+1)$-dimensional Newton's constant and $V_{d-2}=l_y l_2...l_{d-2}$ is the spatial volume of the boundary and $p'^d=\left(\frac{z_t^\perp}{z_0}\right)^d$, $q'^d=\beta^2\gamma^2\left(\frac{z_t^\perp}{z_0}\right)^d$. S_{div} represents the subsystem independent divergent term $S_{div}=\frac{V_{d-2}}{2G_{d+1}(d-2)}\frac{1}{\epsilon^{d-2}}$.

Now we would obtain the subsystem length in terms of the turning point. Under the thin strip approximation, the relation between the subsystem size l and the turning point $z_t^\perp$ reads [192, 193]

$$l \approx 2z_t^\perp\left[b_0+\frac{1}{2}\left(\frac{z_t^\perp}{z_0}\right)^d\left(b_1+\beta^2\gamma^2 I_l\right)\right] \ . \tag{3.71}$$

On the other hand, the relationship between $z_t^\perp$ and $\bar{z}_t$ (where $\bar{z}_t$ is turning point for pure AdS back ground) is obtained to be

$$z_t^\perp = \frac{l/2}{b_0+\frac{1}{2}\left(\frac{z_t^\perp}{z_0}\right)^d\left[b_1+\beta^2\gamma^2 I_l\right]} \approx \frac{\bar{z}_t}{1+\frac{1}{2}\left(\frac{\bar{z}_t}{z_0}\right)^d\left(\frac{b_1}{b_0}+\frac{\beta^2\gamma^2}{b_0}I_l\right)} \ . \tag{3.72}$$

Now the HEE in terms of the subsystem size can be written down as [192, 193]

$$S_{EE}^\perp = S_{div}+\frac{V_{d-2}a_0}{2G_{d+1}}\left(\frac{2b_0}{l}\right)^{d-2}+\frac{V_{d-2}b_1(d+1)l^2}{32G_{d+1}b_0^2 z_0^d}\left(\frac{d-1}{d+1}+\beta^2\gamma^2\right) \ . \tag{3.73}$$

The change in HEE due to boost can be computed by using eq.(3.73) and eq.(3.20). Thus the change in HEE reads

$$\delta S_{EE}^\perp \equiv S_{EE}^\perp - S_{EE}^{pure} = \frac{V_{d-2}b_1(d+1)l^2}{32G_{d+1}b_0^2 z_0^d}\left(\frac{d-1}{d+1}+\beta^2\gamma^2\right) \ . \tag{3.74}$$

Furthermore, the relation between $\delta S_{EE}^\perp$ and $\delta S_{EE}^\parallel$ reads

$$\delta S_{EE}^\parallel = \left[\frac{1+\frac{2}{d-1}\beta^2\gamma^2}{1+\frac{d+1}{d-1}\beta^2\gamma^2}\right]\delta S_{EE}^\perp \ . \tag{3.75}$$

From equations (3.21) and (3.74), it is evident that $S^{\perp}_{EE} \geq S^{\parallel}_{EE}$. This indicates that the entanglement entropy of a strip oriented perpendicular to the boost direction is greater than that of a strip aligned parallel to the boost. This observation underscores the anisotropic nature induced by the boost in the boundary theory, as the boost breaks the rotational symmetry of the boundary field theory [182]. The increased entanglement entropy in the perpendicular direction, compared to the parallel case, arises from the pressure asymmetry in the conformal field theory (CFT). Specifically, the CFT 'pressure' differs between the perpendicular and parallel directions, with the parallel direction experiencing higher pressure due to the boost [195]. This pressure imbalance results in excitations in the CFT requiring more energy in the parallel strip than in the perpendicular strip. Consequently, the entanglement entropy is enhanced in the perpendicular case relative to the parallel case [192, 193]. This reasoning highlights the significant role of CFT 'pressure' in the boundary in determining the entanglement entropy of subsystems within the boundary.

3.4.2 EWCS and Holographic mutual information

We now proceed to compute the minimal cross-section of the entanglement wedge for subsystems oriented perpendicular to the direction of the boost. Consider two subsystems, A and B, each of equal length l and separated by a distance x. In this setup, we aim to determine the minimal area of a vertical constant x_1 hyper-surface that divides the entanglement wedge M_{AB} into two regions corresponding to A and B. The induced metric on this constant x_1 hyper-surface is given by

$$ds^2|_{ind} = \frac{1}{z^2}\left(Kdy^2 + ... + dx^2_{d-2} + \frac{dz^2}{f(z)}\right) . \tag{3.76}$$

The above mentioned induced metric leads to the following expression for EWCS

$$E^{\perp}_W = \frac{V_{d-2}}{4G_{d+1}} \int_{z^{\perp}_t(x)}^{z^{\perp}_t(2l+x)} \frac{dz}{z^{d-1}} \sqrt{\frac{K(z)}{f(z)}} . \tag{3.77}$$

Under the thin strip approximation, the explicit expression of $E^{\perp}_W$ is found to be

$$E^{\perp}_W = \frac{V_{d-2}}{4G_{d+1}(d-2)} \left[\frac{1}{(z^{\perp}_t(x))^{d-2}} - \frac{1}{(z^{\perp}_t(2l+x))^{d-2}}\right] + \frac{V_{d-2}(1+\beta^2\gamma^2)}{16G_{d+1}z_0^d} \left[(z^{\perp}_t(2l+x))^2 - (z^{\perp}_t(x))^2\right] . \tag{3.78}$$

By using eq.(3.72) in the above expression, we get EWCS in terms of the subsystem size l and distance of separation x. This reads

$$E_W^{\perp} = \frac{V_{d-2}}{2G_{d+1}}\left[\frac{(2b_0)^{d-2}}{2(d-2)}\left[\frac{1}{x^{d-2}}-\frac{1}{(2l+x)^{d-2}}\right]+\frac{[(2l+x)^2-x^2]}{4z_0^d(2b_0)^2}\left(\frac{1+\beta^2\gamma^2}{2}-\left(\frac{b_1}{b_0}+\frac{\beta^2\gamma^2 I_l}{b_0}\right)\right)\right] . \tag{3.79}$$

Now we introduce the following scaling similar to the parallel case

$$\bar{E}_W^{perp} = \frac{2G_{d+1}}{V_{d-2}}E_W^{\perp} . \tag{3.80}$$

Furthermore, the change in EWCS in this set up stands to be

$$\begin{aligned}\delta E_W^{\perp} &\equiv E_W^{\perp} - E_W^{pure} \\ &= \frac{V_{d-2}}{32G_{d+1}z_0^d b_0^2}\left[\frac{1}{2}\left(1+\beta^2\gamma^2\right)-\left(\frac{b_1}{b_0}+\beta^2\gamma^2\frac{I_l}{b_0}\right)\right]\left[(2l+x)^2-x^2\right] .\end{aligned} \tag{3.81}$$

We can express $\delta E_W^{\perp}$ in terms of $\delta E_W^{\parallel}$ by using eq(s).(3.33,3.81). This results

$$\delta E_W^{\perp} = \left[\frac{\frac{1}{2}(1+\beta^2\gamma^2)-\left(\frac{b_1}{b_0}+\frac{\beta^2\gamma^2 I_l}{b_0}\right)}{\frac{1}{2}-\left(1+\frac{2\beta^2\gamma^2}{d-1}\right)\frac{b_1}{b_0}+\frac{\beta^2\gamma^2}{d-1}}\right]\delta E_W^{\parallel} . \tag{3.82}$$

We can now relate this change in EWCS (given in eq.(3.81)) with excitation energy and pressure of the boundary theory. To do this we again consider the adjacent subsystem limit ($x \to 0$). In this limit the change in EWCS, $\delta E_W^{\perp}$ can be written as

$$\delta E_W^{\perp} = \frac{V_{d-2}l^2}{8G_{d+1}z_0^d b_0^2}\left[\frac{1}{2}\left(1+\beta^2\gamma^2\right)-\left(\frac{b_1}{b_0}+\beta^2\gamma^2\frac{I_l}{b_0}\right)\right] . \tag{3.83}$$

In this limit (adjacent subsystem limit), the relation given in eq.(3.82) stands to be true. Now comparing the above expression with the one given in eq.(3.74), we get

$$\delta E_W^{\perp} = \lambda_3\ \delta S_{EE}^{\perp} . \tag{3.84}$$

In order to relate $\delta E_W^{\perp}$ to the boundary CFT quantities, we recall the following relation [192, 193]

$$\delta S_{EE}^{\perp} = \frac{1}{T_E}\left(\Delta E_{\perp}-\frac{d-1}{d+1}\mathcal{V}\Delta P_{\perp}\right) \tag{3.85}$$

where $\Delta E_{\perp} = \Delta E_{\parallel}$, $\Delta P_{\perp} = \frac{1}{z_0^d}\frac{1}{16\pi G_{d+1}}$. The expression of entanglement temperature T_E is given in eq.(3.37). Now by using the abve relation in eq.(3.84), we get

$$\delta E_W^{\perp} = \frac{\lambda_3}{T_E}\left(\Delta E_{\perp}-\frac{d-1}{d+1}\mathcal{V}\Delta P_{\perp}\right) . \tag{3.86}$$

On the other hand, the HMI in this set up is given by

$$I^{\perp}(A:B) = \frac{V_{d-2}}{2G_{d+1}}\left[\frac{2^{d-2}b_0^{d-1}}{(d-2)}\left(-\frac{2}{l^{d-2}}+\frac{1}{x^{d-2}}+\frac{1}{(2l+x)^{d-2}}\right)\right.$$
$$\left. + \frac{b_1(d+1)}{16b_0^2z_0^d}\left(\frac{d-1}{d+1}+\beta^2\gamma^2\right)\left[2l^2-x^2-(2l+x)^2\right]\right] . \tag{3.87}$$

Similar to the EWCS, we now compute the change in HMI due to the boost. This reads

$$\delta I^{\perp}(A:B) \equiv I^{\perp}(A:B) - I^{pure}(A:B)$$
$$= \frac{V_{d-2}b_1(d+1)}{32G_{d+1}b_0^2z_0^d}\left(\frac{d-1}{d+1}+\beta^2\gamma^2\right)\left[2l^2-x^2-(2l+x)^2\right] \tag{3.88}$$

where $I^{pure}(A:B)$ is the HMI with pure AdS_{d+1} geometry in the bulk, given in eq.(3.29). Further, the relation between $\delta I^{\perp}(A:B)$ and $\delta I^{\parallel}(A:B)$ can be obtained by using eq.(3.34) and eq.(3.88)

$$\delta I^{\perp}(A:B) = \left[\frac{\frac{d-1}{d+1}+\beta^2\gamma^2}{\frac{d-1}{d+1}+\frac{2\beta^2\gamma^2}{d+1}}\right]\delta I^{\parallel}(A:B) . \tag{3.89}$$

We again introduce the following scaling for the sake of simplicity

$$\bar{I}^{perp}(A:B) = \frac{2G_{d+1}}{V_{d-2}}I^{\perp}(A:B) . \tag{3.90}$$

Similar to the parallel case, we now graphically represent our results to show the effect of boost on EWCS and HMI. This we have done in fig.(3.4). To make these polts we have set $l=3$, $d=3$ and $z_0=10$. In the left panel, we present the derived expressions for EWCS and HMI, as given in eq.(3.80) and eq.(3.90). It is evident that for fixed subsystem length and boost parameter the mutual information vanishes at particular value of the separtion distance x_c, hence the EWCS shows a phase transition from connected phase to disconnected phase at this particular value of the separation distance. It is also observed that, the critical separation length, x_c , decreases as the boost parameter increases. In the right panel, we compare the result of EWCS and HMI computed in both perpendicular and parallel set up. This we have ploted for a particular value of the boost parameter, namely, $\beta=0.99$. TWe observe that for the same value of the β, the discontinuity in EWCS occurs at a early value of x, for the perpendicular case.

One can obtain the critical separation distance x_c in terms of the subsystem length and boost parameter. In order to do this we use the fact that mutual information vanishes at $x=x_c$. For

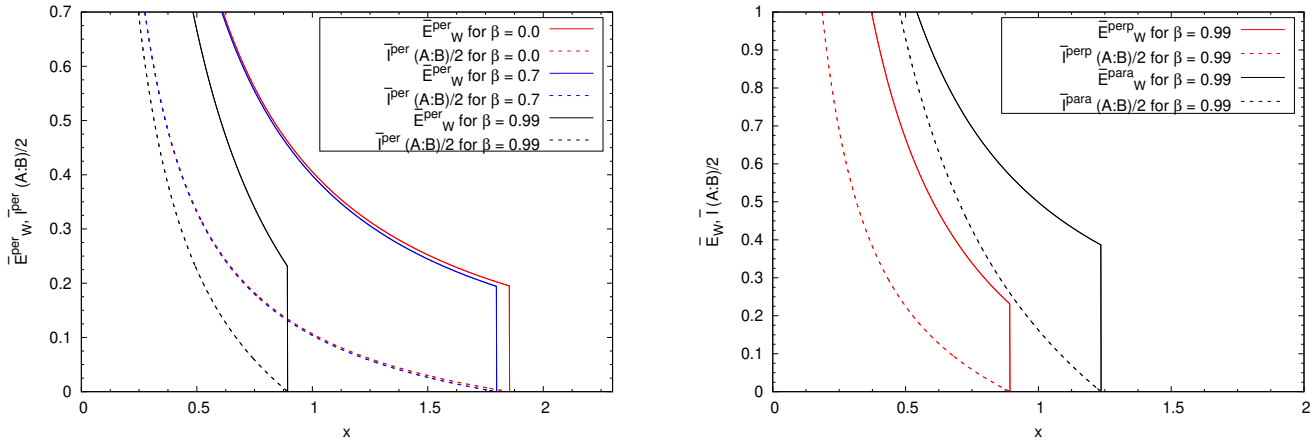

Figure 3.4: In this figure we have shown the variation of EWCS and HMI as a function of separation distance x between two subsystems of fixed length l. In the left panel, we have represented the result of EWCS and HMI when the subsystems are placed perpendicular to the boost direction. In the right panel, we have compared the result of EWCS and HMI between the perpendicular and parallel set up. This we have done for $\beta = 0.99$. For these plots we have also set $l = 3$, $d = 3$ and $z_0 = 10$.

$d = 3$, $I^{\perp}(A:B) = 0$ at $x = x_c$ condition gives

$$2\left(\frac{\sqrt{\pi}\Gamma(3/4)}{\Gamma(1/5)}\right)^2\left[-\frac{2}{l}+\frac{1}{x_c}+\frac{1}{2l+x_c}\right]+\frac{4\sqrt{\pi}\frac{\Gamma(3/4)}{4}(\frac{1}{2}+\beta^2\gamma^2)}{16(10)^3\left(\frac{\sqrt{\pi}\Gamma(3/4)}{\Gamma(1/5)}\right)^2}\left[2l^2-x_c^2-(2l+x_c)^2\right] = 0 \quad (3.91)$$

Similarly, for $d = 4$ we get

$$2\left(\sqrt{\pi}\frac{\Gamma(4/6)}{\Gamma(1/7))}\right)^3\left[-\frac{2}{l^2}+\frac{1}{x_c^2}+\frac{1}{(2l+x_c)^2}\right]+\frac{4\frac{\sqrt{\pi}\Gamma(4/3)}{5\Gamma(5/6)}(\frac{3}{5}+\beta^2\gamma^2)}{16(10)^4\left(\sqrt{\pi}\frac{\Gamma(4/6)}{\Gamma(1/7)}\right)^2}\left[2l^2-x_c^2-(2l+x_c)^2\right] = 0 \quad (3.92)$$

In order to obtain the analytical expression the critical separation x_c, one needs to solve the above equation ($d = 3$). As it is already mentioned that, the point x_c is defined as the critical point at which the mutual information vanishes and the EWCS shows the phase transition from the connected phase to the disconnected phase. We can get a qualitative comparison between critical points computed in the parallel and perpendicular to the boost scenario by using the expressions of $\bar{I}^{perp}(A:B)$ and $\bar{I}^{para}(A:B)$. This we show in fig.(3.5). We observe that the deviation between the critical separation lengths is prominent for relatively larger value of the boost parameter β.

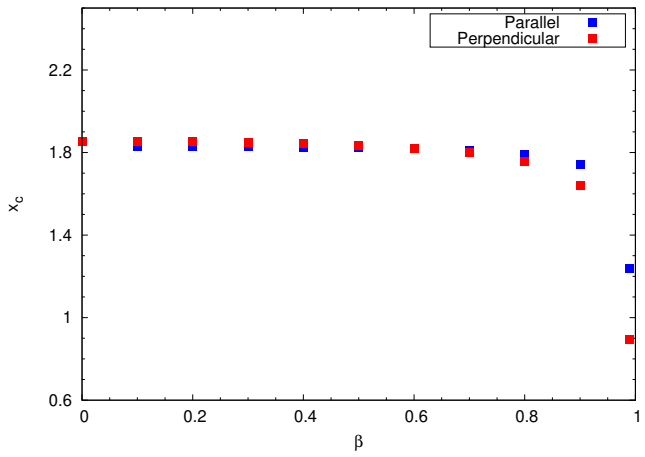

Figure 3.5: The above figure describes a comparison between the critical separation length x_c (where the HMI vanishes) for both the parallel (denoted by blue points) and perpendicular case(denoted by red points).

3.4.3 Entanglement negativity

We now proceed to compute the entanglement negativity (E_N) for the perpendicular case. Similar to the parallel case, we again consider two different configurations to compute E_N holographically. Firstly, we consider two adjacent subsystems of length l_1 and l_2 and then two disjoint subsystems of length l_1 and l_2, separated by a distance x.

For the adjacent set up, entanglement negativity can be obtained by using the following result

$$E^{\perp}_{N_{adj}} = \frac{3}{4}\left[S^{\perp}_{EE}(l_1) + S^{\perp}_{EE}(l_2) - S^{\perp}_{EE}(l_1+l_2)\right] \ . \tag{3.93}$$

In the above expression S_{EE} represents the HEE of a subsystem perpendicular to the boost, given by eq.(3.70). With this above result in hand we can compute the E_N for two adjacent subsystems. This reads

$$\begin{aligned} E^{\perp}_{N_{adj}} &= \frac{3}{4}S_{div} + \frac{3V_{d-2}a_0(2b_0)^{d-2}}{8G_{d+1}}\left(\frac{1}{l_1^{d-2}} + \frac{1}{l_2^{d-2}} - \frac{1}{(l_1+l_2)^{d-2}}\right) \\ &+ \frac{3V_{d-2}b_1(d+1)}{128G_{d+1}b_0^2 z_0^d}\left(\frac{d-1}{d+1} + \beta^2\gamma^2\right)\left[l_1^2 + l_2^2 - (l_1+l_2)^2\right] \ . \end{aligned} \tag{3.94}$$

The above expression of E_N suggests that, the entanglement negativity for adjacent subsystems is a divrgent quantity. On the other hand, the change in E_N reads

$$\begin{aligned}\delta E^{\perp}_{N_{adj}} &\equiv E^{\perp}_{N_{adj}} - E^{pure}_{N_{adj}} \\ &= \frac{3V_{d-2}b_1(d+1)}{128G_{d+1}b_0^2 z_0^d}\left(\frac{d-1}{d+1}+\beta^2\gamma^2\right)\left[l_1^2+l_2^2-(l_1+l_2)^2\right] \end{aligned} \tag{3.95}$$

where $E^{pure}_{N_{adj}}$ is given in eq.(3.41). One can now observe a relation between $\delta E^{\parallel}_{N_{adj}}$ and $\delta E^{\perp}_{N_{adj}}$ by using eq.(s)(3.42), (3.95). This reads

$$\delta E^{\perp}_{N_{adj}} = \left[\frac{d+1}{2}\right]\left[\frac{\frac{d-1}{d+1}+\beta^2\gamma^2}{\frac{d-1}{2}+\beta^2\gamma^2}\right]\delta E^{\parallel}_{N_{adj}} \ . \tag{3.96}$$

Now if we consider that the lengths corresponding to both of the subsystems are equal, that is, $l_1 = l_2 = l$, we then obtain

$$\delta E^{\perp}_{N_{adj}}|_{l_1=l_2} = -\frac{3V_{d-2}b_1(d+1)l^2}{64G_{d+1}b_0^2 z_0^d}\left(\frac{d-1}{d+1}+\beta^2\gamma^2\right) \ . \tag{3.97}$$

Next we move on to compute the entanglement negativity holographically for disjoint subsystems. To do that we consider two disjoint subsystems A and B of length l_1 and l_2 perpendicular to the boost direction, with a separation of x. In this set up one can obtain entanglement negativity by using the following formula [99, 100]

$$E^{\perp}_{N_{dis}} = \frac{3}{4}\left[S^{\perp}_{EE}(l_1+x)+S^{\perp}_{EE}(l_2+x)-S^{\perp}_{EE}(l_1+l_2+x)-S^{\perp}_{EE}(x)\right] \ . \tag{3.98}$$

Thus using the result of HEE given in eq.(3.70) in the above expression we can obtain the following result of entanglement negativity for two disjoint subsystems

$$\begin{aligned} E^{\perp}_{N_{dis}} &= \frac{3}{8}\frac{V_{d-2}a_0(2b_0)^{d-2}}{G_{d+1}}\left[\frac{1}{(l_1+x)^{d-2}}+\frac{1}{(l_2+x)^{d-2}}-\frac{1}{(l_1+l_2+x)^{d-2}}-\frac{1}{x^{d-2}}\right] \\ &+ \frac{3V_{d-2}b_1(d+1)}{128b_0^2G_{d+1}z_0^d}\left(\frac{d-1}{d+1}+\beta^2\gamma^2\right)\left[(l_1+x)^2+(l_2+x)^2-(l_1+l_2+x)^2-x^2\right] \end{aligned} \tag{3.99}$$

The above result suggests that, the entanglement negativity for two disjoint subsystems is a UV finite quantity. Similar to the parallel case, if we take the length of subsystems to be equal, that is $l_1 = l_2 = l$, then the entanglement of negativity (disjoint configuration) reads

$$\begin{aligned} \bar{E}^{per}_{N_{dis}}|_{l_1=l_2} &= \frac{3}{4}\Bigg[a_0(2b_0)^{d-2}\left(\frac{2}{(l+x)^{d-2}}-\frac{1}{(2l+x)^{d-2}}-\frac{1}{x^{d-2}}\right) \\ &+ \frac{b_1(d+1)}{32b_0^2z_0^d}\left(\frac{d-1}{d+1}+\beta^2\gamma^2\right)\left[2(l+x)^2-(2l+x)^2-x^2\right]\Bigg] \end{aligned} \tag{3.100}$$

where $\bar{E}_N^{perp} = \frac{2G_{d+1}}{V_{d-2}} E_N^{\perp}$.

We now graphically represent the variation of entanglement negativity of two disjoint subsystems

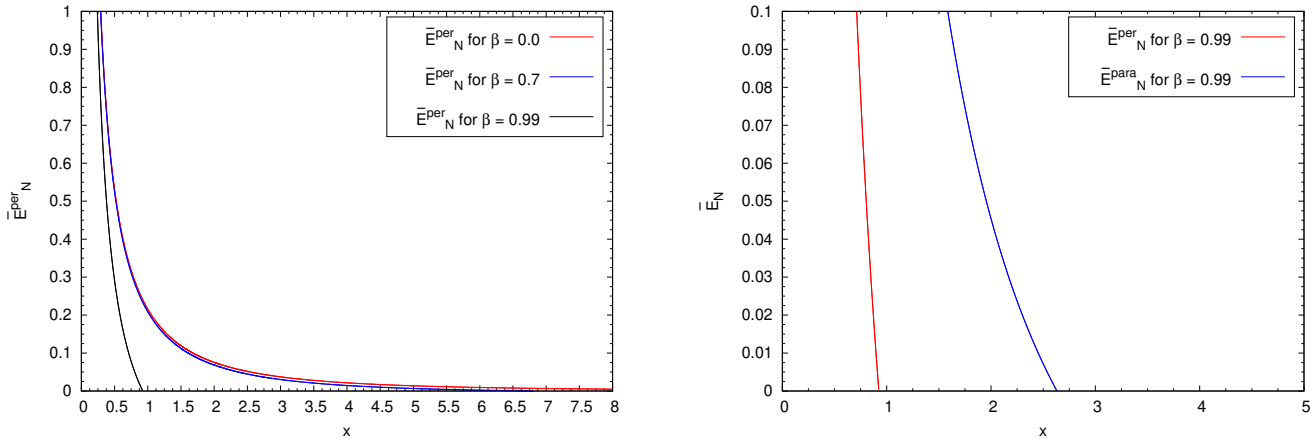

Figure 3.6: We have shown the variation of entanglement negativity for two disjoint subsystems (by considering the fact that, the subsystems are perpendicular to the boost) with same length l, with the separation distance (x) between the subsystems in the above figure. In the left panel of the above figure, we have shown the effect of the boost parameter on the entanglement negativity, computed in the perpendicular set up. On the other hand, in the right panel, we have compared the results of entanglement negativity (for two disjoint subsystems of equal length) for two different configurations. The blue curve depicts the result of E_N, when the subsystems are along the boost and the red curve represents the result when the subsystems are perpendicular to the boost. In both the cases we have taken the boost parameter $\beta = 0.99$. We have set $d = 3$, $l = 3$ and $z_0 = 10$.

(given in eq.(3.100)) with respect to the subsystem separation for different values of the boost parameter in the right panel of the abive figure. We find that E_N computed in the limit $\beta \to 0$ and $z_0 \to \infty$ does not vanishes at any value of the separation distance. However, for a non-zero, finite value of the β, E_N vanishes at a finite value of the separation distance. Further, as we increase the boost, entanglement negativity vanishes at a smaller value of the separation length. This is very much clear from the fig.(3.6). Furthermore, from the right panel of fig.(3.6) we observe that, entanglement negativity vanishes earlier for the perpendicular case, at the same value of the boost parameter (in this case $\beta = 0.99$). This we have observed in the parallel scenario also. We denote this length scale (at which E_N vanishes) as the critical separation length x_c for the entanglement negativity. We now compare the values of this length scale, computed in

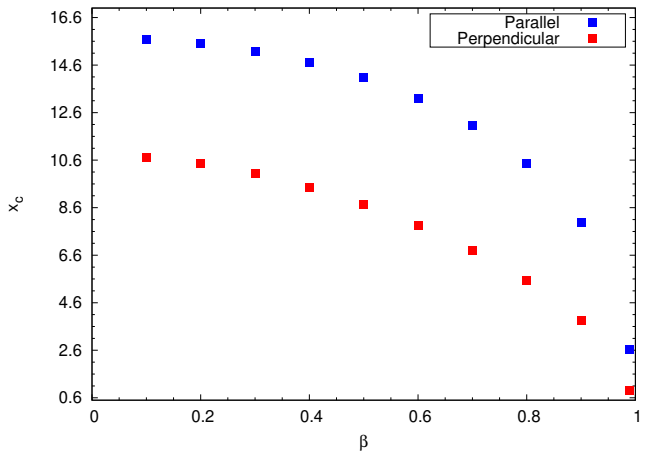

Figure 3.7: The above figure presents a comparison of the critical separation length x_c, at which the entanglement negativity between two disjoint subsystems of equal length vanishes, for both the parallel (denoted by blue dots)and perpendicular configurations (denoted by red dots).

both parallel and perpendicular set up. This we have shown in fig.(3.7). We observe that in the perpendicular set up, the entanglement negativity vanishes for a smaller value of x_c, for the same value of the boost parameter. Furthermore, x_c decreases with the increase in the boost parameter. With this computed result (given in eq.(3.99)) in hand, we can now compute the quantity $\delta E^{\perp}_{N_{dis}}$. This reads

$$\delta E^{\perp}_{N_{dis}} = \frac{3V_{d-2}b_1(d+1)}{128b_0^2 G_{d+1} z_0^d}\left(\frac{d-1}{d+1}+\beta^2\gamma^2\right)\left[(l_1+x)^2+(l_2+x)^2-(l_1+l_2+x)^2-x^2\right] . \tag{3.101}$$

Furthermore, when the length of the two subsystems are equal, that is, $l_1 = l_2 = l$, the change in entanglement negativity reads

$$\delta E^{\perp}_{N_{dis}}|_{l_1=l_2} = \frac{3V_{d-2}b_1(d+1)}{128b_0^2 G_{d+1} z_0^d}\left(\frac{d-1}{d+1}+\beta^2\gamma^2\right)\left[2(l+x)^2-(2l+x)^2-x^2\right] . \tag{3.102}$$

With the help of the above expression and eq.(3.50), we can find the following relation

$$\delta E^{\perp}_{N_{dis}} = \left[\frac{d+1}{2}\right]\left[\frac{\frac{d-1}{d+1}+\beta^2\gamma^2}{\frac{d-1}{2}+\beta^2\gamma^2}\right]\delta E^{\parallel}_{N_{dis}} . \tag{3.103}$$

By looking at the above relation and the one given in eq.(3.97), we can conclude that the relation between $\delta E^{\perp}_N$ and $\delta E^{\parallel}_N$ stands to be unchanged irrespective of the adjacent or disjoint subsystem

choice. Further, it is also reassuring to observe the fact that in the limit $x \to 0$, eq.(3.102) reproduces eq.(3.97). Similar to the parallel set up, once again we construct a relation between $\delta E^{\perp}_{N_{adj}}|_{l_1=l_2}$ and $\delta S^{\perp}_{EE}$. This reads

$$\delta E^{\perp}_{N_{adj}}|_{l_1=l_2} = \lambda_4 \ \delta S^{\perp}_{EE} \ . \tag{3.104}$$

3.4.4 Holographic subregion complexity

In this section we compute the holographic subregion complexity of a strip like subsystem say A which is perpendicular to the direction of boost. In this set up, the HSC is obtained to be

$$C^{\perp}_{V} \ = \ \frac{V_{\perp}(\Gamma)}{8\pi G_{d+1}} \tag{3.105}$$

where $V_{\perp}(\Gamma)$ denotes the volume enclosed by the co-dimension two static minimal Ryu-Takayanagi (RT) surfaces in the bulk. Following similar procedure as we have done in case of the subsystem parallel to boost scenario, we compute the co-dimension one volume $V_{\perp}(\Gamma)$ and substitute in eq.(3.105). This leads to the following [212]

$$\begin{aligned} C^{\perp}_{V} \ &= \ \frac{1}{8\pi G_{d+1}}\Bigg[\frac{V_{d-2}}{d-1}\frac{l}{\epsilon^{d-1}} - \frac{2^{d-2}\pi^{\frac{d-1}{2}}}{(d-1)^2}\left(\frac{\Gamma(\frac{d}{2d-2})}{\Gamma(\frac{1}{(2d-2)})}\right)^{d-3}\frac{V_{d-2}}{l^{d-2}} - \frac{V_{d-2}l^2}{4b_0^2(d-1)z_0^d}\Bigg[\left(\frac{(d-2)\pi b_1}{2(d-1)b_0^2} + (2-d)c_0\right) \\ &+ \ \beta^2\gamma^2\left(\frac{(d-2)\pi I_l}{2b_0^2(d-1)} + c_2 - (d-1)c_0\right)\Bigg]\Bigg] \ . \end{aligned} \tag{3.106}$$

On the other hand, the change in HSC is obtained to be

$$\delta C^{\perp}_{V} = -\frac{V_{d-2}l^2}{32G_{d+1}b_0^2(d-1)z_0^d}\left[\left(\frac{(d-2)\pi b_1}{2(d-1)b_0^2} + (2-d)c_0\right) + \beta^2\gamma^2\left(\frac{(d-2)\pi I_l}{2b_0^2(d-1)} + c_2 - (d-1)c_0\right)\right] . \tag{3.107}$$

Now we will relate this change in the HSC with the boundary field theoretic quatities. This provides a thermodynamics like law for HSC. The change in the holographic subregion complexity ($\delta C^{\perp}_{V}$) related to $\delta S^{\parallel}_{EE}$ (given in eq.(3.21)) and $\delta S^{\perp}_{EE}$ (given in eq.(3.74)) reads [212]

$$\delta C^{\perp}_{V} \ = \ \frac{1}{2(d-1)^3}\left[\frac{\delta S^{\parallel}_{EE}}{(d+1)b_1^2} - \left(\frac{d-2}{b_0^2} - \frac{d-3}{(d+1)b_1^2}\right)\delta S^{\perp}_{EE}\right] \ . \tag{3.108}$$

Now using eqs.(3.36,3.85), one can relate the change in the holographic subregion complexity with the boundary field theoretic quantities like excitation energy, pressure in the following way.

$$\delta C_V^{\perp} = \frac{1}{2(d-1)^3 T_E}\left[\Delta E\left(\frac{d-2}{(d+1)b_1^2}-\frac{d-2}{b_0^2}\right)-\mathcal{V}\left(\frac{d-1}{d+1}\right)\left(\frac{\Delta P_{\parallel}}{b_1^2}-\Delta P_{\perp}\left(\frac{d-2}{b_0^2}-\frac{d-3}{(d+1)b_1^2}\right)\right)\right] . \tag{3.109}$$

Similarly following [212], we can write $\delta C_V^{\parallel}$ (given in eq.(3.56)) in the following way

$$\begin{aligned}\delta C_V^{\parallel} &= \frac{1}{2(d-1)^3 T_E}\left[\Delta E\left(\frac{d-2}{(d+1)b_1^2}-\frac{d-2}{b_0^2}\right)-\mathcal{V}\left(\frac{d-1}{d+1}\right)\left(\frac{\Delta P_{\parallel}}{b_1^2}-\Delta P_{\perp}\left(\frac{d-2}{b_0^2}-\frac{d-3}{(d+1)b_1^2}\right)\right)\right] \\ &+ \frac{\mathcal{V} l\beta^2\gamma^2 c_0}{32\pi G_{d+1}(d-1)b_0^2 z_0^d}\left[1+(d-2)(d+1)\frac{b_1^2}{b_0^2}\right] .\end{aligned} \tag{3.110}$$

From both the eqs.(3.109,3.110), we observe an interesting fact that the change in complexity for strip placed along the perpendicular to the boost direction is related to the CFT pressure perendicular to boost and also on the pressure parallel to the boost. The same is true for the change in HSC for parallel strip (placed along y-direction).

With the computed result of HSC (given in eq.(3.106)) in hand, we now proceed to calculate the mutual complexity between two subsystems A and B which are in perpendicular orientation with respect to the direction of boost. For that we will consider two subsystems of equal length l and with a separation of x. In this setup, the mutual complexity reads

$$\Delta\mathcal{C}^{\perp} = \mathcal{C}_V^{\perp}(A)+\mathcal{C}_V^{\perp}(B)-\mathcal{C}_V^{\perp}(A\cup B) \equiv 2\mathcal{C}_V^{\perp}(l)-\mathcal{C}_V^{\perp}(2l+x)+\mathcal{C}_V^{\perp}(x) . \tag{3.111}$$

For the above mentioned configuration, mutual complexity reads

$$\begin{aligned}\Delta\mathcal{C}^{\perp} &= \frac{V_{d-2}}{8\pi G_{d+1}(d-1)}\left[\frac{2^{d-2}\pi^{\frac{d-1}{2}}}{(d-1)}\left(\frac{\Gamma(\frac{d}{2d-2})}{\Gamma(\frac{1}{(2d-2)})}\right)^{d-3}\left(\frac{1}{(2l+x)^{d-2}}-\frac{1}{x^{d-2}}-\frac{2}{l^{d-2}}\right)\right. \\ &- \left.\frac{1}{4b_0^2 z_0^d}\left[\left(\frac{(d-2)\pi b_1}{2(d-1)b_0^2}+(2-d)c_0\right)+\beta^2\gamma^2\left(\frac{(d-2)\pi I_l}{2b_0^2(d-1)}+c_2-(d-1)c_0\right)\right]\left[2l^2+x^2-(2l+x)^2\right]\right] .\end{aligned} \tag{3.112}$$

Furthermore, the change in mutual complexity $\delta\mathcal{C}^{\perp} \equiv \Delta\mathcal{C}^{\perp} - \Delta\mathcal{C}^{pure}$ is obtained to be

$$\begin{aligned}\delta\mathcal{C}^{\perp} = -\frac{V_{d-2}}{8\pi G_{d+1}(d-1)}\frac{1}{4b_0^2 z_0^d}\left[\left(\frac{(d-2)\pi b_1}{2(d-1)b_0^2}+(2-d)c_0\right)\right. &+ \left.\beta^2\gamma^2\left(\frac{(d-2)\pi I_l}{2b_0^2(d-1)}+c_2-(d-1)c_0\right)\right] \\ &\times\left[2l^2+x^2-(2l+x)^2\right] .\end{aligned} \tag{3.113}$$

The relation between $\delta\mathcal{C}^{\parallel}$ and $\delta\mathcal{C}^{\perp}$ reads

$$\frac{\delta\mathcal{C}^{\parallel}}{\delta\mathcal{C}^{\perp}} = \frac{\left[\left(\frac{(d-2)\pi b_1}{2(d-1)b_0^2}+(2-d)c_0\right)+\beta^2\gamma^2\left(\frac{(d-2)\pi}{2(d-1)^2 b_0}\left(\frac{2b_1}{b_0}-1\right)+c_2-c_0 d\right)\right]}{\left[\left(\frac{(d-2)\pi b_1}{2(d-1)b_0^2}+(2-d)c_0\right)+\beta^2\gamma^2\left(\frac{(d-2)\pi I_l}{2b_0^2(d-1)}+c_2-(d-1)c_0\right)\right]} . \quad (3.114)$$

To obtain the above expression we have used eqs.(3.60,3.113). Similar to parallel case, we now introduce the scaling $\bar{I}_C^{per} = \frac{2G_{d+1}}{V_{d-2}}\Delta\mathcal{C}^{\perp}$ and proceed to represent our findings graphically. This we show in fig.(3.8), where we set $d = 3$, $l = 3$ and $z_0 = 10$. Similar to the parallel case, the mutual complexity in this scenario is also superadditive.

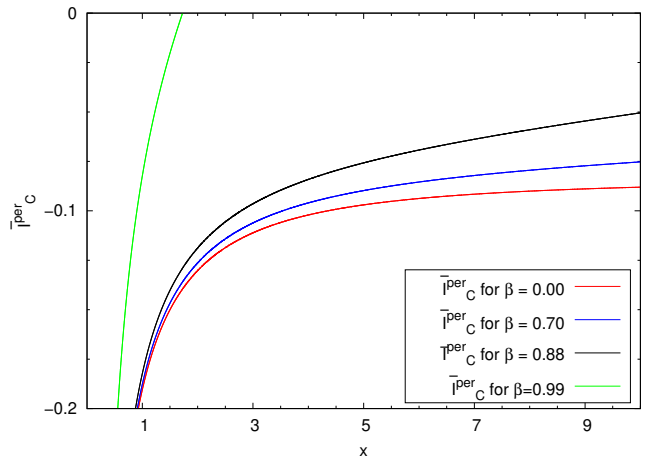

Figure 3.8: The above figure represents the variation of mutual complexity between two subsystems taken perpendicular to the direction of boost with respect to the separation distance between the subsystems for different values of boost parameter.

3.5 Asymmetry ratio of different holographic measures

In this section we compute asymmetry ratio of different information theoretic measures. For entanglement entropy the asymmetry ratio is defined as

$$\mathcal{A}_{S_{EE}} = \frac{\delta S_{EE}^{\perp} - \delta S_{EE}^{\parallel}}{\delta S_{EE}^{\perp} + \delta S_{EE}^{\parallel}} . \quad (3.115)$$

By using eq.(3.21) and eq.(3.74), $\mathcal{A}_{S_{EE}}$ can be computed. This reads

$$\mathcal{A}_{S_{EE}} = \frac{\beta^2\gamma^2}{\left(2+\frac{d+3}{d-1}\beta^2\gamma^2\right)} \ . \tag{3.116}$$

It is clear from the above result that the asymmetry ratio for HEE is independent of the subsystem size. It depends only on the boost parameter and the value of the spacetime dimension. In the large boost limit ($\beta \to 1$), eq.(3.116) can be recast to the form

$$\mathcal{A}_{S_{EE}}|_{\beta\to 1} = \frac{d-1}{d+3} \ . \tag{3.117}$$

Similarly, the asymmetry ratio for mutual information is obtained to be

$$\mathcal{A}_I = \frac{\delta I^{\perp} - \delta I^{\parallel}}{\delta I^{\perp} + \delta I^{\parallel}} = \frac{\beta^2\gamma^2}{\left(2+\frac{d+3}{d-1}\beta^2\gamma^2\right)} \ . \tag{3.118}$$

In the above computation, we have used eq.(3.34) and eq.(3.88) to get the explicit expression. The above result again implies that $\mathcal{A}_I$ is independent of the subsystem size. Again in the large boost limit ($\beta \to 1$), eq.(3.118) reads

$$\mathcal{A}_I|_{\beta\to 1} = \frac{d-1}{d+3} \ . \tag{3.119}$$

The results given in eq.(s)(3.118,3.119) are similar to the ones we have obtained for HEE. This is quite natural as HMI is nothing but a certain combination of the HEE. On the other hand, the asymmetry ratio for the entanglement wedge cross-section reads (we use eq(s).(3.33,3.81))

$$\mathcal{A}_{E_W} = \frac{\delta E_W^{\perp} - \delta E_W^{\parallel}}{\delta E_W^{\perp} + \delta E_W^{\parallel}} = \frac{\beta^2\gamma^2\left[1-2\frac{b_1}{b_0}\right]}{(1-2\frac{b_1}{b_0}) + \frac{\beta^2\gamma^2}{2}\left[1+2\frac{b_1}{b_0}-4\frac{I_l}{b_0}\right]} \ . \tag{3.120}$$

In the limit $\beta \to 1$, the above expression simplifies to the following form

$$\mathcal{A}_{E_W}|_{\beta\to 1} = \frac{2(1-2\frac{b_1}{b_0})}{1+2\frac{b_1}{b_0}-4\frac{I_l}{b_0}} \ . \tag{3.121}$$

From the obtained expression, given in the eq(s).(3.120,3.121), it is clear that the asymmetry ratio for EWCS is independent of shape and size of the subsystem. Asymmetry ratio for the HSC reads [212]

$$\mathcal{A}_{C_V} = \frac{\delta C_V^{\perp} - \delta C_V^{\parallel}}{\delta C_V^{\perp} + \delta C_V^{\parallel}} = \left[\frac{\frac{2-d}{2(d-1)^3 b_0^2} - \frac{1}{2(d-1)^3(d+1)b_1^2}}{\frac{2-d}{2(d-1)^3 b_0^2} + \frac{\mathcal{R}+2d-5}{2(d-1)^3(d+1)b_1^2}}\right]\mathcal{A}_{S_{EE}} \tag{3.122}$$

where $\mathcal{A}_{S_{EE}}$ is given in eq.(3.116) and $\mathcal{R}$ is

$$\mathcal{R} = \frac{\delta S^{\parallel}_{EE}}{\delta S^{\perp}_{EE}} = \frac{1+\frac{2}{d-1}\beta^2\gamma^2}{1+\frac{d+1}{d-1}\beta^2\gamma^2} \ . \tag{3.123}$$

The above result corresponding to HSC, matches with the ones given in [212]. In the limit $\beta \to 1$ eq.(3.122) reduces to

$$\mathcal{A}_{C_V}|_{\beta\to 1} = \left[\frac{\frac{2-d}{2(d-1)^3 b_0^2} - \frac{1}{2(d-1)^3(d+1)b_1^2}}{\frac{2-d}{2(d-1)^3 b_0^2} + \frac{\frac{2}{d+1}+2d-5}{2(d-1)^3(d+1)b_1^2}}\right]\frac{d-1}{d+3} \ . \tag{3.124}$$

Now by using eq(s).(3.50,3.102) the asymmetry ratio for entanglement negativity for disjoint intervals is obtained to be

$$\mathcal{A}_{E_{N_{dis}}} = \frac{\delta E^{\perp}_{N_{dis}} - \delta E^{\parallel}_{N_{dis}}}{\delta E^{\perp}_{N_{dis}} + \delta E^{\parallel}_{N_{dis}}} = \frac{\beta^2\gamma^2\frac{d-1}{2}}{(d+1)+\beta^2\gamma^2\frac{d+3}{2}} \ . \tag{3.125}$$

On the other hand, for adjacent intervals the asymmetry ratio for the entanglement negativity reads

$$\mathcal{A}_{E_{N_{adj}}} = \frac{\delta E^{\perp}_{N_{adj}} - \delta E^{\parallel}_{N_{adj}}}{\delta E^{\perp}_{N_{adj}} + \delta E^{\parallel}_{N_{adj}}} = \frac{\beta^2\gamma^2\frac{d-1}{2}}{(d+1)+\beta^2\gamma^2\frac{d+3}{2}} \ . \tag{3.126}$$

It is interesting to observe that for both the adjacent and disjoint interval case, the asymmetry ratio for entanglement negativity is same and independent of the subsystem size. In the large boost limit ($\beta \to 1$), both the eqs.(3.125,3.126) reduces to the following expression

$$\mathcal{A}_{E_{N_{dis}}}|_{\beta\to 1} = \mathcal{A}_{E_{N_{adj}}}|_{\beta\to 1} = \frac{d-1}{d-3} \ . \tag{3.127}$$

Further, the asymmetry ratio for mutual complexity reads

$$\mathcal{A}_{\Delta\mathcal{C}} = \frac{\beta^2\gamma^2\left(\frac{(d-2)\pi I_l}{2b_0^2(d-1)} + c_2 - (d-1)c_0 - \frac{(d-2)\pi}{2(d-1)^2 b_0}\left(\frac{2b_1}{b_0}-1\right) - c_2 + c_0 d\right)}{2\left(\frac{(d-2)\pi b_1}{2(d-1)b_0^2} + (2-d)c_0\right) + \beta^2\gamma^2\left(\frac{(d-2)\pi I_l}{2b_0^2(d-1)} + c_2 - (d-1)c_0 + \frac{(d-2)\pi}{2(d-1)^2 b_0}\left(\frac{2b_1}{b_0}-1\right) + c_2 - c_0 d\right)} \ . \tag{3.128}$$

In the large boost limit ($\beta \to 1$), the above expression simplifies to the following form

$$\mathcal{A}_{\Delta\mathcal{C}}|_{\beta\to 1} = \frac{\left(\frac{(d-2)\pi I_l}{2b_0^2(d-1)} + c_2 - (d-1)c_0 - \frac{(d-2)\pi}{2(d-1)^2 b_0}\left(\frac{2b_1}{b_0}-1\right) - c_2 + c_0 d\right)}{\left(\frac{(d-2)\pi I_l}{2b_0^2(d-1)} + c_2 - (d-1)c_0 + \frac{(d-2)\pi}{2(d-1)^2 b_0}\left(\frac{2b_1}{b_0}-1\right) + c_2 - c_0 d\right)} \tag{3.129}$$

We would like to mention that the asymmetry ratios computed in this section are bounded from above [193] and the bound saturates in the large boost limit, that is, $\beta \to 1$.

3.6 AdS wave geometry

In this section we consider a very special class of geometry which arises from the boosted black brane geometry in certain limit. Thus one can obtain the AdS wave geometry by taking the limits $\beta \to 1, z_0 \to \infty$ in eq.(3.1), with the following condition

$$\frac{\beta^2\gamma^2}{z_0^d} = \frac{1}{z_I^d} = \text{fixed} \tag{3.130}$$

where $z = z_I$ is an scale which determines momentum of the wave traveling in the y direction. In this limit, the boosted black brane metric (given in eq.(3.1) reduces to following [193]

$$ds^2 = \frac{1}{z^2}\left(-\frac{dt^2}{K} + K(dy-\omega)^2 + dx_1^2 + ... + dx_2^2 + dz^2\right) \tag{3.131}$$

with

$$K(z) = 1 + \frac{z^d}{z_I^d}\ ,\ \omega = \left(1 - \frac{1}{K(z)}\right)dt\ \ . \tag{3.132}$$

We shall now compute various information theoretic measures of the conformal field theory living at the boundary using the above geometry holographically. Here we will again consider two different cases, first, the subsystem is taken along the boost and then the subsystem is perpendicular to the boost. We follow the same approach as we have shown in case of the boosted black brane.

3.6.1 Holographic entanglement entropy

Subsystem along the boost

Similar to the parallel subsystem scenario of boosted black brane, let us consider a subsystem, specified by the volume $V_{sub} = L^{d-2}l$, with $-\frac{l}{2} \le y \le \frac{l}{2}$, and $x_1, ..., x_{d-2} \in [0, L]$ with $L \to \infty$. Further we assume that in this case the length can vary only along the direction of the boost, that is along y-direction and the lengths in other directions are taken to be fixed. Following the same procedure as we have shown for the boosted black brane and by incorporating the thin strip approximation we compute the HEE in this case also. This is obtained to be

$$S_{EE}^{\parallel} = S_{div} + \frac{V_{d-2}}{2G_{d+1}}\left[a_0\left(\frac{2b_0}{l}\right)^{d-2} + \left(\frac{l}{2b_0}\right)^2\frac{b_1}{2z_I^d}\right] \tag{3.133}$$

where we have used the following relation

$$z_t^{\parallel} \approx \frac{l}{2\left[b_0 - \frac{1}{2}\left(\frac{z_t}{z_I}\right)^d(b_1 - I_l)\right]} \approx \frac{\bar{z}_t}{1 - \frac{1}{2}\left(\frac{\bar{z}_t}{z_I}\right)^d\left(\frac{b_1}{b_0} - \frac{I_l}{b_0}\right)}\ . \tag{3.134}$$

In the above $\bar{z}_t$ is the turning point corresponding to the pure AdS_{d+1} geometry in the bulk. In the second line we have use eq.(3.16) to express $z_t^{\parallel}$ in terms of $\bar{z}_t$. Now the change in HEE ($\delta S_{EE}^{\parallel} = S_{EE}^{\parallel} - S_{EE}^{pure}$) is found to be

$$\delta S_{EE}^{\parallel} = \frac{V_{d-2}}{2G_{d+1}} \left(\frac{l}{2b_0}\right)^2 \frac{b_1}{2z_I^d} \tag{3.135}$$

Subsystem perpendicular to the boost

Now we consider a strip-like subsystem, perpendicular to the boost. The system is specified by volume $V = ll_y...l_{d-2}$, with $-\frac{l}{2} \leq x_1 \leq \frac{l}{2}$,$0 \leq y \leq l_y$, and $0 \leq x_i \leq l_i$. l_y and l_i is taken to be very very large, that is $l_y, l_i >> l$. The length along x_1 direction changes and length along other directions is fixed. In this set up, the HEE in terms of the subsystem size is found to be

$$S_{EE}^{\perp} = S_{div} + \frac{V_{d-2}}{2G_{d+1}} \left[a_0 \left(\frac{2b_0}{l}\right)^{d-2} + \frac{a_1}{z_I^d} \left(\frac{l}{2b_0}\right)^2 \right] . \tag{3.136}$$

to obtain the above result we have used the following result

$$z_t^{\perp} \approx \frac{l}{2b_0 \left[1 + \left(\frac{z_t}{z_I}\right)^d I_l\right]} \approx \frac{\bar{z}_t}{\left[1 + \left(\frac{\bar{z}_t}{z_I}\right)^d I_l\right]} . \tag{3.137}$$

Now we will compute change in the entanglement entropy ($\delta S_{EE}^{\perp} = S_{EE}^{\perp} - S_{EE}^{pure}$) using eqs.(3.136,3.20). The expression of $\delta S_{EE}^{\perp}$ reads

$$\delta S_{EE}^{\perp} = \frac{V_{d-2}}{2G_{d+1}} \frac{a_1}{z_I^d} \left(\frac{l}{2b_0}\right)^2 . \tag{3.138}$$

Furthermore, we observe that $\delta S_{EE}^{\perp}$ and $\delta S_{EE}^{\parallel}$ are related by the following relation

$$\delta S_{EE}^{\perp} = \left(\frac{2a_1}{b_1}\right) \delta S_{EE}^{\parallel} . \tag{3.139}$$

3.6.2 EWCS and Holographic mutual information

We now compute the EWCS and HMI by following the same procedure we have shown for the boosted brane. To do that we have considered two disjoint subsystems of equal length l, separated by a distance x.

Subsystems along the boost

When the subsystems are along the boost, the EWCS is found to be

$$E_W^{\parallel} = \frac{V_{d-2}}{2G_{d+1}}\left[\frac{(2b_0)^{d-2}}{2(d-2)}\left(\frac{1}{x^{d-2}}-\frac{1}{(2l+x)^{d-2}}\right)+\frac{\left(\frac{I_l}{b_0}-\frac{b_1}{b_0}\right)}{4(2b_0)^2 z_I^d}\left(x^2-(2l+x)^2\right)\right]. \tag{3.140}$$

On the other hand, HMI corresponding to this set up reads

$$I^{\parallel}(A:B) = \frac{V_{d-2}}{2G_{d+1}}\left[a_0(2b_0)^{d-2}\left(\frac{2}{l^{d-2}}-\frac{1}{x^{d-2}}-\frac{1}{(2l+x)^{d-2}}\right)+\frac{b_1}{(2b_0)^2 z_I^d}\left(l^2-\frac{x^2}{2}-\frac{(2l+x)^2}{2}\right)\right]. \tag{3.141}$$

The changes in EWCS and HMI due to the presence of boost read

$$\delta E_W^{\parallel} = \frac{V_{d-2}}{2G_{d+1}}\frac{\left(\frac{I_l}{b_0}-\frac{b_1}{b_0}\right)}{4(2b_0)^2 z_I^d}\left(x^2-(2l+x)^2\right) \tag{3.142}$$

$$\delta I^{\parallel}(A:B) = \frac{V_{d-2}}{2G_{d+1}}\frac{b_1}{(2b_0)^2 z_I^d}\left(l^2-\frac{x^2}{2}-\frac{(2l+x)^2}{2}\right) . \tag{3.143}$$

Subsystems perpendicular to the boost

When the subsystems are perpendicular to the boost, the EWCS is found to be

$$E_W^{\perp} = \frac{V_{d-2}}{2G_{d+1}}\left[\frac{(2b_0)^{d-2}}{2(d-2)}\left(\frac{1}{x^{d-2}}-\frac{1}{(2l+x)^{d-2}}\right)+\frac{1}{4z_I^d(2b_0)^2}\left(1-\frac{I_l}{b_0}\right)\left[(2l+x)^2-x^2\right]\right]. \tag{3.144}$$

In this set up, HMI reads

$$I^{\perp}(A:B) = \frac{V_{d-2}}{2G_{d+1}}\left[a_0(2b_0)^{d-2}\left(\frac{2}{l^{d-2}}-\frac{1}{x^{d-2}}-\frac{1}{(2l+x)^{d-2}}\right)+\frac{a_1}{z_I^d(2b_0)^2}\left(2l^2-x^2-(2l+x)^2\right)\right]. \tag{3.145}$$

We now compute the changes in EWCS and HMI due to the presence of boost. This reads

$$\delta E_W^{\perp} = \frac{V_{d-2}}{2G_{d+1}}\frac{1}{4z_I^d(2b_0)^2}\left(1-\frac{I_l}{b_0}\right)\left[(2l+x)^2-x^2\right] \tag{3.146}$$

$$\delta I^{\perp}(A:B) = \frac{V_{d-2}}{2G_{d+1}}\frac{a_1}{z_I^d(2b_0)^2}\left(2l^2-x^2-(2l+x)^2\right) . \tag{3.147}$$

3.6.3 Entanglement negativity

We now holographically compute the entanglement negativity for the AdS wave geometry. Firstly, we consider two adjacent subsystems with lengths l_1 and l_2 and compute the entanglement negativity for this configuration. We then consider two disjoint subsystems with lengths l_1 and l_2, separated by a distance x.

Subsystems along the boost

When two adjacent subsystems of length l_1 and l_2 are taken along the boost, the entanglement negativity is reads

$$E^{\parallel}_{N_{adj}} = \frac{3}{4}S_{div} + \frac{3}{4}\frac{V_{d-2}}{2G_{d+1}}\left[a_0(2b_0)^{d-2}\left(\frac{1}{l_1^{d-2}}+\frac{1}{l_2^{d-2}}-\frac{1}{(l_1+l_2)^{d-2}}\right)+\frac{b_1}{2z_I^d(2b_0)^2}\left(l_1^2+l_2^2-(l_1+l_2)^2\right)\right]. \tag{3.148}$$

On the other hand, when we consider two disjoint subsystems (with length l_1 and l_2), separated by a distance x, the entanglement negativity is obtained to be

$$\begin{aligned} E^{\parallel}_{N_{dis}} &= \frac{3}{4}\frac{V_{d-2}}{2G_{d+1}}\left[a_0(2b_0)^{d-2}\left(\frac{1}{(l_1+x)^{d-2}}+\frac{1}{(l_2+x)^{d-2}}-\frac{1}{(l_1+l_2+x)^{d-2}}-\frac{1}{x^{d-2}}\right)\right. \\ &+ \left.\frac{b_1}{2(2b_0)^2z_I^d}\left((l_1+x)^2+(l_2+x)^2-(l_1+l_2+x)^2-x^2\right)\right]. \end{aligned} \tag{3.149}$$

With the above expressions in hand, we can now proceed to compute the change in entanglement negativity due to the involvement of the boost. This we do for both adjacent and disjoint case. The findings are given below

$$\delta E^{\parallel}_{N_{adj}} = \frac{3V_{d-2}b_1}{16(2b_0)^2G_{d+1}z_I^d}\left[l_1^2+l_2^2-(l_1+l_2)^2\right] \tag{3.150}$$

$$\delta E^{\parallel}_{N_{dis}} = \frac{3}{4}\frac{V_{d-2}}{2G_{d+1}}\frac{b_1}{2(2b_0)^2z_I^d}\left((l_1+x)^2+(l_2+x)^2-(l_1+l_2+x)^2-x^2\right). \tag{3.151}$$

Subsystems perpendicular to the boost

Once again we consider two adjacent subsystems of length l_1 and l_2 in perpendicular orientation with respect to the direction of boost. This leads to the following expression for the entanglement

negativity

$$E^{\perp}_{N_{adj}} = \frac{3}{4}S_{div} + \frac{V_{d-2}}{2G_{d+1}}\frac{3}{4}\left[a_0(2b_0)^{d-2}\left(\frac{1}{l_1^{d-2}}+\frac{1}{l_2^{d-2}}-\frac{1}{(l_1+l_2)^{d-2}}\right)+\frac{a_1}{z_I^d(2b_0)^2}\left(l_1^2+l_2^2-(l_1+l_2)^2\right)\right]. \tag{3.152}$$

Furthermore, when we consider two disjoint subsystems with length l_1 and l_2 in the perpendicular direction (with respect to the boost), separated by a distance x, we get the following result for the entanglement negativity

$$\begin{aligned} E^{\perp}_{N_{dis}} &= \frac{3}{4}\frac{V_{d-2}}{2G_{d+1}}\left[a_0(2b_0)^{d-2}\left(\frac{1}{(l_1+x)^{d-2}}+\frac{1}{(l_2+x)^{d-2}}-\frac{1}{(l_1+l_2+x)^{d-2}}-\frac{1}{x^{d-2}}\right)\right. \\ &+ \left.\frac{a_1}{(2b_0)^2 z_I^d}\left((l_1+x)^2+(l_2+x)^2-(l_1+l_2+x)^2-x^2\right)\right]. \end{aligned} \tag{3.153}$$

Similar to the parallel case, we now compute the change in entanglement negativity (for both adjacent and disjoint case) due to the boost. This reads

$$\begin{aligned} \delta E^{\perp}_{N_{adj}} &= \frac{3}{4}\frac{V_{d-2}}{2G_{d+1}}\frac{a_1}{z_I^d(2b_0)^2}\left(l_1^2+l_2^2-(l_1+l_2)^2\right). \\ \delta E^{\perp}_{N_{dis}} &= \frac{3}{4}\frac{V_{d-2}}{2G_{d+1}}\frac{a_1}{z_I^d(2b_0)^2}\left((l_1+x)^2+(l_2+x)^2-(l_1+l_2+x)^2-x^2\right) \end{aligned} \tag{3.154}$$

3.6.4 Holographic subregion complexity

We now proceed to compute the HSC for the AdS wave geometry. Once again we will use the formula given in eq.(3.53).

Subsystem along the boost

When we consider a subsystem of length l in the direction along the boost, the HSC is found to be

$$\begin{aligned} C_V^{\parallel} &= \frac{V_{d-2}}{8\pi G_{d+1}}\left[\frac{1}{d-1}\frac{l}{\epsilon^{d-1}}-\frac{2^{d-2}\pi^{\frac{d-1}{2}}}{(d-1)^2}\left(\frac{\Gamma(\frac{d}{2d-2})}{\Gamma(\frac{1}{(2d-2)})}\right)^{d-3}\frac{1}{l^{d-2}}\right. \\ &- \left.\frac{1}{z_I^d(2b_0)^2(d-1)}\left[c_2-c_0 d+\frac{(d-2)\pi}{2(d-1)b_0}\left(\frac{I_l}{b_0}-\frac{b_1}{b_0}\right)\right]l^2\right] \end{aligned} \tag{3.155}$$

and the change in HSC due to the presence of boost reads

$$\delta C_V^{\parallel} = -\frac{V_{d-2}}{8\pi G_{d+1}}\frac{1}{z_I^d(2b_0)^2(d-1)}\left[c_2 - c_0 d + \frac{(d-2)\pi}{2(d-1)b_0}\left(\frac{I_l}{b_0} - \frac{b_1}{b_0}\right)\right] l^2 \ . \tag{3.156}$$

This change in the subregion complexity can be related to the boundary field theoretic quantities in the following way

$$\delta C_V^{\parallel} = -\frac{\left[c_2 - c_0 d + \frac{(d-2)\pi}{2(d-1)b_0^2}\left(I_l - b_1\right)\right]}{4\pi b_1 (d-1) T_E}\left[\Delta E - \frac{d-1}{d+}\mathcal{V}\Delta P_{\parallel}\right] \tag{3.157}$$

where T_E, ΔE, $\Delta P_{\parallel}$ are given in eq.(3.37).

Subsystem perpendicular to the boost

On the other hand, when we consider a subsystem of length l in the direction perpendicular to the boost, the computed expression of HSC reads

$$\begin{aligned} C_V^{\perp} &= \frac{V_{d-2}}{8\pi G_{d+1}}\left[\frac{1}{d-1}\frac{l}{\epsilon^{d-1}} - \frac{2^{d-2}\pi^{\frac{d-1}{2}}}{(d-1)^2}\left(\frac{\Gamma(\frac{d}{2d-2})}{\Gamma(\frac{1}{(2d-2)})}\right)^{d-3}\frac{1}{l^{d-2}}\right. \\ &- \left.\frac{1}{z_I^d(d-1)(2b_0)^2}\left[c_2 - c_0(d-1) + \frac{I_l(d-2)}{2(d-1)b_0^2}\right] l^2\right] . \end{aligned} \tag{3.158}$$

With the above expression in hand, we can compute the change in HSC due to the boost , in the perpendicular set up. This reads

$$\delta C_V^{\perp} = -\frac{V_{d-2}}{8\pi G_{d+1}}\frac{1}{z_I^d(d-1)(2b_0)^2}\left[c_2 - c_0(d-1) + \frac{I_l(d-2)}{2(d-1)b_0^2}\right] l^2 \ . \tag{3.159}$$

The change in the HSC ($\delta C_V^{\perp}$) can be written in terms of the CFT excitation energy and entanglement temperature in the following way

$$\delta C_V^{\perp} = -\frac{\left[c_2 - c_0(d-1) + \frac{I_l(d-2)}{2(d-1)b_0^2}\right]}{4\pi a_1 T_E}\Delta E \ . \tag{3.160}$$

3.6.5 Mutual complexity

In this section, we compute the mutual complexity by incorporating the HSC conjecture. We do this by considering two subsystems of equal length l, separated by a distance x.

Subsystems along the boost

In this set up, we consider the equal length subsystems (separated by the distance x) are along the direction of the boost. This configuration leads to the following expression of mutual complexity

$$\begin{aligned}\Delta\mathcal{C}^{\parallel} &= \frac{V_{d-2}}{2G_{d+1}}\frac{1}{4\pi}\Bigg[-\frac{2^{d-2}\pi^{\frac{d-1}{2}}}{(d-1)^2}\left(\frac{\Gamma(\frac{d}{2d-2})}{\Gamma(\frac{1}{(2d-2)})}\right)^{d-3}\left(\frac{2}{l^{d-2}}+\frac{1}{x^{d-2}}-\frac{1}{(2l+x)^{d-2}}\right)\\ &- \frac{1}{z_I^d(2b_0)^2(d-1)}\left[c_2-c_0d+\frac{(d-2)\pi}{2(d-1)b_0}\left(\frac{I_l}{b_0}-\frac{b_1}{b_0}\right)\right]\left(2l^2+x^2-(2l+x)^2\right)\Bigg] \quad (3.161)\end{aligned}$$

Subsystems perpendicular the boost

We now consider that the equal length subsystems (separated by the distance x) are in a direction perpendicular to the boost. The mutual complexity then reads

$$\begin{aligned}\Delta\mathcal{C}^{\perp} &= \frac{V_{d-2}}{8\pi G_{d+1}}\Bigg[-\frac{2^{d-2}\pi^{\frac{d-1}{2}}}{(d-1)^2}\left(\frac{\Gamma(\frac{d}{2d-2})}{\Gamma(\frac{1}{(2d-2)})}\right)^{d-3}\left(\frac{2}{l^{d-2}}+\frac{1}{x^{d-2}}-\frac{1}{(2l+x)^{d}}\right)\\ &- \frac{1}{z_I^d(d-1)(2b_0)^2}\left[c_2-c_0(d-1)+\frac{I_l(d-2)}{2(d-1)b_0^2}\right]\left(2l^2+x^2-(2l+x)^2\right)\Bigg]\ . \quad (3.162)\end{aligned}$$

The changes in mutual complexity due to involvement of boost can be written down with the help of the above expressions. For the parallel set up this reads

$$\delta\mathcal{C}^{\parallel} = -\frac{V_{d-2}}{8\pi G_{d+1}}\frac{1}{z_I^d(2b_0)^2(d-1)}\left[c_2-c_0d+\frac{(d-2)\pi}{2(d-1)b_0}\left(\frac{I_l}{b_0}-\frac{b_1}{b_0}\right)\right]\left(2l^2+x^2-(2l+x)^2\right)\ . \quad (3.163)$$

On the other hand, for the perpendicular set up, it reads

$$\delta\mathcal{C}^{\perp} = -\frac{V_{d-2}}{8\pi G_{d+1}}\frac{1}{z_I^d(d-1)(2b_0)^2}\left[c_2-c_0(d-1)+\frac{I_l(d-2)}{2(d-1)b_0^2}\right]\left(2l^2+x^2-(2l+x)^2\right) \quad (3.164)$$

3.7 Conclusion

Now we make a summary of our work presented in this chapter. In this chapter we have computed different measures of quantum correlation for mixed state holographically. It is to be mentioned that, in the boundary CFT we have considered a strongly coupled plasma moving along a particular direction with constant velocity and the corresponding theory of gravity in the bulk is

described by boosted Schwarzschild black brane. Thus by considering this boosted geometry in the bulk we are able to investigate the effect of boost in different measures of quantum correlation. By considering this geometry in the bulk theory we can look into the effect of IR deformation on the quantum information theoretic measures. The bulk geometry we have considered in this paper is the boosted black brane geometry with the direction of boost compactified on a circle. One of the motivations to consider this geometry lies in the fact that this type of geometry leads to Kaluza-Klein gauge charges.

The presencce of boost in a specific direction allows for the selection of subsystems either aligned with the boost direction or oriented perpendicular to it. In this geometric setup we initially calculate the holographic entanglement entropy for strip-like subsystems aligned both parallel and perpendicular to the boost direction. These computations are carried out using the thin strip approximation, as our focus is on determining the leading-order corrections (beyond pure AdS) to information-theoretic quantities resulting from the introduction of the boost. The spacetime geometry for boosted black brane suggests that, it is not a static one. So to compute the HEE we use the HRT formalism instead of RT prescription. In this work we are interested in computing the leading order change in HEE arises due to the boost. We observe that as long we are interested to the leading order change in the HEE, both the HRT prescription and RT prescription produces the same result. The reason for this is that the static minimal surface emerges as the dominating piece of the HRT surface if one neglects the higher order terms. It is shown earlier that, one can relate this leading order change in HEE to the CFT excitation energy and pressure. This relation gives rise to the thermodynamics like law as it introduces the notion of an entanglement temperature. The boost on the bulk spacetime can be thought as a charged excitation in the CFT side. A key observation is that the holographic entanglement entropy increases as the boost parameter increases, both for subsystems oriented perpendicular to the boost and those aligned parallel to it. A possible reason for this increase in the entanglement entropy can be an increase in the strip area of the subsystem living on the CFT side. Furthermore, we have also observed that the change in HEE for perpendicular strip is larger compared to the parallel one. This asymmetry arises due to the difference in the 'pressure' of the CFT in the perpendicular and the parallel case. It is to be noted that, the pressure being more in the parallel case due to the effect of boost.

Keeping this result of HEE in mind we then proceed to compute the holographic mutual informa-

tion between two disjoint subsystems of equal length. Then we move on to the computation of EWCS (which is the gravity dual of EoP) in the similar setup. We have done our computation for both the parallel and perpendicular scenario. We have graphically shown that, in both the cases the HMI vanishes at a particular value of the separation distance (critical separation, x_c) for fixed subsystem length and boost parameter. This implies that, at this particular value of the separation distance EWCS shows a phase transition from connected phase to disconnected phase. We have also observed that, due to the inclusion of boost the HMI vanishes earlier comapred to the $\beta = 0$ scenario, this implies that, the entanglement wedge also undergoes from connected phase to disconnected phase at smaller value of the separation distance in compared to zero boost case. The graphical representation shows that, the value of this critical separation decreases with the increase in the boost parameter. We have observed this in both the parallel and perpendicular setups. We have compared the results of HMI and EWCS graphically for both the parallel and perpendicular case. This observation suggests that HMI for perpendicular configaration vanishes earlier in compare to the parallel configaration for fixed subsystem length and boost parameter. This in turn also means that the connected entanglement wedge gets disconnected earlier for perpendicular configaration. It is to be noted that, in the adjacent subsystem limit (if we take the separation distance $x \to 0$), the change in EWCS due to the boost is proportional to the change in the HEE. Thus we relate the change in EWCS (arises due to the inclusion of boost) to the pressure and excitation energy of the boundary filed theory by employing the the generalized first law of entanglement. This results the thermodynamic like law for EWCS.

Then we proceed to compute the another measures of quantum correlation for mixed state, entanglement negativity holographically. To compute E_N holographically, we consider two different setups. First we consider two adjacent subsystems of different length and then compute E_N holographically by using the result of HEE. We find that, for adjacent subsystems E_N is a divergent quantity. On the other hand for disjoint subsystems of different length, we observe that , E_N is an UV finite quantity. To proceed further we consider that, both the subsystems have same length. Then we polt this result of E_N for two disjoint subsystems of equal length with respect to the separation distance. We observe that, for disjoint subsystems of equal length entanglement negativity vanishes at particular value of separation distance (x_c') for a fixed value of the subsystem length and boost parameter. We have also found that, this critical separation x_c' decrease with increase

in the boost parameter. It is to be noted that due the effect of boost E_N vanishes earlier comapred to zero boost scenario. Furthermore it is to be mentioned that, $x_c' > x_c$, this implies that, even if the subsystems are not in the connected phase, E_N can still measures the quantum correlation between them. This observations hold for both the paralle and perpendicular configaration. We have also compared the result of negativity between the parallel and perpendicular case graphically. Furthermore we show that the change in entanglement negativity for disjoint subsystems of equal length is related to the change in the HEE, in the limit adjacent subsystems. Thus we can relate the this change in E_N with boundary field theoretic quantities similar to EWCS.

In addition to quantifying quantum correlations, we also calculate the subregion complexity for a boosted black brane, enabling us to determine the mutual complexity. Our findings reveal that the mutual complexity exhibits superadditive behavior in this scenario. Furthermore, we establish a thermodynamic-like law for holographic subregion complexity (HSC) applicable to both parallel and perpendicular strip geometries. Lastly, we investigate the AdS wave geometry, derived by applying specific limits to the boosted black brane geometry. We once again compute the aforementioned information-theoretic quantities for this geometry.

We conclude with a final observation regarding entanglement asymmetry. We find that the entanglement asymmetry reaches its maximum for the AdS wave geometry, which corresponds to a zero-temperature conformal field theory (CFT) at the boundary. This phenomenon can be understood through the concept of entanglement pressure. In the zero-temperature CFT, wave-like excitations generate finite entanglement pressure along the direction of the wave, while the pressure in the transverse direction vanishes. However, for a finite-temperature CFT at the boundary (which corresponds to including a black brane geometry in the bulk), entanglement pressure also arises in the transverse direction. As a result, entanglement entropy asymmetry emerges when there is a uniform wave-like excitation or a uniform flow in the CFT. Boosted black brane systems are utilized in this study because they are currently the only known examples suitable for analyzing asymmetric systems. It would also be intriguing to investigate other systems, such as Bianchi models, which exhibit more generic forms of asymmetry, to further explore these dynamics.

3.8 Appendix A: List of beta function identities

In this appendix, we will give some useful integrals which have been used in this paper.

$$
\begin{aligned}
b_0 &= \int_0^1 dt\ t^{d-1}\frac{1}{\sqrt{R}} = \frac{1}{2(d-1)}B\left(\frac{d}{2d-2},\frac{1}{2}\right) = \frac{\sqrt{\pi}\Gamma(\frac{d}{2d-2})}{\Gamma(\frac{1}{2d-2})} \\
b_1 &= \int_0^1 dt\ t^{2d-1}\frac{1}{\sqrt{R}} = \frac{1}{2(d-1)}B\left(\frac{d}{d-1},\frac{1}{2}\right) = \frac{\sqrt{\pi}\Gamma(\frac{d}{d-1})}{(d+1)\Gamma(\frac{1}{2}+\frac{1}{d-1})} \\
b_2 &= \int_0^1 dt\ t^{3d-1}\frac{1}{\sqrt{R}} = \frac{1}{2(d-1)}B\left(\frac{3d}{2d-2},\frac{1}{2}\right) \\
I_l &= \int_0^1 dt\ t^{d-1}(1-t^d)\frac{1}{R^{\frac{3}{2}}} = \frac{d+1}{d-1}b_1 - \frac{1}{d-1}b_0 \\
c_0 &= \int_0^1 dt\ \frac{t^d}{\sqrt{R}} = \frac{1}{2(d-1)}B\left(\frac{d+1}{2(d-1)},\frac{1}{2}\right) = \frac{\pi}{2(d^2-1)b_1} \\
c_1 &= \int_0^1 dt\ \frac{t^{2d}}{\sqrt{R}} = \frac{1}{2(d-1)}B\left(\frac{2d+1}{2(d-1)},\frac{1}{2}\right) = \frac{\pi}{2(d-1)(2d+1)b_2} \\
c_2 &= \int_0^1 dt\ \frac{(1-t^d)}{R^{\frac{3}{2}}} = \frac{2}{d-1}c_0 + \frac{d-2}{2(d-1)^2}B\left(\frac{1}{2(d-1)},\frac{1}{2}\right) = \frac{\pi}{(d+1)(d-1)^2b_1} + \frac{\pi(d-2)}{2(d-1)^2b_0} \\
c_3 &= \int dt\ \frac{t^d(1-t^d)}{R^{\frac{3}{2}}} = \frac{2}{d-1}c_0 + \frac{d+2}{d-1}c_1\int_0^1 \frac{dt}{\sqrt{1-t^{2(d-1)}}} = \frac{\pi}{2(d-1)b_0} \\
J_l &= \int_0^1 dt\ t^{d-1}\left(\frac{\beta^2\gamma^2}{4}t^d + \beta^4\gamma^4\left(\frac{3(1-t^d)}{8(1-t^{2(d-1)})} - \frac{1}{2}\right)\right)\frac{(1-t^d)}{R^{\frac{3}{2}}} = \beta^2\gamma^2 J_1 + \beta^4\gamma^4 J_2 \\
K_l &= \int_0^1 dt\ t^{d-1}\left(\frac{\beta^2\gamma^2}{4}t^d + \beta^4\gamma^4\left(\frac{3(1-t^d)}{8(1-t^{2(d-1)})} - \frac{1}{2}\right)\right)\frac{(1-t^d)}{R^{\frac{3}{2}}} = \beta^2\gamma^2 K_1 + \beta^4\gamma^4 K_2 \qquad (3.165)
\end{aligned}
$$

where $R = 1-t^{2d-2}$ and J_1, J_2, K_1, K_2 are given by

$$
\begin{aligned}
J_1 &= \frac{1}{4(d-1)}\left((2d+1)b_2 - (d+1)b_1\right) \\
J_2 &= \frac{1}{8(d-1)^2}\left((3-2d)b_0 - 2(d+1)(3-d)b_1 + 3(2d+1)b_2\right) - \frac{I_l}{2} \\
K_1 &= \frac{1}{2(d-1)}c_0 + \frac{d+2}{4(d-1)}c_1 \\
K_2 &= -\frac{d-4}{2(d-1)^2}c_0 + \frac{(d+2)(d-4)}{8(d-1)^2}c_1 + \frac{d}{8(d-1)}c_2\ . \qquad (3.166)
\end{aligned}
$$

Note that $B(m,n) = \frac{\Gamma(m)\Gamma(n)}{\Gamma(m+n)}$ is the standard beta function and we have used the identity

$$
B(x,\frac{1}{2})B(x+\frac{1}{2},\frac{1}{2}) = \frac{\pi}{x}\ . \qquad (3.167)
$$

Some more integrals are as follows

$$
\begin{aligned}
a_0 &= \int_0^1 dt\ t^{-d+1}\frac{1}{\sqrt{R}} = \frac{1}{2(d-1)}B\left(\frac{1-(d/2)}{d-1},\frac{1}{2}\right) \\
a_1 &= \int_0^1 dt\ t^{-d+1}\frac{t^d}{\sqrt{R}} = \frac{1}{2(d-1)}B\left(\frac{1}{d-1},\frac{1}{2}\right) \\
a_2 &= \int_0^1 dt\ t^{-d+1}\frac{t^{2d}}{\sqrt{R}} = \frac{1}{2(d-1)}B\left(\frac{1+(d/2)}{d-1},\frac{1}{2}\right) \\
I_a &= \int_0^1 dt\ t^{d-1}(1-t^{2d})\frac{1}{R^{\frac{3}{2}}} = \frac{2d+1}{d-1}b_0 - \frac{1}{d-1}b_0\ . \qquad (3.168)
\end{aligned}
$$

We record some more identities given as

$$
b_0 = (2-d)a_0\ ,\quad b_1 = \frac{2}{d+1}a_1\ ,\ b_2 = \frac{2+d}{2d+1}a_2\quad . \qquad (3.169)
$$

3.9 Appendix B: Expressions of λ_1, λ_2, λ_3 and λ_4

In this appendix, we provide explicit expressions of λ_1, λ_2, λ_3 and λ_4 which have appeared in our analysis. This reads

$$
\begin{aligned}
\lambda_1 &= \left[\frac{4}{b_1(d+1)}\right]\left[\frac{\frac{1}{2}-\left(1+\frac{2\beta^2\gamma^2}{d-1}\right)\frac{b_1}{b_0}+\frac{\beta^2\gamma^2}{d-1}}{\frac{d-1}{d+1}+\frac{2\beta^2\gamma^2}{d+1}}\right] \qquad (3.170) \\
\lambda_2 &= -\left[\frac{3}{d+1}\right]\left[\frac{\frac{d-1}{2}+\beta^2\gamma^2}{\frac{d-1}{d+1}+\frac{2\beta^2\gamma^2}{d+1}}\right] \qquad (3.171) \\
\lambda_3 &= \left[\frac{4}{b_1(d+1)}\right]\left[\frac{\frac{1}{2}\left(1+\beta^2\gamma^2\right)-\left(\frac{b_1}{b_0}+\beta^2\gamma^2\frac{I_I}{b_0}\right)}{\frac{d-1}{d+1}+\beta^2\gamma^2}\right] \qquad (3.172) \\
\lambda_4 &= -\frac{3}{2}\quad . \qquad (3.173)
\end{aligned}
$$

Chapter 4

Page curve, island and mutual information

4.1 Introduction

Black hole physics has fascinated researchers since its discovery, generating immense interest. To understand the physcis of black holes fully, one requires a complete theory of quantum gravity. A key challenge in this context is the information loss paradox, which remains a significant issue. Though it still remains unsolved, notable progress has been achieved recently via holography, a fundamental aspect of quantum gravity. Since the paradox arises at the semiclassical level, so to understand this completely one must go beyong this semiclassical framework. Our goal is to understand the black hole information paradox and its recent progress.

It is very well known that, black holes classical solutions of Eistein field equation.Black holes are the densest astrophysical objects, so massive that even light cannot escape their gravitational pull. This classical view shifted when Hawking demonstrated in his groundbreaking work that black holes can emit thermal radiation within the framework of quantum theory [213, 214]. If a black hole emits particles without absorbing any, it will eventually leads to the black hole evaporation. The evaporation of a black hole, as studied in semiclassical physics, conflicts with quantum mechanics because it transforms a pure state into a mixed state, violating the principles of information conservation and unitarity. This confliction is given the name information loss paradox. However, some researchers, including Hawking initially, thought quantum mechanics needed modification

due to the accuracy of the calculations, today, nearly all scientists agree that quantum mechanics must remain intact. The semiclassical approach is deemed insufficient, as quantum mechanics has consistently described various theories accurately, and violating it would lead to significant issues, such as energy non-conservation. We adopt this perspective here, assuming the calculations are flawed and that moving beyond semiclassical physics is necessary to understand the underlying reasons.

Another approach to understanding this paradox is through the Page curve [215, 216]. In this framework, the paradox can be expressed using the concept of entropy rather than states. Specifically, it concerns the entropy of the radiation emitted by the black hole. The entanglement entropy of the radiation increases over time as more particles are emitted. However, Page argued that to maintain unitarity during evaporation, the entanglement entropy of the radiation must decrease after a certain point. Based on this fact, the paradox can be expressed as follows: We must identify the appropriate semiclassical formula that ensures the entanglement entropy of the radiation adheres to the Page curve. This means the entropy should initially increase, reach a peak, and then decrease at a specific point, eventually returning to its original value.

A major breakthrough in understanding quantum gravity is the idea of holography. This concept proposes that a theory of quantum gravity can be described in a space with one less dimension than the physical space it represents. As a result, a region of spacetime is defined not by its volume, as in quantum field theory, but by the area of its boundary. One of the most well known example of holographic theory is the AdS/CFT correspondence. This relates a gravitational theory in the AdS spacetime (which is also called as the bulk theory), to a conformal field theory (CFT) with one less dimension (the boundary theory). This correspondence states that, physics on the both sides are equivalent, therefore they can be related. One of the well known example of this duality is that, black holes in AdS spacetime is equivalent to thermal states in the CFT side. However, the most important relationship for our purposes is the holographic entanglement entropy. Initially inspired by the Bekenstein-Hawking entropy, this principle essentially states that the entropy of a region in a conformal field theory is proportional to a specific area in the corresponding anti-de Sitter spacetime. A modification of this relationship is the island rule, which is relevant for quantum field theories coupled with a gravitational theory. Another key idea is entanglement wedge reconstruction, which allows us to retrieve information about the bulk region of spacetime solely

from the data present on its boundary. This principle underscores the profound link between the boundary and the bulk in holographic frameworks.

The application of holography to address the information paradox has led to significant and remarkable progress. By leveraging the principles of holography, researchers have gained deeper insights into how information is preserved in black hole evaporation. In [217, 218, 219], the authors have obtained correct Page curve by considereing AdS black hole, with the help of holographic principle of holography and island rule. It is to be mentioned that the island rule is semiclassical formula. But its derivation needs inputs from quantum gravity. Thus it is belived that it the correct semiclassical formula to compute the entanglement entropy of radiation (or the fine grained entropy).

4.2 Hawking radiation and the information loss paradox

In this chapter, we derive the key result that black holes emit a thermal spectrum of particles, a phenomenon that lies at the core of the information paradox. It was first shown by Hawking in [213, 214], by considering the quantum field theory in classical black hole spacetime. This result gives rise to the black hole evaporation process, as the emission of particles causes black holes to lose mass and eventually evaporate. In the same year, Hawking recognized that this evaporation process implies a loss of unitarity and information, which contradicts the principles of quantum mechanics. This realization led to the formulation of the information paradox, highlighting a fundamental conflict between general relativity and quantum theory.

We now derive the spectrum of Hawking radiation by following [220]. Let us consider a black hole with a spherically symmetric, static spacetime, characterized by an asymptotically flat metric of the form

$$ds^2 = -f(r)dt^2 + \frac{dr^2}{f(r)} + r^2 d\Omega^2 \tag{4.1}$$

In [221, 222], it was demonstrated that Hawking radiation can be studied through tunneling by focusing solely on the radial trajectory. Therefore we restrict ourselves only to the $(t-r)$ sector. Now, we consider the massless Klein-Gordon equation in this background spacetime (given in

eq.(4.1)). This results

$$\begin{aligned} g^{\mu\nu}\nabla_\mu\nabla_\nu\phi &= 0 \\ -\frac{1}{f(r)}\partial_t^2\phi + f^{'}(r)\partial_r\phi + f(r)\partial_r^2\phi &= 0 \end{aligned} \tag{4.2}$$

To proceed further, we adopt the standard WKB ansatz of the following form

$$\phi(r,t) = e^{-\frac{i}{\hbar}S(r,t)} \tag{4.3}$$

with

$$S(r,t) = S_0(r,t) + \sum_{i=1}^{\infty}\hbar^i S_i(r,t)\ . \tag{4.4}$$

Now, upon substituting eqs.(4.3, 4.4) into eq.(4.2) and considering the semiclassical limit, we obtain (i.e. $\hbar \to 0$),

$$\partial_t S_0(r,t) = \pm F(r)\partial_r S_0(r,t)\ . \tag{4.5}$$

The positive sign corresponds to the left-moving solution, whereas the negative sign represents the right-moving solution. Since the metric (4.1) is stationary, it possesses a timelike Killing vector. Therefore, we choose the ansatz for $S_0(r,t)$ as

$$S_0(r,t) = \omega t + \tilde{S}_0(r) \tag{4.6}$$

where ω is the conserved quantity associated with the timelike Killing vector. Now substituting the above ansatz in eq.(4.5) we get

$$S_0(r,t) = \omega(t \pm r_*); \quad r_* = \int \frac{dr}{F(r)}\ . \tag{4.7}$$

For further analysis, it is useful to introduce the null tortoise coordinates, defined as follows

$$u = t - r_*, \quad v = t + r_*\ \ . \tag{4.8}$$

It's worth noting that by expressing eq.(4.7) in these above coordinates, which are defined both inside and outside the event horizon, and then substituting into eq.(4.3), one can derive the right and left modes for both regions. This results

$$\begin{aligned} \left(\phi^{(R)}\right)_{\text{in}} &= e^{-\frac{i}{\hbar}\omega u_{\text{in}}}; \quad \left(\phi^{(L)}\right)_{\text{in}} = e^{-\frac{i}{\hbar}\omega v_{\text{in}}} \\ \left(\phi^{(R)}\right)_{\text{out}} &= e^{-\frac{i}{\hbar}\omega u_{\text{out}}}; \quad \left(\phi^{(L)}\right)_{\text{out}} = e^{-\frac{i}{\hbar}\omega v_{\text{out}}} \end{aligned} \tag{4.9}$$

In the tunneling formalism, a virtual pair of particles is generated inside the black hole. One particle from this pair can quantum mechanically tunnel through the horizon and is subsequently observed at infinity. On the other hand the other particle moves towards the singularity. As the particle crosses the horizon, the nature of the spacetime coordinate changes. This can be addressed by using Kruskal coordinates, which remain well-defined on both sides of the horizon. The Kruskal time T and space X coordinates, which are well-defined on both sides of the horizon, are given by

$$\begin{aligned} T_{\rm in} &= e^{\kappa(r_*)_{\rm in}}\,\cosh(\kappa t_{\rm in}) \quad ; \quad X_{\rm in} = e^{\kappa(r_*)_{\rm in}}\,\sinh(\kappa t_{\rm in}) \\ T_{\rm out} &= e^{\kappa(r_*)_{\rm out}}\,\sinh(\kappa t_{\rm out}) \quad ; \quad X_{\rm out} = e^{\kappa(r_*)_{\rm out}}\,\cosh(\kappa t_{\rm out}) \end{aligned} \tag{4.10}$$

where κ is the surface gravity, given by $\kappa = \frac{f'(r_H)}{2}$. Now these two sets of coordinates are related

$$t_{\rm in} \to t_{\rm out} - i\frac{\pi}{2\kappa} \quad ; \quad (r_*)_{\rm in} \to (r_*)_{\rm out} + i\frac{\pi}{2\kappa} \tag{4.11}$$

Now, following the definition (4.8), we derive the relations that connect the null coordinates defined on either side of the horizon. This yields

$$\begin{aligned} u_{\rm in} &= t_{\rm in} - (r_*)_{\rm in} \to u_{\rm out} - i\frac{\pi}{\kappa} \\ v_{\rm in} &= t_{\rm in} + (r_*)_{\rm in} \to v_{\rm out} \end{aligned} \tag{4.12}$$

Under these transformations, the inside and outside modes are related by

$$\begin{aligned} \left(\phi^{(R)}\right)_{\rm in} &\to e^{-\frac{\pi\omega}{\hbar K}}\left(\phi^{(R)}\right)_{\rm out} \\ \left(\phi^{(L)}\right)_{\rm in} &\to \left(\phi^{(L)}\right)_{\rm out} . \end{aligned} \tag{4.13}$$

Using these transformations, the density matrix operator for an observer outside the event horizon can be constructed, leading to the derivation of the blackbody spectrum and the thermal flux corresponding to the semiclassical Hawking temperature. To proceed further we consider the Schwarzschild spacetime. To determine the blackbody spectrum and Hawking flux, we first consider n non-interacting virtual pairs created inside the black hole. Each of these pairs is described by the modes defined in the first set of eq.(4.9). Therefore, the physical state of the system, as observed from the outside, is given by

$$|\Psi\rangle = N\sum_n \left|n^{(L)}_{\rm in}\right\rangle \otimes \left|n^{(R)}_{\rm in}\right\rangle \to N\sum_n e^{-\frac{\pi n\omega}{\hbar\kappa}} \left|n^{(L)}_{\rm out}\right\rangle \otimes \left|n^{(R)}_{\rm out}\right\rangle \tag{4.14}$$

where N is the normalisation constant. Now we can compute the density matrix associated with state $|\Psi\rangle$. Therefore the expression of the density matrix reads

$$\begin{aligned}\rho &= |\Psi\rangle\langle\Psi| \\ &= |N|^2 \sum_n \sum_m e^{-4\pi M\omega(m+n)} \left|n_{\text{out}}^{(L)}\right\rangle \left\langle m_{\text{out}}^{(R)}\right| \otimes \left|n_{\text{out}}^{(R)}\right\rangle \left\langle m_{\text{out}}^{(L)}\right| \ . \end{aligned} \tag{4.15}$$

Keeping this density matrix in hand we can compute the reduced density matrix of the outgoing Hawking radiation by tracing out the left part. This results

$$\rho_R = \text{Tr}_L(\rho) = |N|^2 \sum_n e^{-8\pi M\omega n} \left|n_{\text{out}}^{(R)}\right\rangle \left\langle n_{\text{out}}^{(R)}\right| \ . \tag{4.16}$$

We can fix the normalisation constant by the fact that, $\text{Tr}(\rho_R) = 1$. This yeilds

$$\rho_R = (1 - e^{-8\pi M\omega}) \sum_n e^{-8\pi M\omega n} \left|n_{\text{out}}^{(R)}\right\rangle \left\langle n_{\text{out}}^{(R)}\right| \ . \tag{4.17}$$

It is important to note that the calculation of the normalization factor depends on the nature of the particle, whether it is a boson or a fermion. Our derivations so far correspond to a Klein-Gordon field, meaning the particles have spin zero and are therefore bosons. Now keeping this density matrix in mind we now compute the average number of particles. This results

$$\langle n \rangle = \text{Tr}(n\rho_R) = \frac{1}{e^{8\pi m\omega} - 1} \ . \tag{4.18}$$

Now indentifying energy E as ω the temperature of the radiation is obtained as

$$T = \frac{1}{8\pi M k_B} \ . \tag{4.19}$$

The above temperature is nothing but the Hawking temperature corresponds to the Schwarzschild black hole. So far, we have seen that black holes can emit radiation through a quantum mechanical process, and this radiation is thermal. This process can continue until the black hole has completely evaporated. However, this leads to a loss of information, which presents a significant challenge in fundamental physics. To be more precise this violets the unitarity principle.

We assume that when the black hole forms, it is in a pure state. As it begins to emit radiation, which is thermal, the system appears to evolve into a mixed state. After the black hole has completely evaporated, only the Hawking radiation remains. This was Hawking's original statement, but it implies loss of information, which challenges the principles of quantum mechanics. We begin

with the initial pure state $|\Psi\rangle$ of the black hole. After complete evaporation, only the Hawking radiation remains, described by the density matrix ρ_R. It is easily seen that this density matrix corresponds to a mixed state, which can be verified by computing the von-Neumann entropy. We can compute the von Neumann entropy of the radiation using the expression

$$S_{vN}(\rho_R) = -\mathrm{Tr}(\rho_R \ln \rho_R) = -\ln |N|^2 + 8\pi M\omega \langle n \rangle \tag{4.20}$$

where $\langle n \rangle$ is the average number of particles given in eq.(4.18). Identifying the partition function Z as $1/|N|^2$ the von-Neumann entropy of Hawking radiation can be written as

$$S_{vN}(\rho_R) = \ln Z + 8\pi M\omega \langle n \rangle \ . \tag{4.21}$$

The above analysis suggests that, the von-Neumann entropy of the radiation is non-zero, that is $S_{vN}(\rho_R) \neq 0$. This implies that the desnisty matrix ρ_R describing the radiation is in a mixed state. So, it is observed that, from an initial pure state $|\Psi\rangle$, we end up with a mixed thermal state ρ_R. Since no unitary operator U can describe the evolution of the black hole evaporation process, the transformation from an initial pure state to a final mixed state implies a loss of information. This apparent violation of unitarity, poses a major challenge to our understanding of quantum mechanics and black hole physics.

4.3 Page curve

There is also another way to understand this information loss problem. One can look into this problem from the entropic presprective. It was first demonstrated by Page to resolve the paradox. Page urged that, in order to obey the unitarity the fine grained entropy of Hawking radiation should follow the Page curve. In this section we discuss the concept of Page curve in details.

To understand the Page curve, it is essential to distinguish between fine-grained and coarse-grained entropy. Fine-grained entropy, also known as von Neumann entropy, measures the quantum entanglement of a system and is given by $S_{fin} = -\mathrm{Tr}(\rho \ln \rho)$. This entropy remains constant under unitary evolution. On the other hand, On the other hand, coarse-grained entropy, often associated with thermodynamic entropy, accounts for the lack of detailed knowledge about a system's microstates. It typically increases over time obeying the $2nd$ law of thermodynamics.

In this case the fin-grained entropy of radiation is identified with the entanglement entropy of the matter field located on the region R outside the black hole. However, the thermodynamic entropy of the black hole (S_{BH}) is related to the area of the black hole horizon [223, 224, 225].

Now we describe the information loss paradox for evaporating black hole. This is represented graphically in the left panel of Fig.(4.1). This figure suggests that at the begining of the evaporation the von-Neumann entropy of the radiation $S_{vN}(R)$ is zero, on the other hand the thermodynamic entropy of the black is maximum. Now as time passes black hole statrs to evaporate. Deu to the evaporation black looses mass, so the area of the event horizon decreases. This in turn means that, the thermodynamic entropy of the black hole decreases with time, represented by black line. However, the fin-grained entropy of the radiation monotonically increases with time (represented by the red line). This implies the thermal nature of the Hawking radiation. Now there exists a particular value of the observer's time at which the S_{BH} and $S_{vN}(R)$ are equal. This particular time is known as the Page time. Upto the Page time, that for the time domain $t < t_{Page}$, the thermodynamic entropy of the black hole is greater than the fine-grained entropy of the radiation. This implies in this time domain ($t < t_{Page}$), there is no paradoxial situation. But after the Page time doamin, that for the domain $t > t_{Page}$ it is observed that the fine-grained entropy of the radiation exceeds the thermal entropy of the black hole, that is $S_{vN}(R) > S_{BH}$. This fact is self-contradictory as the basic definition of coarse-grained entropy is associated to the fact that it is obtained by maximizing the fine-grained entropy over all possible states .Therefore the paradox appears just after the Page time. The above mentioned observation provides us an entropic way to understand the paradoxical situation.

This naturally leads to the question of how the von Neumann entropy of Hawking radiation evolves over time. This issue was elegantly resolved by the concept of the *Page curve*. The Page curve suggests that, in order to preserve unitarity, the von Neumann entropy of Hawking radiation should start at zero, increase monotonically until it reaches the Page time, and then decrease back to zero, indicating the completion of the black hole evaporation process (depicted by the dotted line) [226, 227]. The contradiction only emerges after the Page time as after this particular time one usually gets $S_{vN}(R) > S_{BH}$.

We wolud like to mention that, there are several different approaches have been proposed to address and resolve this issue [228, 229, 230, 231].

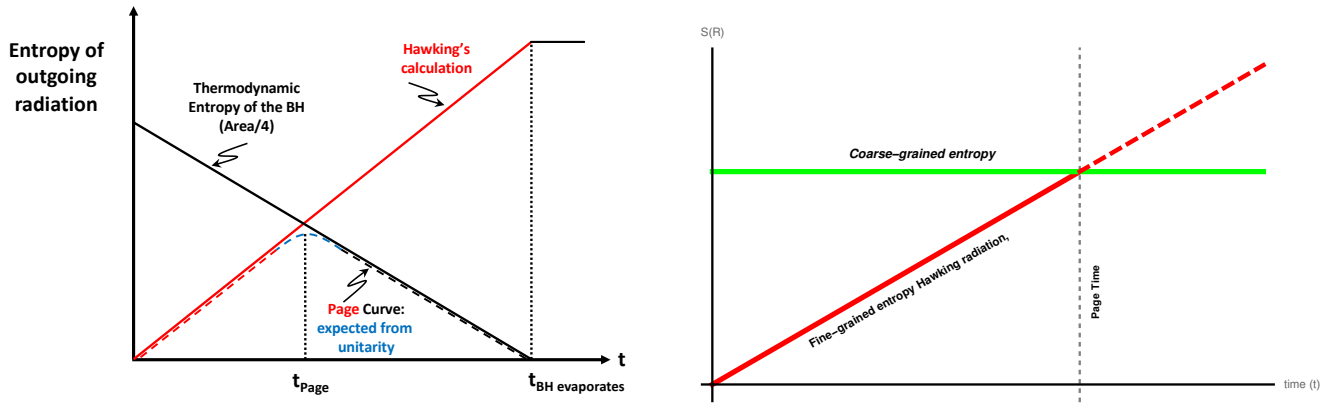

Evaporating black hole Eternal black hole

Figure 4.1: The left panel of the above figure represents the Page curve of evaporating black hole, while the right panel depicts that of for the eternal black hole.

4.4 Island formalism to compute the fine-grained entropy in gravitational back ground

In this section, we explore the methodology for computing the fine-grained entropy in a gravitational background in details. We start our discussion by reviewing some historial results. Motivated by the complexity of computing geometric entropy in higher-dimensional quantum field theories, Ryu and Takayanagi proposed its holographic generalization in [74, 75]. This formulation, developed within the framework of the AdS/CFT correspondence, provides a more tractable approach, as mentioned earlier. They proposed that the entanglement entropy of subsystem in the CFT side can be determined from a geometric quantity in AdS, which is significantly easier to compute. However, this proposal was valid only for time-independent scenarios, where a time-independent state in the CFT is mapped to a static spacetime in AdS. One year later, Hubeny, Ryu, and Takayanagi proposed a covariant generalization of this prescription, extending its applicability to time-dependent scenarios [232]. The conjecture was proven for the static case using gravitational path integrals in [77] and for covariant case in [233]. The covariant version of the Ryu-Takayanagi formula states that the entanglement entropy of a region A is proportional to the area of the

extremal surface X, which is anchored to the boundary of A and extends into the bulk spacetime. The covariant version of the RT formula reads

$$S_{RT}(A) = \frac{\text{Area}(X)}{4G_N^{d+1}} \ . \tag{4.22}$$

It obeys all the properties of entanglement entropy. This formula represents the leading-order classical contribution to the holographic entanglement entropy that we aim to compute. The quantum correction to this formula was first computed by Faulkner, Lewkowycz and Maldacena in [234]. The leading quantum correction is determined by the bulk entanglement entropy between Σ_X and its complement in the bulk, or equivalently, the entanglement entropy of quantum fields confined within Σ_X, where Σ_X is d-dimensional volume in the bulk which is defined as $\partial\Sigma_X = A \cup X$. Now incorporating this fact, one can write the quantum corrected formula for the HEE as follows

$$S_{\text{gen}}(A) = \frac{\text{Area}(X)}{4G_N^{(d+1)}} + S_{\text{bulk}}(\Sigma_X) + O(G_N) \tag{4.23}$$

where $S_{\text{bulk}}(\Sigma_X)$ represents the von-Neumann entropy of matter field localised on Σ_X. It is to be noted that, this formula provides only the leading order correcrtion to the HRT fomula. This formula is also refferd to as the generalised entropy. Now to incorporate all the quantum correction to the expression of generalised entropy, we need to follow the proposal given in [235]. Roughly, this procedure involves extremizing the entire generalized entropy rather than just the area term and subsequently adding the bulk contribution as a correction. More precisely, the holographic fine-grained gravitational entropy is given by

$$S(A) = \min_X \left(\text{ext}_X \left[\frac{\text{Area}(X)}{4G_N} + S_{\text{bulk}}(\Sigma_X) \right] \right) . \tag{4.24}$$

Here, X is a $(d-1)$-dimensional surface with the same boundary as A and homologous to A, which extremizes the generalized entropy. This surface is referred to as the quantum extremal surface (QES). Again Σ_X is d-dimensional volume in the bulk which is defined as $\partial\Sigma_X = A \cup X$. The QES is referred to as a quantum surface, even though it is a classical surface, because it also extremizes the term involving quantum fields. The procedure involves first finding all quantum extremal surfaces (QES) that are extrema of the generalized entropy, and then selecting the one with the smallest generalized entropy. However, it should be kept in mind that, this formula is for effective field theory, hence it is a semi-classical formula. However, initially these formulas

appeared in the context of AdS/CFT correpondence, but these formulas can be applied for any spacetime. Their proof does not rely on holography but instead utilizes the replica trick in the gravitational path integral. This implies that the fine-grained gravitational entropy can be used to compute the entropy of a black hole in Minkowski spacetime, rather than being limited to an AdS background.

Keeping the above discussion in mind, we now introduce the concept of the island formalism, which provides a framework for computing the fine-grained entropy of Hawking radiation. The island rule is a refined version of the fine-grained gravitational entropy, specifically applicable to QFTs those are coupled to a gravitational theory. It was first propose in [219].Recently, the sophisticated idea of entanglement wedge reconstruction from Hawking radiation has suggested that certain non-trivial auxiliary regions within the black hole interior contribute to the fine-grained entropy of radiation [218, 217, 219, 236]. According to the idea, the fine-grained entropy of Hawking radiation is a generalized (quantum-mechanically corrected) version of the von Neumann entropy, which includes the standard von-Neumann term along with an additional surface term [234] . This surface is denoted as the *quantum extremal surface* (QES)[1] [235, 238, 239, 240].On the other hand, the aforementioned auxiliary regions within the black hole interior are referred to as *islands*. According to the recently proposed framework, the correct expression for the fine-grained entropy of Hawking radiation is given by [217, 219, 236]

$$S(\mathsf{R}) = \min \ \underset{\mathrm{I}}{\mathrm{ext}} \left\{ \frac{\mathrm{Area}(\partial \mathrm{I})}{4G_N} + S_{vN}(\mathrm{I} \cup \mathsf{R}) \right\} . \tag{4.25}$$

In the formula above, "I" denotes the island region located within the black hole interior, and the boundaries of this region define the quantum extremal surfaces, which we label as ∂I.

The origin of island formulation is related to the applicability of replica trick in presence of a curved spacetime as the background. According to the replica technique, computation of the von Neumann entropy of matter fields located on region R is to be performed by constructing the partition function as the gravitational path integral on this replicated geometry [241, 242, 243, 244]. One of the saddle points of this path integral is the replica wormholes (associated with correct boundary conditions) which connects different (replica) copies of the original spacetime. The mentioned saddle points in turn lead us to the island formula (given in eq.(4.25)).

[1]These are quantum corrected version of the classical maximin surfaces [237, 232].

Due to the fact that the island formulation has led us to the correct Page curve (compatible with the unitary evolution), it has gained the reputation as an necessary formalism to be studied [245, 246, 247, 248, 249, 250, 251, 252, 253, 175, 254, 255, 256, 257, 258, 259, 260, 176].

4.5 Role of mutual information in the Page curve

In this work [2], we give two proposals regarding the status of connectivity of entanglement wedges and the associated saturation of mutual information. The first proposal has been given for the scenario before the Page time depicting the fact that at a particular value of the observer's time $t_b = t_R$ (where $t_R \ll \beta$), the mutual information $I(R_+ : R_-)$ vanishes representing the disconnected phase of the radiation entanglement wedge. We argue that this time is the Hartman-Maldacena time at which the fine-grained entropy of radiation goes as $S(R) \sim \log(\beta)$, where β is the inverse of Hawking temperature of the black hole. On the other hand, the second proposal probes the crucial role played by the mutual information of black hole subsystems in obtaining the correct Page curve of radiation. In [175], the role played by the mutual information has been probed in the context of the fine grained entropy of Hawking radiation of BTZ black hole. It was shown that the condition of vanishing mutual information between the subsystems leads to a time independent expression for the fine grained entropy of the Hawking radiation which is consistent with the correct Page curve. In this work, we present some more new insights and proposals. In this chapter we consider two dimensional eternal black hole in Jackiw-Teitelboim gravity to carry out our analysis.

4.5.1 Gravitational set up: JT gravity + flat baths

Let us start by considering the two dimensional eternal black hole solution of Jackiw-Teitelboim (JT) gravity [261, 262] which is coupled to a pair of flat thermal baths (non-gravitational space-times). JT gravity is one of many solutions of the two dimensional dilaton gravity theory. The generalised action of two dimensional gravity theory in the presence of dilaton reads [263, 264]

$$\begin{aligned} I_{2d} &= \frac{1}{16\pi G_N}\int_V \sqrt{-g}\left[\phi R + U(\phi)(\nabla\phi)^2 + V(\phi)\right] d^2x \\ &\quad + \frac{1}{8\pi G_N}\int_{\partial V}\sqrt{-h}\phi K dx \ . \end{aligned} \tag{4.26}$$

[2] This work is based on [176]

We can obtain the JT gravity solution can be obtained by the following choice of $U(\phi)$ and $V(\phi)$

$$U(\phi) = 0 \;\; ; \;\; V(\phi) = \frac{2\phi}{l^2} \;\; . \tag{4.27}$$

where ϕ represents the dilaton field profile $\phi(r) = \frac{r}{l}$. We can also obtain the CGHS black hole [265] from the above action by considering different form of the functions $U(\phi)$ and $V(\phi)$ [264]. In this work we only consider black hole in JT gravity.

The spacetime metric describing black hole in JT gravity reads

$$ds^2 = -f(r)dt^2 + \frac{dr^2}{f(r)}; \;\; f(r) = \frac{(r^2 - r_+^2)}{l^2} \;\; . \tag{4.28}$$

The above metric is written in the Schwarzschild gauge. The Hawking temperature and thermal entropy of the black hole in JT gravity are given by $T_H = \beta^{-1} = \frac{r_+}{2\pi l^2}$ and $S_{BH} = \frac{r_+}{4G_N l}$.

We now consider that, the black hole geometry described by the above metric is coupled to non-gravitational thermal bath. Furthermore, we also assume that, the full spacetime is filled with two dimensional conformal field. This method of connecting thermal baths to an eternal AdS black hole ensures the implementation of absorbing boundary conditions for the outgoing Hawking radiation [266, 229, 267].

To proceed further we now represent the above black hole metric in Kruskal coordinates. Therefore the black hole metric in Kruskal coordinates reads (inside the AdS spacetime reads)

$$ds^2_{JT} = -F^2(r)dudv \;\; ; \;\; F^2(r) = -\frac{f(r)}{\kappa^2 uv} \;\; . \tag{4.29}$$

We would like to mention that, the above metric is valid only in the graviatational region. Additionally, we assume that the influence of the curved spacetime governed by JT gravity diminishes at a specific hypothetical cut-off distance, denoted as $r_{R(L)} = \xi$, which lies within the AdS boundary , depicted by the vertical lines in Fig.(4.2) and Fig.(5.4). Beyond this point, the spacetime can be treated as flat, aligning with the description of the non-gravitational thermal baths. This assumption helps in defining a clear boundary between the curved AdS spacetime and the flat bath regions, simplifying the analysis of the system. The metric corresponds to the flat bath region can be obtained by following the approach given in [236] and [256]. To ensure that the metrics associated with the thermal baths and the JT gravity spacetime are smoothly connected at the cut-off boundary $r_{R(L)} = \xi$, we extend the Kruskal coordinates into the bath regions. This extension is

achieved by imposing the normalization condition on the tortoise coordinate, specifically requiring that $\lim_{r\to\infty} r^*(r) = 0$. These conditions allow us to express the bath metric as follows [256]

$$ds^2_{Bath} = -F^2(\xi, r)dudv \ ; \ F^2(\xi, r) = -\frac{f(\xi)}{\kappa^2 uv} \tag{4.30}$$

where $\xi = \alpha r_+$ and $\alpha \gg 1$. Before we proceed further we specify the Kruskal coordinates. For the right wedge (RW), this reads

$$\begin{aligned} u &= -e^{-\kappa(t-r^*(r))} \\ v &= e^{\kappa(t+r^*(r))} \end{aligned} \tag{4.31}$$

and for the left wedge (LW) reads

$$\begin{aligned} u &= e^{\kappa(t+r^*(r))} \\ v &= -e^{-\kappa(t-r^*(r))} \end{aligned} \tag{4.32}$$

where $\kappa = \frac{r_+}{l^2}$ is the surface gravity.

4.5.2 Before Page time scenario: role of $I(R_+ : R_-)$

In this section we focus on the before Page time scenario, that is, $t_{obs} < t_P$. As we have already discussed that, before Page time there is no paradox. In this time domain Hawking saddel point dominates and therefore the fine grained entropy of radiation can be computed by computing the von Neumann entropy of the matter fields loacted on $R = R_+ \cup R_-$. This is depicted in the Fig.(4.2), given below. As there is no paradox appears in this time domain, we can neglect the contribution of island to the von Neumann entropy of Hawking radiatiion. Therefore eq.(4.25) suggests that, $S(R) = S_{vN}(R)$. The region outside the black hole is consists of two disjoint regions labeled by R_+ and R_- (where the $\pm$ signifies the right and left wedges of the Pensrose-Carter diagram in Fig.(4.25)). The region $R_\pm$ are extended to spatial infinity from the inner boundary $b_\pm = (\pm t_b, b)$. Furthermore, we introduce the end points $e_\pm$ in order to regularize it, that is, $e_\pm = (0, e)$. We will eventually take $e \to \infty$. This has been shown graphically in the Penrose diagram given in Fig.(4.2). In this set up, the fine-grained entropy of radiation reads

$$S_{vN}(R) = S_{vN}(R_+ \cup R_-) \ , \ R = R_+ \cup R_- \ . \tag{4.33}$$

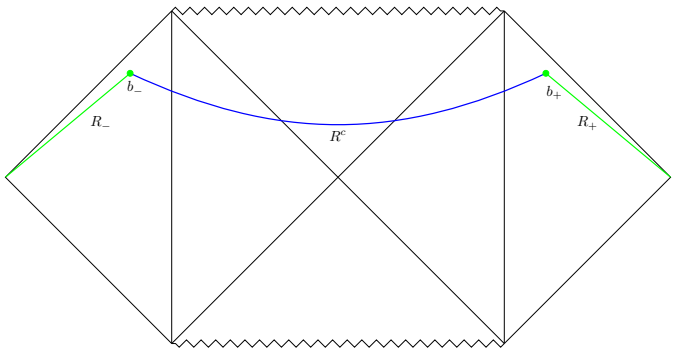

Figure 4.2: The above figure represents the Penrose diagram of eternal black hole in JT gravity attached with the flat auxiliary thermal bath. The $R_\pm$ regions have been shown in green with the inner boundaries $b_\pm = (\pm t_b, b)$.

Additionally, since the state of matter across the entire Cauchy slice is in a pure state, we can express $S_{vN}(R)$ as follows

$$S_{vN}(R_+ \cup R_-) \quad = \quad S_{vN}(R^c) \tag{4.34}$$

where R^c is the complement region of $R = R_+ \cup R_-$. Therefore, to calculate the entanglement entropy of the matter fields (specifically, a free $2D$ conformal field theory) on region $R = R_+ \cup R_-$, we have to calculate the following

$$S_{vN}(R^c) = \left(\frac{c}{3}\right) \log d(b_+, b_-) \ . \tag{4.35}$$

The distance $d(b_+, b_-)$, given in the above expression can be computed explicitly from the metric given in eq.(4.30) as the points $b_\pm$ lie in the non gravitational sector. The expression of $d(b_+, b_-)$ reads

$$d(b_+, b_-) = 2F(\xi, b) e^{\kappa r^*(b)} \cosh(\kappa t_b) \ . \tag{4.36}$$

Now to compute the EE of Hawking radiation we have to use the above result in eq.(4.35). This results the following expression

$$\begin{aligned} S_{vN}(R) &= S_{vN}(R_+ \cup R_-) \\ &= \left(\frac{c}{3}\right) \log \left[\left(\frac{\beta}{2\pi}\right) \sqrt{f(\xi)} \cosh\left(\frac{2\pi t_b}{\beta}\right) \right] \ . \end{aligned} \tag{4.37}$$

The result suggests that, at the early times ($t_b \ll \beta$), the von Neumann entropy of Hawking radiation $S(R) = S_{vN}(R_+ \cup R_-)$ reduces to the following form

$$S_{vN}(R) \approx \left(\frac{c}{3}\right) \log\left[\left(\frac{\beta}{2\pi}\right)\sqrt{f(\xi)}\right] + \left(\frac{c}{6}\right)\left(\frac{2\pi t_b}{\beta}\right)^2 . \tag{4.38}$$

However, on the other hand, at late times ($t_P > t_b \gg \beta$), where t_P is the Page time, we obtain the following form of $S_{vN}(R_+ \cup R_-)$

$$S_{vN}(R) \approx \left(\frac{c}{3}\right) \log\left[\left(\frac{\beta}{2\pi}\right)\sqrt{f(\xi)}\right] + \left(\frac{c}{3}\right)\left(\frac{2\pi t_b}{\beta}\right). \tag{4.39}$$

Now we would like to make few comments on the above analysis. It is to be noted that, as long as the Hawking saddel point dominates, there is no contribution of island to the EE of Hawking radiation, the entropy of radiation $S(R)$ increases in both early and late times, with respect to the observer's time t_b. In particular in the early times it increases quadritically with observer's time, that is $S(R) \sim t_b^2$. On the other hand, in the late times, it increases linearly, that is, $S(R) \sim t_b$. This observation firmly agrees with the one shown in [268].

Further, we can calculate the von Neumann entropy of matter fields on the individual intervals R_+ and R_-. This can computed by the following expressions

$$\begin{aligned} S_{vN}(R_+) &= \left(\frac{c}{3}\right) \log d(b_+, e_+) \\ S_{vN}(R_-) &= \left(\frac{c}{3}\right) \log d(b_-, e_-) . \end{aligned} \tag{4.40}$$

To compute the distances mentioned in the above result we have to use the flat metric given in eq.(4.30). The expressions of $d(b_+, e_+)$ and $d(b_-, e_-)$ read

$$\begin{aligned} d(b_+, e_+) &= \sqrt{2F(\xi, b)F(\xi, e)e^{\kappa r^*(b)}[\cosh(\kappa r^*(b)) - \cosh(\kappa t_b)]} \\ &= d(b_-, e_-) . \end{aligned} \tag{4.41}$$

Now we substitute the above result in eq.(4.40). This yields

$$S_{vN}(R_+) = S_{vN}(R_-) = \left(\frac{c}{6}\right) \log\left[2\left(\frac{\beta}{2\pi}\right)^2 f(\xi)\left\{|\cosh\left(\frac{2\pi r^*(b)}{\beta}\right) - \cosh\left(\frac{2\pi t_b}{\beta}\right)|\right\}\right] . \tag{4.42}$$

Keeping this results in mind we now proceed to compute the the mutual information between the matter fields located on the intervals R_+ and R_-, $(I(R_+ : R_-))$. We can compute this mutual information $I(R_+ : R_-)$ with the help of eq.(4.37) and eq.(4.42). Therefore, the mutual information between R_+ and R_- reads

$$\begin{aligned} I(R_+ : R_-) &= S_{vN}(R_+) + S_{vN}(R_-) - S_{vN}(R_+ \cup R_-) \\ &= \left(\frac{c}{3}\right) \log \left[\left(\frac{\beta}{2\pi}\right) \sqrt{f(\xi)} \left\{ \frac{|\cosh\left(\frac{2\pi r^*(b)}{\beta}\right) - \cosh\left(\frac{2\pi t_b}{\beta}\right)|}{\cosh\left(\frac{2\pi t_b}{\beta}\right)} \right\} \right] . \end{aligned} \tag{4.43}$$

Keeping this result of $I(R_+ : R_-)$ in mind, we now move on to look at how $I(R_+ : R_-)$ behaves in both early $(t_b \ll \beta)$ and late time $(t_b \gg \beta)$.

Now, at the early time doamin $(t_b \ll \beta)$, we find that the expression of $I(R_+ : R_-)$ reduces to following form

$$\begin{aligned} I(R_+ : R_-) &\approx \left(\frac{c}{3}\right) \left[\log \left[\left(\frac{\beta}{2\pi}\right) \sqrt{f(\xi)} \cosh\left(\frac{2\pi r^*(b)}{\beta}\right) \right] - \operatorname{sech}\left(\frac{2\pi r^*(b)}{\beta}\right) \right. \\ &- \left. \left(\frac{2\pi^2}{\beta^2}\right) \left\{ 1 + \operatorname{sech}\left(\frac{2\pi r^*(b)}{\beta}\right) \right\} t_b^2 \right] . \end{aligned} \tag{4.44}$$

The above expression suggests that, at the early time doamin $I(R_+ : R_-)$ decreases with the time-scaling $\sim t_b^2$. However, at the late times $(t_b \gg \beta)$, we obtain the following result of the mutual information

$$I(R_+ : R_-) \approx \left(\frac{c}{3}\right) \left[\log \left[\left(\frac{\beta}{2\pi}\right) \sqrt{f(\xi)} \right] - 2\cosh\left(\frac{2\pi r^*(b)}{\beta}\right) e^{-\left(\frac{2\pi t_b}{\beta}\right)} \right] . \tag{4.45}$$

It is to be noted that, at late times $(t_b \gg \beta)$, $I(R_+ : R_-)$ increases with respect to the observer's time t_b. It is also interesting to observe the fact that, at $t_b = 0$ the mutual information between R_+ and R_- is nonzero. In particular, we find that, $I(R_+ : R_-)|_{t_b=0} \approx 1.17$, for $l = 10r_+, b \sim \alpha = 15r_+$ and $r_+ = 10$. This implies that, at the very beginning of evaporation, the mutual information between R_+ and R_- is non-zero and the associated radiation entanglement wedge $(R_+ \cup R_-)$ is in connected phase.

Interestingly, one can note by looking at eq.(4.44) that there exists a particular value of t_b at which the mutual information will be zero and the entanglement wedge $R_+ \cup R_-$ will be disconnected[3]. With this observation in mind, we give the following proposal [176].

Proposal I: *Starting from a finite, non-zero value (at $t_b = 0$), the mutual information between R_+ and R_- vanishes at a particular value of the observer's time ($t_b = t_R$).*

The above proposal suggests that, we can find the explicit form of t_R by using the expression of mutual information given in eq.(4.43). According to the above proposal we have to solve the following equation to find the form of t_R

$$I(R_+ : R_-)|_{t_b=t_R} \;=\; 0 \; . \tag{4.46}$$

Now by solving the above equation we get the following form of t_R

$$t_R = \left(\frac{\beta}{2\pi}\right) \cosh^{-1}\left\{\left(\frac{\frac{\beta}{2\pi}\sqrt{f(\xi)}}{1+\frac{\beta}{2\pi}\sqrt{f(\xi)}}\right)\cosh\left(\frac{2\pi r^*(b)}{\beta}\right)\right\}. \tag{4.47}$$

We would like to mention that, this particular value of observer's time $t_b = t_R$ is much smaller than the time scale $t_b = \beta$. This in turn means that, this particular time-scale $t_b = t_R$ is in the early time domain as $t_R \ll \beta$. Before proceeding further, we now find the expression of $S_{vN}(R_+ \cup R_-)$ at $t_b = t_R$. To do this we have to substitute the above result in eq.(4.37). This yields

$$\begin{aligned} S_{vN}^{t_b=t_R}(R_+ \cup R_-) \;&=\; \frac{c}{3}\log\left[\frac{\left(\frac{\beta\sqrt{f(\xi)}}{2\pi}\right)^2}{1+\frac{\beta\sqrt{f(\xi)}}{2\pi}}\cosh\left(\frac{2\pi r^*(b)}{\beta}\right)\right] \\ &\approx\; \frac{c}{3}\log\left[\frac{\beta}{2\pi}\sqrt{f(\xi)}\right] + \frac{c}{6}\left(\frac{r_+}{b}\right)^2 \; . \end{aligned} \tag{4.48}$$

To get the above result we have used the fact that $\frac{\beta\sqrt{f(\xi)}}{2\pi} \gg 1$ and $b \gg r_+$.

Now we would like to make few remarks. We have found that the mutual information between the matter field localised on R_+ and R_-, that is $I(R_+ : R_-)$ starts from a maximum value at the

[3]As we know mutual information between two subsystems, namely, A and B satisfies the non-negative property, that is, $I(A : B) \geq 0$. This means zero is the lowest possible value mutual information can have where the correlation between A and B vanishes.

begining of the evaporation process, then in the time domain $0 \leq t_b < t_R$, $I(R_+ : R_-)$ decreases with observer's time. This implies that, the entanglement wedge associated to $R_+ \cup R_-$ is in the connected phase during this time interval $0 \leq t_b < t_R$. Then at $t_b = t_R$, the mutual information between R_+ and R_- ($I(R_+ : R_-)$) vanishes excatly and the entanglement wedge of $R_+ \cup R_-$ moves to the disconnected phase. Once again it is to be noted that $t_R \ll \beta$. These findings strongly suggest that, this particular value of observer's time $t_b = t_R$ is nothing but the Hartman-Maldacena time t_{HM}. This observation agrees with the one given in [269]. Furthermore, the expression of $I(R_+ : R_-)$ at $t_b = \beta$ (by substituting $t_b = \beta$ in eq.(4.43)), reads

$$I(R_+ : R_-) \quad = \quad \left(\frac{c}{3}\right) \log \left[\left(\frac{\beta}{2\pi}\right) \sqrt{f(\xi)} \cosh \left(\frac{2\pi r^*(b)}{\beta}\right)\right] \ . \tag{4.49}$$

The above result suggests that, the mutual correlation between R_+ and R_- starts to increase after $t_b = t_R$. This can be observed from eq.(4.43).

4.5.3 After Page time scenario: probing the role of $I(B_+ : B_-)$

In this section we focus on the after Page time scenario, that is, $t_{obs} > t_P$. In this time domain replica wormhole saddel point dominates in the gravitational path integral. As we have mentioned earlier, just after the Page time, island statrs contribute to the von Neumann entropy of Hawking radiation. Thus to compute the von Neumann entropy of radiation after the Page time we have to apply the formula given in eq.((4.25)). It can be observed that, the trem $S_{vN}(I \cup R)$ (in eq.((4.25))) can be written as $S_{vN}(I \cup R_+ \cup R_-) = S_{vN}(B_+ \cup B_-)$. The regions of $B_\pm$ are indetified as $(b_\pm \to a_\pm)$ where $a_\pm = (\pm t_a, a)$ are the boundaries of the island. This we can represent graphically with the help of a Penrose diagram, as given in Figure (4.3). Now as we have mentioned earlier that, . This in turn means that the expression associated to $S_{vN}(B_+ \cup B_-)$ can be evaluated by utilizing the following formula [50]

$$S_{vN}(B_+ \cup B_-) = \left(\frac{c}{3}\right) \log \left[\frac{d(a_+, a_-) d(b_+, b_-) d(a_+, b_+) d(a_-, b_-)}{d(a_+, b_-) d(a_-, b_+)}\right] \ . \tag{4.50}$$

To compute the explict form of $S_{vN}(B_+ \cup B_-)$ we need to substitute the expression of different distances in the above equation. These distances can be obtained from the black hole metric (given

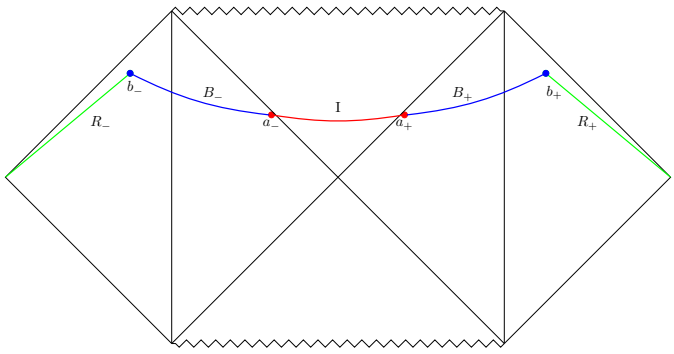

Figure 4.3: Penrose diagram with the island region (depicted by red line) with the boundary $a_\pm = (\pm t_a, a)$, along with the $B_\pm$ regions (in blue). The inner boundaries of the $B_\pm$ regions coincide with $a_\pm = (\pm t_a, a)$, while the outer boundaries are located at $b_\pm = (\pm t_b, b)$.

in eq.(4.29)) and bath metric (given in eq.(4.30)) written in Kruskal coordinates. It can be shown that for the eternal black hole in JT gravity, the expression of $S_{vN}(B_+ \cup B_-)$ can be written as

$$\begin{aligned} S_{vN}(B_+ \cup B_-) &= S_{vN}(B_+) + S_{vN}(B_-) \\ &\quad + \sim \mathcal{O}(e^{-\frac{2\pi t_a}{\beta}}) + \sim \mathcal{O}(e^{-\frac{2\pi t_b}{\beta}}) \end{aligned} \tag{4.51}$$

where the expression of $S_{vN}(B_\pm)$ is given by

$$S_{vN}(B_\pm) = \frac{c}{3}\log(d(b_\pm, a_\pm)) \ . \tag{4.52}$$

However, in recent works in this direction, it is shown that at the late times ($t_a, t_b \gg \beta$), one can make the following approximation [247, 270]

$$S_{vN}(B_+ \cup B_-) \approx S_{vN}(B_+) + S_{vN}(B_-) \ . \tag{4.53}$$

In obtaining the above result one ignores the trems $\mathcal{O}(e^{-\frac{2\pi t_{a,b}}{\beta}})$. Now substituting the above approximated result of $S_{vN}(B_+ \cup B_-)$ in eq.(4.25) with the correct *area term* and then performing the extremization with respect to island parameter, we get time-independent expression of $S(R)$, that is $S(R) = 2S_{BH} + ..$ (for a two-sided eternal black hole).

It is to be noted that the above late-time approximation (given in eq.(4.53)) indirectly gives the hint of vanishing mutual correlation (only in the leading order) between B_+ and B_-. Keeping this in mind, we give our *after Page time proposal* [175]. This reads

Proposal II: *The mutual information between the subsystems B_+ and B_- vanishes once the island*

starts to contribute.

According to our proposal, we have

$$\begin{aligned} I(B_+ : B_-) &= 0 \\ S_{vN}(B_+) + S_{vN}(B_-) &= S_{vN}(B_+ \cup B_-) \ . \end{aligned} \tag{4.54}$$

Now using results given in eq.(4.50) and eq.(4.52) in the above result we have the following relation involving the distances

$$d(a_-, b_+)d(a_+, b_-) = d(a_+, a_-)d(b_+, b_-) \ . \tag{4.55}$$

Substituting this condition in $S_{vN}(R_+ \cup R_-)$ gives

$$S_{vN}(B_+ \cup B_-) = \frac{c}{3}\log(d(a_+, b_+)d(a_-, b_-)) \ . \tag{4.56}$$

By utilizing the gravitational metric provided in eq.(4.28) and the flat metric given in eq.(4.30), we have the following explicit expressions

$$d(a_\pm, b_\pm) = \sqrt{2F(a)F(\xi, b)e^{\kappa(r^*(b)+r^*(a))}}\Big[\cosh[\kappa(r^*(a) - r^*(b))] - \cosh[\kappa(t_a - t_b)]\Big]^{\frac{1}{2}} \tag{4.57}$$

$$d(a_\pm, b_\mp) = \sqrt{2F(a)F(\xi, b)e^{\kappa(r^*(b)+r^*(a))}}\Big[\cosh[\kappa(r^*(a) - r^*(b))] + \cosh[\kappa(t_a + t_b)]\Big]^{\frac{1}{2}} \tag{4.58}$$

$$d(b_+, b_-) = 2F(\xi, b)e^{\kappa r^*(b)}\cosh(\kappa t_b) \tag{4.59}$$

$$d(a_+, a_-) = 2F(a)e^{\kappa r^*(a)}\cosh(\kappa t_a) \ . \tag{4.60}$$

By plugging the expressions above into eq.(4.55)

$$t_a - t_b = |r^*(a) - r^*(b)| \ . \tag{4.61}$$

Now substituting the expression of $d(a_\pm, b_\pm)$ given in eq.(4.57) and using the above condition in eq.(4.56) we have following result of $S_{vN}(B_+ \cup B_-)$

$$S_{vN}(B_+ \cup B_-) = \frac{c}{3}\log\left[\left(\frac{\beta}{\pi}\right)\sqrt{(\alpha^2 - 1)(a^2 - r_+^2)}\right] \ . \tag{4.62}$$

The most remarkable aspect of the expression above is that it does not depend on time. Now, if we insert the expression above into eq.(4.25) along with the area term, $\frac{\text{Area}(\partial I)}{4G_N} = 2 \times \frac{a}{4G_N l}$ and then extremizing it with respect to the island parameter "a", we obtain

$$a = r_+ + \left(\frac{2cG_N l}{3}\right)^2 \frac{1}{8r_+} + \ldots \ . \tag{4.63}$$

Inserting the extremized value of "a" from above in eq.(4.62) yields the final expression for the fine-grained entropy of Hawking radiation. This results

$$S_{vN}(R) = 2S_{BH} - \frac{2c}{3}\log\left(\frac{S_{BH}}{\sqrt{\alpha}}\right) + \frac{\left(\frac{c}{2}\right)^2}{2S_{BH}} + \frac{\left(\frac{c}{3}\right)^3}{32S_{BH}^2} + ... \tag{4.64}$$

to get the above result we have used the fact that $\frac{c}{3}\ln\left(\sqrt{\alpha^2-1}\right) \approx -\frac{2c}{3}\ln\left(\alpha^{-\frac{1}{2}}\right)$, since α is large compared to 1. The result above for the fine-grained entropy of Hawking radiation is time independent, which is necessary to achieve the correct Page curve in the post Page time scenario. Additionally, it should be observed that the result above includes logarithmic and inverse power-law correction terms [175]. Now substituting the extremised value of the island parameter "a" (given by eq.(4.63)) in eq.(4.61), we get

$$t_a - t_b = \left(\frac{\beta}{2\pi}\right)\log\left(S_{BH}\right) = t_{Scr} \tag{4.65}$$

where t_{Scr} is the *Scrambling time*[271, 272]. On the other hand, the explicit expression of the Page time is found to be

$$t_p = \left(\frac{3\beta}{\pi c}\right)S_{BH} - \left(\frac{\beta}{\pi}\right)\log\left(S_{BH}\right) + \left(\frac{3c}{8}\right)\frac{\beta}{2\pi S_{BH}} + ... \ . \tag{4.66}$$

In the above expression, the leading piece is the familiar form of the Page time, where the rest represent the sub-leading corrections to it.

We now provide a holographic interpretation of the above proposal. We suggest that shortly after the Page time, when the replica wormhole saddle points begin to dominate over the Hawking saddle point (which gives $S(R) \sim t_b$), the entanglement wedge associated with $B_+ \cup B_-$ makes a phase transition from connected to disconnected phase [4, 38, 114], which yields $I(B_+ : B_-) = 0$. The striking observation highlighted above indicates that shortly after the Page time t_P, the replica wormhole saddle points begin to dominate. This dominance coincides with the emergence of an island in the black hole interior, leading to the disconnected phase of the entanglement wedge $B_+ \cup B_-$.

4.6 Conclusions

We now present an overview of our results. In this work, we provide two proposals to investigate the importance of mutual information in obtaining the Page curve. The first proposal focuses on the pre-Page time domain. In this time domain, the Hawking saddle point dominates, resulting in $S_{vN}(R) \sim t_b$ in the late-time approximation, where $t_b \gg \beta$. Conversely, in the early-time regime ($t_b \ll \beta$), the von-Neumann entropy of radiation evolves as $S_{vN}(R) \sim t_b^2$. Keeping this result of $S_{vN}(R)$ in hand, we move on to compute the von Neumann entropy of matter fields on the individual regions R_+ and R_-. Based upon the obtained results of $S_{vN}(R_+)$, $S_{vN}(R_-)$ and $S_{vN}(R_+ \cup R_+)$, we compute the mutual information ($I(R_+ : R_-)$) between these two individual regions. Next we proceed to analyze how the mutual information, $I(R_+ : R_-)$ behaves in both early and late times. Inspired by this insight, we suggest that at a specific value of observer's time, that is, $t_b = t_R$, the mutual correlation between the matter fields on R_+ and R_- disappears, indicating the fact that, the corresponding entanglement wedge $R_+ \cup R_-$ becomes disconnected. Additionally, we observe that $t_R \ll \beta$, that is, this time lies in the early time domain and that the von Neumann entropy $S_{vN}(R)|_{t_b=t_R} \sim \log \beta$. These observations suggests that t_R is nothing but the Hartman-Maldacena time t_{HM}. On the other hand, it is also observed that after $t_b = t_R$, $I(R_+ : R_-)$ starts to increase which implies, the entanglement wedge of $R_+ \cup R_-$ is in the connected phase.

We now make few comments about the second proposal, which is given for the after Page time scenario. In this case, the replica wormholes emerge as the dominant saddle points, and the island appears within the interior of the black hole. The recent studies indicate that, one needs to incorporate the late-time approximation for $S_{vN}(B_+ \cup B_-)$ to derive the correct Page curve, which in turn leads to the extremization condition $t_a \approx t_b$ [247]. Motivated by this we propose that just after the Page time when island starts to contribute to the fine-grained entropy radiation, the entnaglement wedge associated with $B_+ \cup B_-$ becomes disconnected. In other words once the island starts to dominate, the mutual information between B_+ and B_- vanishes. This proposal suggests that the mutual information between B_+ and B_- vanishes when $t_a - t_b = t_{Scr}$ where t_{Scr} is the *Scrambling time* [271, 272]. According to the proposal, as long as $t_a - t_b < t_{Scr}$, the entanglement wedge of $B_+ \cup B_-$ is in connected phase and once the condition $t_a - t_b = t_{Scr}$ is satisfied, the entanglement wedge of $B_+ \cup B_-$ gets disconnected. We also find that this condition

of vanishing mutual information leads to a time-independent expression of $S_{vN}(I \cup R)$ and we also find the final expression of $S_{vN}(R)$ contains universal corrections (logarithmic and inverse power law corrections). This in turn means that our proposals and observations related to mutual information gives strong realization of the concept given in [269, 273].

To conclude, we propose that in the before Page time scenario, there is a particular time-scale at which the radiation $(R_+ \cup R_-)$ entanglement wedge makes transition from connected to disconnected phase and in the after page time scenario, there is a time-scale at which the black hole $(B_+ \cup B_-)$ entanglement wedge makes the same transition. Furthermore, the above observations can also be extended to higher dimensional scenarios with s-wave approximation in the conformal field theory matter sector [274, 266].

Chapter 5

Mutual information of subsystems and the Page curve for Schwarzschild de-Sitter black hole

In this work [1], we show that the two proposals related to the mutual information of matter fields can be formulated for an eternal Schwarzschild black hole in de Sitter spacetime. These proposals also illustrate the status of the associated entanglement wedges and their role in obtaining the correct Page curve of radiation.The first proposal is formulated for the pre-Page time domain, which states that the mutual information between R_H^+ and R_H^-, that is, $I(R_H^+ : R_H^-)$ vanishes at a specific value of the observer's time $t_{b_H} = t_H$ (where $t_H \ll \beta_H$). We argue that this corresponds to the Hartman-Maldacena time, at which the entanglement wedge associated to $R_H^+ \cup R_H^-$ gets disconnected and the fine-grained radiation entropy has the form $S(R_H) \sim \log(\beta_H)$. On the other hand, the second proposal states that just after the Page time, when replica wormholes saddle points dominant , the mutual information between B_H^+ and B_H^-,that is, $I(B_H^+ : B_H^-)$ vanishes as the time difference $t_{a_H} - t_{b_H}$ equals the scrambling time. Holographically, this proposal indicates the fact that, the entanglement wedge associated to $B_H^+ \cup B_H^-$ gets disconnected at this particular time-scale. Furthermore, these two proposals guide us to the correct time evolution of the fine-grained entropy of radiation, as depicted by the Page curve. We have also demonstrated that

[1] This work is based on [177].

similar observations hold for the radiation associated with the cosmological horizon.

Hawking radiation is one of the most intriguing and enigmatic phenomena in theoretical physics, arising from pair production occurring in the near-horizon region of a black hole[213].This phenomenon has attracted considerable interest in modern theoretical physics. As a quantum mechanical effect, its presence provides key insights into the microscopic foundations of general relativity. This motivation has led to probing its quantum mechanical aspects, by computing the von Neumann entropy of radiation [2]. However, the study of the von Neumann entropy of Hawking radiation has, in turn, revealed a paradox. The paradox can be formulated as follows.

It has been observed that the formation of a black hole, resulting from the gravitational collapse of a massive shell, corresponds to a pure state. This implies that, at the begining of the evaporation process the von Neumann entropy of radiation is zero. Additionally, according to the principle of unitary evolution, the final state at the end of the evaporation process must also be a pure state. This implies that the von Neumann entropy must return to zero at the completion of the evaporation process. However, Hawking's semiclassical analysis showed that for an evaporating black hole, the von Neumann entropy of Hawking radiation monotonically increases with the observer's time [275], and it does not vanish even after the black hole has completely evaporated.

The paradox can also be understood in terms of the Page curve [215], which describes the time evolution of the von Neumann entropy of radiation. It is suggested that a black hole forms from the collapse of a massive shell initially in a pure state. Consequently, the entanglement entropy (or fine-grained entropy) of the radiation[2] is initially zero. On the other hand, at the onset of evaporation, the thermodynamic entropy (also known as coarse-grained entropy [223, 224, 225]) is at its maximum since no radiation is present at the beginning. As time progresses, the fine-grained entropy of the radiation increases, while the thermal entropy of the black hole decreases due to the shrinking event horizon. Importantly, after a specific time known as the Page time, the fine-grained entropy of radiation surpasses the black hole's thermal entropy, leading to a paradoxical situation where $S_{vN}(R) > S_{BH}$. This situation appears self-contradictory, as the definition of coarse-grained entropy implies that it is obtained by maximizing the fine-grained entropy over all possible states. This observation thus provides an entropic perspective on understanding the paradox.

[2]Notably, the entanglement entropy of the radiation corresponds to the von Neumann entropy of the matter fields confined to the region R outside the black hole.

A fundamental question concerns the correct time evolution of the von Neumann entropy of Hawking radiation. This was effectively addressed by the so-called *Page curve*, which proposes that, to maintain unitarity, the von Neumann entropy of the radiation should initially be zero, grow monotonically until the *Page time*, and then decline back to zero, signaling the completion of the evaporation process [226, 227]. The contradiction arises only after the Page time, as beyond this point, one typically finds $S_{vN}(R) > S_{BH}$.

Several approaches have been proposed to address this problem while ensuring the unitary evolution of radiation [228, 229, 230, 231]. Recently, the idea of entanglement wedge reconstruction from Hawking radiation has proposed that certain regions in the interior of a black hole may be responsible for the fine-grained entropy of that radiation [218, 217, 219, 236].These auxiliary regions are referred to as *islands*, while the surfaces at their boundaries are known as *quantum extremal surfaces* (QES) [235, 238, 239, 240]. It is to be mentioned that the quantum extremal surfaces are the quantum corrected classical extremal surfaces [237, 232].The fine-grained entropy of Hawking radiation, in the presence of an island within the black hole interior, is determined by

$$S(R) = \min \underset{\text{I}}{\text{ext}} \left\{ \frac{\text{Area}(\partial I)}{4G_N} + S_{vN}(I \cup R) \right\} . \tag{5.1}$$

From a semi-classical perspective, islands originate from the replica wormhole saddle points of the gravitational path integral, imposed by appropriate boundary conditions. These saddle points arise as a consequence of applying the replica method in a dynamical gravitational background [241, 242, 243, 244]. This remarkable observation has led to the emergence of the island formulation as a crucial framework for further investigation [245, 246, 247, 248, 249, 250, 251, 252, 253, 276, 277, 254, 278, 255, 256, 257, 258, 279, 259, 260, 280, 281, 282, 283].

It is important to note that while most of the aforementioned studies focus on black holes in asymptotically flat or AdS spacetimes, but recent findings suggest that our universe is de Sitter in nature. Therefore, it is natural to explore the impact of a positive cosmological constant in the context of the information paradox. With this motivation, we consider the eternal Schwarzschild-de Sitter (SdS) spacetime as the black hole background in this work. Since these black holes are formed during the early inflationary stage of our universe, the information paradox for Schwarzschild-de Sitter black holes becomes a crucial issue to investigate. It also serves as an ideal toy model for studying the global structure of isolated black holes in our universe, considering the current

phase of accelerated expansion. De-Sitter space contains causally separated areas, resembling the situation observed with black holes.As a result, an observer can only perceive the parts of the universe contained within their own horizon. Additionally, cosmological event horizons both emit and absorb radiation, known as the Gibbons-Hawking radiation. Generally, the entropy generated by the cosmological horizon depends on the observer, unlike the case with black holes. This arises from uncertainty about what lies beyond the cosmic horizon. In this study, we aim to derive the accurate Page curve for the black hole horizon of the Schwarzschild-de Sitter (SdS) black hole, as well as a Page-like curve for the cosmological horizon of that same spacetime. We shall carry this out while keeping the island formulation in mind. It is worth noting that, in addition to the approach (gravitational framework) we have adopted in this study, there exists an alternative method (gravitational framework) to tackle this entropic paradox, referred to as the doubly holographic setup [284, 285, 286, 287, 288, 289, 290, 291, 292]. Some very interesting works in this set up can be found in [217, 246, 293, 294, 295, 296, 297, 298, 299, 283].

In earlier studies [175, 176] it was highlighted that the mutual information of various subsystems plays a vital role in obtaining the correct Page curve of Hawking radiation. In particular, it is worth mentioning that in [175], pointed out that just after the Page time, the mutual information of matter fields localized on R_+ and R_- intervals vanishes, which ultimately results in a time-independent profile of the fine-grained entropy $S(R)$. Furthermore, in [176], the previous proposal was analyzed in detail, and a new proposal was introduced concerning the saturation of mutual information for various subsystems in the pre-Page time scenario. However, these studies were solely confined to eternal black holes in AdS and asymptotically flat spacetimes. In this work, we will investigate whether these proposals hold for eternal black holes in de Sitter spacetime. However, it is to be noted that, our work does not account for certain subtleties in gravitational theories, such as diffeomorphism invariance, which allows for an arbitrary definition of a subregion. A discussion on this aspect can be found in [300, 301, 302] which shows that it can have important implications to quantum gravity.

5.1 Brief discussion on the Kottler spacetime

In this section we would discuss briefly about the Schwarzschild black hole in de-Sitter spacetime. It is a solution of Einstein's vacuum field equation in the presence of positive cosmological constant in $(3+1)$- spacetime dimensions. This solution is sometimes also denoted as the Kottler solution. The metric of the SdS solution reads [303]

$$\begin{aligned} ds^2 &= -f(r)dt^2 + \frac{dr^2}{f(r)} + r^2(d\theta^2 + \sin^2\theta d\phi^2); \\ f(r) &= 1 - \frac{2M}{r} - \frac{\Lambda r^2}{3} \end{aligned} \tag{5.2}$$

where M is the mass parameter and Λ is the cosmological constant. In terms of the AdS radius the lapse function $(f(r))$ can be written as

$$f(r) = 1 - \frac{2M}{r} - \frac{r^2}{L^2_{\rm AdS}} \quad . \tag{5.3}$$

In the limit $\Lambda \to 0$ (or $L_{\rm AdS} \to \infty$), we can recover the asymptotically flat Schwarzschild spacetime. We now proceed to discuss the horizon structure of the Kottler metric. The horizon structure of SdS spacetime depends on the value of the cosmological constant (Λ). It is to be noted that, there is a critical value of cosmological constant $\Lambda = \Lambda_{crit} = \frac{1}{9M^2}$ beyond which the event horizon no longer exists, and the solution is then referred to as a naked singularity. However, within this range of cosmological constant, $0 < \Lambda < \Lambda_{crit}$ (or $\frac{m}{L_{\rm AdS}} < \frac{1}{3\sqrt{3}}$), there exists three different solutions to $f(r) = 0$. Among these three solutions, only two are physically relevant [303, 304], one of them is termed as the black hole horizon (r_H) and the other one is known as the cosmological horizon (r_c), $r_c > r_H$. Furthermore, it is to be noted that, in the limit $\Lambda \to \Lambda_{crit}$ there is a degenerate horizon [303]. In this chapter, we only consider the range $0 < \Lambda < \Lambda_{crit}$ along with the following form of the lapse function [305]

$$f(r) = \frac{1}{L^2_{\rm AdS} r}(r_H - r)(r - r_c)(r + r_H + r_c) \ . \tag{5.4}$$

The expressions for the black hole horizon (r_H) and cosmological horizon (r_c)(in terms of the mass parameter and the cosmological constant) are given by [304, 306, 307]

$$\begin{aligned} r_H &= \frac{2}{\sqrt{\Lambda}}\cos\left(\frac{\pi}{3}+\frac{\arccos\left(3M\sqrt{\Lambda}\right)}{3}\right) \\ r_c &= \frac{2}{\sqrt{\Lambda}}\cos\left(\frac{\pi}{3}-\frac{\arccos\left(3M\sqrt{\Lambda}\right)}{3}\right) \ . \end{aligned} \tag{5.5}$$

To proceed further, we now express the metric in Kruskal coordinates. Since there are two distinct horizon choices, there exist two different sets of Kruskal coordinates. This arises because the Kruskal coordinate transformations involve the surface gravity, which takes different values for different event horizons. The surface gravity associated to the black hole horizon (r_H) and cosmological horizon (r_c) are denoted by κ_H and κ_c repectively. Keeping this fact in mind, one can express the metric in two alternative forms using the two different Kruskal coordinates. These correspond to the black hole horizon representation and the cosmological horizon representation of the metric.

To express the metric in Kruskal coordinates, we first introduce the light cone corredinates given as follows

$$u = t - r^*(r) \ , \ v = t + r^*(r) \tag{5.6}$$

where $r^*(r)$ is the tortoise coordinate, given as

$$r^*(r) = \alpha_H \ln(|r_H - r|) - \alpha_c \ln(|r - r_c|) + \alpha' \ln(r + r_H + r_c). \tag{5.7}$$

The expressions of α_H, α_c and α' are given by

$$\begin{aligned} \alpha_H &= \frac{L^2_{\rm AdS} r_H}{(r_c - r_H)(2r_H + r_c)} \\ \alpha_c &= \frac{L^2_{\rm AdS} r_c}{(r_c - r_H)(2r_c + r_H)} \\ \alpha' &= \frac{L^2_{\rm AdS}(r_H + r_c)}{(2r_c + r_H)(2r_H + r_c)} \ . \end{aligned} \tag{5.8}$$

We begin by presenting the black hole horizon description of the metric. The Kruskal coordinates for the the right wedge of the black hole horizon are given by

$$\begin{aligned} U_H &= -e^{-\kappa_H (t - r^*(r))} \\ V_H &= e^{\kappa_H (t + r^*(r))} \end{aligned} \tag{5.9}$$

and for the left wedge it read

$$\begin{aligned} U_H &= e^{\kappa_H (t+r^*(r))} \\ V_H &= -e^{-\kappa_H (t-r^*(r))} \end{aligned} \tag{5.10}$$

where the expression of the surface gravity associated with the black horizon (κ_H) is given by

$$\kappa_H = \frac{(r_c - r_H)(2r_H + r_c)}{2L^2_{\rm AdS} r_H} \ . \tag{5.11}$$

Furthermore, we can derive the following expression for the Hawking temperature associated with the black hole horizon

$$T_H = \frac{\kappa_H}{2\pi} = \frac{(r_c - r_H)(2r_H + r_c)}{4\pi L^2_{\rm AdS} r_H} = \frac{1}{\beta_H} \ . \tag{5.12}$$

Furthermore, the expression of surface gravity and the Hawking temperature associated with the black hole horizon in terms of the cosmological constant and the mass parameter read [307]

$$\kappa_H = \sqrt{\Lambda}\left[\frac{1}{4\cos\left(\frac{1}{3}\arccos\left(3M\sqrt{\Lambda}\right)+\frac{\pi}{3}\right)} - \cos\left(\frac{1}{3}\arccos\left(3M\sqrt{\Lambda}\right)+\frac{\pi}{3}\right)\right] \tag{5.13}$$

$$T_H = \frac{\sqrt{\Lambda}}{2\pi}\left[\frac{1}{4\cos\left(\frac{1}{3}\arccos\left(3M\sqrt{\Lambda}\right)+\frac{\pi}{3}\right)} - \cos\left(\frac{1}{3}\arccos\left(3M\sqrt{\Lambda}\right)+\frac{\pi}{3}\right)\right] \ . \tag{5.14}$$

Further, the Bekenstein-Hawking entropy associated with the black hole horizon is given by $S_{BH} = \frac{\pi r_H^2}{G_N}$. Finally, the metric for the black hole patch in terms of the Kruskal coordinates (given in eqs.(5.9,5.10)) reads

$$ds^2 = -F^2(r) dU_H dV_H + r^2 \Omega_2^2 \ ; \ F^2(r) = \frac{f(r)}{\kappa_H^2} e^{-2\kappa_H r^*(r)} \tag{5.15}$$

where the detailed expression of $F(r)$ reads

$$F(r) = \frac{2L_{\rm AdS} r_H}{\sqrt{r}} \frac{|r - r_c|^{\frac{1}{2}(1+\frac{r_c}{r_H}\left(\frac{2r_H+r_c}{2r_c+r_H}\right))} (r + r_c + r_H)^{\frac{1}{2}(1-\frac{r_c^2-r_H^2}{r_H(2r_c+r_H)})}}{(2r_H + r_c)(r_c - r_H)} \ . \tag{5.16}$$

We now proceed to represent the metric in terms of the cosmological horizon. The Kruskal coordinates for the right wedge of the cosmological horizon read

$$\begin{aligned} U_c &= -e^{-\kappa_c (t-r^*(r))} \\ V_c &= e^{\kappa_c (t+r^*(r))} \end{aligned} \tag{5.17}$$

and for the left wedge, it read

$$\begin{aligned} U_c &= e^{\kappa_c(t+r^*(r))} \\ V_c &= -e^{-\kappa_c(t-r^*(r))} \ . \end{aligned} \tag{5.18}$$

The surface gravity (κ_c) and the Hawking temperature (T_c) of the cosmological horizon read

$$\kappa_c = \frac{(r_c - r_H)(2r_c + r_H)}{2L^2_{\rm AdS} r_c} \tag{5.19}$$

$$T_c = \frac{\kappa_c}{2\pi} = \frac{(r_c - r_H)(2r_c + r_H)}{4\pi L^2_{\rm AdS} r_c} = \frac{1}{\beta_c} \ . \tag{5.20}$$

In terms of the cosmological constant and mass parameter the expression of κ_c and T_c are given as [307]

$$\kappa_c = \sqrt{\Lambda}\left[\frac{1}{4\cos\left(\frac{1}{3}\arccos\left(3M\sqrt{\Lambda}\right) - \frac{\pi}{3}\right)} - \cos\left(\frac{1}{3}\arccos\left(3M\sqrt{\Lambda}\right) - \frac{\pi}{3}\right)\right] \tag{5.21}$$

$$T_c = \frac{\sqrt{\Lambda}}{2\pi}\left[\frac{1}{4\cos\left(\frac{1}{3}\arccos\left(3M\sqrt{\Lambda}\right) - \frac{\pi}{3}\right)} - \cos\left(\frac{1}{3}\arccos\left(3M\sqrt{\Lambda}\right) - \frac{\pi}{3}\right)\right] \ . \tag{5.22}$$

Furter, we can describe the cosmological horizon of the metric in terms of the Kruskal coordinates as

$$ds^2 = -G^2(r) dU_c dV_c + r^2 d\Omega_2^2 \ ; \ G^2(r) = \frac{f(r)}{\kappa_c^2} e^{-2\kappa_c r^*(r)} \tag{5.23}$$

where the conformal factor $G(r)$ reads

$$G(r) = \frac{2L_{\rm AdS} r_c}{\sqrt{r}} \frac{|r_H - r|^{\frac{1}{2}\left(1 - \frac{r_H}{r_c}\frac{r_H + 2r_c}{r_c + 2r_H}\right)} (r + r_c + r_H)^{\frac{1}{2}\left(1 + \frac{r_c^2 - r_H^2}{r_c(2r_H + r_c)}\right)}}{(r_c - r_H)(2r_c + r_H)} \ . \tag{5.24}$$

The two alternative descriptions of the Schwarzschild de- Sitter metric can be visualized using Penrose-Carter diagrams, which depict the global causal structure of the spacetime.This is illustrated in Fig.(5.1), where the two physical horizons are indicated, either of which can be used to equivalently describe the spacetime. In this work, our goal is to analyze the Page curve of radiation corresponding to both Hawking radiation and Gibbons-Hawking radiation.This can be achieved by isolating different patches of the spacetime through the introduction of a thermal opaque membrane [308, 309, 310, 311, 312, 313]. These regions are commonly referred to as the black hole

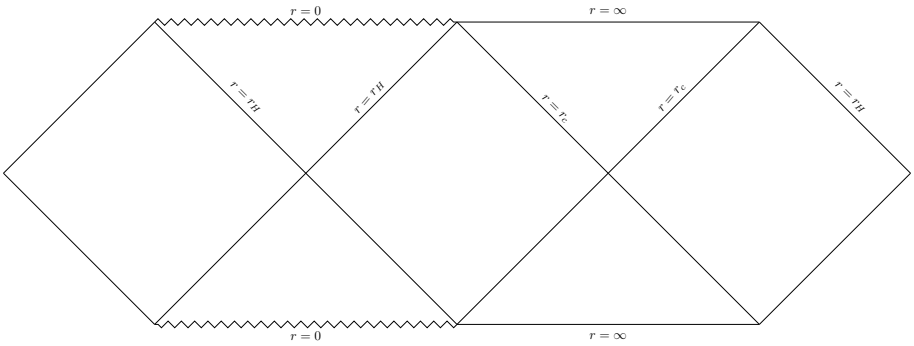

Figure 5.1: The above figure depicts the Penrose-Carter diagram of Schwarzschild de-Sitter spacetime where $r = r_H$ denotes the black hole event horizon and $r = r_c$ represents the cosmological event horizon.

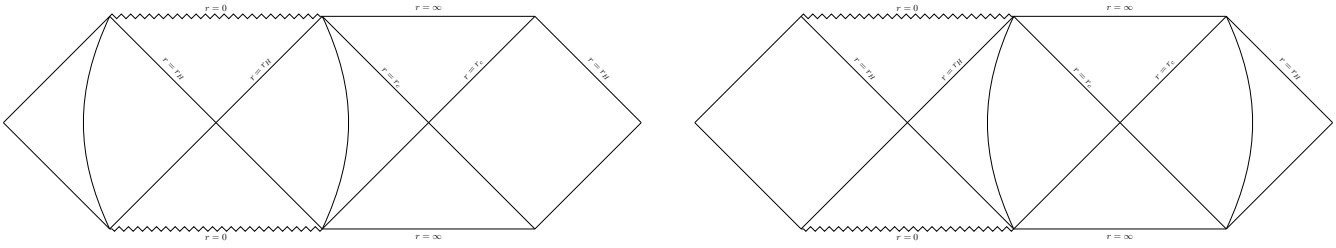

Black hole patch Cosmological patch

Figure 5.2: SAdS spacetime with thermal opaque membrane.

patch and the cosmological patch in the literature. We have shown this in Fig.(5.2). The primary reason for introducing this thermally opaque membrane is that any of these Kruskal coordinates are not capable of removing the coordinate singularities from both the black hole horizon and the cosmological horizon simultaneously. Furthermore, the SdS spacetime has two distinct horizons, namely the back hole horizon and the cosmlogical horizon. These can be regarded as two separate thermodynamic systems, each with its own temperature. Therefore, they are not in thermal equilibrium. For a non-equilibrium system, studying its thermodynamic properties becomes significantly challenging. To simplify the analysis, one must ensure that the system, whether the black hole horizon or the cosmological horizon should be thermal equilibrium. This is achieved by the thermal opaque membrane [308, 309, 310, 311, 312, 313].In a multi-horizon spacetime, a thermal opaque membrane can be used to analyze one horizon while treating the other as a boundary. This concept can be better understood by following the approach presented in [307, 312].

Now we briefly discuss the radial part of Klein-Gordon equation in SdS background. It can be

shown that the radial part of KG equation in SdS spacetime reads [307, 312]

$$\left(-\frac{\partial^2}{\partial t^2}+\frac{\partial^2}{\partial r^{*2}}\right)\psi(r)+V_{eff}(r)\psi(r)=0 \tag{5.25}$$

where V_{eff} is the effective potential which depends on the lapse function. Therefore, the expression of the effective potential reads [307, 312]

$$V_{eff}=\left(1-\frac{2M}{r}-\frac{\Lambda r^2}{3}\right)\left(\frac{l(l+1)}{r^2}+\frac{2M}{r^3}-\frac{\Lambda}{3}\right)\ .$$

It can be shown that the above expression of effective potential vanishes at the both the black hole and cosmological horizon. In [307, 312], it was urged that, this effective potential can be interpreted as the partition between the black hole and cosmological horizons. To visualize this in the Penrose diagram, one can introduce the Kruskal time-like and space-like coordinates for the black hole patch as follows

$$U_H=T_H-R_H\ ,\ V_H=T_H+R_H \tag{5.26}$$

and similarly for the cosmological patch

$$U_c=T_c-R_c\ ,\ V_c=T_c+R_c\ . \tag{5.27}$$

Using the Kruskal time-like and space-like coordinates mentioned above, one can obtain the following. [307]

$$-U_HV_H = R_H^2-T_H^2=e^{2\kappa_H r^*(r)} \tag{5.28}$$

$$-U_cV_c = R_c^2-T_c^2=e^{2\kappa_c r^*(r)}\ . \tag{5.29}$$

The above results indicate that for $r=constant$, a hyperbola (membrane) in the $R_{H(c)}-T_{H(c)}$ plane can be realized in both the black hole and the cosmological patch.

On the other hand, it has been proposed that the analogue of a "defect" in wedge holography corresponds to the "thermal opaque membrane" in a Schwarzschild-de Sitter eternal black hole. Gravity can be considered sufficiently weak at these membranes since they are located far from the black hole/de-Sitter patch. We now proceed to explore the role of mutual information between various subsystems in the Page curve associated with a multi-event horizon black hole spacetime.

5.2 Analysis for the black hole patch

We now proceed to investigate the Page curve of Hawking radiation for the Schwarzschild de-Sitter (SdS) eternal black hole in $(3+1)$ spacetime dimensions. As previously mentioned, to analyze Hawking radiation, we must restrict our study to the black hole patch by introducing a thermal opaque membrane to effectively freeze the cosmological horizon. We will use the metric form given in eq.(5.15), which corresponds to the black hole horizon description of the SdS solution.

Furthermore we assume that, the entire spacetime is filled with conformal matter of central charge c. More specifically, we consider the matter to be a free CFT. Additionally, we will incorporate the s-wave approximation in the conformal matter sector [314, 315, 247]. The reason behind this is that the process of the Hawking radiation is dominated by the s-wave modes. Under this approximation we can neglect the angular part of the metric. So we can compute the entanglement entropy of the Hawking radiation by using the $2d$ CFT formula [50, 49]. Furthermore, the s-wave approximation in the matter sector implies that we can neglect the massive modes of the matter fields. This is justified because the entangling regions are widely separated, effectively reducing the theory of conformal matter fields to a $2d$ conformal field theory.

In this work, our objective is to investigate whether the proposals presented in [175, 176], which are limited to eternal black holes in asymptotically AdS and flat spacetimes, also hold for a spacetime geometry with a positive cosmological constant. In this section, we specifically examine the black hole patch of the Schwarzschild-de Sitter spacetime and investigate whether the results reported in [175, 176] hold in this context.

As mentioned earlier, The black hole patch is equivalent to the Penrose diagram of the flat Schwarzschild black hole embedded in the de Sitter spacetime with cosmological horizons in both sides. We will focus on two scenarios here. Firstly, we will discuss what happens before the Page time (t_H^{Page}), then we will proceed to probe the after Page time scenario. In the before the Page time scenario, we intend to discuss the role of mutual information between R_H^+ and R_H^- (shown in the Penrose diagram Fig.(5.3)) on the Page curve, as there is no island contribution in the entropy of the Hawking radiation in this time domain. However, in the after Page time scenario one has to consider the contribution from the island region which resides in the black hole interior.

5.2.1 Before Page time scenario: the role of $I(R_H^+ : R_H^-)$

In this section, we carry out our analysis in the pre-Page time scenario. As previously mentioned, in the time domain $0 < t_{obs} < t_H^{Page}$, no paradox arises. It is important to note that within this regime, the Hawking saddle point dominates the gravitational path integral. Consequently, in the pre-Page time scenario, there is no contribution from an island to the von Neumann entropy of Hawking radiation. Therefore, for $t_{obs} < t_H^{Page}$, the entanglement entropy of the Hawking radiation is determined by computing the von Neumann entropy of the matter fields in two disjoint intervals, R_H^+ and R_H^-[3]. This leads to the von Neumann entropy of radiation being given by

$$S_{vN}(R_H) = S_{vN}(R_H^+ \cup R_H^-), \tag{5.30}$$

where $R_H = R_H^+ \cup R_H^-$, with the $\pm$ signifying the right and left wedges of the Penrose-Carter diagram, as shown in Fig. (5.3).

We now specify the disjoint regions $R_H^{\pm}$. The endpoints of these regions are given by $[e_H^{\pm} : b_H^{\pm}]$. It is important to note that $R_H^{\pm}$ extends to spatial infinity (up to the thermal opaque membrane) from the inner boundary $b_H^{\pm} = (\pm t_{b_H}, b_H)$. To regularize this, we introduce the point $e_H^{\pm}$, defined as $e_H^{\pm} = (0, e_H)$. Eventually, we take the limit $e_H \to \infty$. This set up can be decribed by the Penrose diagram given in Fig.(5.3). In this configuration, that is, in the absence of an island, the fine-grained entropy of radiation is given by

$$S_{vN}(R_H) = S_{vN}(R_H^+ \cup R_H^-) = S_{vN}(R_H^c) \tag{5.31}$$

where R_H^c denotes the complementary region of $R_H = R_H^+ \cup R_H^-$. In the discussion above, we have assumed that the state on the entire Cauchy slice is a pure state.As mentioned earlier, we consider the matter fields to be $2d$ free conformal matter, which can be obtained using the s-wave approximation. Therefore the expression of fine-grained entropy of Hawking radiation in the absence of island can be computed by the following formula

$$S_{vN}(R_H^c) = \left(\frac{c}{3}\right) \log d(b_H^+, b_H^-) \ . \tag{5.32}$$

We can compute the explicit form of the distance $d(b_H^+, b_H^-)$, appearing in the above expression by using the metric for We can determine the explicit form of the distance $d(b_H^+, b_H^-)$, appearing in

[3]Here "H" stands for the Hawking radiation or black hole radiation

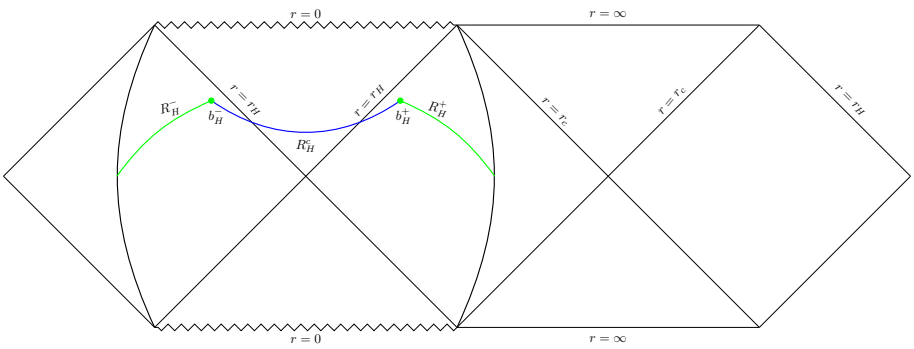

Figure 5.3: Penrose diagram describing the black hole patch of Schwarzschild de-Sitter spacetime with thermal opaque membrane covering the cosmological patch. The $R_H^{\pm}$ regions are shown by green curve with the inner boundary $b_H^{\pm} = (\pm t_{b_H}, b_H)$. On the other hand, the blue line denotes the complementary region of $R_H = R_H^+ \cup R_H^-$.

the above expression, by using the metric describing the black hole patch given in eq.(5.15). This leads to the following result

$$d(b_H^+, b_H^-) = 2F(b_H) e^{\kappa_H r^*(b_H)} \cosh(\kappa_H t_{b_H}) \ . \tag{5.33}$$

Substituting the above expression into eq. (5.32), we obtain the following form for entanglement entropy of Hawking radiation

$$\begin{aligned} S_{vN}(R_H) &= S_{vN}(R_H^+ \cup R_H^-) \\ &= \left(\frac{c}{3}\right) \log\left[\left(\frac{\beta_H}{\pi}\right)\sqrt{f(b_H)}\cosh\left(\frac{2\pi t_{b_H}}{\beta_H}\right)\right]. \end{aligned} \tag{5.34}$$

The above result suggests that in the early time domain, that is in the domain $t_{b_H} \ll \beta_H$, the fin-grained entropy of radiation reduces to the following

$$S_{vN}(R_H) \approx \left(\frac{c}{3}\right) \log\left[\left(\frac{\beta_H}{\pi}\right)\sqrt{f(b_H)}\right] + \left(\frac{c}{6}\right)\left(\frac{2\pi t_{b_H}}{\beta_H}\right)^2 . \tag{5.35}$$

However, at late times ($t_{b_H} \gg \beta_H$), the entropy of the Hawking radiation takes the following form

$$S_{vN}(R_H) \approx \left(\frac{c}{3}\right) \log\left[\left(\frac{\beta_H}{\pi}\right)\sqrt{f(b_H)}\right] + \left(\frac{c}{3}\right)\left(\frac{2\pi t_{b_H}}{\beta_H}\right). \tag{5.36}$$

The above analysis suggests that both in the early and late times the fine-grained entropy of radiation increases with time. Furthermore, it is to be mentioned that, in the above analysis we donot take the contribution of island. However, it can be observed that, the nature of this time

evolution of $S_{vN}(R_H)$ is completely different for these two different time doamins. In particular, in the early time $S_{vN}(R_H)$ shows quadratic behaviour with time, that is $S_{vN}(R_H) \sim t_{b_H}^2$, and in the late time domain it grows linearly in time, that is $S_{vN}(R_H) \sim t_{b_H}$. This observation firmly agrees with the one shown in [268].

Now we proceed to calculate the entanlement entropy of the matter fields localized on the individual regions R_H^+ and R_H^-. This can be computed by using the following result

$$S_{vN}(R_H^{\pm}) = \left(\frac{c}{3}\right) \log d(b_H^{\pm}, e_H^{\pm}) \ . \tag{5.37}$$

To obtain an explicit form of $S_{vN}(R_H^{\pm})$ we have to compute the distance $d(b_H^{\pm}, e_H^{\pm}$ by using the balck hole metric given in eq.(5.15). The expressions of $d(b_H^+, e_H^+)$ and $d(b_H^-, e_H^-)$ read

$$d(b_H^+, e_H^+) = \left[2F(b_H)F(e_H)e^{\kappa_H r^*(b_H)} \left(\cosh(\kappa_H r^*(b_H)) - \cosh(\kappa_H t_{b_H})\right)\right]^{\frac{1}{2}} = d(b_H^-, e_H^-) \ . \tag{5.38}$$

To get the above result we have used the fact that in the limit $e \to \infty$, $r^*(e)$ vanishes, that is, $\text{Limit}_{e\to\infty} r^*(e) = 0$. Therefore, the von-Neumann entropy of matter field localised on the individual regions $R_H^{\pm}$ can be computed by substituting the above expression in eq.(5.37). This results

$$S_{vN}(R_H^{\pm}) = \left(\frac{c}{6}\right) \log \left[2\left(\frac{\beta_H}{2\pi}\right)^2 \sqrt{f(b_H)f(e_H)} \left\{ |\cosh\left(\frac{2\pi r^*(b_H)}{\beta_H}\right) - \cosh\left(\frac{2\pi t_{b_H}}{\beta_H}\right)| \right\}\right] \ . \tag{5.39}$$

Keeping these computed results of fine-grained entropies (given in eq.(5.34) and eq.(5.39)) in mind we now proceed to find the expression of the mutual information (MI) between the matter fields localised on the individual regions R_H^+ and R_H^-. This yields

$$\begin{aligned} I(R_H^+ : R_H^-) &= S_{vN}(R_H^+) + S_{vN}(R_H^-) - S_{vN}(R_H^+ \cup R_H^-) \\ &= \left(\frac{c}{3}\right) \log \left[\left(\frac{\beta_H}{2\pi}\right) \sqrt{f(e_H)} \left\{ \frac{|\cosh\left(\frac{2\pi r^*(b_H)}{\beta_H}\right) - \cosh\left(\frac{2\pi t_{b_H}}{\beta_H}\right)|}{\cosh\left(\frac{2\pi t_{b_H}}{\beta_H}\right)} \right\}\right] \ . \end{aligned} \tag{5.40}$$

To thoroughly understand the behavior of mutual information (MI) in both the early and late time scenarios, we compute its form by considering the appropriate limiting cases. The expression of mutual information in the early time domain ($t_{b_H} \ll \beta_H$), reads

$$\begin{aligned} I(R_H^+ : R_H^-) &\approx \left(\frac{c}{3}\right) \left[\log\left[\left(\frac{\beta_H}{2\pi}\right)\sqrt{f(e_H)}\cosh\left(\frac{2\pi r^*(b_H)}{\beta_H}\right)\right] - \text{sech}\left(\frac{2\pi r^*(b_H)}{\beta_H}\right) \right. \\ &- \left. \left(\frac{2\pi^2}{\beta_H^2}\right)\left\{1 + \text{sech}\left(\frac{2\pi r^*(b_H)}{\beta_H}\right)\right\} t_{b_H}^2 \right] \ . \end{aligned} \tag{5.41}$$

According to the above expression the mutual information at the early time decreases with the observer's time. In particular, in this time domain $I(R_H^+ : R_H^-)$ decreases with the time-scaling $\sim t_{b_H}^2$. However, it is to be noted that, at the late times ($t_{b_H} \gg \beta_H$), the mutual information between R_H^+ and R_H^- reduces to the following form

$$I(R_H^+ : R_H^-) \approx \left(\frac{c}{3}\right)\left[\log\left[\left(\frac{\beta_H}{2\pi}\right)\sqrt{f(e_H)}\right] - 2\cosh\left(\frac{2\pi r^*(b_H)}{\beta_H}\right)e^{-\left(\frac{2\pi t_{b_H}}{\beta_H}\right)}\right] . \quad (5.42)$$

The above result of $I(R_H^+ : R_H^-)$ suggests that, at the late times the mutual information between R_H^+ and R_H^- increases with observer's time. Interestingly, from eqs.(5.41),(5.42), one can observe that there exists a specific value of observer's time t_{b_H} at which the mutual information vanishes. This observation also reflects to the fact that, the entanglement wedge corresponding to $R_H^+ \cup R_H^-$ will be in disconnected phase. This observation supports the following proposal given in [176]

Proposal I: *For an eternal black hole in de-Sitter spacetime, starting from a finite, non-zero value (at $t_{b_H} = 0$), the mutual information between R_H^+ and R_H^+ vanishes at a particular value of the observer's time ($t_{b_H} = t_H$).*

According to the above proposal, we can obtain the explicit form of t_H (at this particular value of the observer's time the mutual information between R_H^+ and R_H^- vanishes) we have to solve the following equation

$$I(R_H^+ : R_H^-)|_{t_{b_H}=t_H} = 0 \quad (5.43)$$

where the expression of $I(R_H^+ : R_H^-)$ is given by eq.(5.40). Now by solving the above equation we get the following result of t_H

$$t_H = \left(\frac{\beta_H}{2\pi}\right)\cosh^{-1}\left\{\left(\frac{\frac{\beta_H}{2\pi}\sqrt{f(e_H)}}{1+\frac{\beta_H}{2\pi}\sqrt{f(e_H)}}\right)\cosh\left(\frac{2\pi r^*(b_H)}{\beta_H}\right)\right\} . \quad (5.44)$$

The above result of t_H suggests that the time scale t_H is much smaller compared to $t_{b_H} = \beta_H$, that is $t_H \ll \beta_H$. This implis the fact that, this particular value ofobserver's time scale $t_{b_H} = t_H$ lies in the early time domain. We now compute the expression of the von-Neumann entropy of hawking radiation, at this particular time ($t_{b_H} = t_H$), by using the above result in eq.(5.34). This results

the following

$$S_{vN}^{t_{b_H}=t_H}(R_H^+ \cup R_H^-) = \frac{c}{3}\log\left[\frac{\left(\frac{\beta_H\sqrt{f(e_H)}}{2\pi}\right)^2}{1+\frac{\beta_H\sqrt{f(e_H)}}{2\pi}}\cosh\left(\frac{2\pi r^*(b_H)}{\beta_H}\right)\right]$$
$$\approx \frac{c}{3}\log\left[\frac{\beta_H}{2\pi}\sqrt{f(e_H)}\right]+\frac{c}{6}\left(\frac{r_H}{b_H}\right)^2 . \quad (5.45)$$

Now we would like to make few comments regarding the above analysis. According to the above proposal the mutual information between R_H^+ and R_H^- is non-vanishing for the time interval $0 \leq t_{b_H} < t_H$. It is to be noted that, $I(R_+ : R_-)$ is maximum at $t_{b_H} = 0$ and then it starts to decrease with the observer's time $t_{b_H} \leq t_H$ and it vanishes exactly at $t_{b_H} = t_H$. This in turn means that, the entnaglement wedge associated to $R_H^+ \cup R_H^-$ is in connected phase in the time domain $t_{b_H} \leq t_H$. Then, at $t_{b_H} = t_H$, as the mutual information between R_H^+ and R_H^- vanishes, the entanglement wedge associated to $R_H^+ \cup R_H^-$ makes the transition to the disconnected phase. Once again we would like to mention that $t_H \ll \beta_H$. These observations strongly suggests that this time t_H is nothing but the Hartman-Maldacena time t_{HM}, as reported in our previous work [176]. Furthermore, the expression of mutual information, $I(R_H^+ : R_H^-)$ at $t_{b_H} = \beta_H$ is obtained to be

$$I(R_H^+ : R_H^-) = \left(\frac{c}{3}\right)\log\left[\left(\frac{\beta_H}{2\pi}\right)\sqrt{f(e_H)}\cosh\left(\frac{2\pi r^*(b_H)}{\beta_H}\right)\right] . \quad (5.46)$$

The above result tells us that after the Hartman- Maldacena time, the mutual correlation between R_H^+ and R_H^- ($I(R_+ : R_-)$) starts to increase with respect to the observer's time t_{b_H}.

5.2.2 After Page time scenario: probing the role of $I(B_H^+ : B_H^-)$

In this section, we focus on the post-Page time scenario, specifically in the time domain where, $t_{b_H} \geq t_H^{Page}$. As previously mentioned, just after the Page time, the replica wormhole saddle point dominates over the Hawking saddle point in the gravitational path integral. Consequently, in this time domain, the island begins to contribute to the von Neumann entropy of Hawking radiation. Therefore, in the presence of island the fine-grained entropy of Hawking radiation can be computed by using the formula given in eq.(5.1). It is to be noted that, the formula for fine-grained entropy consists of two terms: the first term represents a geometric contribution, while the second term, $S_{vN}(I_H \cup R_H)$, corresponds to the von Neumann entropy of the matter fields.

It is to be mentioned that, the fine-grained entropy of the matter field, that is, $S_{vN}(I_H \cup R_H)$ obeys the identity $S_{vN}(I_H \cup R_H^+ \cup R_H^-) = S_{vN}(B_H^+ \cup B_H^-)$. We can specify the regions of $B_H^\pm$ by $(b_H^\pm \to a_H^\pm)$ where $a_H^\pm = (\pm t_{a_H}, a_H)$ are the end points of the island. This set up is described by the Penrose diagram, given in Fig(5.4. As mentioned earlier, in this study, we consider a 2D free conformal field theory (CFT) as the matter sector. So to compute the explicit form of $S_{vN}(B_H^+ \cup B_H^-)$, we must use the following formula for the entanglement entropy of two disjoint subsystems [50]

$$S_{vN}(B_H^+ \cup B_H^-) = \left(\frac{c}{3}\right) \log \left[\frac{d(a_H^+, a_H^-) d(b_H^+, b_H^+) d(a_H^+, b_H^+) d(a_H^-, b_H^-)}{d(a_H^+, b_H^-) d(a_H^-, b_H^+)}\right] . \tag{5.47}$$

To explicitly compute the entanglement entropy of the matter fields, we substitute the distances

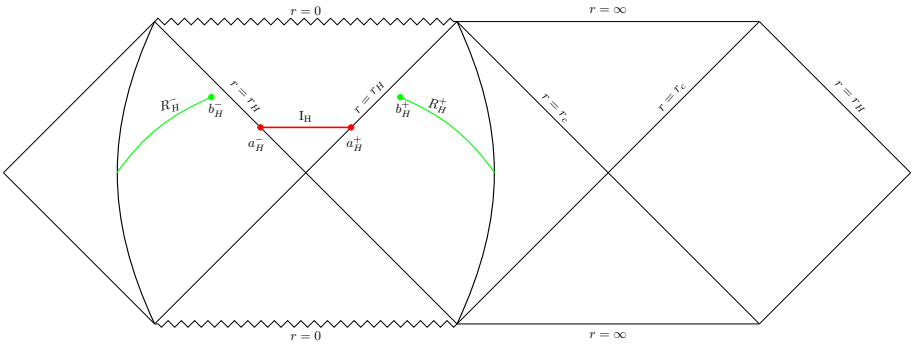

Figure 5.4: Penrose diagram of the black hole patch (with thermal opaque membrane covering the cosmological patch) with the island region (denoted by red region) with outer boundary $a_H^\pm = (\pm t_{a_H}, a_H)$. The radiation regions $(R_H^\pm)$ are shown by the green line.

into eq.(5.47). These distances can be determined using the black hole metric given in eq.(5.15). Recent works in this direction suggest that at late times $(t_{a_H}, t_{b_H} \gg \beta_H)$,the following approximation can be made [247, 270]

$$S_{vN}(B_H^+ \cup B_H^-) \approx S_{vN}(B_H^+) + S_{vN}(B_H^-) \tag{5.48}$$

where

$$S_{vN}(B_H^\pm) = \left(\frac{c}{3}\right) \log d(b_H^\pm, a_H^\pm) \tag{5.49}$$

Now substituting the above approximated result of $S_{vN}(B_H^+ \cup B_H^-)$ in the expression of fine-grained entropy of radiation given in eq.(5.1) and then extremizing this result of $S_{vN}(R_H)$ with respect

to the island parameter one can obtain a time independent result for the fine-entropy of Hawking radiation in post Page time regime. In particular, by following this one can obtain $S(R_H) = 2S_{BH} + ...$. This has already been shown in [307, 276].

However, in [175, 176] it was mentioned that, to get the approximated result of $S_{vN}(B_H^{\pm})$ given in eq.(5.48), one needs to igonre the terms $\sim e^{-\frac{2\pi t_{b_H}}{\beta_H}}$. Therefore this approximation suggests that, the mutual information between B_H^+ and B_H^- , that is $I(B_H^+ : B_H^-)$ ($I(B_H^+ : B_H^-) = S_{vN}(B_H^+) + S_{vN}(B_H^-) - S_{vN}(B_H^+ \cup B_H^-)$), vanishes approximately. In other words this approximation suggests that $I(B_H^+ : B_H^-)$ vanishes only at the leading order. It is also to be noted that, if the contribution of these terms are taken in account, then this leads us to a time dependent expression of $S_{vN}(R_H)$. We have addressed this issue in our previous works [175, 176]. Based upon our previous work, we now extend our analysis to de Sitter spacetime by introducing the following proposal.

Proposal II: *For a spherically symmetric static eternal black hole in de-Sitter spacetime, the mutual information between B_H^+ and B_H^- vanishes exactly, just after the Page time when the island starts to contribute.*

Holographically the above proposal implies that just after the Page time, when the replica wormhole saddle points starts to dominate, the entanglement wedge of $B_H^+ \cup B_H^-$ makes the transition from connected to disconnected phase [4, 38, 114] and this results in $I(B_H^+ : B_H^-) = 0$.

Now, the above proposal suggests the following

$$\begin{aligned} I(B_H^+ : B_H^-) &= 0 \\ S_{vN}(B_H^+) + S_{vN}(B_H^-) &= S_{vN}(B_H^+ \cup B_H^-) \ . \end{aligned} \tag{5.50}$$

To proceed further, we have to substitute the expressions of $S_{vN}(B_H^{\pm})$ and $S_{vN}(B_H^+ \cup B_H^-)$ (given by eq.(5.49) and eq.(1.43)) in the above condition. This results

$$d(a_H^+, b_H^-)d(a_H^-, b_H^+) = d(a_H^+, a_H^-)d(b_H^+, b_H^-) \ . \tag{5.51}$$

Substituting this above result in the expression of $S_{vN}(B_H^+ \cup R_H^-)$ (given in eq.(1.43)), we get

$$S_{vN}(B_H^+ \cup B_H^-) = \frac{c}{3} \log \left(d(a_H^+, b_H^+)d(a_H^-, b_H^-) \right) \ . \tag{5.52}$$

To proceed further we need to calculate the explicit form of various distances. One can compute these distances by using the metric describing the black hole patch, given in eq.(5.15). This yields

$$\begin{aligned}
d(a_H^{\pm}, b_H^{\pm}) &= \sqrt{2F(a_H)F(b_H)e^{\kappa_H(r^*(b_H)+r^*(a_H))}}\Big[\cosh[\kappa_H(r^*(a_H)-r^*(b_H))]-\cosh[\kappa_H(t_{a_H}-t_{b_H})]\Big]^{\frac{1}{2}} \\
d(a_H^{\pm}, b_H^{\mp}) &= \sqrt{2F(a_H)F(b_H)e^{\kappa_H(r^*(b_H)+r^*(a_H))}}\Big[\cosh[\kappa_H(r^*(a_H)-r^*(b_H))]+\cosh[\kappa(t_{a_H}+t_{b_H})]\Big]^{\frac{1}{2}} \\
d(b_H^{+}, b_H^{-}) &= 2F(b_H)e^{\kappa_H r^*(b_H)}\cosh(\kappa_H t_{b_H}) \\
d(a_H^{+}, a_H^{-}) &= 2F(a_H)e^{\kappa_H r^*(a_H)}\cosh(\kappa_H t_{a_H})\ .
\end{aligned} \tag{5.53}$$

The above results of these distances indicate that

$$\begin{aligned}
d(a_H^{+}, b_H^{+}) &= d(a_H^{-}, b_H^{-}) \\
d(a_H^{+}, b_H^{-}) &= d(a_H^{-}, b_H^{+}).
\end{aligned} \tag{5.54}$$

Therefore, by substituting the above result in the expression of $S_{vN}(B_H^+ \cup B_H^-)$ (given in eq.(5.52)) we obtain the following result

$$S_{vN}(B_H^+ \cup B_H^-) = \frac{2c}{3}\log d(a_H^+, b_H^+) \tag{5.55}$$

Now by plugging these expressions of distances in eq.(5.51) along with the result given in eq.(5.54), we obtain the following condition

$$t_{a_H} - t_{b_H} = |r^*(a_H) - r^*(b_H)|\ . \tag{5.56}$$

The condition derived above is particularly noteworthy because it allows us to express t_{a_H} in terms of the other variables. Now by substituting this above result in eq.(**??**) we have the following result

$$S_{vN}(B_H^+ \cup B_H^-) = \frac{c}{3}\log\left(\frac{2}{\kappa_H^2}\right) + \frac{c}{6}\log[f(a_H)f(b_H))]\ . \tag{5.57}$$

The most striking features about the above result is that, the matter field entropy is independent of time. Now by substituting the above result in eq.(5.1) alongwith the *area term*, that is $\frac{\text{Area}(\partial I_H)}{4G_N} = 2 \times \frac{4\pi a_H^2}{4G_N}$, we obtain the following expression of the fine grained entropy of the Hawking radiation

$$S(R_H) = 2 \times \frac{4\pi a_H^2}{4G_N} + \frac{c}{3}\log\left(\frac{2}{\kappa_H^2}\right) + \frac{c}{6}\log[f(a_H)f(b_H)]\ . \tag{5.58}$$

We now aim to determine the value of the island parameter 'a_H'. This is achieved by extremizing the result obtained above. This results

$$a_H = r_H - \left(\frac{cG_N}{24\pi}\right)\frac{1}{r_H} + \dots \,. \tag{5.59}$$

The above results indicate that the quantum extremal surfaces are located within the black hole event horizon [307, 305]. However, for eternal black holes in AdS, it has been observed that these surfaces lie just outside the event horizon [175, 176]. This distinction highlights that the positions of the island endpoints differ between dS and AdS spacetimes. By substituting the above result for "a_H" in eq.(5.58), we obtain the following expression for the fine-grained entropy of Hawking radiation

$$S_{vN}(R_H) = 2S_{BH} + \frac{c}{3}\log\left(S_{BH}\right) - \frac{\left(\frac{c}{2}\right)^2}{2S_{BH}} + \dots \,. \tag{5.60}$$

From the above expression, it is evident that the result is time-independent and includes both logarithmic and inverse power-law correction terms [175, 176]. Now substituting the expression of "a_H" (given in eq.(5.60)) in eq.(5.56), we get

$$t_{a_H} - t_{b_H} = \left(\frac{\beta_H}{8\pi}\right)\log\left(S_{BH}\right) = t_H^{Scr} \tag{5.61}$$

where t_H^{Scr} is the *Scrambling time*[271, 272] for the black hole patch. The remarkable observation made above in turn tells that just after the Page time t_H^P, the replica wormhole saddle points start to dominate and the emergence of island in the black hole interior leads to the disconnected phase of the entanglement wedge $B_H^+ \cup B_H^-$, characterized by the condition given in eq.(5.61). On the other hand, the explicit expression of the Page time is found to be

$$t_H^{Page} = \left(\frac{3\beta_H}{\pi c}\right)S_{BH} - \left(\frac{\beta_H}{\pi}\right)\log\left(S_{BH}\right)\dots \,. \tag{5.62}$$

In the above expression, the leading term corresponds to the well-known form of the Page time, while the remaining terms represent subleading corrections.

5.3 Analysis for the cosmological patch

In this section, we analyze the Page curve associated with the entanglement entropy of Gibbons-Hawking radiation (GH radiation). To do this, we restrict our analysis to the cosmological patch

while treating the black holes on each side as frozen. As in the previous section, we introduce two thermal opaque membranes on either side of the black hole patch. The metric corresponding to the region of interest is presented in eq.(5.23). Studies in this field have primarily focused on black holes in asymptotically flat or AdS spacetimes. However, recent observations indicate that the universe is expanding at an accelerated rate, exhibiting de Sitter-like characteristics. In this framework, cosmological event horizons exhibit radiation emission and absorption similar to black hole event horizons. This phenomenon is termed as Gibbons-Hawking radiation. In general, the entropy creation of the cosmic horizon is an observer-dependent feature in contrast to the black hole. It develops as a result of ignorance regarding what exists beyond the cosmological horizon. Now carrying out our analysis in the cosmological patch we have to freeze the black hole patch by introducing the thermal opaque membranes on the both sides. Once again, we will discuss two scenarios here, namely, the before cosmological Page time (t_c^{Page}) scenario and the after cosmological Page time scenario.

5.3.1 Before cosmological Page time scenario: The role of $I(R_c^+ : R_c^-)$

In this section we restrict ourselves to the pre cosmological Page time scenario. that is $t_c \ll t_c^{Page}$. As mentioned earlier, in this time domain there is no cosmological island contribution to the fine-grained entropy of GH radiation. Therefore the entanglement entropy of the Gibbons-Hawking radiation ($S_{vN}(R_c)$) is given by the von Neumann entropy of the matter fields on $R_c = R_c^+ \cup R_c^-$, that is $S_{vN}(R_c) = S_{vN}(R_c^+ \cup R_c^-)$. The end points of the disjoint regions R_c^+ and R_c^- can be specified by $[e_c^\pm : b_c^\pm]$. However, these disjoint regions span from the inner boundary ,$b_c^\pm = (\pm t_{b_c}, b_c)$ to spatial infinity (up to the thermal opaque). This can be regularised by introducing the points $e_c^\pm$, that is $e_c^\pm = (0, e_c)$. It is also to be noted that, at the end we have to take the limit $e_c \to \infty$. This set can be visualized by the Penrose diagram given in Fig.(5.5). Now, to compute the fine-grained entropy of the GH radiation in the before cosmological Page time doamin we have to use the following result

$$S_{vN}(R_c) \quad = \quad S_{vN}(R_c^+ \cup R_c^-) \; ; \; R_c = R_c^+ \cup R_c^- \; . \tag{5.63}$$

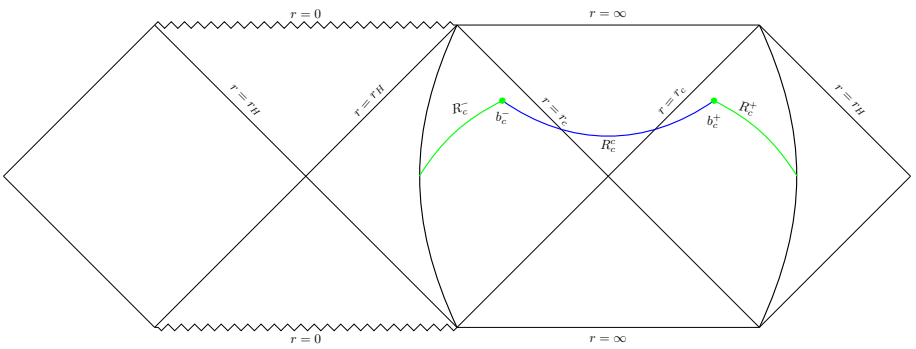

Figure 5.5: The above figure rtepresents the Penrose diagram of cosmological patch of SdS spacetime with thermal opaque covering the black hole patch. The radiation regions $R_c^{\pm}$ are denoted by the green line. On the other hand the complementary region of $R_c = R_c^+ \cup R_c^-$, that is, R_c^c is depicted by the by blue line.

We again assume that the state across the entire Cauchy slice is pure, and thus the fine-grained entropy of the GH radiation reads

$$S_{vN}(R_c) = S_{vN}(R_c^+ \cup R_c^-) \quad = \quad S_{vN}(R_c^c) \tag{5.64}$$

where R_c^c is the complementary region of $R_c^+ \cup R_c^-$. Now, considering the s-wave approximation in the matter sector, we apply the $2d$ conformal field theory formula, which is expressed as

$$S_{vN}(R_c) = S_{vN}(R_c^c) = \left(\frac{c}{3}\right) \log d(b_c^+, b_c^-) \ . \tag{5.65}$$

Now to proceed further we need to compute the distance $d(b_c^+, b_c^-)$, which can be computed by using the metric given in eq.(5.23). This results

$$d(b_c^+, b_c^-) = 2G(b_c) e^{\kappa_c r^*(b_c)} \cosh(\kappa_c t_{b_c}) \tag{5.66}$$

where κ_c denotes the surface gravity of the cosmological patch, given by eq.(5.19). Substituting the above expression of $d(b_c^+, b_c^-)$ in eq.(5.65) we get the following result of fine-grained entropy of GH radiation in the absence of island

$$\begin{aligned} S_{vN}(R_c) &= S_{vN}(R_c^+ \cup R_c^-) \\ &= \left(\frac{c}{3}\right) \log \left[\left(\frac{\beta_c}{\pi}\right) \sqrt{f(b_c)} \cosh\left(\frac{2\pi t_{b_c}}{\beta_c}\right) \right] . \end{aligned} \tag{5.67}$$

We now retrace the steps outlined in the previous section to calculate the form of $S_{vN}(R_c)$ for both the early and late time regimes. In the early time domain ($t_{b_c} \ll \beta_c$), the expression of fine-grained entropy of GH radiation ($S_{vN}(R_c)$, given in eq.(5.65)) reduces to the following form

$$S_{vN}(R_c) \approx \left(\frac{c}{3}\right) \log\left[\left(\frac{\beta_c}{\pi}\right)\sqrt{f(b_c)}\right] + \left(\frac{c}{6}\right)\left(\frac{2\pi t_{b_c}}{\beta_c}\right)^2 . \tag{5.68}$$

However, it is to be noted that in late time domain ($t_c^{Page} > t_{b_c} \gg \beta_c$), the expression of $S_{vN}(R_c)$ reads

$$S_{vN}(R_c) \approx \left(\frac{c}{3}\right) \log\left[\left(\frac{\beta_c}{\pi}\right)\sqrt{f(b_c)}\right] + \left(\frac{c}{3}\right)\left(\frac{2\pi t_{b_c}}{\beta_c}\right). \tag{5.69}$$

We again point out that, in the absence of the island the fine-grained entropy of GH radiation, $S_{vN}(R_c)$ displays a quadratic growth with time in the early time regime ($t_{b_c} \ll \beta_c$), $S(R_c) \sim t_{b_c}^2$, and it scales linearly with time, that is, $S_{vN}(R_c) \sim t_{b_c}$, in the late time regime ($t_c^{Page} > t_{b_c} \gg \beta_c$). Additionally, the entanglement entropy of the matter fields confined to the distinct regions R_c^+ and R_c^- is determined by

$$S_{vN}(R_c^{\pm}) = \frac{c}{3}\log d(b_c^{\pm}, e_c^{\pm}) \tag{5.70}$$

By employing the metric on the cosmological patch given in eq.(5.23), we can compute the distances. The expressions of $d(b_c^+, e_c^+)$ and $d(b_c^-, e_c^-)$ read

$$d(b_c^+, e_c^+) = \left[2G(b_c)G(e_c)e^{\kappa_c r^*(b_c)}\left(\cosh(\kappa_c r^*(b_c)) - \cosh(\kappa_c t_{b_c})\right)\right]^{\frac{1}{2}} = d(b_c^-, e_c^-) . \tag{5.71}$$

To get the above resukt we are using the fact that, in the limit $e_c \to \infty$, $r^*(e)$ vanishes. By substituting the aforementioned expression of $d(b_c^{\pm}, e_c^{\pm})$ into eq.(5.70), we obtain the following result

$$S_{vN}(R_c^+) = S_{vN}(R_c^-) = \left(\frac{c}{6}\right)\log\left[2\left(\frac{\beta_c}{2\pi}\right)^2\sqrt{f(b_c)f(e_c)}\left\{\left|\cosh\left(\frac{2\pi r^*(b_c)}{\beta_c}\right) - \cosh\left(\frac{2\pi t_{b_c}}{\beta_c}\right)\right|\right\}\right] \tag{5.72}$$

We now proceed to compute the mutual information between R_c^+ and R_c^- by incorporating the expressions given by eq.(5.67) and eq.(5.72). This yields

$$\begin{aligned} I(R_c^+ : R_c^-) &= S_{vN}(R_c^+) + S_{vN}(R_c^-) - S_{vN}(R_c^+ \cup R_c^-) \\ &= \left(\frac{c}{3}\right)\log\left[\left(\frac{\beta_c}{2\pi}\right)\sqrt{f(e_c)}\left\{\frac{\left|\cosh\left(\frac{2\pi r^*(b_c)}{\beta_c}\right) - \cosh\left(\frac{2\pi t_{b_c}}{\beta_c}\right)\right|}{\cosh\left(\frac{2\pi t_{b_c}}{\beta_c}\right)}\right\}\right] . \end{aligned} \tag{5.73}$$

In a manner analogous to the black hole patch analysis, it is observed that, starting from a non-zero value (at $t_{b_c} = 0$) , $I(R_c^+ : R_c^-)$ decreases with observer's time (with a time dependence of $\sim t_{b_c}^2$) in the early time regime, while in the late time regime ($t_{b_c} \gg \beta_c$), $I(R_c^+ : R_c^-)$ grows with respect to the observer's time t_{b_c}. This further highlights the existence of a specific time t_c at which the mutual information between R_c^+ and R_c^- drops to zero, resulting in the disconnection of the entanglement wedge corresponding to $R_c^+ \cup R_c^-$. With this consideration, it can be argued that the following proposal holds true for the cosmological patch as well

Proposal I: *For an eternal black hole in de-Sitter spacetime, starting from a finite, non-zero value (at $t_{b_c} = 0$), the mutual information between R_c^+ and R_c^+ vanishes at a particular value of the observer's time ($t_{b_c} = t_c$).*

In this case, the expression of the time-scale t_c is obtained by solving the following equation

$$I(R_c^+ : R_c^-)|_{t_{b_H}=t_c} = 0 \tag{5.74}$$

where the expression of $I(R_c^+ : R_c^-)$ is given by eq.(5.73). Therefore, solving the above equation we get the following

$$t_c = \left(\frac{\beta_c}{2\pi}\right) \cosh^{-1}\left\{\left(\frac{\frac{\beta_c}{2\pi}\sqrt{f(e_c)}}{1+\frac{\beta_c}{2\pi}\sqrt{f(e_c)}}\right)\cosh\left(\frac{2\pi r^*(b_c)}{\beta_c}\right)\right\}. \tag{5.75}$$

We again observe that the time scale t_c is significantly smaller than $t_{b_c} = \beta_c$, meaning $t_c \ll \beta_c$. This implies the fact that, the time scale t_c belongs to the early time domain. Moreover, the expression for $S_{vN}(R_c^+ \cup R_c^-)$ at this specific time is given by

$$\begin{aligned} S_{vN}^{t_{b_c}=t_c}(R_c^+ \cup R_c^-) &= \frac{c}{3}\log\left[\frac{\left(\frac{\beta_c\sqrt{f(e_c)}}{2\pi}\right)^2}{1+\frac{\beta_c\sqrt{f(e_c)}}{2\pi}}\cosh\left(\frac{2\pi r^*(b_c)}{\beta_c}\right)\right] \\ &\approx \frac{c}{3}\log\left[\frac{\beta_c}{2\pi}\sqrt{f(e_c)}\right] + \frac{c}{6}\left(\frac{r_c}{b_c}\right)^2 . \end{aligned} \tag{5.76}$$

Now we would make few comments. It is to be noted that, for the cosmological patch as well, the mutual correlation between R_c^+ and R_c^- starts from a maximum value at $t_{b_c} = 0$ and remains non-zero during the time interval $0 \leq t_{b_c} < t_c$. Then at $t_{b_c} = t_c$, the mutual information disappears.This further indicates that the connected phase of the entanglement wedge associated with $R_c^+ \cup R_c^-$

becomes disconnected at $t_{b_c} = t_c$. These results once more strongly imply that t_c represents the Hartman-Maldacena time for the cosmological patch. After this time (Hartman-Maldacena time) the mutual information between R_c^+ and R_c^- increases with respect to the observer's time.

5.3.2 After Cosmological Page time scenario: The role of $I(B_c^+ : B_c^-)$

Now in this section we once again proceed to study the post-cosmological Page time scenario. As discussed earlier, immediately afte the cosmological Page time (t_c^{Page}), the island starts contributing to the fine-grained entropy of Gibbons-Hawking radiation. Therefore in this time domain matter

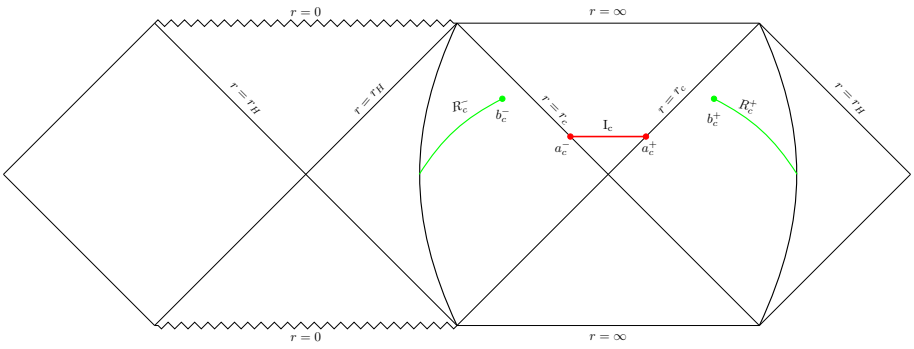

Figure 5.6: The above Penrose diagram denotes the cosmological patch of SdS spacetime with the thermal opaque membrane covering the black hole patch. The red line represents the cosmological island surface with outer boundary $a_c^{\pm} = [\pm t_{a_c}, a_c]$. The radiation regions are denoted by the green lines.

field entropy can be computed by incorporating the fact that, the matter part of eq.(5.1) satisfies the property $S_{vN}(I_c \cup R_c^+ \cup R_c^-) = S_{vN}(B_c^+ \cup B_c^-)$. Now we can identify the disjoint regions $B_c^{\pm}$ by $(b_c^{\pm} \to a_c^{\pm})$, where the endpoints of the island are denoted as $a_c^{\pm} = (\pm t_{a_c}, a_c)$.The Penrose diagram in Fig.(5.6) provides a clear visualization of this configuration. We now proceed by following the steps outlined in the black hole patch scenario. As we mentioned earlier, the matter sector in this study is take to be $2d$ free conformal field theory. Thus, the expression for $S_{vN}(B_c^+ \cup B_c^-)$ can be computed using the following formula [50]

$$S_{vN}(B_c^+ \cup B_c^-) = \left(\frac{c}{3}\right) \log \left[\frac{d(a_c^+, a_c^-) d(b_c^+, b_c^-) d(a_c^+, b_c^+) d(a_c^-, b_c^-)}{d(a_c^+, b_c^-) d(a_c^-, b_c^+)}\right] \tag{5.77}$$

To obtain the explicit form of the entanglement entropy of the matter field, we have to substitute the distances which can be derived from the metric given in eq. (5.23). On the other hand, the entropy of the matter field in the individual regions can be determined using the following expression

$$S_{vN}(B_c^{\pm}) \;=\; \left(\frac{c}{3}\right)\log d(b_c^{\pm}, a_c^{\pm})\ . \tag{5.78}$$

Now, as discussed earlier in the black hole patch analysis, at late time the expression of $S_{vN}(B_c^{+}\cup B_c^{-})$ simplifies to the following form

$$S_{vN}(B_c^{+}\cup B_c^{-}) \sim S_{vN}(B_c^{+}) + S_{vN}(B_c^{-})\ . \tag{5.79}$$

The aforementioned approximation is again based on the assumption that terms of the order $\sim e^{-\frac{2\pi t_{bc}}{\beta_c}}$ can be neglected. This suggests that, at leading order, the mutual correlation between B_c^{+} and B_c^{-} vanishes. This finding aligns with what we previously observed in the black hole patch scenario, indicating that the same proposal should also apply to the cosmological patch:

Proposal II: *For an eternal black hole in de-Sitter spacetime, the mutual information between the between the matter fields localised on B_c^{+} and B_c^{-} vanishes exactly just after the cosmological Page time.*

The above proposal leads us to the following condition

$$t_{a_c} - t_{b_c} = |r^*(a_c) - r^*(b_c)| \tag{5.80}$$

By employing the same approach we have already outlined for the black hole patch, one can determine the time-independent expression for the fine-grained entropy of Gibbons-Hawking (GH) radiation based on the proposal provided above. This results

$$S(R_c) = 2\times\frac{4\pi a_c^2}{4G_N} + \frac{c}{3}\log\left(\frac{2}{\kappa_c^2}\right) + \frac{c}{6}\log[f(a_c)f(b_c)]\ . \tag{5.81}$$

By extremizing the result above with respect to the cosmological island parameter a_c, we obtain

$$a_c = r_c - \left(\frac{cG_N}{24\pi}\right)\frac{1}{r_c} + \ldots\ . \tag{5.82}$$

The result above suggests that the endpoints of the cosmological island, known as quantum extremal surfaces, lie inside the cosmological horizon [307]. Now substituting the above result in eq.(5.81) we obtain the desired result of fine-grained entropy of Gibbons-Hawking radiation

$$S(R_c) = 2S_{GH} + \frac{c}{3}\log\left(S_{GH}\right) - \frac{\left(\frac{c}{2}\right)^2}{2S_{GH}} + \dots \ . \tag{5.83}$$

Moreover, the extremized value of the cosmological island parameter simplifies the condition for the vanishing of mutual information into the following form

$$t_{a_c} - t_{b_c} = \left(\frac{\beta_c}{8\pi}\right)\log\left(S_{GH}\right) = t_c^{Scr} \ . \tag{5.84}$$

where t_c^{Scr} scrambling time for the cosmological patch. Furthermore, the expression of the cosmological Page reads [307]

$$t_c^P \approx \left(\frac{3\beta_c}{\pi c}\right) S_{GH} \ . \tag{5.85}$$

5.4 Conclusions

We now summarize our findings. In this work, we have investigated whether our previously reported proposals [175, 176] hold in the case of eternal black holes in de Sitter spacetime. Initially, the proposals were formulated for eternal black holes in both AdS and flat spacetime. In this work, we have found that these proposals also hold for eternal black holes in de Sitter spacetime. The motivation for considering an eternal black hole solution in de Sitter spacetime arises from the intricate structure of its event horizon. As we noted earlier, for a specific range of the cosmological constant, two distinct horizons emerge. In this work we have probed how mutual information between various subsystems contributes to the Page curve for both Hawking radiation and Gibbons-Hawking radiation, taking into account the latest advancements in the island formulation. It should be noted that, given the presence of two distinct horizons, we must introduce the concept of a thermally opaque membrane to study the Page curve for two different types of radiation. This membrane facilitates the independent study of the two different radiations by dividing the whole system into two regions, namely the black hole patch and the cosmological patch. Moreover, the insights we gained from investigating the role of mutual information in our previous works, have inspired us to propose two distinct proposals for both the black hole patch and the cosmological

patch in Schwarzschild de-Sitter spacetime.

We begin by discussing the significance of these proposals by considering the black hole patch. The first proposal addresses the regime in which the observer's time is shorter than the Page time (t_P^{Page}). In this regime, there is no contribution of island in the entanglement entropy of Hawking radiation. Therefore, the entropy of the radiation in this time domain is represented by the von Neumann entropy of the conformal matter fields localised on $R_H^+ \cup R_H^-$. It is to be noted that, we have assumed the s-wave approximation in the matter sector. Therefore we can compute $S_{vN}(R_H) = S_{vN}(R_H^+ \cup R_H^-)$ by using the formula for $2d$ free CFT. Keeping this in mind we have observed that, in the early time domain, that is for $t_{b_H} \ll \beta_H$, the EE of Hawking radiation $S_{vN}(R_H)$ exhibits quadratic nature ($S_{vN}(R_H) \sim t_{b_H}^2$) and in the late time domain ($t_{b_H} \gg \beta_H$), it increases linearly with respect to the observer's time ($S_{vN}(R_H) \sim t_{b_H}$). Then we proceed to compute the mutual information between R_H^+ and R_H^-, that is $I(R_H^+ : R_H^-)$, by calculating $S_{vN}(R_H^+)$ and $S_{vN}(R_H^-)$. Keeping this general result of mutual information $I(R_H^+ : R_H^-)$ in hand we move on to investigate its behaviour in both the early and late time domain. We have observed that, starting from the maximum value at $t_{b_H} = 0$, $I(R_H^+ : R_H^-)$ decreases with the observer's time. On the other hand, in the late time domain we find that $I(R_H^+ : R_H^-)$ increases with respect to t_{b_H}.

This nature of the mutual information motivates our first proposal, which asserts that there exists a specific time , $t_{b_H} = t_H$ $(0 < t_H < \beta_H)$ at which the mutual correlation between R_H^+ and R_H^- vanishes. This means that, the entanglement wedge associated to $R_H^+ \cup R_H^-$ becomes disconnected. It is to be noted that, at $t_{b_H} = t_H$, the entropy of Hawking radiation is proportional to the logarithm of the inverse temperature of the black hole, that is $S_{vN}(R_H)|_{t_{b_H}=t_H} \sim \log \beta_H$. This observation indicates that this particular time scale, t_H, represents the Hartman-Maldacena time associated with the black hole patch. It is also observed that, after the Hartman-Maldacena time $t_{b_H} = t_H$, $I(R_H^+ : R_H^-)$ starts to increase. This implies the associated entanglement wedge is once again in its connected phase. We have also carried out the similar analysis for the cosmological patch in the pre cosmological "Page time" scenario. For the cosmological patch also we have found the Hartmann-Maldacena time t_c at which the mutual information between R_c^+ and R_c^- vanishes.

Now we will discuss about our second proposal. This proposal is associated to the time domain where the observer's time is greater than the Page time. In case of the black hole patch, after the Page time (t_H^{Page}), the entropy of Hawking radiation includes the island contribution. This

inclusion of island contribution provides appropriate Page curve which portrays the time evolution of the entropy of the Hawking radiation. Following the works in this direction, it has been noted that to obtain the correct Page curve we have to use the late time approximation $S_{vN}(B_H^+ \cup B_H^-) \approx S_{vN}(B_H^+) + S_{vN}(B_H^-)$ [247] which can also be understood as $I(B_H^+ : B_H^-)$ but only at the leading order. This approximation is associated to the fact that one has to ignore terms $\sim e^{-\frac{2\pi t_{b_H}}{\beta_H}}$. This creates a dilemma as the the core issue in this context is regarding time-dependency. However, if these terms are incorporated one gets a time-dependent form of $S(R)$ in the after Page time scenario. We address this crucial issue by demanding that the inclusion of island (replica wormhole saddle-point contributions) leads to the disconnected phase of the entanglement wedge associated to $B_H^+ \cup B_H^-$. This in turns means that just after the Page time (t_H^P), island in turn gifts us the vanishing mutual information between B_H^+ and B_H^-. This condition of vanishing mutual information, that is $I(B_H^+ : B_H^-) = 0$ leads to the remarkable result $t_{a_H} - t_{b_H} = t_H^{Scr}$ where t_H^{Scr} is the *scrambling time* [271, 272]. Using the subadditivity condition of von Neumann entropy we can reforge our observation in the following way. The entanglement wedge associated to $B_H^+ \cup B_H^+$ is in connected phase as long as $t_{a_H} - t_{b_H} < t_H^{Scr}$, and when this time difference equals the scrambling time t_H^{Scr}, the entanglement wedge associated to $B_H^+ \cup B_H^+$ jumps to the disconnected phase. Most importantly this condition of vanishing mutual information condition gives us the time-independent expression of the entropy of the Hawking radiation. Our proposals and observations related to mutual information gives strong realization of the concept given in [269, 273]. For the cosmological patch also our second proposal implies that after the cosmological Page time when the island statrs contributes the entanglement wedge associated to $B_c^+ \cup B_c^-$ is in the disconnected phase. Our proposal also implies that for the cosmological patch we have $t_{a_c} - t_{b_c} = t_c^{Scr}$, with t_c^{Scr} is the *Scrambling time* for the cosmological patch. Similar to the black hole patch scenario, we also obtain a time independent result of the entropy of the Gibbons-Haking entropy by imposing the condition of vanishing mutual information between B_c^+ and B_c^-. Another interesting fact to point out is that in both of the cases the quantum extremal surfaces lie inside the respective horizons. This behaviour is opposite to the one we observe for the eternal black hole in AdS spacetime.

Chapter 6

Summary of the thesis

In this thesis, we have investigated various aspects of the Anti-de Sitter/Conformal Field Theory (AdS/CFT) correspondence, focusing on its fundamental principles, mathematical formulation, and physical implications. Specifically, we have investigated the methods for calculating various information theoretic quantities in strongly coupled field theories by leveraging the idea of AdS/CFT duality. In particular we have computed entanglement entropy of strip like subsystem kept at the conformal field theory side by applying the Ryu-Takayanagi prescription. Instead of computing the entnaglement entropy from the field theory side, we have computed it by considering a dual gravity theory in one higher dimension. That is why this entropy is termed as the holographic entanglement entropy. We have also computed the mutual information between two strip like subsystem with the help of the result of the holographic entanglement entropy. Apart from these quantities we have computed some measures of quantum correlation for mixed states. In this context we have computed entanglement wedge cross section (which is the gravity dual of the entanglement of purification), entanglement negativity. Apart from those quantities we have also computed complexity and purification complexity holographically. We have computed these mentioned quantities for $\mathcal{N} = 4$ noncommutative super Yang-Mills theory, $\mathcal{N} = 4$ dipole deformed super Yang-Mills theory and uniformly boosted $\mathcal{N} = 4$ strongly coupled thermal plasma by considering their gravity dual within the framework of AdS/CFT duality. On the other hand, we have also studied the information loss paradox by employing the recently proposed island formalism, which provides a novel perspective on the resolution of the black hole information problem. In these couple of works we have shown that, the mutual information between concerned subsystem

plays a vital role in obtaining the Page curve. In this context we have provided two proposals in two different time domains regarding the connectivity of entanglement wedge. In these works, we have shown that our proposed methods accurately reproduce the correct Page curve for eternal black holes. We have also found that our proposals hold for eternal black holes in both asymptotically AdS and asymptotically dS spacetimes. We have considered the eternal black hole solution in JT gravity as well as the Schwarzschild de-Sitter black hole to make our analysis.

In chapter (1), we have started our discussion with different measures of quantum correlation in the context of quantum information theory. We start our analysis with von-Neumann entropy, which measures quantum correlation, when the system under consideration is in the mixed state. Keeping this concept of von-Neumann entropy in mind we move on to discuss the concept of mutual information. Then we have also studied some measures of cquantum correlation for mixed states. In this context we have discussed two quantities, namely the entanglement of purification and entanglement negativity. We have also discuss the concept of quantum complexity (for pure state) and purification complexity (mutual complexity for mixed state). Then we have moved on to discuss entanglement entropy in the context of quantum field theory. Then we move on to discuss the gauge/gravity duality. Keeping this discussion in mind, we then proceed to discuss the holographic description of different measures of quantum correlation.

In chapter(2), we have computed these mentioned quantities for deformed $\mathcal{N} = 4$ supersymmetric Yang-Mills theory holographically. In particular, we have considered two different kinds of deformation, namely, the noncommutative deformation and the dipole defromation. For noncommutative Yang Mills theory we have found that there exists a critical length scale ($\frac{l_c}{a}$, in dimensionless form) which depends on the UV cut-off. This gives us a hint of UV-IR mixing. Furthermore, the domain where the subsystem length ($\frac{l}{a}$, in dimensionless form) is larger than the critical length can be devided into different regimes. We have computed different information theoretic measures for different domains of the theory. We have found that, the holographic entanglement entropy has different behavior in these two different domains. If the subsystem length is greater than this critical length the HEE obey the area law. On the other hand if the length of the subsystem is smaller than the critical length, HEE obey the volume law. However, in the domain $\frac{l}{a} < \frac{l_c}{a}$, the divergent piece in the HEE depends on the subsystem length, this implies that fact that in this domain HEE is not a finite quantity. On the othe hand in the domain $\frac{l}{a} > \frac{l_c}{a}$, the divergent

piece in HEE is independent of the subsystem length, implying the fact that in this doamin the divergent piece is universal. We have also ploted this result of HEE with respect to the subsystem length. Furthermore, the computation of holographic mutual information (HMI) and EWCS for two disjiont subsystems (in the domain $\frac{l}{a} > \frac{l_c}{a}$) suggests that the HMI between two subsystems vanihes for a particular separation distance. This in turn means that the entnaglemnet wedge associated with the total system shows a phase transition from a connected pahse to a disconnected phase. On the other hand in the domain $\frac{l}{a} < \frac{l_c}{a}$ these qunatities are UV divergent. We have also explored the UV-IR mixing property holographically. We have also carried out similar kind of computation for finite temperature noncommutative Yang Mills theory by considering black hole geometry in the bulk. On the other hand to compute these mentioned information theoretic quantities for dipole deformed supersymmetric Yang-Mills theory we again consider a dual gravity theory. In this case also we have found that there is a critical length scale. But in contrast to the noncommutative case, in this case the critical length scale does not depend on the UV-cutoff. This implies for dipole deformed theory there is no UV-IR mixing. In this case also we have computed the HEE of strip like subsystem (placed at the boundary) by using the RT prescription. Simliar to the NC case, here also we have observed that if the subsystem length is larger than this critical length the HEE obey the area like law, and in the domain where the subsystem length is smaller in compared to this critical length the HEE obey the volume like law. We have also expressed the subsystem length in terms of the bulk corrdinate. Then we have ploted this result of subsystem length with respect to the turning point and observed that for every subsystem length there exist a unique turing point. This implies that for every subsystem there there is only one unique RT surface. This feature is quite different from the noncommutative scenario. Then we have moved forward to compute the HMI and EWCS bwteen two disjoint subsystems for two different domains of the theory. We have observed that if the subsyestem length lies above the critical length scale these quantities are finite and physically relevant. On the other hand if the the subsystem length is smaller than the critical length these quantities are not finite.

Next, in chapter(3) we have computed different information theoretic quantities for strongly coupled boosted plasma holographically. To do this we have consider boosted black brane geometry in the bulk theory. The geometry suggests that the spacetime metric is not stationary. First we will consider a strip like subsytem along the boost. To the compute the HEE of strip like subsystem

(along the boost) we will use the HRT prescription instead of the RT prescription, because in this case the dual spacetime metric is not stationary. Furthermore, we have compute the result of HEE under the thin strip approximation. Then with this result of HEE we have computed HMI for two disjoint strip like subsystem (along the boost) of equal lenght. In this setup we have also computed the EWCS. We have represented the results of HMI and EWCS graphically. We have found that for a particular value of the separation distance the HMI between two subsystems vanishes. This implies the the fact that, the connected phase becomes disconnected. Furthermore we have also found that HMI for boosted geometry vanishes earlier in comparison with unboosted geometry. Then we have proceed to compute the entanglement negativity holographically for both the adjacent and disjoint subsystems. This computation suggests that, the entanglement negativity is divergent quantity for adjacent subsyatems. On the other hand the entanglement negativity for disjoint subsystem in an UV- finite quantity and it vanishes for a critical separation between two subsystems of fixed length. We have also found that due the boost the entanglement negativity vanishes earlier. Now we have moved on compute the holographic sub-region complexity for a strip like subsystem placed along the boost. Further for the mixed states we have computed the complexity of purification with the help of the result of sub region complexity. Similar to parallel case have also computed all the above mentioned quantites for subsystems placed perpendicular to the boost. We have also made a comparative study of different results of mentioned information theoretic measures in both the scenario. For the completeness of the study we have calculated the mentioned quatitiies for "*AdS wave*" geometry. This geometry can be obtained by taking appropriate limits of the boosted black brane geometry.

In chapters(4,5), we have provided two proposals regarding the saturation of mutual information in the two different time doamins. In chapter(4), we have considered black hole solution in two dimensional JT gravity attached with flat thermal bath to carry out our analysis. The first proposal is given for the pre-Page time domain. It was observed that, in this time doamin Hawking saddel point dominates which leads to $S_{vN}(R) \sim t_b^2$ in early times ($t_b \ll \beta$) and $S_{vN}(R) \sim t_b$ at late times ($t_b \gg \beta$). Then computing the von-Neumann entropy of matter field on the individual regions $R_{\pm}$, that is $S_{vN}(R_{\pm})$ and $S_{vN}(R_+ \cup R_-)$, we calculated the mutual information between $R_{\pm}$, that is $I(R_+ \cup R_-)$. Then analyzing the nature of $I(R_+ \cup R_-)$ in early and late time domain, we proposed that, the mutual information between R_+ and R_- vanishes at a particular value of observer's

time, $t_b = t_R$. This indicates the fact that, the entanglement wedge associated with $R_+ \cup R_-$ becomes disconnected. However, it is to be noted that, this time scale lies in the early time domain, $t_R << \beta$. This particular value of observer's time is reffered to as the Hartman-Maldacena time (t_{HM}). On the other hand, the second proposal is given for the post Page time scenario. In this time doamin replica wormhole saddel points dominates and the island starts to contribute to the von-Neumann entropy of Hawking radiation. Some earlier studies in this direction suggest that late time approximation (that is, $S_{vN}(B_+ \cup B_-) \approx S_{vN}(B_+) + S_{vN}(B_-)$) leads to the mutual information, $I(B_+ : B_-)$ vanishes in the leading order which in turn leads to extremization condition $t_a \approx t_b$. Our proposal suggets that, just after the Page time when island starts to contribute the mutual information between B_+ and B_-, that is $I(B_+ : B_-)$ vanishes exactly, which leads to the extremization condition $t_a - t_b = t_{\rm scr} + ...$. The conceptual foundation of this proposal lies in the observation that the replica wormhole saddle points (which account for the island contribution) lead to a disconnected phase for the entanglement wedge associated with $B_+ \cup B_-$. Consequently, the mutual correlation between B_+ and B_- should vanish at all orders, rather than just at the leading order as indicated in previous studies. This condition of vanishing mutual information B_+ and B_- leads to a time independent result for the fine-grained entropy of Hawking radiation which also includes logarithmic and power law corrections. Our proposal suggests that as long as the time difference $t_a - t_b$ is less than the scrambling time the entanglement wedge associated with $B_+ \cup B_-$ is in the connected phase which means $I(B_+ \cup B_-) \neq 0$. Then at $t_a - t_b = t_{\rm scr} + ...$, the entanglement wedge of $B_+ \cup B_-$ becomes disconnected.

On the other hand in chapter(5), we have consider eternal Schwarzschild ds-Sitter black hole. The motivation for considering an eternal black hole solution in de Sitter spacetime stems from the intricate structure of its event horizon, which exhibits multiple causal boundaries, including the black hole horizon and the cosmological horizon. In this work, we have investigated the validity of our previously reported proposals [175, 176] in the context of eternal black holes in de Sitter spacetime. While these proposals were initially formulated for eternal black holes in AdS and flat spacetime, our analysis confirms that they remain applicable in the de-Sitter case as well. We have separtely carried out our analysis in both the black hole patch and the cosmological patch. We have made a similar observations (for both the black hole and cosmological patch) to what was previously discussed in chapter (4).

In summary, the application of gauge/gravity duality within the framework of information theory yields profound insights that cannot be achieved through conventional perturbative approaches in field theory. In this thesis, we have primarily focused on key quantities such as entanglement entropy, complexity, and measures of entanglement and complexity for mixed states. However, numerous other information-theoretic quantities hold significant importance in their own right. Given this, extending holographic techniques to study these additional quantities presents a compelling avenue for future research. From the current perspective, it is evident that the holographic investigation of information-theoretic measures will play a crucial role in deepening our understanding of the fundamental principles of nature.

Bibliography

[1] E. Schrödinger, "Quantisierung als Eigenwertproblem", *Annalen Phys.* **384**[4] (1926) 361.

[2] M. A. Nielsen and I. L. Chuang, Quantum Computation and Quantum Information, Cambridge University Press 2000.

[3] B. M. Terhal, M. Horodecki, D. W. Leung and D. P. DiVincenzo, "The entanglement of purification", *Journal of Mathematical Physics* **43**[9] (2002) 4286–4298.

[4] T. Takayanagi and K. Umemoto, "Entanglement of purification through holographic duality", *Nature Phys.* **14**[6] (2018) 573, arXiv:1708.09393 [hep-th].

[5] P. Jain, V. Malvimat, S. Mondal and G. Sengupta, "Holographic entanglement negativity conjecture for adjacent intervals in AdS_3/CFT_2", *Phys. Lett. B* **793** (2019) 104, arXiv:1707.08293 [hep-th].

[6] G. Vidal and R. Werner, "Computable measure of entanglement", *Phys. Rev. A* **65** (2002) 032314, arXiv:quant-ph/0102117.

[7] M. Ghasemi, A. Naseh and R. Pirmoradian, "Odd entanglement entropy and logarithmic negativity for thermofield double states", *JHEP* **10** (2021) 128, arXiv:2106.15451 [hep-th].

[8] J. K. Basak, H. Chourasiya, V. Raj and G. Sengupta, "Odd entanglement entropy in Galilean conformal field theories and flat holography", arXiv:2203.03902 [hep-th].

[9] S. Dutta and T. Faulkner, "A canonical purification for the entanglement wedge cross-section", arXiv:1905.00577 [hep-th].

[10] J. Chu, R. Qi and Y. Zhou, "Generalizations of Reflected Entropy and the Holographic Dual", *JHEP* **03** (2020) 151, arXiv:1909.10456 [hep-th].

[11] J. K. Basak, H. Chourasiya, V. Raj and G. Sengupta, "Reflected entropy in Galilean conformal field theories and flat holography", arXiv:2202.01201 [hep-th].

[12] M. J. Vasli, M. R. Mohammadi Mozaffar, K. Babaei Velni and M. Sahraei, "Holographic study of reflected entropy in anisotropic theories", *Phys. Rev. D* **107**[2] (2023) 026012, arXiv:2207.14169 [hep-th].

[13] S. Arora and B. Barak, "Computational complexity: A modern approach, Cambridge University Press (2009)", .

[14] C. Moore and S. Mertens, "The nature of computation, Oxford University Press (2011)", .

[15] M.A.Nielsen, "A geometric approach to quantum circuit lower bound", arXiv:0502070 [quant-ph].

[16] M. G. A. C. D. Michael A. Nielsen, Mark R. Dowling, " Quantum Computation as Geometry", *Science* , arXiv:0603161 [quant-ph].

[17] L. Susskind, "Three Lectures on Complexity and Black Holes", SpringerBriefs in Physics, Springer 2018, arXiv:1810.11563 [hep-th].

[18] T. Ali, A. Bhattacharyya, S. Shajidul Haque, E. H. Kim and N. Moynihan, "Time Evolution of Complexity: A Critique of Three Methods", *JHEP* **04** (2019) 087, arXiv:1810.02734 [hep-th].

[19] M. A. Nielsen, "A geometric approach to quantum circuit lower bounds", *Quantum Inf. Comput.* **6** (2006) 213.

[20] L. Susskind, "Entanglement is not enough", *Fortsch. Phys.* **64** (2016) 49, arXiv:1411.0690 [hep-th].

[21] L. Susskind, "Computational Complexity and Black Hole Horizons", *Fortsch. Phys.* **64** (2016) 24, [Addendum: Fortsch.Phys. 64, 44–48 (2016)], arXiv:1403.5695 [hep-th].

[22] M. A. Nielsen, M. R. Dowling, M. Gu and A. C. Doherty, "Quantum Computation as Geometry", *Science* **311**[**5764**] (2006) 1133, arXiv:https://www.science.org/doi/pdf/10.1126/science.1121541.

[23] M. R. Dowling and M. A. Nielsen, "The geometry of quantum computation", *Quantum Information & Computation* **8**[**10**] (2008) 861.

[24] T. Ali, A. Bhattacharyya, S. S. Haque, E. H. Kim and N. Moynihan, "Time evolution of complexity: a critique of three methods", *Journal of High Energy Physics* **2019**[**4**] (2019) 1.

[25] T. Ali, A. Bhattacharyya, S. S. Haque, E. H. Kim, N. Moynihan and J. Murugan, "Chaos and complexity in quantum mechanics", *Physical Review D* **101**[**2**] (2020) 026021.

[26] S. Chapman, J. Eisert, L. Hackl, M. P. Heller, R. Jefferson, H. Marrochio and R. Myers, "Complexity and entanglement for thermofield double states", *SciPost physics* **6**[**3**] (2019) 034.

[27] S. Lloyd and C. Weedbrook, "Quantum generative adversarial learning", *Physical review letters* **121**[**4**] (2018) 040502.

[28] M. Svítek, O. Kosheleva, V. Kreinovich and T. N. Nguyen, "Why quantum (wave probability) models are a good description of many non-quantum complex systems, and how to go beyond quantum models", *in* International Econometric Conference of Vietnam, p. 168–175, Springer 2019.

[29] M. Guo, Z.-Y. Fan, J. Jiang, X. Liu and B. Chen, "Circuit complexity for generalized coherent states in thermal field dynamics", *Physical Review D* **101**[**12**] (2020) 126007.

[30] G. Di Giulio and E. Tonni, "Subsystem complexity after a global quantum quench", *Journal of High Energy Physics* **2021**[**5**] (2021) 1.

[31] R. A. Jefferson and R. C. Myers, "Circuit complexity in quantum field theory", *Journal of High Energy Physics* **2017**[**10**] (2017) 1.

[32] M. Alishahiha, K. Babaei Velni and M. R. Mohammadi Mozaffar, "Black hole subregion action and complexity", *Phys. Rev. D* **99**[**12**] (2019) 126016, arXiv:1809.06031 [hep-th].

[33] E. Cáceres, J. Couch, S. Eccles and W. Fischler, "Holographic purification complexity", *Phys. Rev. D* **99** (2019) 086016.

[34] E. Caceres, S. Chapman, J. D. Couch, J. P. Hernandez, R. C. Myers and S.-M. Ruan, "Complexity of Mixed States in QFT and Holography", *JHEP* **03** (2020) 012, arXiv:1909.10557 [hep-th].

[35] C. A. Agón, M. Headrick and B. Swingle, "Subsystem Complexity and Holography", *JHEP* **02** (2019) 145, arXiv:1804.01561 [hep-th].

[36] S.-M. Ruan, Circuit Complexity of Mixed States, Ph.D. thesis, Waterloo U. 2021.

[37] A. Chowdhury Roy, A. Saha and S. Gangopadhyay, "Mixed state information theoretic measures in boosted black brane", *Annals Phys.* **452** (2023) 169270, arXiv:2204.08012 [hep-th].

[38] A. Saha and S. Gangopadhyay, "Holographic study of entanglement and complexity for mixed states", *Phys. Rev. D* **103**[**8**] (2021) 086002, arXiv:2101.00887 [hep-th].

[39] A. Bhattacharyya, S. S. Haque and E. H. Kim, "Complexity from the reduced density matrix: a new diagnostic for chaos", *Journal of High Energy Physics* **2021**[**10**] (2021) 1.

[40] L.-C. Qu, J. Chen and Y.-X. Liu, "Chaos and complexity for inverted harmonic oscillators", *Physical Review D* **105**[**12**] (2022) 126015.

[41] V. Balasubramanian, M. DeCross, A. Kar and O. Parrikar, "Quantum complexity of time evolution with chaotic Hamiltonians", *Journal of High Energy Physics* **2020**[**1**] (2020) 1.

[42] S. Chapman and G. Policastro, "Quantum computational complexity from quantum information to black holes and back", *The European Physical Journal C* **82**[**2**] (2022) 1.

[43] G. Policastro and S. Chapman, "Quantum Computational Complexity–From Quantum Information to Black Holes and Back", .

[44] A. Bhattacharyya, W. Chemissany, S. S. Haque, J. Murugan and B. Yan, "The multi-faceted inverted harmonic oscillator: Chaos and complexity", *SciPost Physics Core* **4**[**1**] (2021) 002.

[45] H. A. Camargo, P. Caputa, D. Das, M. P. Heller and R. Jefferson, "Complexity as a novel probe of quantum quenches: universal scalings and purifications", *Physical Review Letters* **122**[**8**] (2019) 081601.

[46] P. Calabrese and J. L. Cardy, "Entanglement entropy and quantum field theory", *J. Stat. Mech.* **0406** (2004) P06002, arXiv:hep-th/0405152.

[47] P. Calabrese and J. L. Cardy, "Evolution of entanglement entropy in one-dimensional systems", *J. Stat. Mech.* **0504** (2005) P04010, arXiv:cond-mat/0503393.

[48] P. Calabrese and J. L. Cardy, "Entanglement entropy and quantum field theory: A Non-technical introduction", *Int. J. Quant. Inf.* **4** (2006) 429, arXiv:quant-ph/0505193.

[49] P. Calabrese and J. Cardy, "Entanglement entropy and conformal field theory", *J. Phys. A* **42** (2009) 504005, arXiv:0905.4013 [cond-mat.stat-mech].

[50] P. Calabrese, J. Cardy and E. Tonni, "Entanglement entropy of two disjoint intervals in conformal field theory", *J. Stat. Mech.* **0911** (2009) P11001, arXiv:0905.2069 [hep-th].

[51] M. Srednicki, "Entropy and area", *Phys. Rev. Lett.* **71** (1993) 666, arXiv:hep-th/9303048.

[52] M. Cramer, J. Eisert, M. B. Plenio and J. Dreissig, "An Entanglement-area law for general bosonic harmonic lattice systems", *Phys. Rev. A* **73** (2006) 012309, arXiv:quant-ph/0505092.

[53] M. B. Plenio, J. Eisert, J. Dreissig and M. Cramer, "Entropy, entanglement, and area: analytical results for harmonic lattice systems", *Phys. Rev. Lett.* **94** (2005) 060503, arXiv:quant-ph/0405142.

[54] H. Casini and M. Huerta, "Universal terms for the entanglement entropy in 2+1 dimensions", *Nucl. Phys. B* **764** (2007) 183, arXiv:hep-th/0606256.

[55] M. Rangamani and T. Takayanagi, Holographic Entanglement Entropy, volume 931, Springer 2017, arXiv:1609.01287 [hep-th].

[56] R. Blumenhagen and E. Plauschinn, Introduction to Conformal Field Theory, Lecture Notes in Physics, Springer Berlin, Heidelberg 2009.

[57] E. Witten, "Bound states of strings and p-branes", *Nucl. Phys. B* **460** (1996) 335, arXiv:hep-th/9510135.

[58] L. Brink, J. H. Schwarz and J. Scherk, "Supersymmetric Yang-Mills Theories", *Nucl. Phys. B* **121** (1977) 77.

[59] F. Gliozzi, J. Scherk and D. I. Olive, "Supersymmetry, Supergravity Theories and the Dual Spinor Model", *Nucl. Phys. B* **122** (1977) 253.

[60] J. M. Maldacena, "The Large N limit of superconformal field theories and supergravity", *Int. J. Theor. Phys.* **38** (1999) 1113, arXiv:hep-th/9711200.

[61] S. S. Gubser, I. R. Klebanov and A. M. Polyakov, "Gauge theory correlators from noncritical string theory", *Phys. Lett. B* **428** (1998) 105, arXiv:hep-th/9802109.

[62] E. Witten, "Anti-de Sitter space and holography", *Adv. Theor. Math. Phys.* **2** (1998) 253, arXiv:hep-th/9802150.

[63] G. 't Hooft, "A Planar Diagram Theory for Strong Interactions", *Nucl. Phys. B* **72** (1974) 461.

[64] O. Aharony, S. S. Gubser, J. M. Maldacena, H. Ooguri and Y. Oz, "Large N field theories, string theory and gravity", *Phys. Rept.* **323** (2000) 183, arXiv:hep-th/9905111.

[65] S. S. Gubser, "Einstein Manifolds and Conformal Field Theories", *Phys. Rev. D* **59** (1999) 025006, arXiv:hep-th/9807164.

[66] L. Susskind, "The World as a hologram", *J. Math. Phys.* **36** (1995) 6377, arXiv:hep-th/9409089.

[67] L. Susskind and E. Witten, "The Holographic Bound in Anti-de Sitter Space", arXiv:hep-th/9805114.

[68] D. Bigatti and L. Susskind, "TASI lectures on the holographic principle", *in* Theoretical Advanced Study Institute in Elementary Particle Physics (TASI 99): Strings, Branes, and Gravity, p. 883–933 1999, arXiv:hep-th/0002044.

[69] M. Natsuume, AdS/CFT Duality User Guide, Lecture Notes in Physics, Springer Japan 2015.

[70] J. Casalderrey-Solana, H. Liu, D. Mateos, K. Rajagopal and U. A. Wiedemann, Gauge/String Duality, Hot QCD and Heavy Ion Collisions, Cambridge University Press 2014.

[71] M. Ammon and J. Erdmenger, Gauge/Gravity Duality, Cambridge University Press 2015.

[72] H. Năstase, Introduction to AdS/CFT Correspondence, Cambridge University Press 2015.

[73] J. Zaanen, Y. Liu, Y.-W. Sun and K. Schalm, Holographic Duality in Condensed Matter Physics, Cambridge University Press 2015.

[74] S. Ryu and T. Takayanagi, "Holographic derivation of entanglement entropy from AdS/CFT", *Phys. Rev. Lett.* **96** (2006) 181602, arXiv:hep-th/0603001.

[75] S. Ryu and T. Takayanagi, "Aspects of Holographic Entanglement Entropy", *JHEP* **08** (2006) 045, arXiv:hep-th/0605073.

[76] T. Nishioka, S. Ryu and T. Takayanagi, "Holographic Entanglement Entropy: An Overview", *J. Phys. A* **42** (2009) 504008, arXiv:0905.0932 [hep-th].

[77] A. Lewkowycz and J. Maldacena, "Generalized gravitational entropy", *JHEP* **08** (2013) 090, arXiv:1304.4926 [hep-th].

[78] N. Jokela and A. Pönni, "Notes on entanglement wedge cross sections", *JHEP* **07** (2019) 087, arXiv:1904.09582 [hep-th].

[79] K. Babaei Velni, M. R. Mohammadi Mozaffar and M. Vahidinia, "Some Aspects of Entanglement Wedge Cross-Section", *JHEP* **05** (2019) 200, arXiv:1903.08490 [hep-th].

[80] P. Nguyen, T. Devakul, M. G. Halbasch, M. P. Zaletel and B. Swingle, "Entanglement of purification: from spin chains to holography", *JHEP* **01** (2018) 098, arXiv:1709.07424 [hep-th].

[81] J. Kudler-Flam and S. Ryu, "Entanglement negativity and minimal entanglement wedge cross sections in holographic theories", *Phys. Rev. D* **99**[**10**] (2019) 106014, arXiv:1808.00446 [hep-th].

[82] Y. Kusuki, J. Kudler-Flam and S. Ryu, "Derivation of holographic negativity in AdS_3/CFT_2", *Phys. Rev. Lett.* **123**[**13**] (2019) 131603, arXiv:1907.07824 [hep-th].

[83] D. D. Blanco, H. Casini, L.-Y. Hung and R. C. Myers, "Relative Entropy and Holography", *JHEP* **08** (2013) 060, arXiv:1305.3182 [hep-th].

[84] P. Chaturvedi, V. Malvimat and G. Sengupta, "Entanglement negativity, Holography and Black holes", *Eur. Phys. J. C* **78**[**6**] (2018) 499, arXiv:1602.01147 [hep-th].

[85] P. Chaturvedi, V. Malvimat and G. Sengupta, "Holographic Quantum Entanglement Negativity", *JHEP* **05** (2018) 172, arXiv:1609.06609 [hep-th].

[86] P. Jain, V. Malvimat, S. Mondal and G. Sengupta, "Holographic entanglement negativity for adjacent subsystems in AdS_{d+1}/CFT_d", *Eur. Phys. J. Plus* **133**[**8**] (2018) 300, arXiv:1708.00612 [hep-th].

[87] P. Jain, V. Malvimat, S. Mondal and G. Sengupta, "Covariant holographic entanglement negativity for adjacent subsystems in AdS_3 /CFT_2", *Nucl. Phys. B* **945** (2019) 114683, arXiv:1710.06138 [hep-th].

[88] V. Malvimat, H. Parihar, B. Paul and G. Sengupta, "Entanglement Negativity in Galilean Conformal Field Theories", *Phys. Rev. D* **100**[**2**] (2019) 026001, arXiv:1810.08162 [hep-th].

[89] V. Malvimat, S. Mondal and G. Sengupta, "Time Evolution of Entanglement Negativity from Black Hole Interiors", *JHEP* **05** (2019) 183, arXiv:1812.04424 [hep-th].

[90] D. Rogerson, F. Pollmann and A. Roy, "Entanglement entropy and negativity in the Ising model with defects", arXiv:2204.03601 [hep-th].

[91] A. Matsumura, "Role of coherence in entanglement due to gravity", arXiv:2204.00324 [quant-ph].

[92] B. Bertini, K. Klobas and T.-C. Lu, "Entanglement Negativity and Mutual Information after a Quantum Quench: Exact Link from Space-Time Duality", arXiv:2203.17254 [quant-ph].

[93] J. Roik, K. Bartkiewicz, A. Černoch and K. Lemr, "Entanglement quantification from collective measurements processed by machine learning", arXiv:2203.01607 [quant-ph].

[94] X. Dong, S. McBride and W. W. Weng, "Replica Wormholes and Holographic Entanglement Negativity", arXiv:2110.11947 [hep-th].

[95] A. Bhattacharya, A. Bhattacharyya, P. Nandy and A. K. Patra, "Partial islands and subregion complexity in geometric secret-sharing model", *JHEP* **12** (2021) 091, arXiv:2109.07842 [hep-th].

[96] K. Hejazi and H. Shapourian, "Symmetry protected entanglement in random mixed states", arXiv:2112.00032 [quant-ph].

[97] M. Afrasiar, J. Kumar Basak, V. Raj and G. Sengupta, "Holographic Entanglement Negativity for Disjoint Subsystems in Conformal Field Theories with a Conserved Charge", arXiv:2106.14918 [hep-th].

[98] D. Basu, H. Parihar, V. Raj and G. Sengupta, "Entanglement negativity, reflected entropy and anomalous gravitation", arXiv:2202.00683 [hep-th].

[99] V. Malvimat, S. Mondal, B. Paul and G. Sengupta, "Covariant holographic entanglement negativity for disjoint intervals in AdS_3/CFT_2", *Eur. Phys. J. C* **79[6]** (2019) 514, arXiv:1812.03117 [hep-th].

[100] J. Kumar Basak, H. Parihar, B. Paul and G. Sengupta, "Holographic entanglement negativity for disjoint subsystems in $\mathrm{AdS}_{\mathrm{d}+1}/\mathrm{CFT}_{\mathrm{d}}$", arXiv:2001.10534 [hep-th].

[101] J. Couch, S. Eccles, T. Jacobson and P. Nguyen, "Holographic Complexity and Volume", *JHEP* **11** (2018) 044, arXiv:1807.02186 [hep-th].

[102] A. R. Brown, D. A. Roberts, L. Susskind, B. Swingle and Y. Zhao, "Holographic Complexity Equals Bulk Action?", *Phys. Rev. Lett.* **116**[**19**] (2016) 191301, arXiv:1509.07876 [hep-th].

[103] A. R. Brown, D. A. Roberts, L. Susskind, B. Swingle and Y. Zhao, "Complexity, action, and black holes", *Phys. Rev. D* **93**[**8**] (2016) 086006, arXiv:1512.04993 [hep-th].

[104] S. Lloyd, "Ultimate physical limits to computation", *Nature* **406**[**6799**] (2000) 1047.

[105] L. Lehner, R. C. Myers, E. Poisson and R. D. Sorkin, "Gravitational action with null boundaries", *Phys. Rev. D* **94**[**8**] (2016) 084046, arXiv:1609.00207 [hep-th].

[106] D. Carmi, R. C. Myers and P. Rath, "Comments on Holographic Complexity", *JHEP* **03** (2017) 118, arXiv:1612.00433 [hep-th].

[107] J. W. York, "Role of Conformal Three-Geometry in the Dynamics of Gravitation", *Phys. Rev. Lett.* **28** (1972) 1082.

[108] G. W. Gibbons and S. W. Hawking, "Action integrals and partition functions in quantum gravity", *Phys. Rev. D* **15** (1977) 2752.

[109] K. Parattu, S. Chakraborty, B. R. Majhi and T. Padmanabhan, "A Boundary Term for the Gravitational Action with Null Boundaries", *Gen. Rel. Grav.* **48**[**7**] (2016) 94, arXiv:1501.01053 [gr-qc].

[110] G. Hayward, "Gravitational action for spacetimes with nonsmooth boundaries", *Phys. Rev. D* **47** (1993) 3275.

[111] D. Brill and G. Hayward, "Is the gravitational action additive?", *Phys. Rev. D* **50** (1994) 4914.

[112] M. Alishahiha, "Holographic Complexity", *Phys. Rev. D* **92**[**12**] (2015) 126009, arXiv:1509.06614 [hep-th].

[113] M. Ghodrati, X.-M. Kuang, B. Wang, C.-Y. Zhang and Y.-T. Zhou, "The connection between holographic entanglement and complexity of purification", *JHEP* **09** (2019) 009, arXiv:1902.02475 [hep-th].

[114] A. R. Chowdhury, A. Saha and S. Gangopadhyay, "Entanglement wedge cross-section for noncommutative Yang-Mills theory", *JHEP* **02** (2022) 192, arXiv:2106.04562 [hep-th].

[115] A. Roy Chowdhury, A. Saha and S. Gangopadhyay, "Mixed state entanglement measures for the dipole deformed supersymmetric Yang–Mills theory", *Annals Phys.* **460** (2024) 169565, arXiv:2307.13712 [hep-th].

[116] M. R. Douglas and N. A. Nekrasov, "Noncommutative field theory", *Rev. Mod. Phys.* **73** (2001) 977.

[117] S. Minwalla, M. Van Raamsdonk and N. Seiberg, "Noncommutative perturbative dynamics", *JHEP* **02** (2000) 020, arXiv:hep-th/9912072.

[118] A. Armoni, "Comments on perturbative dynamics of noncommutative Yang-Mills theory", *Nucl. Phys. B* **593** (2001) 229, arXiv:hep-th/0005208.

[119] R. J. Szabo, "Quantum field theory on noncommutative spaces", *Phys. Rept.* **378** (2003) 207, arXiv:hep-th/0109162.

[120] N. Seiberg and E. Witten, "String theory and noncommutative geometry", *JHEP* **09** (1999) 032, arXiv:hep-th/9908142.

[121] A. Hashimoto and N. Itzhaki, "Noncommutative Yang-Mills and the AdS/CFT Correspondence", *Phys. Lett. B* **465** (1999) 142, arXiv:hep-th/9907166.

[122] J. M. Maldacena and J. G. Russo, "Large N Limit of Noncommutative Gauge Theories", *JHEP* **09** (1999) 025, arXiv:hep-th/9908134.

[123] W. Fischler, A. Kundu and S. Kundu, "Holographic Entanglement in a Noncommutative Gauge Theory", *JHEP* **01** (2014) 137, arXiv:1307.2932 [hep-th].

[124] J. L. F. Barbon and C. A. Fuertes, "Holographic entanglement entropy probes (non)locality", *JHEP* **04** (2008) 096, arXiv:0803.1928 [hep-th].

[125] J. L. Karczmarek and C. Rabideau, "Holographic entanglement entropy in nonlocal theories", *JHEP* **10** (2013) 078, arXiv:1307.3517 [hep-th].

[126] H. Casini and M. Huerta, "A Finite entanglement entropy and the c-theorem", *Phys. Lett. B* **600** (2004) 142, arXiv:hep-th/0405111.

[127] H. Casini and M. Huerta, "A c-theorem for the entanglement entropy", *J. Phys. A* **40** (2007) 7031, arXiv:cond-mat/0610375.

[128] A. Zamolodchikov, ""Irreversibility" of the Flux of the Renormalization Group in a 2D Field Theory", *JETP Lett.* **43** (1986) 730.

[129] I. R. Klebanov, D. Kutasov and A. Murugan, "Entanglement as a Probe of Confinement", *Nucl. Phys. B* **796** (2008) 274, arXiv:0709.2140 [hep-th].

[130] R. C. Myers and A. Singh, "Comments on Holographic Entanglement Entropy and RG Flows", *JHEP* **04** (2012) 122, arXiv:1202.2068 [hep-th].

[131] O. Ben-Ami, D. Carmi and J. Sonnenschein, "Holographic Entanglement Entropy of Multiple Strips", *JHEP* **11** (2014) 144, arXiv:1409.6305 [hep-th].

[132] J. Bhattacharya, M. Nozaki, T. Takayanagi and T. Ugajin, "Thermodynamical Property of Entanglement Entropy for Excited States", *Phys. Rev. Lett.* **110**[**9**] (2013) 091602, arXiv:1212.1164 [hep-th].

[133] S. Karar, D. Ghorai and S. Gangopadhyay, "Holographic entanglement thermodynamics for higher dimensional charged black hole", *Nucl. Phys. B* **938** (2019) 363, arXiv:1810.08037 [hep-th].

[134] A. Saha, S. Gangopadhyay and J. P. Saha, "Holographic entanglement entropy and generalized entanglement temperature", *Phys. Rev. D* **100**[**10**] (2019) 106008, arXiv:1906.03159 [hep-th].

[135] A. Saha, S. Gangopadhyay and J. P. Saha, "Generalized entanglement temperature and entanglement Smarr relation", *Phys. Rev. D* **102** (2020) 086010, arXiv:2004.00867 [hep-th].

[136] S. Karar and S. Gangopadhyay, "Holographic information theoretic quantities for Lifshitz black hole", *Eur. Phys. J. C* **80**[**6**] (2020) 515, arXiv:2002.08272 [hep-th].

[137] H. Ouyang, "Semiclassical spectrum for BMN string in Sch5× S5", *Journal of High Energy Physics* **2017[12]** (2017) 1.

[138] M. Guica, F. Levkovich-Maslyuk and K. Zarembo, "Integrability in dipole-deformed $\mathcal{N} = 4$ super Yang–Mills", *J. Phys. A* **50[39]** (2017) 39, arXiv:1706.07957 [hep-th].

[139] U. Gursoy and C. Nunez, "Dipole deformations of N=1 SYM and supergravity backgrounds with U(1) x U(1) global symmetry", *Nucl. Phys. B* **725** (2005) 45, arXiv:hep-th/0505100.

[140] K. Landsteiner and S. Montero, "KK-Masses in Dipole Deformed Field Theories", *Journal of High Energy Physics* **2006**.

[141] A. Bergman and O. J. Ganor, "Dipoles, twists and noncommutative gauge theory", *JHEP* **10** (2000) 018, arXiv:hep-th/0008030.

[142] F. Delduc, M. Magro and B. Vicedo, "An integrable deformation of the $AdS_5 \times S^5$ superstring action", *Phys. Rev. Lett.* **112[5]** (2014) 051601, arXiv:1309.5850 [hep-th].

[143] A. Dumitru, H. Mäntysaari and R. Paatelainen, "High-energy dipole scattering amplitude from evolution of low-energy proton light-cone wave functions", *Phys. Rev. D* **107** (2023) 114024.

[144] K. Dasgupta and M. M. Sheikh-Jabbari, "Noncommutative dipole field theories", *JHEP* **02** (2002) 002, arXiv:hep-th/0112064.

[145] T. Araujo, I. Bakhmatov, E. O. Colgáin, J. Sakamoto, M. M. Sheikh-Jabbari and K. Yoshida, "Yang-Baxter σ-models, conformal twists, and noncommutative Yang-Mills theory", *Phys. Rev. D* **95[10]** (2017) 105006, arXiv:1702.02861 [hep-th].

[146] T. Araujo, I. Bakhmatov, E. O. Colgáin, J.-i. Sakamoto, M. M. Sheikh-Jabbari and K. Yoshida, "Conformal twists, Yang–Baxter σ-models & holographic noncommutativity", *J. Phys. A* **51[23]** (2018) 235401, arXiv:1705.02063 [hep-th].

[147] S. Chakravarty, K. Dasgupta, O. J. Ganor and G. Rajesh, "Pinned branes and new non-Lorentz invariant theories", *Nucl. Phys. B* **587** (2000) 228, arXiv:hep-th/0002175.

[148] K. Dasgupta, O. J. Ganor and G. Rajesh, "Vector deformations of N=4 superYang-Mills theory, pinned branes, and arched strings", *JHEP* **04** (2001) 034, arXiv:hep-th/0010072.

[149] F. Ardalan, H. Arfaei and M. M. Sheikh-Jabbari, "Noncommutative geometry from strings and branes", *JHEP* **02** (1999) 016, arXiv:hep-th/9810072.

[150] I. Kawaguchi, T. Matsumoto and K. Yoshida, "Jordanian deformations of the $AdS_5 x S^5$ superstring", *JHEP* **04** (2014) 153, arXiv:1401.4855 [hep-th].

[151] V. V. Flambaum, B. M. Roberts and Y. V. Stadnik, "Comment on "Axion induced oscillating electric dipole moments"", *Phys. Rev. D* **95**[5] (2017) 058701, arXiv:1507.05265 [hep-ph].

[152] C. T. Hill, "Axion induced oscillating electric dipole moments", *Phys. Rev. D* **91** (2015) 111702.

[153] S. Afonin and T. Solomko, "Confinement Potential in a Soft-Wall Holographic Model with a Hydrogen-like Spectrum", *Universe* **9**[3], URL.

[154] C. Nunez, M. Oyarzo and R. Stuardo, "Confinement in $(1+1)$ dimensions: a holographic perspective from I-branes", 2023.

[155] A. Bergman, K. Dasgupta, O. J. Ganor, J. L. Karczmarek and G. Rajesh, "Nonlocal field theories and their gravity duals", *Phys. Rev. D* **65** (2002) 066005, arXiv:hep-th/0103090.

[156] W. Fischler and S. Kundu, "Strongly Coupled Gauge Theories: High and Low Temperature Behavior of Non-local Observables", *JHEP* **05** (2013) 098, arXiv:1212.2643 [hep-th].

[157] J. Erdmenger and N. Miekley, "Non-local observables at finite temperature in AdS/CFT", *JHEP* **03** (2018) 034, arXiv:1709.07016 [hep-th].

[158] N. I. Gushterov, A. O'Bannon and R. Rodgers, "On Holographic Entanglement Density", *JHEP* **10** (2017) 137, arXiv:1708.09376 [hep-th].

[159] D. Giataganas, N. Pappas and N. Toumbas, "Holographic observables at large d", *Phys. Rev. D* **105**[2] (2022) 026016, arXiv:2110.14606 [hep-th].

[160] M. Sahraei, M. J. Vasli, M. R. M. Mozaffar and K. B. Velni, "Entanglement wedge cross section in holographic excited states", *JHEP* **08** (2021) 038, arXiv:2105.12476 [hep-th].

[161] K. Tamaoka, "Entanglement Wedge Cross Section from the Dual Density Matrix", *Phys. Rev. Lett.* **122[14]** (2019) 141601, arXiv:1809.09109 [hep-th].

[162] H.-S. Jeong, K.-Y. Kim and M. Nishida, "Reflected Entropy and Entanglement Wedge Cross Section with the First Order Correction", *JHEP* **12** (2019) 170, arXiv:1909.02806 [hep-th].

[163] Y. Kusuki and K. Tamaoka, "Entanglement Wedge Cross Section from CFT: Dynamics of Local Operator Quench", *JHEP* **02** (2020) 017, arXiv:1909.06790 [hep-th].

[164] Y. Kusuki, Y. Suzuki, T. Takayanagi and K. Umemoto, "Looking at Shadows of Entanglement Wedges", *PTEP* **2020[11]** (2020) 11B105, arXiv:1912.08423 [hep-th].

[165] J. Boruch, "Entanglement wedge cross-section in shock wave geometries", *JHEP* **07** (2020) 208, arXiv:2006.10625 [hep-th].

[166] M. Ghodrati, "Correlations of mixed systems in confining backgrounds", *Eur. Phys. J. C* **82[6]** (2022) 531, arXiv:2110.12970 [hep-th].

[167] M. Ghodrati, "Encoded information of mixed correlations: the views from one dimension higher", arXiv:2209.04548 [hep-th].

[168] M. Ghodrati, "String amplitudes and mutual information in confining backgrounds: the partonic behavior", arXiv:2307.13454 [hep-th].

[169] K. Babaei Velni, M. R. Mohammadi Mozaffar and M. H. Vahidinia, "Evolution of entanglement wedge cross section following a global quench", *JHEP* **08** (2020) 129, arXiv:2005.05673 [hep-th].

[170] P. Liu, C. Niu, Z.-J. Shi and C.-Y. Zhang, "Entanglement wedge minimum cross-section in holographic massive gravity theory", *JHEP* **08** (2021) 113, arXiv:2104.08070 [hep-th].

[171] D. Basu, A. Chandra, V. Raj and G. Sengupta, "Entanglement Wedge in Flat Holography and Entanglement Negativity", arXiv:2106.14896 [hep-th].

[172] Z. Yang, F.-J. Cheng, C. Niu, C.-Y. Zhang and P. Liu, "The mixed-state entanglement in holographic p-wave superconductor model", arXiv:2301.13574 [hep-th].

[173] M. Asadi, B. Amrahi and H. Eshaghi-Kenari, "Probing phase structure of strongly coupled matter with holographic entanglement measures", *Eur. Phys. J. C* **83**[**1**] (2023) 69, arXiv:2209.01586 [hep-th].

[174] K. Babaei Velni, M. R. Mohammadi Mozaffar and M. H. Vahidinia, "Entanglement Wedge Cross Section Growth During Thermalization", arXiv:2302.12882 [hep-th].

[175] A. Saha, S. Gangopadhyay and J. P. Saha, "Mutual information, islands in black holes and the Page curve", *Eur. Phys. J. C* **82**[**5**] (2022) 476, arXiv:2109.02996 [hep-th].

[176] A. Roy Chowdhury, A. Saha and S. Gangopadhyay, "The role of mutual information in the Page curve", arXiv:2207.13029 [hep-th].

[177] A. Roy Chowdhury, A. Saha and S. Gangopadhyay, "Mutual information of subsystems and the Page curve for Schwarzschild de-Sitter black hole", arXiv:2303.14062 [hep-th].

[178] S. Khoeini-Moghaddam, F. Omidi and C. Paul, "Aspects of hyperscaling violating geometries at finite cutoff", *Journal of High Energy Physics* **2021**[**2**] (2021) 1.

[179] P. Jain and S. Mahapatra, "Mixed state entanglement measures as probe for confinement", *Phys. Rev. D* **102** (2020) 126022, arXiv:2010.07702 [hep-th].

[180] P. Jain, S. S. Jena and S. Mahapatra, "Holographic confining-deconfining gauge theories and entanglement measures with a magnetic field", *Phys. Rev. D* **107**[**8**] (2023) 086016, arXiv:2209.15355 [hep-th].

[181] D. Mateos and D. Trancanelli, "The anisotropic N=4 super Yang-Mills plasma and its instabilities", *Phys. Rev. Lett.* **107** (2011) 101601, arXiv:1105.3472 [hep-th].

[182] A. Bhatta, S. Chakrabortty, S. Dengiz and E. Kilicarslan, "High temperature behavior of non-local observables in boosted strongly coupled plasma: A holographic study", *Eur. Phys. J. C* **80**[**7**] (2020) 663, arXiv:1909.03088 [hep-th].

[183] E. Shuryak, "What RHIC experiments and theory tell us about properties of quark–gluon plasma?", *Nuclear Physics A* **750**[1] (2005) 64, quark-Gluon Plasma. New Discoveries at RHIC: Case for the Strongly Interacting Quark-Gluon Plasma. Contributions from the RBRC Workshop held May 14-15, 2004, URL.

[184] J. et al, "The PHOBOS perspective on discoveries at RHIC", *Nuclear Physics A* **757**[1] (2005) 28.

[185] E. Shuryak, "Physics of strongly coupled quark–gluon plasma", *Progress in Particle and Nuclear Physics* **62**[1] (2009) 48, URL.

[186] E. Shuryak, "Strongly coupled quark-gluon plasma in heavy ion collisions", *Rev. Mod. Phys.* **89** (2017) 035001, arXiv:1412.8393 [hep-ph].

[187] M. Panero, "Thermodynamics of the QCD Plasma and the Large-N Limit", *Phys. Rev. Lett.* **103** (2009) 232001.

[188] M. J. Bhaseen, B. Doyon, A. Lucas and K. Schalm, "Far from equilibrium energy flow in quantum critical systems", *Nature Phys.* **11** (2015) 5, arXiv:1311.3655 [hep-th].

[189] R. Mishra and H. Singh, "Entanglement entropy at higher orders for the states of $a = 3$ Lifshitz theory", *Nucl. Phys. B* **938** (2019) 307, arXiv:1804.01361 [hep-th].

[190] V. Balasubramanian and P. Kraus, "A Stress tensor for Anti-de Sitter gravity", *Commun. Math. Phys.* **208** (1999) 413, arXiv:hep-th/9902121.

[191] P. Kraus, F. Larsen and R. Siebelink, "The gravitational action in asymptotically AdS and flat space-times", *Nucl. Phys. B* **563** (1999) 259, arXiv:hep-th/9906127.

[192] R. Mishra and H. Singh, "Perturbative entanglement thermodynamics for AdS spacetime: Renormalization", *JHEP* **10** (2015) 129, arXiv:1507.03836 [hep-th].

[193] R. Mishra and H. Singh, "Entanglement asymmetry for boosted black branes and the bound", *Int. J. Mod. Phys. A* **32**[16] (2017) 1750091, arXiv:1603.06058 [hep-th].

[194] V. E. Hubeny, M. Rangamani and T. Takayanagi, "A covariant holographic entanglement entropy proposal", *Journal of High Energy Physics* **2007**[07] (2007) 062.

[195] R. Mishra, Study of Geometrical Aspects of Holographic Entanglement Entropy and First Law, Ph.D. thesis, HOMI BHABHA NATIONAL INSTITUTE 2018.

[196] S. Maulik and H. Singh, "Entanglement entropy and the first law at third order for boosted black branes", *JHEP* **04** (2021) 065, arXiv:2012.09530 [hep-th].

[197] R. Emparan, A. M. Frassino, M. Sasieta and M. Tomašević, "Holographic complexity of quantum black holes", *JHEP* **02** (2022) 204, arXiv:2112.04860 [hep-th].

[198] A. Bhattacharyya, G. Katoch and S. R. Roy, "Complexity of warped conformal field theory", arXiv:2202.09350 [hep-th].

[199] M. Alishahiha, S. Banerjee, J. Kames-King and E. Loos, "Complexity as a holographic probe of strong cosmic censorship", *Phys. Rev. D* **105[2]** (2022) 026001, arXiv:2106.14578 [hep-th].

[200] M. Alishahiha, K. Babaei Velni and M. Reza Tanhayi, "Complexity and near extremal charged black branes", *Annals Phys.* **425** (2021) 168398, arXiv:1901.00689 [hep-th].

[201] N. Engelhardt and r. Folkestad, "General bounds on holographic complexity", *JHEP* **01** (2022) 040, arXiv:2109.06883 [hep-th].

[202] A. Mounim and W. Mück, "Reparameterization dependence is useful for holographic complexity", *JHEP* **07** (2021) 010, arXiv:2101.10909 [hep-th].

[203] N. Ghanbarian and M. R. Tanhayi, "'Mutual complexity' in hyperscaling violating background", *Int. J. Mod. Phys. D* **30[02]** (2021) 2150013.

[204] Z. Borvayeh, M. R. Tanhayi and S. Rafibakhsh, "Holographic Complexity of Subregions in the Hyperscaling Violating Theories", *Mod. Phys. Lett. A* **35[23]** (2020) 2050191, arXiv:2006.08478 [hep-th].

[205] S. A. Hosseini Mansoori and M. M. Qaemmaqami, "Complexity growth, butterfly velocity and black hole thermodynamics", *Annals Phys.* **419** (2020) 168244, arXiv:1711.09749 [hep-th].

[206] A. Akhavan and F. Omidi, "On the Role of Counterterms in Holographic Complexity", *JHEP* **11** (2019) 054, arXiv:1906.09561 [hep-th].

[207] F. Omidi, "Regularizations of Action-Complexity for a Pure BTZ Black Hole Microstate", *JHEP* **07** (2020) 020, arXiv:2004.11628 [hep-th].

[208] S. S. Hashemi, G. Jafari and A. Naseh, "First law of holographic complexity", *Phys. Rev. D* **102[10]** (2020) 106008, arXiv:1912.10436 [hep-th].

[209] M. Doroudiani, A. Naseh and R. Pirmoradian, "Complexity for Charged Thermofield Double States", *JHEP* **01** (2020) 120, arXiv:1910.08806 [hep-th].

[210] A. Akhavan, M. Alishahiha, A. Naseh and H. Zolfi, "Complexity and Behind the Horizon Cut Off", *JHEP* **12** (2018) 090, arXiv:1810.12015 [hep-th].

[211] M. Alishahiha, A. Faraji Astaneh, A. Naseh and M. H. Vahidinia, "On complexity for F(R) and critical gravity", *JHEP* **05** (2017) 009, arXiv:1702.06796 [hep-th].

[212] S. Karar, R. Mishra and S. Gangopadhyay, "Holographic complexity of boosted black brane and Fisher information", *Phys. Rev. D* **100[2]** (2019) 026006, arXiv:1904.13090 [hep-th].

[213] S. W. Hawking, "Particle Creation by Black Holes", *Commun. Math. Phys.* **43** (1975) 199, [Erratum: Commun.Math.Phys. 46, 206 (1976)].

[214] S. W. Hawking, "Breakdown of Predictability in Gravitational Collapse", *Phys. Rev. D* **14** (1976) 2460.

[215] D. N. Page, "Time Dependence of Hawking Radiation Entropy", *JCAP* **09** (2013) 028, arXiv:1301.4995 [hep-th].

[216] D. Page, "Information in black hole radiation", *Phys. Rev. Lett.* **71** (1993) 3743, arXiv:hep-th/9306083.

[217] A. Almheiri, N. Engelhardt, D. Marolf and H. Maxfield, "The entropy of bulk quantum fields and the entanglement wedge of an evaporating black hole", *JHEP* **12** (2019) 063, arXiv:1905.08762 [hep-th].

[218] G. Penington, "Entanglement Wedge Reconstruction and the Information Paradox", *JHEP* **09** (2020) 002, arXiv:1905.08255 [hep-th].

[219] A. Almheiri, R. Mahajan, J. Maldacena and Y. Zhao, "The Page curve of Hawking radiation from semiclassical geometry", *JHEP* **03** (2020) 149, arXiv:1908.10996 [hep-th].

[220] R. Banerjee and B. R. Majhi, "Hawking black body spectrum from tunneling mechanism", *Phys. Lett. B* **675** (2009) 243, arXiv:0903.0250 [hep-th].

[221] K. Srinivasan and T. Padmanabhan, "Particle production and complex path analysis", *Physical Review D* **60**[**2**].

[222] M. K. Parikh and F. Wilczek, "Hawking Radiation As Tunneling", *Physical Review Letters* **85**[**24**] (2000) 5042–5045.

[223] J. D. Bekenstein, "Black holes and the second law", *Lett. Nuovo Cim.* **4** (1972) 737.

[224] J. D. Bekenstein, "Black holes and entropy", *Phys. Rev. D* **7** (1973) 2333.

[225] S. W. Hawking, "Black holes and thermodynamics", *Phys. Rev. D* **13** (1976) 191.

[226] D. N. Page, "Information in black hole radiation", *Phys. Rev. Lett.* **71** (1993) 3743.

[227] D. N. Page, "Time dependence of Hawking radiation entropy", *Journal of Cosmology and Astroparticle Physics* **2013**[**09**] (2013) 028.

[228] A. Almheiri, D. Marolf, J. Polchinski and J. Sully, "Black Holes: Complementarity or Firewalls?", *JHEP* **02** (2013) 062, arXiv:1207.3123 [hep-th].

[229] A. Almheiri, D. Marolf, J. Polchinski, D. Stanford and J. Sully, "An Apologia for Firewalls", *JHEP* **09** (2013) 018, arXiv:1304.6483 [hep-th].

[230] S. Lloyd and J. Preskill, "Unitarity of black hole evaporation in final-state projection models", *JHEP* **08** (2014) 126, arXiv:1308.4209 [hep-th].

[231] K. Papadodimas and S. Raju, "Black Hole Interior in the Holographic Correspondence and the Information Paradox", *Phys. Rev. Lett.* **112**[**5**] (2014) 051301, arXiv:1310.6334 [hep-th].

[232] V. E. Hubeny, M. Rangamani and T. Takayanagi, "A Covariant holographic entanglement entropy proposal", *JHEP* **07** (2007) 062, arXiv:0705.0016 [hep-th].

[233] X. Dong, A. Lewkowycz and M. Rangamani, "Deriving covariant holographic entanglement", *JHEP* **11** (2016) 028, arXiv:1607.07506 [hep-th].

[234] T. Faulkner, A. Lewkowycz and J. Maldacena, "Quantum corrections to holographic entanglement entropy", *JHEP* **11** (2013) 074, arXiv:1307.2892 [hep-th].

[235] N. Engelhardt and A. Wall, "Quantum Extremal Surfaces: Holographic Entanglement Entropy beyond the Classical Regime", *JHEP* **01** (2015) 073, arXiv:1408.3203 [hep-th].

[236] A. Almheiri, R. Mahajan and J. Maldacena, "Islands outside the horizon", arXiv:1910.11077 [hep-th].

[237] S. Ryu and T. Takayanagi, "Holographic Derivation of Entanglement Entropy from the anti–de Sitter Space/Conformal Field Theory Correspondence", *Phys. Rev. Lett.* **96** (2006) 181602.

[238] N. Engelhardt and S. Fischetti, "Surface Theory: the Classical, the Quantum, and the Holographic", *Class. Quant. Grav.* **36[20]** (2019) 205002, arXiv:1904.08423 [hep-th].

[239] C. Akers, N. Engelhardt, G. Penington and M. Usatyuk, "Quantum Maximin Surfaces", *JHEP* **08** (2020) 140, arXiv:1912.02799 [hep-th].

[240] A. C. Wall, "Maximin Surfaces, and the Strong Subadditivity of the Covariant Holographic Entanglement Entropy", *Class. Quant. Grav.* **31[22]** (2014) 225007, arXiv:1211.3494 [hep-th].

[241] A. Almheiri, T. Hartman, J. Maldacena, E. Shaghoulian and A. Tajdini, "Replica Wormholes and the Entropy of Hawking Radiation", *JHEP* **05** (2020) 013, arXiv:1911.12333 [hep-th].

[242] G. Penington, S. Shenker, D. Stanford and Z. Yang, "Replica wormholes and the black hole interior", arXiv:1911.11977 [hep-th].

[243] K. Goto, T. Hartman and A. Tajdini, "Replica wormholes for an evaporating 2D black hole", *JHEP* **04** (2021) 289, arXiv:2011.09043 [hep-th].

[244] S. Colin-Ellerin, X. Dong, D. Marolf, M. Rangamani and Z. Wang, "Real-time gravitational replicas: Formalism and a variational principle", *JHEP* **05** (2021) 117, arXiv:2012.00828 [hep-th].

[245] A. Almheiri, T. Hartman, J. Maldacena, E. Shaghoulian and A. Tajdini, "The entropy of Hawking radiation", *Rev. Mod. Phys.* **93[3]** (2021) 035002, arXiv:2006.06872 [hep-th].

[246] H. Z. Chen, Z. Fisher, J. Hernandez, R. C. Myers and S.-M. Ruan, "Information flow in black hole evaporation", *Journal of High Energy Physics* **2020[3]** (2020) 1.

[247] K. Hashimoto, N. Iizuka and Y. Matsuo, "Islands in Schwarzschild black holes", *JHEP* **06** (2020) 085, arXiv:2004.05863 [hep-th].

[248] T. Hartman, E. Shaghoulian and A. Strominger, "Islands in Asymptotically Flat 2D Gravity", *JHEP* **07** (2020) 022, arXiv:2004.13857 [hep-th].

[249] T. Anegawa and N. Iizuka, "Notes on islands in asymptotically flat 2d dilaton black holes", *JHEP* **07** (2020) 036, arXiv:2004.01601 [hep-th].

[250] X. Dong, X.-L. Qi, Z. Shangnan and Z. Yang, "Effective entropy of quantum fields coupled with gravity", *JHEP* **10** (2020) 052, arXiv:2007.02987 [hep-th].

[251] V. Balasubramanian, A. Kar and T. Ugajin, "Islands in de Sitter space", *JHEP* **02** (2021) 072, arXiv:2008.05275 [hep-th].

[252] S. Raju, "Lessons from the information paradox", *Phys. Rept.* **943** (2022) 1, arXiv:2012.05770 [hep-th].

[253] M. Alishahiha, A. Faraji Astaneh and A. Naseh, "Island in the presence of higher derivative terms", *JHEP* **02** (2021) 035, arXiv:2005.08715 [hep-th].

[254] S. Azarnia, R. Fareghbal, A. Naseh and H. Zolfi, "Islands in flat-space cosmology", *Phys. Rev. D* **104[12]** (2021) 126017, arXiv:2109.04795 [hep-th].

[255] I. Aref'eva and I. Volovich, "A Note on Islands in Schwarzschild Black Holes", arXiv:2110.04233 [hep-th].

[256] S. He, Y. Sun, L. Zhao and Y.-X. Zhang, "The universality of islands outside the horizon", *JHEP* **05** (2022) 047, arXiv:2110.07598 [hep-th].

[257] F. Omidi, "Entropy of Hawking radiation for two-sided hyperscaling violating black branes", *JHEP* **04** (2022) 022, arXiv:2112.05890 [hep-th].

[258] M.-H. Yu, C.-Y. Lu, X.-H. Ge and S.-J. Sin, "Island, Page curve, and superradiance of rotating BTZ black holes", *Phys. Rev. D* **105**[**6**] (2022) 066009, arXiv:2112.14361 [hep-th].

[259] G. Yadav, "Page Curves of Reissner-Nordström Black Hole in HD Gravity", arXiv:2204.11882 [hep-th].

[260] D.-H. Du, W.-C. Gan, F.-W. Shu and J.-R. Sun, "Unitary Constraints on Semiclassical Schwarzschild Black Holes in the Presence of Island", arXiv:2206.10339 [hep-th].

[261] C. Teitelboim, "Gravitation and Hamiltonian Structure in Two Space-Time Dimensions", *Phys. Lett. B* **126** (1983) 41.

[262] R. Jackiw, "Lower Dimensional Gravity", *Nucl. Phys. B* **252** (1985) 343.

[263] G. Mandal, A. M. Sengupta and S. R. Wadia, "Classical solutions of two-dimensional string theory", *Mod. Phys. Lett. A* **6** (1991) 1685.

[264] D. Grumiller, W. Kummer and D. V. Vassilevich, "Dilaton gravity in two-dimensions", *Phys. Rept.* **369** (2002) 327, arXiv:hep-th/0204253.

[265] C. G. Callan, Jr., S. B. Giddings, J. A. Harvey and A. Strominger, "Evanescent black holes", *Phys. Rev. D* **45**[**4**] (1992) R1005, arXiv:hep-th/9111056.

[266] S. Hemming and E. Keski-Vakkuri, "Hawking radiation from AdS black holes", *Phys. Rev. D* **64** (2001) 044006, arXiv:gr-qc/0005115.

[267] M. Raamsdonk, "Evaporating Firewalls", *JHEP* **11** (2014) 038, arXiv:1307.1796 [hep-th].

[268] T. Hartman and J. Maldacena, "Time Evolution of Entanglement Entropy from Black Hole Interiors", *JHEP* **05** (2013) 014, arXiv:1303.1080 [hep-th].

[269] G. Grimaldi, J. Hernandez and R. C. Myers, "Quantum extremal islands made easy. Part IV. Massive black holes on the brane", *JHEP* **03** (2022) 136, arXiv:2202.00679 [hep-th].

[270] Y. Matsuo, "Islands and stretched horizon", *JHEP* **07** (2021) 051, arXiv:2011.08814 [hep-th].

[271] Y. Sekino and L. Susskind, "Fast Scramblers", *JHEP* **10** (2008) 065, arXiv:0808.2096 [hep-th].

[272] P. Hayden and J. Preskill, "Black holes as mirrors: Quantum information in random subsystems", *JHEP* **09** (2007) 120, arXiv:0708.4025 [hep-th].

[273] M. Van Raamsdonk, "Building up spacetime with quantum entanglement", *Gen. Rel. Grav.* **42** (2010) 2323, arXiv:1005.3035 [hep-th].

[274] J. Polchinski, P. Vieira and O. DeWolfe (Eds.), Proceedings, Theoretical Advanced Study Institute in Elementary Particle Physics: New Frontiers in Fields and Strings (TASI 2015): Boulder, CO, USA, June 1-26, 2015, WSP 2017.

[275] S. W. Hawking, "Breakdown of predictability in gravitational collapse", *Phys. Rev. D* **14** (1976) 2460.

[276] C. Krishnan, "Critical Islands", *JHEP* **01** (2021) 179, arXiv:2007.06551 [hep-th].

[277] C. Krishnan, V. Patil and J. Pereira, "Page Curve and the Information Paradox in Flat Space", arXiv:2005.02993 [hep-th].

[278] M.-H. Yu and X.-H. Ge, "Islands and Page curves in charged dilaton black holes", *Eur. Phys. J. C* **82**[**1**] (2022) 14, arXiv:2107.03031 [hep-th].

[279] B. Ahn, S.-E. Bak, H.-S. Jeong, K.-Y. Kim and Y.-W. Sun, "Islands in charged linear dilaton black holes", *Phys. Rev. D* **105**[**4**] (2022) 046012, arXiv:2107.07444 [hep-th].

[280] S. A. Hosseini Mansoori, O. Luongo, S. Mancini, M. Mirjalali, M. Rafiee and A. Tavanfar, "Planar black holes in holographic axion gravity: Islands, Page times, and scrambling times", *Phys. Rev. D* **106**[**12**] (2022) 126018, arXiv:2209.00253 [hep-th].

[281] D. S. Ageev, I. Y. Aref'eva, A. I. Belokon, A. V. Ermakov, V. V. Pushkarev and T. A. Rusalev, "Entanglement Islands and Infrared Anomalies in Schwarzschild Black Hole", arXiv:2209.00036 [hep-th].

[282] M.-H. Yu and X.-H. Ge, "Entanglement Islands in Generalized Two-dimensional Dilaton Black Holes", arXiv:2208.01943 [hep-th].

[283] P.-J. Hu, D. Li and R.-X. Miao, "Island on codimension-two branes in AdS/dCFT", *JHEP* **11** (2022) 008, arXiv:2208.11982 [hep-th].

[284] T. Takayanagi, "Holographic dual of a boundary conformal field theory", *Physical review letters* **107**[**10**] (2011) 101602.

[285] M. Fujita, T. Takayanagi and E. Tonni, "Aspects of ads/bcft", *Journal of High Energy Physics* **2011**[**11**] (2011) 1.

[286] M. Nozaki, T. Takayanagi and T. Ugajin, "Central charges for BCFTs and holography", *Journal of High Energy Physics* **2012**[**6**] (2012) 1.

[287] R.-X. Miao, C.-S. Chu and W.-Z. Guo, "New proposal for a holographic boundary conformal field theory", *Phys. Rev. D* **96** (2017) 046005.

[288] H. Geng and A. Karch, "Massive islands", *JHEP* **09** (2020) 121, arXiv:2006.02438 [hep-th].

[289] H. Geng, Y. Nomura and H.-Y. Sun, "Information paradox and its resolution in de Sitter holography", *Phys. Rev. D* **103**[**12**] (2021) 126004, arXiv:2103.07477 [hep-th].

[290] H. Geng, S. Lüst, R. K. Mishra and D. Wakeham, "Holographic BCFTs and Communicating Black Holes", *jhep* **08** (2021) 003, arXiv:2104.07039 [hep-th].

[291] Q.-L. Hu, D. Li, R.-X. Miao and Y.-Q. Zeng, "AdS/BCFT and Island for curvature-squared gravity", *Journal of High Energy Physics* **2022**[**9**] (2022) 1.

[292] H. Geng, A. Karch, C. Perez-Pardavila, S. Raju, L. Randall, M. Riojas and S. Shashi, "Entanglement phase structure of a holographic BCFT in a black hole background", *JHEP* **05** (2022) 153, arXiv:2112.09132 [hep-th].

[293] M. Rozali, J. Sully, M. Van Raamsdonk, C. Waddell and D. Wakeham, "Information radiation in BCFT models of black holes", *Journal of High Energy Physics* **2020**[**5**] (2020) 1.

[294] A. Almheiri, R. Mahajan and J. Santos, "Entanglement islands in higher dimensions", *SciPost Physics* **9**[**1**] (2020) 001.

[295] R. Bousso and E. Wildenhain, "Gravity/ensemble duality", *Physical Review D* **102**[**6**] (2020) 066005.

[296] M. Afrasiar, J. K. Basak, A. Chandra and G. Sengupta, "Reflected Entropy for Communicating Black Holes II: Planck Braneworlds", arXiv:2302.12810 [hep-th].

[297] M. Afrasiar, J. Kumar Basak, A. Chandra and G. Sengupta, "Islands for Entanglement Negativity in Communicating Black Holes", arXiv:2205.07903 [hep-th].

[298] C.-Z. Guo, W.-C. Gan and F.-W. Shu, "Page curves and Entanglement Islands for the Step-Function Vaidya Model of Evaporating Black Holes", arXiv:2302.02379 [hep-th].

[299] R.-X. Miao, "Entanglement Island and Page Curve in Wedge Holography", arXiv:2301.06285 [hep-th].

[300] H. Geng, A. Karch, C. Perez-Pardavila, S. Raju, L. Randall, M. Riojas and S. Shashi, "Information Transfer with a Gravitating Bath", *SciPost Phys.* **10**[**5**] (2021) 103, arXiv:2012.04671 [hep-th].

[301] H. Geng, A. Karch, C. Perez-Pardavila, S. Raju, L. Randall, M. Riojas and S. Shashi, "Inconsistency of islands in theories with long-range gravity", *JHEP* **01** (2022) 182, arXiv:2107.03390 [hep-th].

[302] S. Raju, "Failure of the split property in gravity and the information paradox", *Class. Quant. Grav.* **39**[**6**] (2022) 064002, arXiv:2110.05470 [hep-th].

[303] F. Kottler, "Über die physikalischen Grundlagen der Einsteinschen Gravitationstheorie", *Annalen der Physik* **361**[14] (1918) 401, arXiv:https://onlinelibrary.wiley.com/doi/pdf/10.1002/andp.19183611402.

[304] G. W. Gibbons and S. W. Hawking, "Cosmological Event Horizons, Thermodynamics, and Particle Creation", *Phys. Rev. D* **15** (1977) 2738.

[305] K. Goswami and K. Narayan, "Small Schwarzschild de Sitter black holes, quantum extremal surfaces and islands", *JHEP* **10** (2022) 031, arXiv:2207.10724 [hep-th].

[306] S. Bhattacharya and A. Lahiri, "Mass function and particle creation in Schwarzschild-de Sitter spacetime", *Eur. Phys. J. C* **73** (2013) 2673, arXiv:1301.4532 [gr-qc].

[307] G. Yadav and N. Joshi, "Cosmological and black hole islands in multi-event horizon spacetimes", *Phys. Rev. D* **107**[2] (2023) 026009, arXiv:2210.00331 [hep-th].

[308] H. Saida, "To What Extent Is the Entropy-Area Law Universal?: Multi-Horizon and Multi-Temperature Spacetime May Break the Entropy-Area Law", *Progress of Theoretical Physics* **122**[6] (2009) 1515.

[309] M.-S. Ma, R. Zhao and Y.-Q. Ma, "Thermodynamic stability of black holes surrounded by quintessence", *General Relativity and Gravitation* **49**[6] (2017) 1.

[310] Y. Sekiwa, "Thermodynamics of de Sitter black holes: thermal cosmological constant", *Physical Review D* **73**[8] (2006) 084009.

[311] A. Gomberoff and C. Teitelboim, "de Sitter black holes with either of the two horizons as a boundary", *Physical Review D* **67**[10] (2003) 104024.

[312] S. Bhattacharya and N. Joshi, "Entanglement degradation in multi-event horizon spacetimes", *Phys. Rev. D* **105** (2022) 065007.

[313] Y. Sekiwa, "Thermodynamics of de Sitter black holes: Thermal cosmological constant", *Phys. Rev. D* **73** (2006) 084009.

[314] J. Polchinski, "The Black Hole Information Problem", *in* Theoretical Advanced Study Institute in Elementary Particle Physics: New Frontiers in Fields and Strings, p. 353–397 2017, arXiv:1609.04036 [hep-th].

[315] V. E. Hubeny, D. Marolf and M. Rangamani, "Hawking radiation from AdS black holes", *Class. Quant. Grav.* **27** (2010) 095018, arXiv:0911.4144 [hep-th].